THE UNIVERSITY
of EDINBURGH

Investigating the mechanism of FOXG1 in glioblastoma stem cells

Kirsty Megan Ferguson

Supervisor: Professor Steven M. Pollard

A thesis submitted for the degree of Doctor of Philosophy

MRC Centre for Regenerative Medicine
and Edinburgh Cancer Research UK Centre

University of Edinburgh

2019

ABSTRACT

Glioblastoma multiforme (GBM) is the most common and aggressive primary brain cancer in adults. Relapse after conventional surgery and chemo/radiotherapy is thought to be driven by glioblastoma stem cells (GSCs). GSCs have phenotypic similarities to normal neural stem cells (NSCs) and frequently overexpress many key neurodevelopmental transcription factors, including FOXG1, a key forebrain transcription factor with reprogramming activity. Evidence points to an important functional role of FOXG1 in driving the NSC-like identity of GSCs. Here we explore the mechanisms by which FOXG1 acts, by characterising its key downstream transcriptional targets and protein-protein interactions.

Analysis of the transcriptional changes induced by *FOXG1* overexpression identified key targets, including cell cycle and epigenetic regulators, such as *FoxO6* and *Chd3*. FoxO6 was identified as a clear downstream target with a functional role in enabling FOXG1 to drive exit from quiescence. This also revealed that FOXG1, a transcriptional repressor, can lead to gene activation. The H3K4 demethylase JARID1B (KDM5B/PLU-1), a negative regulator of promoter activation, is thought to be a protein partner of FOXG1. We hypothesised that FOXG1 may activate gene expression by sequestration of this repressor. However, our studies suggest JARID1B is not essential for FOXG1's ability to drive a proliferative NS cell-like state, nor transcriptional activation of *FoxO6* or *Chd3*.

FOXG1 immunoprecipitation studies highlighted difficulties in obtaining good quality, protein-specific antibodies for characterising protein partners. We therefore exploited CRISPR/Cas9 technology to epitope-tag endogenous *FOXG1* in patient-derived glioblastoma NS (GNS) cells. These cellular models can now be used in future studies to define FOXG1's key protein partners and aid the identification of ways to therapeutically target FOXG1 in GBM.

LAY SUMMARY

One in two people will be diagnosed with cancer at some point during their lives. In the last 40 years cancer survival has doubled, owing to great strides in improving diagnosis and treatment. However, not all cancers have seen such improvements. Brain tumours remain the biggest cause of cancer death in children and adults. In adults, glioblastoma (GBM) is the most common and aggressive form, with an average survival of 15 months.

A major problem is regrowth of the tumour following conventional treatments. This is caused by cells called 'glioblastoma stem cells' (GSCs), which share many similarities with normal brain stem cells. In development, brain stem cells are tightly controlled by molecules called transcription factors; these determine when certain genes are switched on and off. GSCs have hijacked these controls by producing high levels of these transcription factors. As a result, cells divide uncontrollably leading to tumour growth. One such transcription factor, and a potential therapeutic target, is FOXG1. However, to target FOXG1 we must first understand how it works at the molecular level. Which genes are switched on and off by FOXG1 and how does it achieve this? What other molecules does FOXG1 interact with and how are these important to its function? We address these questions using both normal brain stem cells from mice and GSCs from patient tumours, and by modifying genes in these cells using the latest genetic engineering tool, CRISPR/Cas9.

This knowledge will help us to develop new ways to target FOXG1, to prevent GSCs fuelling tumour regrowth, and ultimately improve survival rates for patients with GBM. Throughout this thesis we present work which we hope brings us one step closer to this aim.

ACKNOWLEDGEMENTS

Firstly, I would like to thank Professor Steven Pollard for his expert guidance throughout this project. I am grateful for his continued support and encouragement, which has helped develop my confidence as a scientist. He has been a great mentor, with endless ideas, enthusiasm and a clear drive to make a difference to patients with glioblastoma.

Thank you also to Steve for giving me the opportunity to work as part of this wonderful group of scientists. The Pollard lab has been welcoming from day one of my PhD and I would like to thank all members, past and present, for their intellectual support and companionship over these last four years. I believe I have made life-long friendships and my PhD experience would not have been the same without them. A special thank you to Raul Bressan and Sabine Gogolok for their endless patience and scientific advice. Thank you to Ester Gangoso, Maria Angeles Marqués-Torrejón, Pooran Dewari and Leanne Bradley for always offering their support as mentors and their good humour. Finally, thank you to my fellow PhD students, Katrina McCarten and Ute Köber, for sharing the highs and lows of PhD life; as the saying goes, a problem shared is a problem halved.

I gratefully acknowledge Cancer Research UK for funding my studentship and thank my thesis committee for providing useful feedback and guidance throughout my PhD. Thank you also to the SCRM facilities and staff for assisting with technical and administrative matters. Thank you to Vivien Grant and Carla Blin for technical support and for keeping the lab running smoothly. Thank you to all who have provided reagents or analysis, as acknowledged in this thesis.

I would like to thank my examiners, Prof Nancy Papalopulu and Dr Andrew Wood, for an intellectually stimulating viva and for providing me with valuable comments on the work presented in this thesis.

Last but not least, I would like to thank all of my family and closest friends. Especially my parents, Alastair and Tamara, my elder sister Helen, and my grandparents, who have always been my number one fans and have supported me throughout my education. Their constant love and support has kept me going through challenging times and enabled me to reach this milestone.

DECLARATION OF ORIGINALITY

I declare that this thesis is of my own composition. The work presented in it is my own, unless stated otherwise by reference or acknowledgement. Any information derived from the published or unpublished work of others has been acknowledged in the text and references are listed in the bibliography. This work has not been submitted, in whole or in part, in any previous application for a degree.

29th August 2019	Kirsty Ferguson
_____	_____
Date	Signature

LIST OF ABBREVIATIONS

ATAC-seq	Assay for Transposase-Accessible Chromatin using sequencing
BMP4	Bone morphogenetic protein-4
bp	Base pair
BSD	Blasticidin-resistance gene
Cas9	CRISPR-associated protein 9
Chd3	Chromodomain Helicase DNA binding protein 3
ChIP-seq	Chromatin Immunoprecipitation sequencing
CNS	Central nervous system
CRISPR	Clustered regularly interspaced short palindromic repeats
crRNA	CRISPR RNA
Ct	Threshold cycle
DAPI	4',6-Diamidino-2-Phenylindole, Dihydrochloride
dCt/ddCt	Delta Ct/ delta delta Ct
Dox	Doxycycline
DMEM	Dulbecco's Modified Eagle's medium
DMR	Differentially methylated region
DMSO	Dimethyl sulfoxide
DNA	Deoxyribonucleic acid
dNTPs	Deoxynucleotide triphosphates
d-qNSC	Dormant quiescent NSC
DSB	Double-strand break
E(12.5)	Embryonic day (12.5)
EdU	5-ethynyl-2'-deoxyuridine
EGF(R)	Epidermal growth factor (receptor)
EGFRvIII	Epidermal growth factor receptor variant III
ESC	Embryonic stem cell
EtBr	Ethidium bromide

FACS	Fluorescence-activated cell sorting
FC	Fold change
FGF-2	Fibroblast growth factor-2
FOXG1	Forkhead Box G1
FoxO6	Forkhead Box O6
5-Aza	5-Azacytidine
4OHT	4-Hydroxytamoxifen
Fox	Forkhead box
GBM	Glioblastoma
GFAP	Glial fibrillary acidic protein
GFP	Green fluorescent protein
GSC	Glioblastoma stem cell
GO	Gene ontology
GNS	Glioblastoma neural stem
H3K4	Histone 3 Lysine 4
HDR	Homology-directed repair
HR	Homologous recombination
ICC	Immunocytochemistry
iPSC	Induced pluripotent stem cell
Jarid1b	Jumonji/ARID domain-containing protein 1b
mRNA	Messenger RNA
MGMT	O6-methylguanine-DNA-methyltransferase
MS	Mass spectrometry
NuRD	Nucleosome Remodelling and Deacetylase
NHEJ	Non-homologous end joining
NS(C)	Neural stem (cell)
nt	Nucleotide
OPC	Oligodendrocyte progenitor cell
PAM	Protospacer adjacent motif

PBS(T)	Phosphate-buffered saline (with Tween-20 or Triton X-100)
PCR	Polymerase chain reaction
PDGFα/β	Platelet-derived growth factor subunit α/β
PFA	Paraformaldehyde
PPI(D)	Protein-protein interaction (disruptor)
PRC	Polycomb repressive complex
PTM	Post-translational modification
qRT-PCR	Quantitative reverse transcription-PCR
rCas9	Recombinant Cas9
RG	Radial glia
RNA	Ribonucleic Acid
RNA-seq	RNA-sequencing
RNP	Ribonucleoprotein
RRBS	Reduced representation bisulfite sequencing
rtTA	Reverse tetracycline-controlled transactivator
SDS	Sodium Dodecyl Sulphate
sgRNA	Single guide RNA
SGZ	Subgranular zone
ssODN	Single-stranded oligonucleotide
SVZ	Subventricular zone
TAP	Tandem affinity purification
TBS-T	Tris-Buffered Saline with Tween-20
TCGA	The Cancer Genome Atlas
TF	Transcription factor
TLDA	TaqMan low-density array
TMZ	Temozolomide
tracrRNA	Trans-activating CRISPR RNA
UTR	Untranslated region

LIST OF FIGURES

TABLE OF CONTENTS

CHAPTER 1 Introduction

Glioblastoma multiforme (GBM) is the most common and aggressive primary adult brain cancer. Approximately 5% of people diagnosed with GBM survive more than 5 years. With a median survival rate of ~15 months, GBM has one of the worst overall survival rates of any human cancer (Tykocki & Eltayeb, 2018; National Cancer Intelligence Network, 2013; Hottinger *et al*, 2016; Stupp *et al*, 2009). Despite decades of research to improve diagnosis and treatments, progress has been poor. There is therefore an urgent need to develop novel therapies to treat this devastating disease.

Improving our understanding of the molecular mechanisms underlying GBM biology will aid the search for new therapeutic targets. That is the goal of this thesis. In this general introduction I cover four key areas: 1) The current landscape of GBM treatments and our knowledge of GBM molecular and cellular biology; 2) The role of master regulatory transcription factors in NSC biology, cellular reprogramming and cancers, including GBM; 3) The literature surrounding the forebrain-specific neurodevelopmental transcription factor, FOXG1; and 4) *In vitro* models of GBM. Finally, I outline the key aims and hypotheses of this thesis.

1.1 The molecular and cellular aetiology of GBM

1.1.1 Diagnosis and current treatments for GBM

Gliomas are a type of tumour that arise in the brain or spinal cord. They are categorised according to the World Health Organisation classification system (Louis *et al*, 2016) based on microscopic morphology, immunohistochemistry and recently added molecular features (Aldape *et al*, 2019). Based on this classification, gliomas can be categorised into three main types according to the predominant cell populations present: astrocytoma, oligodendroglioma and ependymoma. Astrocytomas are the most common. Each type is graded from low grade (I or II) to high grade (III or IV) based on histopathological features.

GBMs are grade IV astrocytomas and are characterised by: anaplastic glial cells, high mitotic activity, microvascular proliferation and large zones of necrotic cell death (Louis *et al*, 2016). GBMs are often diffuse, with no clear boundary between the tumour and the normal brain tissue. They comprise approximately half of all glioma cases (Zhang *et al*, 2012). GBMs are further defined as primary or secondary GBM, depending if they arose *de novo* as a grade IV tumour, or if they developed progressively from a lower grade astrocytoma, respectively. ~90% of cases of GBM are primary and 10% are secondary.

GBMs are still considered a rare, or orphan, disease. Global incidence is 0.59-3.69 per 100,000 live births, and slightly increased in males compared to females (Ghosh *et al*, 2018; Koshy *et al*, 2012; Ostrom *et al*, 2018). However, they remain the most common primary brain tumour found in adults, affecting mainly 45 to 75 year olds, and account for 12-15% of all brain tumours. Furthermore, with a median survival rate of just 15 months (Tykocki & Eltayeb, 2018; Stupp *et al*, 2010; National Cancer Intelligence Network, 2013), GBM accounts for more years of active life lost than any other cancer.

The current standard treatment for GBM, referred to as the 'Stupp protocol', involves surgical resection, followed by radiotherapy and treatment with the chemotherapeutic agent, temozolomide (TMZ) (Stupp *et al*, 2005). Complete surgical removal of the entire tumour is often difficult due to the diffuse nature of GBM and can never be curative (Claes *et al*, 2007).

Following surgery, sensitivity to TMZ can be predicted, albeit quite poorly, using an MGMT promoter methylation test (Hegi *et al*, 2005). The *MGMT* gene encodes the enzyme O6-methylguanine–DNA methyltransferase, that repairs DNA damage caused by TMZ; epigenetic silencing of this gene by promoter methylation is associated with improved treatment response. If tumour recurrence occurs, Gliadel® wafers coated with the chemotherapeutic carmustine can be implanted at the site of surgery. Currently in the UK these are only licensed for use on recurrent tumours after at least 90% of the tumour has been resected; although they can lead to increased wound infection, there is evidence to support their sequential use with radiotherapy and TMZ, as is approved in the US (Chowdhary *et al*, 2015; Ashby *et al*, 2016).

Despite these recent developments, surgery, systemic chemotherapy and radiotherapy are limited in their effectiveness and result in significant tissue toxicities and poor quality of life. There are emerging treatments, such as Tumour Treating Fields, in which electrical fields are used to selectively target dividing cells through interaction with mitotic proteins (Branter *et al*, 2018; Toms *et al*, 2019), and DCVax®-L immunotherapy, a personalised cancer vaccine using patient dendritic cells (Liau *et al*, 2018). However, it is too early to conclude if these have efficacy.

Notably, no current treatments address the problem of GBM tumour recurrence. New approaches are therefore needed which better consider the biology of GBM and the

underlying mechanisms of its initiation and maintenance in order to prevent patient relapse. As we will discuss in the next section, the inter- and intra-tumoural heterogeneity found in GBMs, at the genetic, epigenetic and cellular levels, presents challenges to the development of targeted therapeutics.

1.1.2 GBM genetics

GBMs are intrinsically heterogeneous. Indeed, as the name 'glioblastoma multiforme' implies, this is a complex disease that takes multiple forms. This is especially apparent with regards to the genetic profile of GBMs. The extensive genetic landscape of GBMs recently emerged through the collection and compilation of genomic, expression, methylation, proteomic and clinical data from numerous tumour samples (The Cancer Genome Atlas Research Network, 2008; Madhavan *et al*, 2009; Wick & Kessler, 2018; Brennan *et al*, 2013). For example, The Cancer Genome Atlas (TGCA) analysed 206 GBM patient samples to reveal a common set of pathways disrupted, including aberrant activation of oncogenes, such as *EGFR* and *Akt,* and disruption of tumour suppressors, such as *p53*, *PTEN* and *pRb*. These frequent genetic alternations fall into three critical signalling pathways: the RB, Tp53 and RTK pathways. ~74% of GBMs harbour disruptions to all three. This suggested that deregulation of these core signalling pathways is a key driver of GBM pathogenesis and may aid therapeutic decisions (Figure 1-1 A).

Several studies have shown that GBMs can be molecularly classified into two to four major groups (Verhaak *et al*, 2010; Phillips *et al*, 2006; Huse *et al*, 2011; Brennan *et al*, 2009; Park *et al*, 2019). Based on TCGA GBM gene expression profiles, Verhaak *et al* described four transcriptional subtypes: Proneural, Classical, Mesenchymal and Neural, each associated with a set of common genetic aberrations (Verhaak *et al*, 2010). Later

research, using a more stringent method of distinguishing tumour versus non-malignant mRNAs, suggests the neural subtype arose from contaminating non-tumour cells in the original analysis (Wang *et al*, 2017b; Sidaway, 2017) (Figure 1-1 B). Treatment efficacy and survival were found to differ depending on this classification, raising potential clinical applications of molecularly defining GBMs (Nutt *et al*, 2003; Freije *et al*, 2004; Le Mercier *et al*, 2012; Chen & Xu, 2016).

However, the biological or clinical relevance of these transcriptional subtypes remains unclear. Receptor tyrosine kinases (RTKs) such as epidermal growth factor receptor (EGFR), platelet-derived growth factor receptor α/β (PDGFR α/β) and the hepatocyte growth factor receptor MET are frequently activated in GBMs. *EGFR* mutations and amplifications are found in 45-57% of GBM cases (Brennan *et al*, 2013; The Cancer Genome Atlas Research Network, 2008; Pearson & Regad, 2017) with a truncated, constitutively active form, EGFR variant III (EGFRvIII), frequently expressed. Numerous kinase inhibitors and antibody therapies have been trialled clinically (Lee *et al*, 2015; van Den Bent *et al*, 2009; Jane *et al*, 2009; Sampson *et al*, 2011; Neyns *et al*, 2009), however none have given clear consistent benefits. While ongoing research is being conducted with third-generation EGFR inhibitors to circumvent treatment resistance (Liu *et al*, 2019), targeting molecular drivers such as EGFR currently holds unfulfilled promise (Westphal *et al*, 2017; Artene *et al*, 2018; Pearson & Regad, 2017). As seen in many cancers, the mutational heterogeneity within individual tumours and redundancy at many levels of these core pathways means there is no single actionable driver across all GBMs. Success may require combinatorial targeting of multiple pathways with increased risks of deleterious side effects, or the identification of new biological vulnerabilities.

A

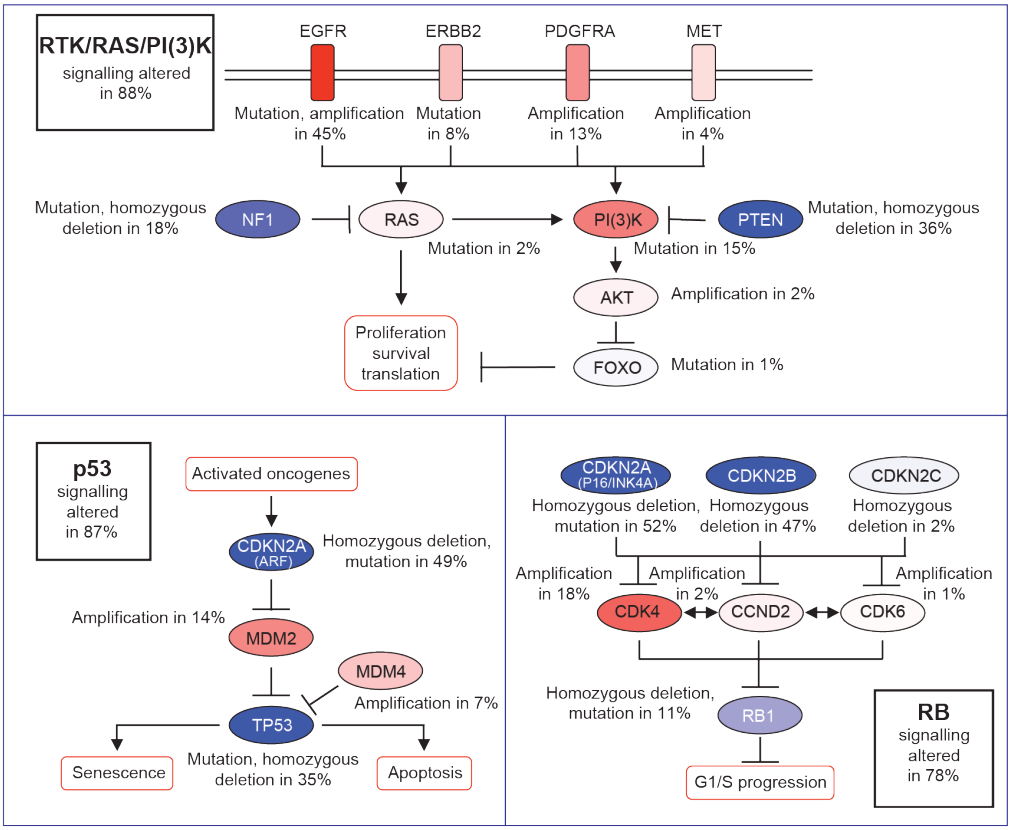

B

Molecular subtype	Expression signature	Common genetic features
Proneural	Oligodendrocytic	*PDGFRα* abnormalities, *IDH1*, *TP53* and *PTEN* mutations
Classical	Astrocytic	Chromosome 7 deletions and amplifications, *EGFR* amplification, homozygous deletion of *Ink4a/Arf* (or *Cdkn2a*) locus
Mesenchymal	Astroglial	*NF1* mutation, high levels of *TNF* and *NF-κB* pathway genes

Figure 1-1 | GBMs display genetic alterations in three key signalling pathways and can be grouped into three molecular subtypes.

(A) The TCGA data on GBM samples reveals common genetic aberrations in RTK/PI3K/RAS, TP53 and RB signalling pathways. Activating mutations are shown in red and inactivating mutations are shown in blue, with more frequent alterations denoted by darker shades. The nature of the alteration and the percentage of tumours possessing this genetic aberration are noted underneath each pathway component. Highlighted boxes show the percentage of GBMs with a genetic alternation in at least one component of the described pathway. Figure adapted with permission from Macmillan Publishers Ltd: Nature, (The Cancer Genome Atlas Research Network, 2008). **(B)** Molecular classification of GBMs based on their genomic profiles. Subtypes described by (Verhaak *et al*, 2010; Wang *et al*, 2017b). Subtypes are shown alongside common genetic features and the predominant expression signature, determined by Verhaak *et al* by comparison with gene sets defined using the brain transcriptome database presented by (Cahoy *et al*, 2008).

In addition to the difficulties posed by treatment resistance, subsequent studies found these molecular subtype classifiers to be expressed variably within each tumour at the cellular level; multiple clones, each with specific functional behaviours, were found to co-exist in the same patient (Patel *et al*, 2014; Sottoriva *et al*, 2013; Meyer *et al*, 2015; Chen *et al*, 2018). This intra-tumoural heterogeneity has been further characterised by the assignment of genomic alterations to key anatomical features (Puchalski *et al*, 2018). Moreover, the genomic instability of GBMs can lead to subclonal diversification and clonal branched evolution (Swanton, 2012; McGranahan & Swanton, 2017). Thus, the genetic makeup of the tumour will vary between diagnosis and recurrence, potentially misleading targeted therapies if only the initial profile is considered (Kim *et al*, 2015a; Johnson *et al*, 2014; Kim *et al*, 2015c). Indeed, a recent study found out of 91 paired samples taken prior to treatment and upon recurrence, only 55% retain their original subtype (Wang *et al*, 2017b; Sidaway, 2017). While GBM relapse was previously associated with progression from a proneural to mesenchymal subtype, more recent studies have not validated this association, suggesting there is no common pattern to shifts in genetic and transcriptional subtypes (Phillips *et al*, 2006; Ozawa *et al*, 2014).

Transcriptional subtypes have been shown to correlate with the immune response (Wang *et al*, 2017b); changes in the tumour microenvironment may therefore also promote transcriptomic adaptability of tumour cells leading to clonal evolution (Olar & Aldape, 2014). Recent single-cell analyses confirm that four cellular states are found within every tumour, with the frequency of cells in each state influenced by both genetics and the microenvironment (Neftel *et al*, 2019).

Although transcriptional profiling provides useful information regarding the molecular pathogenesis of GBMs, caution should therefore be taken when relying on the status of these signatures for therapeutic use. It is possible that with time and changes in the

tumour microenvironment during treatment, the tumour clonally evolves, creating a 'moving target' with regards to subtype. Furthermore, while targeting the predominant molecular subtype may result in debulking of the tumour, the survival of cells driven by other genetic aberrations will ultimately result in patient relapse.

1.1.3 The cellular origin of glioblastoma

The finding that GBMs can be classified into molecular subtypes also raised new questions regarding their cell of origin. This is defined as the cell type in which the transforming mutations that lead to gliomagenesis first occur, and has been subject to controversy for many years. To understand the possible cells of origin in GBM we must first consider the range of cell types within the adult mammalian brain that could potentially undergo malignant transformation (Figure 1-2).

NSC niches have been identified in two regions of the adult mammalian brain, the sub-ventricular zone (SVZ) lining the lateral ventricles and the subgranular zone (SGZ) of the hippocampal denate gyrus (DG) (Alvarez-Buylla *et al*, 2002; Modrek, 2014; Braun & Jessberger, 2014; Doetsch *et al*, 1999; Gage, 2000; Kriegstein & Alvarez-Buylla, 2009). These NSCs are multipotent, self-renewing, and responsible for brain plasticity and repair (Fuentealba *et al*, 2012; Kempermann *et al*, 2018; Bond *et al*, 2015). While SVZ NSCs generate olfactory bulb neurons and corpus callosum oligodendrocytes, SGZ NSCs give rise to DG neurons and astrocytes (Bond *et al*, 2015). These mature cell types arise through distinct lineage-restricted transit-amplifying progenitor cells. For example, SVZ NSCs give rise to type C progenitors, which in turn give rise to type A cells, or neuroblasts, which migrate to the olfactory bulb to become neurons (Modrek, 2014; Kriegstein & Alvarez-Buylla, 2009). Various immature stem and precursor cell types therefore exist with different lineage-restrictions and proliferative capacities (Figure 1-2 A).

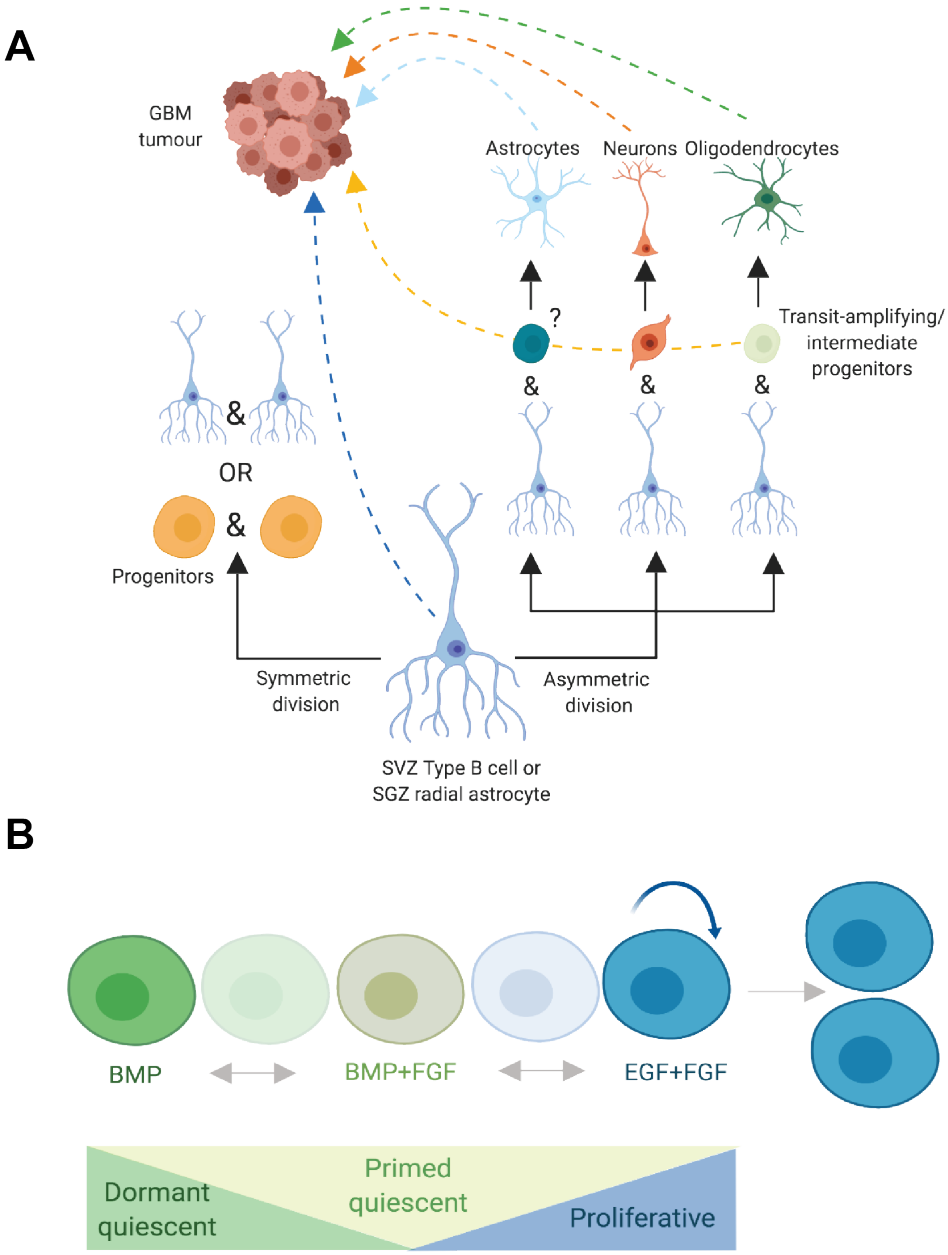

Figure 1-2 | Various cell types exist in the adult mammalian brain with different lineage-restrictions and proliferation capacities.

(A) Diagram describing the diversity of cell types present in the adult brain that could undergo malignant transformation. Adult NSCs can divide either symmetrically or asymmetrically to yield more NSCs and progenitor cells. NSCs may also differentiate directly into mature cell types, or via intermediate progenitor cell types. Experimental evidence does not yet exist for the presence of transit-amplifying astrocyte progenitors *in vivo.* SVZ and SGZ NSCs give rise to different types of mature progeny, however, tripotent differentiation is shown here for simplicity. Adapted using figure from (Bond *et al*, 2015). **(B)** Figure adapted from Marqués-Torrejón *et al* (manuscript in preparation). *In vitro* NSCs can exist along a continuum of states depending on exposure to growth factors, EGF and FGF-2, and differentiation cues such as BMP4. For simplicity, changes in morphology are not depicted. Figure made using BioRender.

The self-renewal and high proliferative capacity of NSCs make them the most likely candidate for malignant transformation; indeed, several studies support NSCs as the cell of origin in mouse models of glioma (Holland, 2000; Alcantara Llaguno & Parada, 2016; Jacques *et al*, 2010). The first genetic evidence of a human SVZ NS cell of origin in GBM samples was recently acquired through deep sequencing and genetic comparison of matched normal SVZ, tumour and normal cortical tissues (Lee *et al*, 2018). However, NSCs *in vivo* can exist in both active proliferating states and non-cycling quiescent states (Codega *et al*, 2014). Indeed, a single cell RNA-seq study identified that NSCs of the mouse SVZ exist along a continuum of states from activation to differentiation (Dulken *et al*, 2017). In agreement with this, the Pollard lab has found *in vitro* cultured NSCs to exist in a range of quiescent and differentiating states depending on their treatment with growth factors (EGF and FGF-2) and differentiation cues (BMP4) (Figure 1-2 B). NSCs can therefore also exist in non-proliferative quiescent states *in vivo* where they are less likely to acquire transformative mutations.

Differentiated cell types and their precursors have also been shown to have some proliferative capacity, suggesting they could also be at risk of acquiring transforming mutations (Zong *et al*, 2015). For example, oligodendrocyte precursor cells (OPCs) continue dividing into adulthood and can outnumber NSCs in the adult brain in humans and rodents (Dawson *et al*, 2003; Dimou *et al*, 2008). Histopathological analysis has revealed OPC marker expression in human GBM samples (Shoshan *et al*, 2002; Lu *et al*, 2001; Ligon *et al*, 2004; Rebetz *et al*, 2008) and overexpression of the OPC mitogen, PDGF, in the brain of mice resulted in the formation of tumours expressing the OPC markers, PDGFRα and NG2 (Assanah *et al*, 2006). Furthermore, loss of the tumour suppressors p53 (encoded by *Trp53)* and *Nf1* in NSCs resulted in tumour growth driven by the expansion of OPCs but not other NSC-derived lineages or NSCs themselves (Liu *et*

al, 2011). Such transformation of committed progenitors has also been shown in other types of cancer such as leukaemia (Krivtsov *et al*, 2006). Evidence for a mature astrocyte cell of origin has been provided by the ability of primary astrocyte cultures with tumour suppressor loss and oncogene activation to form malignant tumours in mice (Bachoo *et al*, 2002). More recently, it was also shown that ectopic co-expression of three core transcription factors in immortalised *Ink4a/Arf*$^{-/-}$ astrocytes can lead to glioma-initiating cells (Singh *et al*, 2017). These experiments clearly show that many brain cell types can undergo malignant transformation on introduction of common GBM driver mutations and are therefore a potential cell of origin. However, experimental conditions that artificially enforce certain genetic events do not signify that this occurs during the aetiology of GBM *in vivo*.

The intrinsic properties of different cell types may determine vastly different susceptibilities to be the cell of origin. Recently, assessment of the tumour-initiating potential of adult neural progenitor cells at various stages of lineage progression revealed a 'glioblastoma cell-of-origin hierarchy', in which there is decreasing susceptibility to transformation with increasing lineage restriction (Alcantara Llaguno *et al*, 2019). The revelation that GBMs can be grouped into different subclasses with common genetic aberrations has also hinted at a difference in cell of origin between subgroups (Verhaak *et al*, 2010); for example the molecular profile of the proneural subtype of GBM closely matched an OPC profile. This suggests that although some cell types are more prone to malignant transformation, patient tumours could arise from diverse cells of origin. However, given the evidence for heterogeneity and genetic plasticity within tumours, it is also possible that the predominant features of an established tumour do not necessarily reflect those of the cell from which it originated. The cell of origin of GBM is therefore difficult to prove.

1.2 Glioblastoma and the cancer stem cell hypothesis

A separate question to where and when GBMs first arise through their cell of origin, is that of how GBMs are maintained; this is perhaps of greater importance for the development of new therapies. Gliomas are comprised of morphologically, genetically and phenotypically heterogeneous cell populations (Wang *et al*, 2013). Are all cells in a tumour equal in their potential to propagate its expansion?

1.2.1 The cancer stem cell hypothesis

Two distinct models have been explored to explain the heterogeneity and continued propagation of tumours: 1) the stochastic clonal evolution model and 2) the hierarchical cancer stem cell (CSC) model (Figure 1-3).

The clonal evolution model posits that any cell within the tumour has equal potential to drive tumour formation (Figure 1-3 A). Functional differences between these cells arise due to stochastic intrinsic and extrinsic influences, including the acquisition of genetic and epigenetic alternations over time and changes in the microenvironment (Rich, 2016; Dick, 2009). It is therefore not possible to predict which cells will be exposed to factors which endow them with malignant properties, and tumour-propagating cells do not share a biological uniqueness enabling their isolation. The selection and expansion of 'advantageous' clones over time results in the formation of a heterogeneous tumour made up of an accumulation of diverse clones, each of which have separately undergone neoplastic transformation. Based on this hypothesis traditional cancer treatments have been based on treating all tumour cells as equally important to eradicate (Bradshaw *et al*, 2016; Sundar *et al*, 2014).

Conversely, the CSC hypothesis postulates that tumour formation and long-term

maintenance is fuelled by a distinct sub-population of cells with stem-cell like properties; namely, the ability to self-renew and to give rise to differentiated, non-malignant progeny (Clarke *et al*, 2006; Sell, 2010; Reya *et al,* 2001) (Figure 1-3 B). Given their biological uniqueness, it must therefore be possible to isolate CSCs based on their intrinsic properties. In this model, the tumour is organised in a differentiation hierarchy reminiscent of that in normal tissues containing tissue stem cells; however, aberrant control of this hierarchy results in tumour formation. A population of CSCs is maintained at the apex, which gives rise to differentiated tumour cell progeny of decreasing proliferative capacity and increasing specialisation. The CSC is therefore responsible for propagating tumour growth and is the therapeutic target.

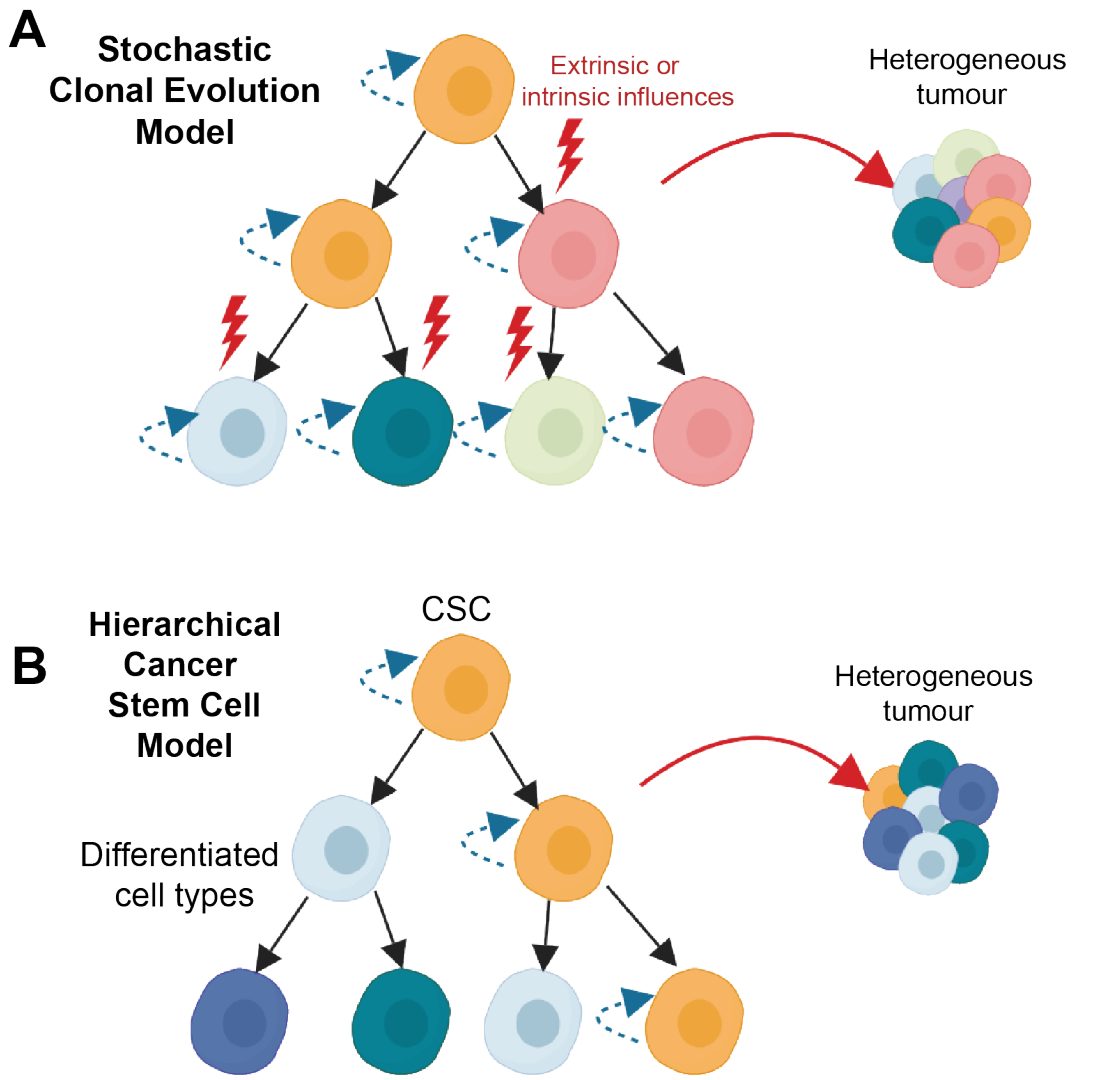

Figure 1-3 | Two predominant models exist to explain the heterogeneity and continued propagation of cancer.

(A) The clonal evolution model suggests that all cells within the tumour have equal potential to gain malignant properties, through exposure to intrinsic and extrinsic influences, and drive tumour formation. This leads to a tumour made up of competing clones with unpredictable behaviour. **(B)** The CSC hypothesis suggests the tumour is organised hierarchically, with CSCs (yellow) at the top of the hierarchy giving rise to all differentiated cell types of the tumour. Only the CSCs have the potential to propagate tumour expansion. Both models result in the formation of a heterogeneous tumour. Figure created with BioRender.

The first strong evidence supporting the CSC hypothesis was reported by Kleinsmith and Pierce in the 1960's, who demonstrated that single teratocarcinoma cells, then named embryonal carcinoma cells, could give rise to multi-differentiated, transplantable tumours in mice (Kleinsmith & Pierce, 1964). The rarity of teratocarcinomas, however, undermined their findings as many dismissed them as unrepresentative of most human cancers.

In 1994, Dick and colleagues provided the first functional evidence for CSCs in leukaemia, characterised by their expression levels of the cell surface markers CD34 and CD38 (Lapidot *et al*, 1994). While work in the haematopoietic system is most advanced with respect to the identification and characterisation of CSCs, there is now mounting evidence that CSCs exist in several types of solid tumour (Visvader & Lindeman, 2008). For example, Al-Hajj and colleagues were the first to isolate a fraction of tumorigenic cells in human breast carcinoma (Al-Hajj *et al*, 2003).

1.2.2 The discovery of CSCs in GBM

Since the first identification of CSCs in solid tumours, several studies have provided support for their existence in GBM (Furnari *et al*, 2007; Singh *et al*, 2003; Hemmati *et al*, 2003; Pollard *et al*, 2009; Galli *et al*, 2004; Yuan *et al*, 2004). In two seminal papers, Singh *et al*. isolated immature stem-like cells from brain cancers, using the marker CD133, a cell surface antigen known to mark multipotent cells in the brain and other tissues (Yuan *et al*, 2004; Galli *et al*, 2004; Singh *et al*, 2003, 2004); they then demonstrated that these cells can give rise to heterogeneous tumours that are serially transplantable and are reminiscent of neural progenitors, upregulating neuronal and glial marker protein expression on exposure to serum (Hemmati *et al*, 2003; Stiles & Rowitch, 2008). These identified glioblastoma stem cells (GSCs) are defined as a tumour sub-population that

can self-renew, are tumour-initiating and can generate differentiating progeny. More recently, new technologies, such as lineage-tracing with DNA barcoding and single-cell RNA-seq, have provided evidence of a proliferative hierarchy in GBM that recapitulates that of normal brain development (Lan *et al*, 2017; Couturier *et al*, 2018).

Although putative cell surface markers such as CD133 were first used for CSC isolation, there are some caveats to this experimental approach (Abbaszadegan *et al*, 2017). For example, GSCs have been identified that do not express CD133 (Pollard *et al,* 2009). Also, CD133 is expressed on other non-tumour cells such as endothelial cells and varies with cell cycle stage (Beier *et al*, 2007; Stiles & Rowitch, 2008; Sun *et al*, 2009). To accurately study the biology of human GBM, novel approaches were therefore required to isolate pure GSC populations for analysis.

In 2009, Pollard *et al* demonstrated that conditions previously established for the propagation of mouse and human adherent NS cell lines can be used to efficiently derive and expand adherent cells from malignant glioma (Conti *et al*, 2005; Pollard *et al*, 2006; Sun *et al*, 2008). When cultured under these serum-free conditions supplemented with EGF, FGF-2 and laminin, patient-derived GSCs can be expanded continuously *in vitro* as an adherent monolayer and are tumorigenic following transplantation *in vivo* (Pollard *et al*, 2009). These cells also display many NS cell properties, such as high motility and expression of the neural progenitor markers Sox2 and Nestin, and hence they are referred to as glioblastoma NS (GNS) cells. The advantages of this culture system compared to conventional glioma cell lines is described further in section 1.5.2.

In addition, Pollard *et al* found GNS cell lines from different patients could be distinguished based on their expression of lineage-specific neural progenitor markers, mirroring some of the differences in transcriptional subtypes described previously

(Pollard *et al*, 2009; Verhaak *et al,* 2010). This suggests that although the GSC population underlies tumour formation, GBMs are not driven by a single type of tumour stem cell and it is possible GSCs arise from different origins. The arguments discussed in section 1.1.3 regarding the cellular aetiology of GBM apply to the development of GSCs; the cells from which they arise is still under debate.

Furthermore, it is increasingly clear that the hierarchical CSC and stochastic clonal evolution models of tumour heterogeneity are not mutually exclusive. Recently a third 'unified' dynamic model has been suggested (Kreso & Dick, 2014; Corrò & Moch, 2018; Rich, 2016) (Figure 1-4 A). This considers that in the course of tumour development, tumour cells may be exposed to influences, such as genetic mutations, that alter their behaviour. This could lead to phenotypic plasticity, with the formation of new CSC branches or the conversion of differentiated cells to a stem cell phenotype. As a result, multiple CSC clones, each competing and giving rise to their own hierarchy, may coexist within a tumour. Furthermore, the 'depth' of tumour developmental hierarchies may alter during tumour progression (Figure 1-4 B). While CSCs may initially exist at low frequencies in the tumour, their numbers may expand in response to accumulative malignant properties, leading to sub-clones with higher frequencies of stem-like cells (Kreso & Dick, 2014). These processes may be accelerated by changes in the microenvironment and could explain the change in predominant transcriptional subtype often found on tumour recurrence. The extent to which this unified 'plasticity' model applies to GSCs is as yet unclear. A recent fate mapping study of barcoded GSCs following xenotransplantation found that the majority of clones showed hierarchical growth, neutral to evolving mutations; however, a minority subset were expanded after TMZ treatment (Lan *et al*, 2017). Nevertheless, despite potential inter- and intra-tumoural differences in GSC clones, all possess the same NSC-like characteristics.

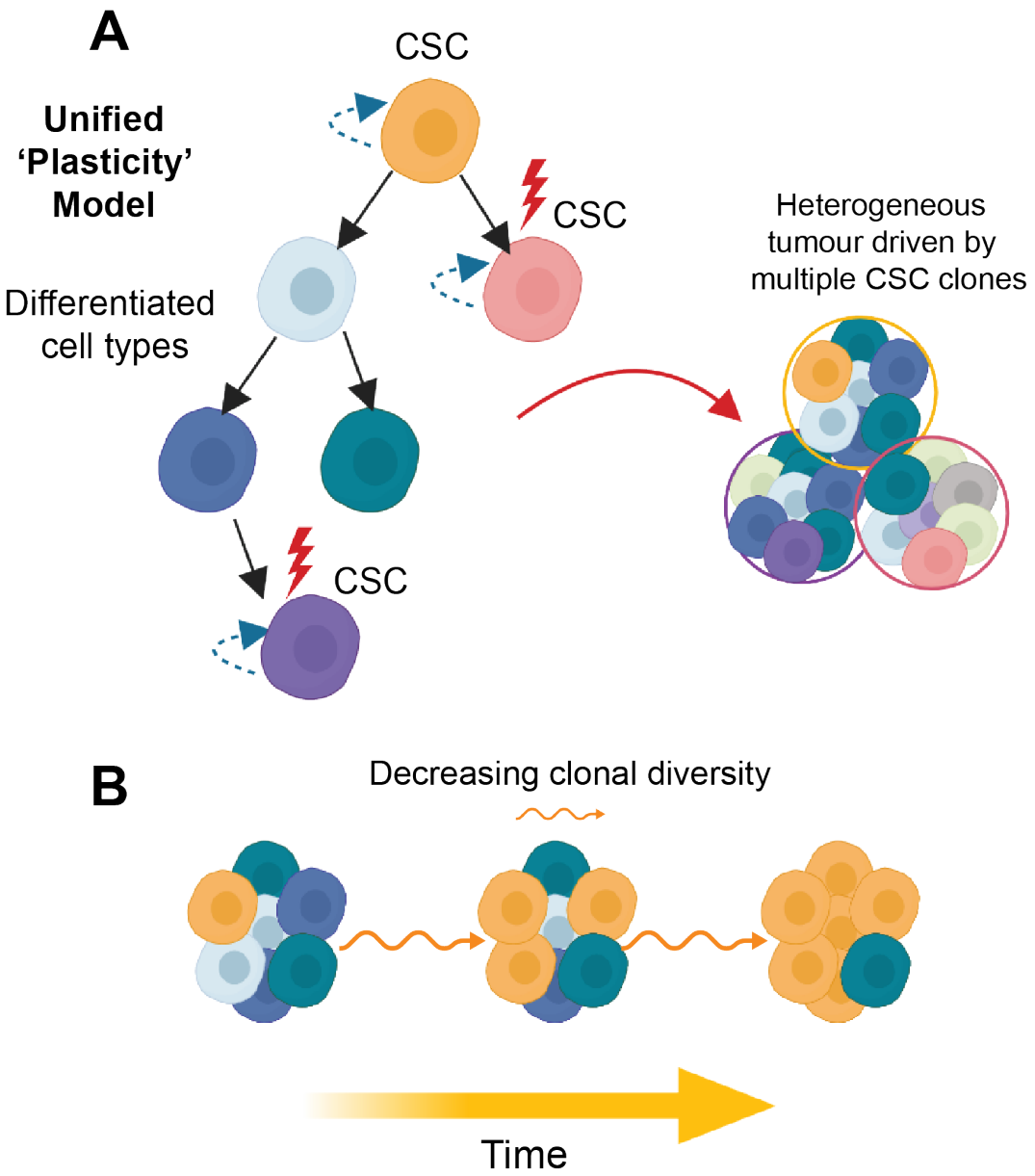

Figure 1-4 | The unified model of GBM heterogeneity.

(A) The unified 'plasticity' model suggests that, over time, tumour cells will be exposed to influences that change their behaviour. For example, CSCs may themselves undergo clonal evolution, or differentiated cells may acquire stem cell characteristics in response to environmental pressures such as treatments. This leads to competing CSC clones within an individual tumour (Kreso & Dick, 2014; Rich, 2016). **(B)** Over time the depth of tumour differentiation hierarchies may alter, with CSC frequencies (yellow cells) expanding during tumour progression (Kreso & Dick, 2014). Figure created with BioRender.

1.2.3 Challenges posed by GSCs for the treatment of GBM

The discovery of a CSC fraction driving tumour formation raised important new considerations for the treatment of GBM. Studies suggest CSCs can evade conventional cytotoxic therapeutic strategies due to a number intrinsic properties (Lathia *et al*, 2015). These include increased DNA repair capacity, higher expression of drug export proteins and radiation resistance (Bao *et al*, 2006; Stiles & Rowitch, 2008; Kim *et al*, 2015b; Bhat *et al*, 2013; Wang *et al*, 2010), mediated through signalling such as Notch, EZH2 and NF-κB. A block of commitment in the presence of differentiation cues is also a feature of GNS cells, resulting in resistance to potential differentiation therapies (Carén *et al*, 2015). Furthermore, like normal adult NSCs *in vivo* and *in vitro*, it is likely that GSCs can adopt a continuum of states, from dormancy to active proliferation (Figure 1-2 B). Quiescent GSCs have been reported in GBM, in a reversible cell-cycle arrest that allows them to evade therapies targeting mitotic cells (Deleyrolle *et al*, 2011; Ishii *et al*, 2016; Chen *et al*, 2012). This selective survival of GSCs is thought to be a major factor leading to tumour recurrence and patient relapse after therapy.

In conclusion, despite controversy surrounding the cell of origin of GBM, it is widely accepted that relapse is driven by GSCs, which express many immature NS and progenitor cell markers and exist in both quiescent and proliferative subpopulations. However, more studies are needed to define the origins of the GSCs and their capacity to undergo terminal differentiation *in vivo*. To effectively treat GBM it is vital to utilise GSC-specific agents, to target this cancer stem cell fraction, alongside traditional therapies to eliminate the tumour bulk. This requires an understanding of the transcriptional networks that limit the differentiation of GSCs and underpin their self-renewal, and hence drive their initiation and maintenance.

1.3 Transcription factors and reprogramming in cancer

1.3.1 Transcription factors control gene expression to determine cell identity

There are ~20,000 protein-coding genes in the human genome, whose expression levels must be tightly regulated, temporally and spatially, to give rise to the abundance of different cell identities found in the body. Cell type identity is governed by the action of transcription factors, proteins that bind to DNA-regulatory sequences, often in combination, to control the rate of transcription. Transcription factors (TFs) belong to two main classes: i) general TFs, which together with the RNA polymerases, form the basal transcriptional machinery around the transcription start site; and ii) sequence-specific TFs, that bind to specific cis-regulatory sequences to regulate gene expression in response to biological signals (Benayoun *et al*, 2011; Spitz & Furlong, 2012; Levine & Tjian, 2003). These factors share common characteristics including specific DNA binding domains and trans-activation or trans-repression effector domains. Many sequence-specific TFs are expressed in a lineage- or cell type-specific manner.

TFs can lead to repression or activation of specific genes by several mechanisms. Some directly recruit RNA polymerase, while others recruit accessory factors to promote specific phases of transcription (Frietze and Farnham, 2011; Lambert *et al*, 2018b). However, most eukaryotic TFs act by recruiting either co-repressors or co-activators, often as multi-subunit complexes. These often contain enzymatic activities, enabling covalent modification of TFs and RNA polymerases themselves, as well as DNA and histones, leading to chromatin remodelling and changes in DNA accessibility. In this way, TF binding to DNA can lead to changes in the epigenetic landscape that facilitate or repress transcription initiation. In addition, some TFs themselves can act as pioneer factors, binding to and derepressing closed chromatin, directly leading to increased DNA

accessibility (Iwafuchi-Doi & Zaret, 2014).

Most transcription factors are known as either repressors or activators of gene expression; however, this is often overly simplistic. There are many reports of single TFs acting as both activators and repressors in a context-dependent manner, for example in response to binding of multiple cofactors with opposing effects (Schmitges *et al*, 2016; Rodriguez *et al*, 2005), covalent modifications resulting from specific signalling cascades (Rosenfeld *et al*, 2006) and the local DNA sequence context (Meijsing *et al*, 2009; Lambert *et al*, 2018b; Seth & Majzoub, 2001). Most likely there is a network of TF and cofactor interactions that result in gene expression changes in a context-dependent manner, to ensure correct progenitor proliferation and cellular differentiation during development (Lambert *et al*, 2018b).

1.3.2 Master transcription factors can lead to cell fate conversions

TFs whose expression is limited to a particular tissue or cellular lineage are described as lineage-specific (Kumar *et al*, 2019). Several examples of such TFs have been reported such as MYOD, which establishes muscle development (Fong & Tapscott, 2014), and PAX5, which is essential for B cell lymphogenesis (Morrison *et al*, 1998). The interaction of a precise combination of these factors results in an, often autoregulatory and self-re-enforcing, TF network that leads to cell-type specific expression patterns and hence lineage specification (Bottardi *et al*, 2007).

Over the last twenty years, several seminal studies have shown the ability of sets of lineage-specific TFs to reprogramme cell lineages. As such, they are often termed 'master regulatory' TFs as their potent function suggests they lie at the top of a regulatory network. In 1978, Davis *et al.* first observed that MyoD alone could drive the conversion of fibroblasts into myoblasts (Davis et al, 1987). Over 25 years later, Yamanaka and

colleagues published their seminal work showing the reprogramming of somatic cells into induced pluripotent stem cells (iPSCs) through the overexpression of four factors, Oct4, Sox2, Klf4 and c-Myc (OKSM) (Takahashi & Yamanaka, 2006).

1.3.3 Epigenetic resetting is facilitated by master regulators

Research into understanding how these master regulators interact with the genome and other molecules to drive these cell fate conversions is of great interest (Soufi, 2014; Fong & Tapscott, 2013; Apostolou & Stadtfeld, 2018). Importantly, they must reset the transcriptional programme to that of the new cell state (Hochedlinger & Plath, 2009). To do this, global and focal changes in reversible histone modifications and DNA methylation, collectively known as 'epigenetic resetting', must occur (Suvà *et al*, 2013; Orkin & Hochedlinger, 2011). This in turn overcomes DNA accessibility barriers to facilitate changes in gene expression. In the formation of iPSCs, genome-wide profiling of TF binding, chromatin state and DNA methylation patterns reveals significant epigenetic changes that lead to activation of pluripotency genes and full cell reprogramming (Hochedlinger & Jaenisch, 2015; Mikkelsen *et al*, 2008).

Since the discovery of methylation of cytosine C-5 within CpG dinucleotides in the 1970s, DNA methylation status has been shown to alter gene expression (Bird, 2002; Stricker & Pollard, 2014). This is facilitated by a set of DNA methyltransferase enzymes, which catalyse both *de novo* DNA methylation (DNMT3a and b) and maintenance of methylation (DNMT1) (Xu *et al*, 2010; Romani *et al*, 2018), and TET methylcytosine dioxygenases (TET1/2/3), which convert 5-methylcytosine to 5-hydroxymethlycytosine to initiate a demethylation process.

Initially DNA methylation was considered generically transcriptionally repressive; methylation at CpG islands in gene promoters generally correlates inversely with

transcription and hypermethylation of intragenic clusters of CpGs have been shown to prevent unwanted initiation at internal promoters. However, the correlations between transcriptomes and DNA methylomes are usually weak, highlighting that the direction of transcriptional change cannot always be easily predicted (Stricker & Pollard, 2014). Nevertheless, global changes in DNA methylation marks are a key barrier to the transition to a stem cell state, acting to modify the interactions of DNA with specific TFs or histone proteins. While CpG methylation is the canonical form of methylation in eukaryotes, methylation at non-CpG sites (CpA, CpT and CpC) has recently been reported to be enriched in mammalian cells such as ES cells, iPSCs, neurons and glial cells; further studies are needed to understand the functions underlying this mark and its importance to cell fate (Carén *et al*, 2013; Patil *et al*, 2014; Jang *et al*, 2017; Xie *et al*, 2012; Lister *et al*, 2009). Furthermore, whether 5-hydroxymethylcytosine (5hmC), the modification catalysed by TET enzymes, has roles other than as an intermediate of DNA methylation remains to be determined (Carén *et al*, 2013).

In addition to modifications of DNA itself, the epigenetic landscape includes chromatin accessibility, primarily regulated by the density of nucleosomes, the basic unit of DNA packaging. This chromatin structure is altered by a series of post-translational modifications present on the tails of the histone proteins around which DNA is structured. More than 100 histone-modifying enzymes act together to 'write' and 'erase' this code, made up of marks such as acetylation, methylation and phosphorylation (Allfrey *et al*, 1964), which is then 'read' by effector complexes to control the chromatin structure. These include chromatin architectural proteins, ATP-dependent chromatin-remodellers, of which there are four families in eukaryotes (SWI/SNF, ISWI, CHD and INO80), and chromatin modifiers (Yun *et al*, 2011).

In addition, histone modifications can alter gene expression by directing the recruitment of core transcriptional machinery (Qin *et al*, 2016). Different histone marks are therefore associated with different chromatin landscapes and levels of gene expression. For example, active euchromatin generally has high levels of acetylation and methylation of histone 3 lysine 4 (H3K4), whereas silent heterochromatin has high levels of methylation and low acetylation of histone 3 lysine 27 (H3K27). These processes are often performed by multi-subunit protein complexes, such as the nucleosome remodelling and deacetylase (NuRD) complex (Basta & Rauchman, 2009), polycomb repressive complexes (PRCs) (Chittock *et al*, 2017) and the SWI/SNF complex (Lu & Allis, 2017), which function in equilibrium to stabilise and maintain gene expression patterns (Bracken *et al*, 2019).

1.3.4 The link between reprogramming and tumorigenesis

In addition to the transformative applications that reprogramming research has had on disease modelling and cell therapies, it also demonstrates the ability of master regulatory TFs to drive a complete conversion of cell fate in inappropriate developmental contexts (Suvà *et al*, 2013). The conceptual and mechanistic similarities between *in vitro* reprogramming and tumour development have become increasingly apparent, with the expression of master regulatory lineage-specific TFs playing a vital role in emergence of a stem cell-like phenotype in both cases. Cells that undergo malignant transformation enter an immature state and acquire self-renewal capacity to drive tumour formation. Furthermore, there are numerous examples of TFs and chromatin regulators that have established roles in both cancer and iPSC reprogramming (Suvà *et al*, 2013). For example, c-Myc and the developmental transcription factor, SOX2, both components of the OKSM reprogramming cocktail, have a wide range of functions in human cancers. The transcriptional networks that normally

regulate cell fate during development can be exploited by scientists to reprogramme cell lineages; in an analogous manner, cancer can subvert these developmental programmes to obtain a proliferative stem cell-like state that drives tumour formation.

1.3.5 Master regulatory transcriptional networks in glioblastoma stem cells

The finding that CSCs rely on many of the signalling pathways required for maintenance of the stem cell state can be extended to GSCs (Jackson *et al*, 2014; Guo *et al*, 2011). As described in section 1.2.2, GNS cells were found to possess NS cell-like properties, including the expression of several key NSC markers (e.g. Nestin, Ascl1, Sox2, Olig2), suggesting factors involved in controlling normal NSCs may be important to GSC initiation and maintenance. Indeed, several studies have found transcriptional regulators, normally kept in check by PRCs, to have increased activation in glioma-initiating cells (Singh *et al*, 2017; Rheinbay *et al*, 2013; Bulstrode *et al*, 2017; Garcia *et al*, 2017) which is required for their tumour-propagating potential (Mehta *et al*, 2011; Gangemi *et al*, 2009).

Recent studies have used analysis of active chromatin landscapes to further delineate the transcriptional circuitry driving GSCs (Suvà *et al*, 2014; Singh *et al*, 2017; Mack *et al*, 2019). For example, Suvà *et al.* identified a core set of neurodevelopmental transcription factors (POU3F2, SOX2, SALL2 and OLIG2) that are sufficient to reprogramme differentiated GBM cells into stem-like tumour propagating cells (Suvà *et al*, 2014). The coordinated induction of three core transcription factors (Sox2, Olig2 and Zeb1) was also recently shown to transform immortalised astrocytes without oncogene induction (Singh *et al*, 2017). Furthermore, a recent genome-wide CRISPR/Cas9 screen identified key 'stemness regulators' in GSCs, including SOX2 and SOX9 (MacLeod *et al*, 2019). These factors have important known roles in lineage restriction during neural

development. For example, SOX2 is found in multiple types of stem cells including neural progenitors (Arnold *et al*, 2011) and OLIG2 is a master regulator of oligodendrocyte identity (Meijer *et al*, 2012); both of these factors also have fundamental roles in NSC self-renewal (Mateo *et al*, 2015; Graham *et al*, 2003). SOX9 also plays an essential role in the formation and maintenance of multipotent NSCs (Scott *et al*, 2010).

Notably, in addition to their developmental roles, several of these factors have been shown to possess reprogramming activity *in vitro* (Pang *et al*, 2011; Lujan *et al*, 2012). For example, reprogramming of murine embryonic fibroblasts into tripotent NS cells was achieved using three neural-lineage specific factors, Foxg1, Sox2 and Brn2 (Lujan *et al*, 2012). SOX2 alone was also shown to programme mouse and human fibroblasts to multipotent NSCs at low efficiency (Ring *et al*, 2012). This suggests a core transcriptional network is needed for initiation and/or maintenance of GSCs, in which master regulators act to drive the self-renewal and epigenetics underlying GBM. Several studies suggest that oncogene activation may facilitate the establishment of this transcriptional network (Singh *et al*, 2017; Liu *et al*, 2015; Riddick *et al*, 2017).

Caren *et al* found that GNS cell lines are unable to respond appropriately to the differentiation signal BMP4, known to trigger cell cycle exit and astrocyte differentiation of NSCs (Carén *et al*, 2015; Bonaguidi, 2005); chromatin accessibility revealed that regions that failed to close on BMP4 treatment were enriched in SOX2 motifs. This suggests that the elevated levels of master regulators, such as SOX2, found in GSCs may facilitate their ability to evade differentiation and maintain a stem cell-like state. It is likely that the high levels of master regulators in GSCs are constantly acting to drive cellular reprogramming in the presence of changing environmental challenges to the stem cell state. How these master regulatory TFs are able to control the GSC state, leading to dysregulated self-renewal, is a question of great interest.

As demonstrated by cell reprogramming studies, one mechanism by which master regulators lead to changes in gene expression is through association with cofactors that alter DNA methylation and chromatin structure. The importance of epigenetic resetting in GBM tumorigenesis has been highlighted by several studies, with half of adult GBMs shown to have aberrations in a chromatin modifier gene (Brennan *et* al, 2013; Bruggeman *et al*, 2007; Lee *et al*, 2008; Azzarelli *et al*, 2018). In addition to direct genetic aberrations of epigenetic machinery, epigenetic resetting can be established through gene specific and global changes in epigenetic marks leading to aberrant expression of tumour suppressors, oncogenes and cell differentiation machinery (Carén *et al*, 2013).

Such changes in the epigenetic landscape are thought to drive GSC initiation. Analysis of DNA methylation patterns in primary GBM samples revealed hypermethylation of, not the traditional tumour suppressor genes as expected, but novel tumour suppressor and PRC2-target genes. The replacement of reversible repression of these genes, normally required for determining cell fate choice in ESCs, with permanent silencing is thought to facilitate establishment of a stem cell state (Widschwendter *et al*, 2007; Lai *et al*, 2014). Stricker and colleagues validated this finding, in addition to identifying other hypermethylated genes, *TES* and *CDKN1C*, by comparing the DNA methylation profiles of GNS and normal NSC lines (Stricker *et al*, 2013). To investigate the contribution of the cancer epigenome to malignant behaviour, the team reprogrammed GNS cell lines into GBM iPSCs (GiPSCs) using exogenous expression of *OCT4* and *KLF4*. This resulted in resetting of DNA methylation marks; however this was insufficient to override dysregulated signalling in GiPSC-derived NSCs which remained highly malignant. This is consistent with the 'epigenetic progenitor' model of tumorigenesis, whereby epigenetic silencing of PRC-regulated genes is an early step in tumour formation, prior to global epigenetic resetting and further mutations (Feinberg *et al*, 2006; Stricker & Pollard,

2014; Carén *et al*, 2013). However these early epigenetic changes are not necessarily a key therapeutic target, as genetic pathways later take over the main driver role.

In addition to GSC initiation, epigenetic remodelling is also thought to play key roles in maintaining the CSC state. During cancer progression, changes in the microenvironment trigger reversible epigenetic modifications that threaten CSC maintenance; aberrant expression of chromatin regulators, used to maintain proliferation and pluripotency in normal stem cells, is needed to enable their continued self-renewal (Gervais *et al*, 2019; Keenen & De La Serna, 2009). Numerous epigenetic regulators have been shown to be upregulated in GSCs and implicated in their maintenance, such as the PRC components, EZH2 (Suvà *et al*, 2009) and BMI1 (Gargiulo *et al*, 2013), and the Trithorax-related histone methyltransferase, MLL (Gallo *et al*, 2012). GSCs have also been shown to transition between epigenetic states in response to environmental pressures; in response to RTK inhibitors, a transition to a slow-cycling 'persister' state through upregulation of histone demethylases KDM6A/B and Notch signalling facilitates GSC resistance (Liau *et al*, 2017).

In summary, lineage-specific TFs are key therapeutic targets in GBM. Our advancing knowledge of the core transcriptional and epigenetic networks driving GBM should therefore bring new possibilities for treating this disease (Romani *et al*, 2018).

1.4 FOXG1 in development, reprogramming and cancer

One neurodevelopmental transcription factor of particular interest to the pathogenesis of GBM, and the focus of this thesis, is the Forkhead factor, FOXG1. In this section we will cover the background literature surrounding Forkhead factors and their known roles in development, reprogramming and cancer.

1.4.1 The Forkhead family of TFs possess a conserved Forkhead domain

Sequence-specific TFs can be classified according to the structure and homology of their DNA binding domains. The Forkhead box (FOX) proteins are a superfamily of 'winged helix' or 'Forkhead box' DNA binding domain TFs, evolutionarily conserved in organisms from yeast to humans. The term 'Forkhead' was first used to describe the founding member, a *Drosophila melanogaster* protein whose absence resulted in a characteristic 'forked head' appearance due to abnormal gut development (Weigel *et al*, 1969). To date, over 2000 Forkhead family members have been identified in 108 species of animals and fungi (Benayoun *et al*, 2011). In the human genome, fifty Forkhead proteins have been identified, characterised by their Forkhead box binding domain of approximately 100 residues (Jackson *et al*, 2010). The structure of several Forkhead domains complexed to their target DNA sequences have been resolved; this revealed three N-terminal α-helices, three β-strands and two loops in the C-terminal region (Benayoun *et al*, 2011; Clark *et al*, 1993), in which the folding of the two loops around the helices creates a 'winged helix' appearance. The Forkhead factors bind a seven base pair consensus binding sequence (GTAAACA), with the wings and flanking DNA sequences modulating the binding specificity and affinity (Cirillo & Zaret, 2007). In addition to DNA-binding functions, the Forkhead domain also contains nuclear localisation sequences, primarily at the C-terminal (Romanelli *et al*, 2003), indicating a common nuclear import mechanism.

1.4.2 Varied expression patterns, domain structures, protein partners and PTMs confer Forkhead factors with a diverse range of functions

While the Forkhead domain is highly conserved, regions outside are divergent. In humans, Forkhead factors can be further categorised into 19 subclasses, A to S, based on sequence homology within and outside the Forkhead domain (Kaestner *et al*, 2000; Lam & Gomes, 2014; Golson & Kaestner, 2016), with FoxO factors perhaps the best studied

subfamily. Fox factors possess distinct tissue-specific expression patterns during development and adulthood, reflective of their roles in cell fate determination in all three germ layers after gastrulation (Lehmann *et al*, 2003); these patterns are often divergent even between close paralogs within subclasses (Benayoun *et al*, 2011).

Distinct post-translational modifications (PTMs) and protein interactions introduce a further layer of functional diversity between the Fox factors. While Forkhead factors are thought to mostly bind DNA as monomers, evidence exists for some binding in both homodimeric and heterodimeric forms. For example, the crystal structures of FOXP2 and FOXK1 revealed homodimeric interactions with DNA (Tsai *et al*, 2006; Stroud *et al*, 2006). The interaction between FoxO3 and FoxM1 is required to regulate expression of the oestrogen receptor (Madureira *et al*, 2006), whereas the coordination of FOXP2 and FOXP4 is essential in controlling neural stem and progenitor cell differentiation during neurogenesis (Rousso *et al*, 2012).

Fox protein binding partners are not, however, limited to other family members. Fox factors can also interact with other transcriptional regulators, such as Smad and homeodomain factors (Blount *et al*, 2009; Wijchers *et al*, 2006). Forkhead factors are also known to interact with various protein cofactors, both activators and repressors, to regulate transcription; for example, FoxM1 and FoxA factors can recruit DNA methyltransferases and HDACs to facilitate chromatin compaction (Lam *et al*, 2013). Furthermore, members of the FoxK subfamily contain a 'Forkhead-associated domain' which recognises and binds to phosphorylated threonine residues to mediate protein-protein interactions, and FoxO family members have been shown to associate with multiple nuclear receptors (Wijchers *et al*, 2006). A recent tandem-affinity purification/mass spectrometry study analysed the interactome of 37 Fox factors in human embryonic kidney cells to reveal that each Fox factor interacts with a unique

repertoire of co-regulators (Li *et al*, 2015). In addition, the identified interactors differ when the transcription factors are 'on' or 'off' chromatin, suggesting partners may alter depending on cellular localisation and that this might infer alternative functions within a single cell (Ji & Sharrocks, 2015).

Finally, PTMs are known to modulate the activity, subcellular localisation, stability, binding efficiency and specificity of Forkhead factors; this leads to the hypothesis of a PTM code of TFs (Benayoun *et al*, 2011; Huang & Tindall, 2007) and adds another regulatory level that alters target DNA and protein partner binding (Wijchers *et al*, 2006). Identified modifications include phosphorylation of serine, threonine or tyrosine residues (Greer *et al*, 2007; Tan *et al*, 2007), acetylation of lysines (Li *et al*, 2007) and ubiquitylation (van der Horst *et al*, 2006). For example, FoxO3A and FoxM1 have been shown to interact with the co-activators CBP/p300 in a manner dependent on AMP kinase-mediated phosphorylation of Ser626, or CDK1/2-mediated phosphorylation of Thr596, respectively (Major *et al*, 2004; Wang *et al*, 2009, 2012). Acetylation of FoxO proteins as also been suggested to drive a switch between DNA binding-dependent and independent functions (Heide & Smidt, 2005).

Together these factors enable Forkhead family members to function in a diverse range of biological processes, including differentiation, metabolism, apoptosis and longevity (Myatt & Lam, 2007). Often Forkhead factors are found to act as terminal effectors in key pathways, such as Insulin/IGF, TGFβ/SMAD and Wnt/β-catenin signalling, suggesting they act as central molecular nodes to integrate environmental signals (Benayoun *et al*, 2011; Blount *et al*, 2009; Wolfrum *et al*, 2003). For example, the FoxO subfamily act to maintain homeostasis through their role as signal integrators and crosstalk mediators between numerous pathways, including IGF1-PI3K-Akt signalling, JNK oxidative stress signalling and Wnt signalling (Huang & Tindall, 2007). Although FoxO factors have been

shown to be regulated by a variety of PTMs in different contexts, the most well-described is phosphorylation (Eijkelenboom & Burgering, 2013). Activation of the PI3K-AKT pathway in response to growth factors such as insulin, leads to phosphorylation of FoxO factors and nuclear export, inhibiting their transcriptional activity (Brunet *et al*, 1999).

Single Fox factors can also perform distinct functions during development and in adulthood, as illustrated by FoxA2, which controls liver and pancreas development in the embryo, whilst in adulthood it modulates insulin secretion in the pancreas and gluconeogenesis and bile production in the liver (Le Lay & Kaestner, 2010).

1.4.3 Forkhead factors act as 'multimodal' regulators of gene expression

The differences in tissue-specific expression, protein domains, protein-protein interactions and PTMs discussed above confer the Fox factors with a wide range of functions. A complex set of potential regulatory controls emerge which enable transcription to be controlled in a cell context-dependent manner (Wijchers *et al*, 2006; Lam & Gomes, 2014).

As described by Lam *et al* (2013), Forkhead factors are 'multimodal' regulators of gene expression. Activation of gene expression can occur by multiple mechanisms. Several Forkhead factors are known to bind directly to DNA Forkhead-response elements in promoters, leading to transcriptional activation by recruitment of epigenetic co-activators (Lam *et al*, 2013). Accumulating evidence also suggests that Forkhead factors may possess pioneer activity, a characteristic of many reprogramming factors (Iwafuchi-Doi & Zaret, 2014), enabling them to directly bind and alter the structure of closed chromatin at specific loci to facilitate changes in transcription rate. The most well-known example for this function is FOXA1 and FOXA2, whose pioneer activity is known to be required for oestrogen and androgen receptor binding to DNA (Carroll *et al*, 2005;

Robinson *et al*, 2011). Other Fox factors, such as FoxO1, have also been reported to bind regulatory sequences in compacted chromatin to facilitate DNA remodelling (Hatta & Cirillo, 2007). How this occurs is still unclear, however, the winged conformation of the Forkhead domain bears resemblance to the histones H1 and H5 which can also bind and displace core nucleosomal histones (Wijchers *et al*, 2006). Furthermore, Fox factors may act to recruit other pioneer factors to enable chromatin access, as is demonstrated by FoxM1 recruiting BMYB to activate G2/M genes (Down *et al*, 2012).

Similarly, transcriptional repression can be mediated by the recruitment of epigenetic co-repressors. FoxK1, for example, forms a co-repressor complex with Sin3b, a scaffolding protein that is part of a complex including HDACs and nucleosome remodelling factors (Yang *et al*, 2000). Similarly, FoxP1/2/4 proteins interact with a component of the NuRD-MeCP1 chromatin-remodelling complex, to recruit HDAC1 and HDAC2 to regulate *IL-6* expression in the lung injury response (Chokas *et al*, 2010).

Forkhead factors can be functionally antagonistic in activating and repressing the same target genes, as demonstrated by FoxO3 and FoxM1 in breast cancer cells (Karadedou *et al*, 2012). FoxO3 antagonises FoxM1's action through multiple mechanisms: FoxM1 is negative transcriptional target of FoxO3, FoxO3 acts to physically displace FoxM1 from promoters and FoxO3 recruits chromatin remodellers to limit FoxM1's access to its DNA binding sites (Lam *et al*, 2013). Studies have also shown the ability of individual Fox factors to act as activators or repressors in different contexts. In addition to acting as pioneer factors to facilitate an active chromatin landscape, FOXA1/2 have been shown to inhibit genes required for hepatic differentiation by recruiting HDACs via Groucho-related protein GRG3 (Santisteban *et al*, 2010). While the mechanisms of transcriptional regulation are still not well understood for many of the Fox factors, it is clear the family possess a range of regulatory properties influenced by numerous factors.

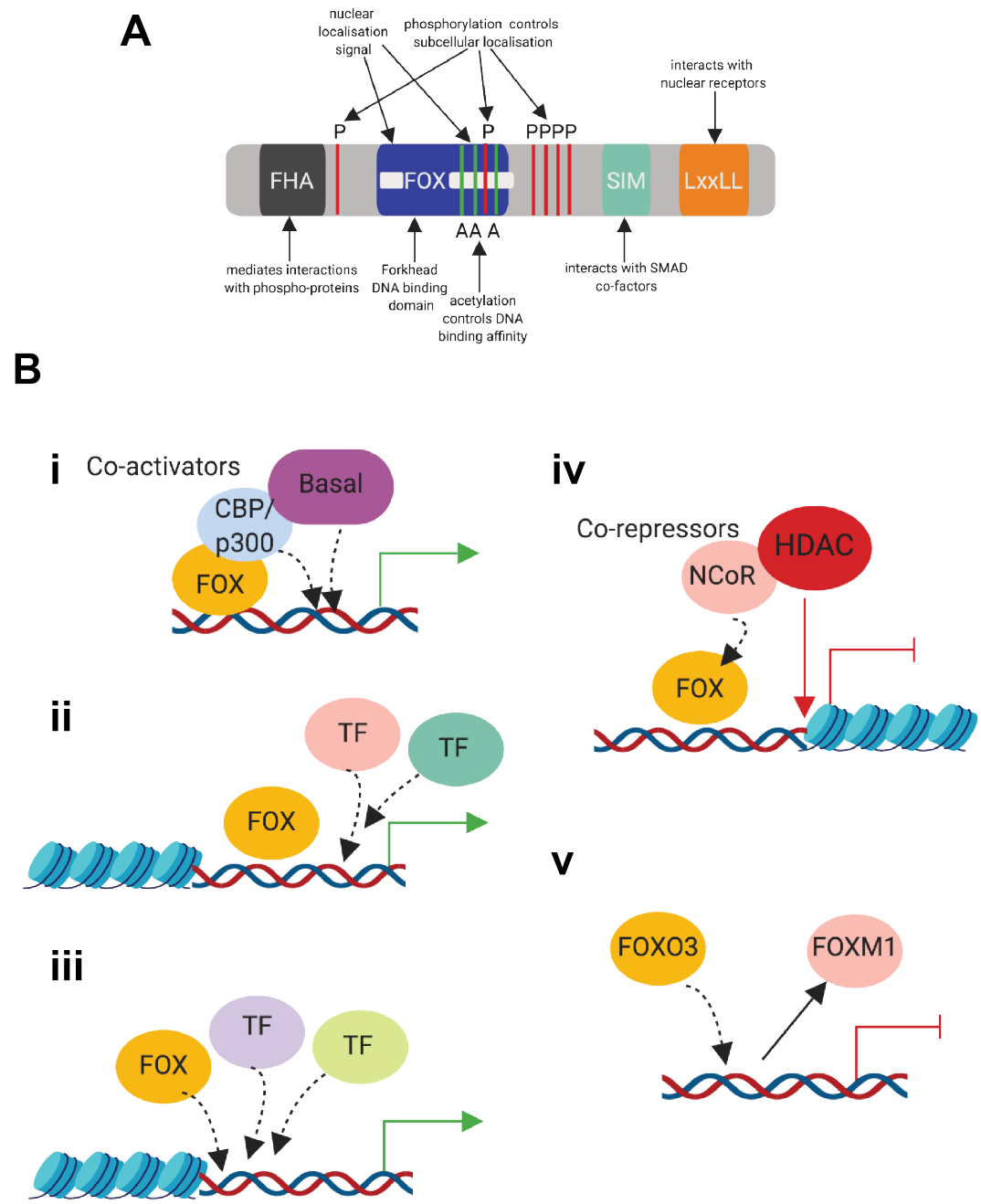

Figure 1-5 | Forkhead factors act in many ways to regulate gene expression.

(A) Schematic representing the known domains and regulatory motifs present in the Forkhead family TF protein structure. Note this represents an overview of the Forkhead family and no single factor contains all of these features. The FHA domain mediates interactions with phosphoproteins via phosphorylated threonine residues. The FOX or Forkhead domain mediates interactions with DNA at Forkhead motifs. The SIM domain mediates interactions with SMAD co-factors at promoters. The LxxLL motif (lysine-rich amino acid motif) is thought to mediate interactions with nuclear receptors. A bipartite nuclear localisation signal is shown by the white boxes in the FOX domain. The red lines labelled P indicates residues that can be phosphorylated to control nuclear export. *Figure legend continued overleaf.*

The green lines labelled A indicate lysine residues that can be acetylated to control DNA binding affinity. Figure adapted from (Wijchers *et al*, 2006). **(B)** Schematics displaying models of FOX-dependent **(i-iii)** transcriptional activation, **(iv)** repression, and **(v)** functional antagonism. **(i)** FOX factors can act to recruit co-activators such as CBP/p300, to mediate recruitment of components of the basal transcriptional machinery. **(ii)** FOX factors can act as pioneer factors, opening chromatin structure directly to facilitate the binding of other TFs. **(iii)** FOX factors can act as co-factors to recruit other TFs into a complex to mediate transcription initiation. **(iv)** FOX factors can recruit co-repressors, which in turn recruit HDACs to compact local chromatin and inhibit active gene transcription. **(v)** FOXO3 acts to functionally antagonise FOXM1 by multiple mechanisms, including direct displacement from target gene promoters. Note that this figure shows an overview of functions in the Forkhead family and no factor possesses all of these functions. Figure adapted from figures in (Lam *et al*, 2013). Figure created with BioRender.

1.4.4 Forkhead factors in cancer and as therapeutic targets

Fox factors are crucial in both development and adulthood, and so it follows that their disruption has drastic consequences on cell fate determination. Their mutation and/or deregulation has been reported in a diverse range of human diseases, including many cancers. Numerous examples exist of Fox proteins being deregulated through genetic mutation or aberrant PTMs in cancer, and their resulting abnormal functions driving tumorigenesis (Lam *et al*, 2013; Myatt & Lam, 2007). In fitting with their capacity to both activate and repress transcription, compelling evidence suggests Fox factors, such as FoxM1 and FoxO3, can act as either oncogenes or tumour suppressors in cancer (Lam & Gomes, 2014). As such, these factors present promising candidate therapeutic targets.

Although studies are being carried out to target TFs therapeutically, for example by modulating protein expression or degradation (Lambert *et al*, 2018a), they are intrinsically difficult to drug using small molecules due to their lack of small, defined ligand binding sites and the large structural changes that occur on DNA binding. Understanding co-factor recruitment and the interactions which may regulate subcellular shuttling and recruitment to transcription start sites may lead to more promising avenues to alter TF function (Yan & Higgins, 2013; Hagenbuchner & Ausserlechner, 2016). Future studies should therefore focus on understanding the mechanisms regulating Fox expression, the protein cofactors and PTMs mediating their functions, and the target genes they regulate (Golson & Kaestner, 2016). This knowledge will enable us to develop improved rationally-designed therapeutic approaches.

1.4.5 FOXG1, a multidomain neurodevelopmental transcription factor

FOXG1 is a predominantly brain-specific Forkhead family TF with important neurodevelopmental functions in cell fate specification. While three *FOXG1* sequences were previously reported, the human *QIN* gene, *HFK1* and *BF1* (Murphy *et al*, 1994; Kastury *et al*, 1994; Wiese *et al*, 1995), these were later found to all map to the same position of chromosome 14q12. FOXG1 is 489 amino acids in length, encoded by a single exon gene, and is highly conserved across mammals (Bredenkamp *et al*, 2007). In addition to the DNA-binding Forkhead domain, the FOXG1 protein has two other mapped functional domains: the Groucho/TLE-1-binding domain and the JARID1B-binding domain (De Filippis *et al*, 2011). Tertiary structure information obtained with Phyre software indicates while the Forkhead domain consists of three α-helices, three β-strands and two loops, the other domains are randomly coiled (Ariani *et al*, 2008).

Like other Forkhead factors, FOXG1 is post-translationally modified by core signalling pathways. Known PTMs include phosphorylation of the conserved residues serine 19 and threonine 271 (Thr279 in humans), whereby serine phosphorylation by casein kinase I induces nuclear import and threonine phosphorylation through FGF signalling causes nuclear export in cortical progenitors (Regad *et al*, 2007); these changes in subcellular localisation have functional consequences in controlling neuronal differentiation. In post-mitotic neurons, Akt-mediated phosphorylation of FOXG1 in response to IGF signalling controls its survival-promoting activity, however this is thought to be through another mechanism as FOXG1 remains predominantly nuclear (Dastidar *et al*, 2011). A fraction of FOXG1 has also been shown to localise to mitochondria in an energy-dependent manner in primary neuronal/glial cell lines and in the mouse cortex (Pancrazi *et al*, 2015), suggesting a role in modulating mitochondrial and metabolic functions. Thus, the subcellular localisation of FOXG1 may play an

important role in controlling cell differentiation and bioenergetics.

The FOXG1 protein was originally found to act as a transcriptional repressor, with its repressive activity mapping to amino acids 252 to 395 (Li *et al*, 1995). Indeed, this is implied by the presence of binding domains for two transcriptional co-repressors, Groucho/TLE-1 and JARID1B. For example, FOXG1 has a well-described role in inhibition of cytostatic TGF-β signalling during forebrain development (Seoane *et al*, 2004; Vezzali *et al*, 2016). Loss of FOXG1 in cortical progenitor cells or brain-tumour initiating cells results in expression changes dominated by upregulation, consistent with a transcriptional repressor function (Vezzali *et al*, 2016; Dali *et al*, 2018). In addition to direct transcriptional repression, FOXG1 acts to sequester TGF-β-activated FoxO-Smad complexes, inhibiting their transactivation of the growth inhibitory gene $p21^{Cip1}$ (Seoane *et al*, 2004). Furthermore, cytoplasmic FOXG1 has been found to inhibit TGFβ signalling through binding to Smad proteins and their partners (Rodriguez *et al*, 2001; Dou *et al*, 2000).

In addition to FOXG1's repressive function, this highlights a DNA-binding independent mode of transcriptional regulation. The first example of such a regulation by a winged-helix protein was reported by Hanashima *et al*, who used a DNA-binding defective form of FOXG1 (BF1) to show it is required for control of neural progenitor proliferation and differentiation through distinct mechanisms, independent or dependent on DNA binding (Hanashima *et al*, 2002). FOXG1 has also been shown to act as a co-repressor through its protein-protein interaction with the androgen receptor, a ligand-dependent transcriptional activator (Obendorf *et al*, 2007).

While the literature describes FOXG1 as having predominantly repressive functions, a dual activity of FOXG1, acting as a transcriptional activator and repressor in a

concentration-dependent manner, has been reported in positioning neurogenesis in the *Xenopus* ectoderm (Bourguignon *et al*, 1998). Although as yet unknown, the winged helix Forkhead domain could also confer pioneer activity to FOXG1. A recent study found 11% of differentially expressed genes were upregulated on *FOXG1* deletion in brain-tumour initiating cells (Dali *et al*, 2018). FOXG1 may therefore have an under-explored role as a transcriptional activator.

1.4.6 Protein-protein interactions of FOXG1

In addition to binding to FoxO-SMAD complexes, FOXG1 has mapped binding domains to the co-repressors Groucho/TLE-1 and JARID1B. The interaction of FOXG1 with co-repressors of the TLE family (Groucho-related proteins) is well-documented. Four full-length paralogues (TLE 1-4) and two shorter isoforms (Groucho-related proteins 5 and 6 (Grg5/6)) are known in mammals (Dali *et al*, 2018). All isoforms, except Grg5, contain a conserved WD40 domain that can recognise two conserved motifs in protein interactors, the WRPW motif or engrailed homology 1 (Eh1) domain. FOXG1 is reported to bind TLE-1 via a C terminal YWPMSPFLSLH sequence that shows similarities to the TLE WRPW motif (Buscarlet *et al*, 2008; Yao *et al*, 2000; Sonderegger & Vogt, 2003). The N terminal Eh1 motif (FSINSLV), however, has been shown to be most critical to FOXG1's physical interaction with another TLE family member, TLE-2, with the C terminal motif required for indirect functional synergism in ventral telencephalon specification (Roth *et al*, 2010). Cooperation between these binding domains may therefore be required for the functional cooperation of FOXG1 with some TLE factors (Roth *et al,* 2010).

Together FOXG1 and TLE-1 have a repressive function via this interaction which is antagonised by binding of Grg6 (Marcal *et al*, 2005). TLE proteins can act as transcriptional co-repressors in a variety of pathways including Notch, Wnt and TGFβ

signalling, through the recruitment of chromatin modifying enzymes such as HDACs. In addition, TLEs have been reported to act as adaptors between FOXG1 and Hes1, a transcriptional repressor of proneural genes activated by Notch signalling (Adesina *et al*, 2007) and an important regulator of adult NS cell quiescence (Harris & Guillemot, 2019). This enables FOXG1 to potentiate Hes1-mediated transcriptional repression (Yao *et al*, 2001).

FOXG1 was first reported to interact with JARID1B (also known as PLU-1 or KDM5B) in a yeast two-hybrid experiment (Tan *et al*, 2003). JARID1B catalyses the removal of H3K4 di- or tri-methylation, associated with active transcription, and subsequent transcriptional silencing through chromatin remodelling (Roesch *et al*, 2008). FOXG1 was reported to bind JARID1B through a novel VP motif, also conserved in PAX9. In a luciferase reporter assay in HEK cells, Tan *et al* show that the transcriptional repression activity of FOXG1 is enhanced by co-expression of PLU-1, and mutation of the VP motif in FOXG1 abolishes this co-repression. Given the presence of a VP motif in Pax9, which also binds to Groucho/TLE proteins, the authors further speculate a role for PLU-1 in competing with Groucho for binding to FOXG1 or a direct involvement in TLE-mediated transcriptional repression.

In mice and humans there are four JARID1 proteins (A-D); these all function as H3K4 demethylases with shared cofactor binding sites, however display distinct expression profiles and functional differences (Yamane *et al*, 2007; Klose *et al*, 2006). JARID1B is essential for embryonic development and known to localise at developmental target genes in ESCs to control acquisition of active histone modifications that lead to differentiation-related gene expression (Schmitz *et al*, 2011; Albert *et al*, 2013; Dey *et al*, 2008). In addition, JARID1B may act to recruit other corepressors, for example it interacts directly with HDACs in breast cancer (Barrett *et al*, 2007).

Owing to its demethylase activity, JARID1B is traditionally known as a co-repressor of transcription; however, some evidence points to a dual activity. For example, JARID1B has been reported to potentiate transcriptional activation by the androgen receptor (Xiang *et al*, 2007), act as a co-activator of retinoic acid signalling (Zhang *et al*, 2014) and in adipogenesis JARID1 family proteins act as dual modulators of gene expression (Brier *et al*, 2017). In *Drosophila*, the *Jarid1b* ortholog, Lid, acts as a co-activator of c-Myc through a conserved interaction (Secombe *et al*, 2007) and an activator of oxidative stress genes by binding and inducing deacetylation of FoxO proteins through HDACs, increasing their DNA binding affinity (Liu *et al*, 2014). Lid has also been reported to bind and inhibit HDAC1 activity, leading to higher levels of H3 acetylation and transcriptional activation (Lee *et al*, 2009). A context-dependent role of other demethylases has also been shown, such as for Jarid1A , through interaction with RB or nuclear receptors (Chan & Hong, 2001; Benevolenskaya *et al*, 2005), and LSD1, which can recruit distinct coactivators or corepressor complexes to activate or repress transcription (Wang *et al*, 2007). The generality of specific histone marks leading to transcriptional activation or repression has also become less defined, suggesting the recognition of a combination of modifications by effector proteins, rather than the modification itself, determine biological outcome (Fischer *et al*, 2008; Vakoc *et al*, 2005). Thus, JARID1B, although established as a regulator of promoter-associated H3K4 demethylation, may possess context-dependent functions.

In conclusion, while the exact mechanism of action of FOXG1 remains unclear, it is clearly a multi-faceted transcription factor with likely context-dependent roles. A TAP/MS screen in HEK cells suggests FOXG1 may also exist in different protein complexes when 'on' or 'off' chromatin, suggesting FOXG1 may also carry out varying roles within a single cell (Li *et al*, 2015).

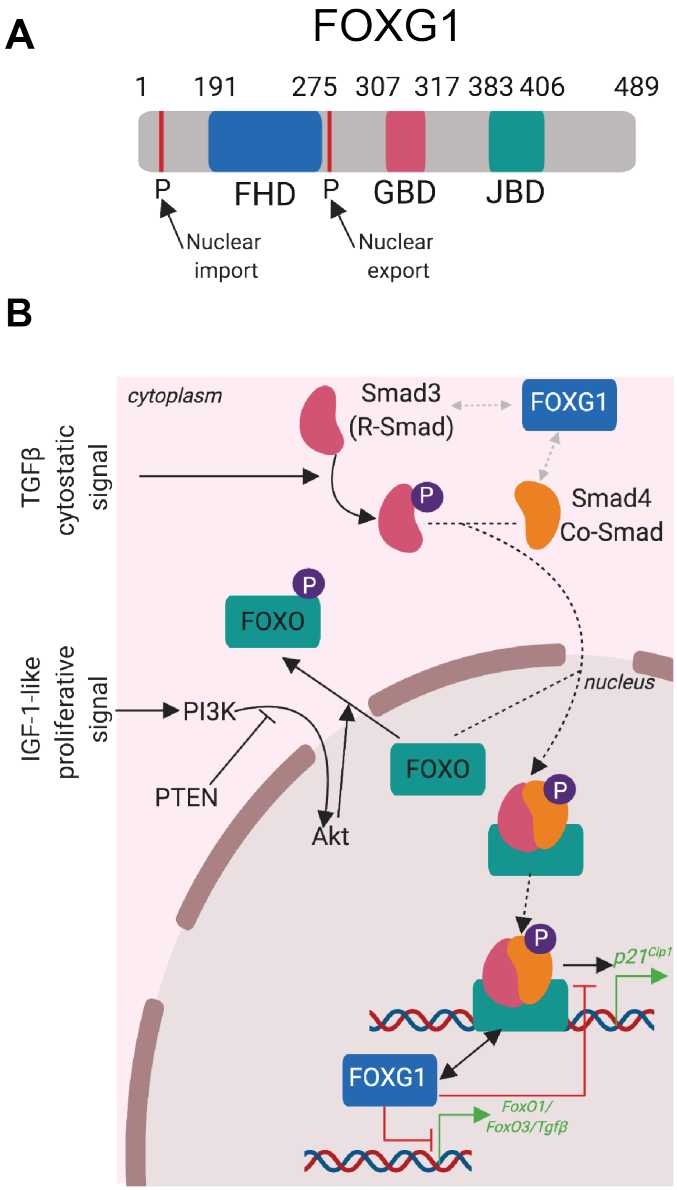

Figure 1-6 | FOXG1 is a multidomain neurodevelopmental transcription factor with DNA binding-dependent and -independent functions.

(A) Schematic representation of FOXG1 protein structure with mapped functional domains. FHD = Forkhead DNA binding domain. GDB = Groucho/TLE-1 binding domain (Sonderegger & Vogt, 2003; Yao *et al*, 2001). JDB = JARID1B binding domain (Tan *et al*, 2003). The red lines labelled P indicate phosphorylation of serine or threonine residues known to control subcellular localisation (Regad *et al*, 2007). Figure adapted from (De Filippis *et al*, 2011). **(B)** Schematic describing reported DNA binding-dependent and -independent functions of FOXG1. FoxO factors act as signal integrators to control cell proliferation through transcription of $p21^{Cip1}$. IGF-1 signalling results in Akt-mediated phosphorylation of FoxO factors and nuclear export, whereas TGFβ signalling results in FoxO-SMAD complex formation. FOXG1 acts to sequester these complexes and prevent DNA binding, thus inhibiting $p21^{cip1}$ expression and exit from cell cycle. FOXG1 has also been shown to bind to Smad proteins and their partners (grey arrows) (Dou *et al*, 2000; Rodriguez *et al*, 2001) and directly repress *FoxO1/FoxO3/Tgfβ* transcription (Vezzali *et al*, 2016). Figure adapted from (Seoane *et al*, 2004). Figure created with BioRender.

1.4.7 FOXG1 in brain development and neurodevelopmental disorders

FOXG1 plays vital roles during brain development. It is one of the earliest TFs expressed in the anterior neural plate that gives rise to the telencephalon. The telencephalon includes progenitors that give rise to the neocortex in mammals (Manuel *et al*, 2010). Deletion of *Foxg1* in mice is lethal, resulting in premature differentiation of neural progenitors in the telencephalon, and hence an excess in early-born neuron production (Xuan *et al*, 1995; Hanashima *et al*, 2004). In contrast, overexpression of *FoxG1* results in increased proliferation of neural progenitors and reduced differentiation (Bourguignon *et al*, 1998). This control over telencephalic proliferation was shown to be cell autonomous, with an underrepresentation of *Foxg1* null cells found in chimeric mouse embryos (Manuel *et al*, 2011) and likely to be mediated through FOXG1's transcriptional repression of cyclin-dependent kinase inhibitors ($p27^{XIC1}$ in *Xenopus,* homologous to mammalian $p21^{CIP1}$ and $p27^{KIP1}$) (Hardcastle & Papalopulu, 2000).

In cortical progenitor cells, FOXG1 opposes the anti-proliferative and differentiating effects of TGFβ signaling through sequestering FoxO-SMAD complexes and thereby preventing transcriptional activation of *Cdkn1a* (Seoane *et al*, 2004; Dou *et al*, 2000; Siegenthaler & Miller, 2008). More recently, Vezzali *et al* found that FOXG1 also directly inhibits the expression of *FoxO1*, *FoxO3* and *Cdkn1a* (Vezzali *et al*, 2016). In addition to proliferation and differentiation defects, disruption of *Foxg1* leads to defective dorsal-ventral patterning of the forebrain, accompanied by complete loss of ventral telencephalic cell fate markers (Martynoga *et al*, 2005); this was associated with loss of Shh in the ventral telencephalon and increased BMP4 expression in the dorsal neuroepithelium (Dou *et al*, 1999). FOXG1 was later confirmed as a central integrator of both Shh and Wnt signalling to control telencephalon regionalisation in zebrafish development (Danesin *et al*, 2009) and is shown to coordinate the production of

neuronal subtypes in the cerebral cortex through a programme of transcriptional repression (Kumamoto *et al*, 2013).

Evidence of a concentration-dependent function of FOXG1 in development is suggested by the differing effects of different dosages of *FoxG1* RNA on neural differentiation and proliferation in *Xenopus laevis* embryos. This dual activity is proposed to underlie the positioning and coordination of neuronal differentiation in the ectoderm through both suppressing and activating neurogenesis/proliferation in a dose-dependent manner (Bourguignon *et al*, 1998). Moreover, siRNA knock-down of *Foxg1*, in comparison to knockout, is able to reset the timing of neurogenesis rather than simply enhance neuron generation (Shen *et al*, 2006). TLE-1, an interactor of FOXG1, also has known roles in regulating forebrain development (Yao *et al*, 2000); together these factors act to co-repress transcription and control cortical neurogenesis (Marcal *et al*, 2005; Roth *et al*, 2010).

Later in neurogenesis, the dynamic expression of *Foxg1* continues to play an important role in post-mitotic neuron precursor cells (Cargnin *et al*, 2018; Miyoshi & Fishell, 2012), with transient downregulation occurring when progenitors begin neuronal differentiation and subsequent upregulation needed to direct their correct migration to the cortical plate. In adulthood, *FOXG1* expression persists in areas of the brain derived from the telencephalon, including the cerebral cortex, hippocampus, olfactory bulbs and the basal ganglia (Dou *et al*, 1999); here it acts as a downstream mediator of IGF-1/Akt signalling to promote survival of postnatally born post-mitotic neurons, in cooperation with TLE-1 (Dastidar *et al*, 2011, 2012; Shen *et al*, 2006).

The role of FOXG1's other previously reported protein partner, JARID1B, in forebrain development is less clear. JARID1B, is required to epigenetically repress two master

regulators, Otx2 and Pax6, in eye and neural development (Albert *et al*, 2013; Elsen *et al*, 2018). Zhou *et al* found that *Jarid1b*-depleted adult mouse SVZ NSCs showed reduced proliferation and neurosphere formation in culture, suggesting JARID1B negatively regulates neurogenesis (Zhou *et al*, 2016). However, it was also shown to be required for the neural differentiation of ESCs, but dispensable for differentiation of established NSCs (Schmitz *et al*, 2011), suggesting its critical effects are at an earlier stage of cell fate specification.

The importance of FOXG1 in development and adulthood is further highlighted by its involvement in a number of neurodevelopmental disorders. Focal malformations of cortical development leading to paediatric epilepsy are thought to be driven by an AKT-FOXG1-reelin signalling pathway (Baek *et al*, 2015). Haplosufficiency of novel *FOXG1* variants have been associated with brain malformations with altered forebrain size similar to microcephaly (Shoichet *et al*, 2005). Haplosufficiency has been suggested to lead to neurological defects through increased expression of neuropeptides (Frullanti *et al*, 2016). Increased dosages of *FOXG1* due to duplications of chromosome 14q12 are associated with developmental epilepsy and mental retardation (Brunetti-Pierri *et al*, 2011; Tohyama *et al*, 2011). *FOXG1* mutations are also responsible for FOXG1 syndrome, a severe neurodevelopmental disorder, previously known as the congenital variant of Rett Syndrome (Vegas *et al*, 2018; Ariani *et al*, 2008; De Filippis *et al*, 2011; Mencarelli *et al*, 2010). The severity of phenotypes can be correlated with the position of mutations relative to FOXG1's known functional domains. For example, Ariani *et al* identified two patients with a stop codon mutation (p.Trp255X) which impaired DNA binding and a 1 bp deletion (p.Ser323ArgfsX325) that caused misfolding of the Groucho/TLE-1-binding domain motif and loss of the JARID1B-binding domain (Ariani *et al*, 2008). In primary neurons, nuclear FOXG1 is normally localised outside of heterochromatic foci indicating

it is not stably bound to chromatin (Ariani *et al*, 2008); a p.R244C mutation has been shown to lead to abnormal localisation of FOXG1 in nuclear foci and altered *CDKN1A* expression (Guen *et al*, 2011). Furthermore, mutations have been reported to lead to altered dynamics of chromatin binding (De Filippis *et al*, 2011). Mitter *et al* recently reviewed 83 patients and found more severe phenotypes were associated with truncating mutations in the N terminal or Forkhead domain (Mitter *et al*, 2018). This provides further evidence of the importance of FOXG1's mapped domains to its function.

1.4.8 FOXG1 in cellular reprogramming

A role for FOXG1 in reprogramming of cell fate has also been recently demonstrated. Together *Foxg1, Sox2* and *Brn2* are able to direct the conversion of mouse fibroblasts or mouse astrocytes into tripotent neural precursors (Lujan *et al*, 2012; Ma *et al*, 2018). Mallamaci and colleagues also demonstrated the conversion of mouse embryonic fibroblasts to NSC-marker Sox1-eGFP-expressing cells through overexpression of *FOXG1* and *PAX6* transgenes (Raciti *et al*, 2013). Together, FOXG1's roles in brain development and cellular programming provide evidence that it is an important factor in controlling cell fate specification.

1.4.9 FOXG1 in cancer

As with many developmental genes, FOXG1 has a role in numerous types of cancer, with reports suggesting actions as both a tumour suppressor and an oncoprotein. For example, in cervical cancer miRNA-mediated downregulation of *FOXG1* is associated with increased cell proliferation and metastasis (Zeng *et al*, 2016). In breast cancer, FOXG1 acts as a tumour suppressor by compromising the formation of a coactivator complex at the promoter of AIB1, a frequently upregulated steroid receptor that potentiates activation by hormonal receptors (Li *et al*, 2013). In contrast, in ovarian

cancer overexpression of FOXG1 inhibits TGFβ cytostatic signalling through suppressing *p21^{cip1}* transcription (Chan *et al*, 2009).

Given GBMs are characterised by a cellular hierarchy similar to that of normal neural development, it follows that FOXG1 may also have important roles in establishing and/or maintaining the stem cell state of GSCs. Data from the TCGA (Brennan *et al*, 2013), accessed via the cBioPortal for Cancer Genomics (developed at the Memorial Sloan Kettering Cancer Centre) reveal FOXG1 is only mutated in 4 out of 291 patient GBM samples, with no amplifications. However, comparison of the transcriptional state of genetically-normal NS cells and GNS cells identified *FOXG1* to be the most consistently overexpressed gene in GBM across tumour subtypes (Engström *et al*, 2012), a finding later confirmed at the protein level (Bulstrode *et al*, 2017). High FOXG1 levels are associated with adverse treatment outcomes and a decrease in overall survival (Robertson *et al*, 2015; Wang *et al*, 2018; Verginelli *et al*, 2013). While the reason for these high FOXG1 levels remains unclear, they could be a result of the widespread epigenetic resetting found in GBM or as a consequence of key driver mutations. FOXG1 has been reported to be downstream of the common GBM variant EGFRvIII (Liu *et al*, 2015). Our investigations, through genetic engineering of driver mutations and deletion of EGFRvIII in mouse GBM model cell lines, are in disagreement with this finding (data not shown). Nevertheless, regardless of the cause of elevated FOXG1 levels, many studies cite an important role for its overexpression in GBM.

Work conducted by the Pollard team prior to this thesis revealed that high levels of the lineage-specific TFs FOXG1 and SOX2 are able to drive the reactivation of astrocytic dormant quiescent NSCs to a proliferative radial glia-like state (as further described in the introduction of Chapter 3). CRISPR/Cas9-mediated ablation of *FOXG1* in primary human GNS cells, in which FOXG1 levels are elevated, resulted in a failure to form

tumours following xenotransplantation into immunocompromised mice (Bulstrode *et al*, 2017). Furthermore, the *FOXG1*-null cells were found to have astrocytic morphology and expressed higher levels of the astrocyte markers, GFAP and S100β, than wild-type controls. This highlights the functional importance of elevated FOXG1 levels in maintaining the tumorigenic potential and restricting the differentiation commitment of GSCs (Bulstrode *et al*, 2017). In agreement, Verginelli *et al* found that shRNA-mediated silencing of *FOXG1* in GBM-derived tumour-initiating cells results in decreased tumour growth upon intracranial transplantation into host mice (Verginelli *et al*, 2013); these effects were phenocopied by knockdown of *TLE-1* or inhibition of the FOXG1:TLE-1 complex. A further report supports a role of FOXG1 in restricting differentiation, maintaining stem cell marker expression and enhancing proliferation of GBM cells even in the presence of TMZ (Wang *et al*, 2018). A novel role of FOXG1 in driving proliferation through inhibition of apoptosis by negative transcriptional regulation of caspases has also been recently reported (Chen *et al*, 2018a).

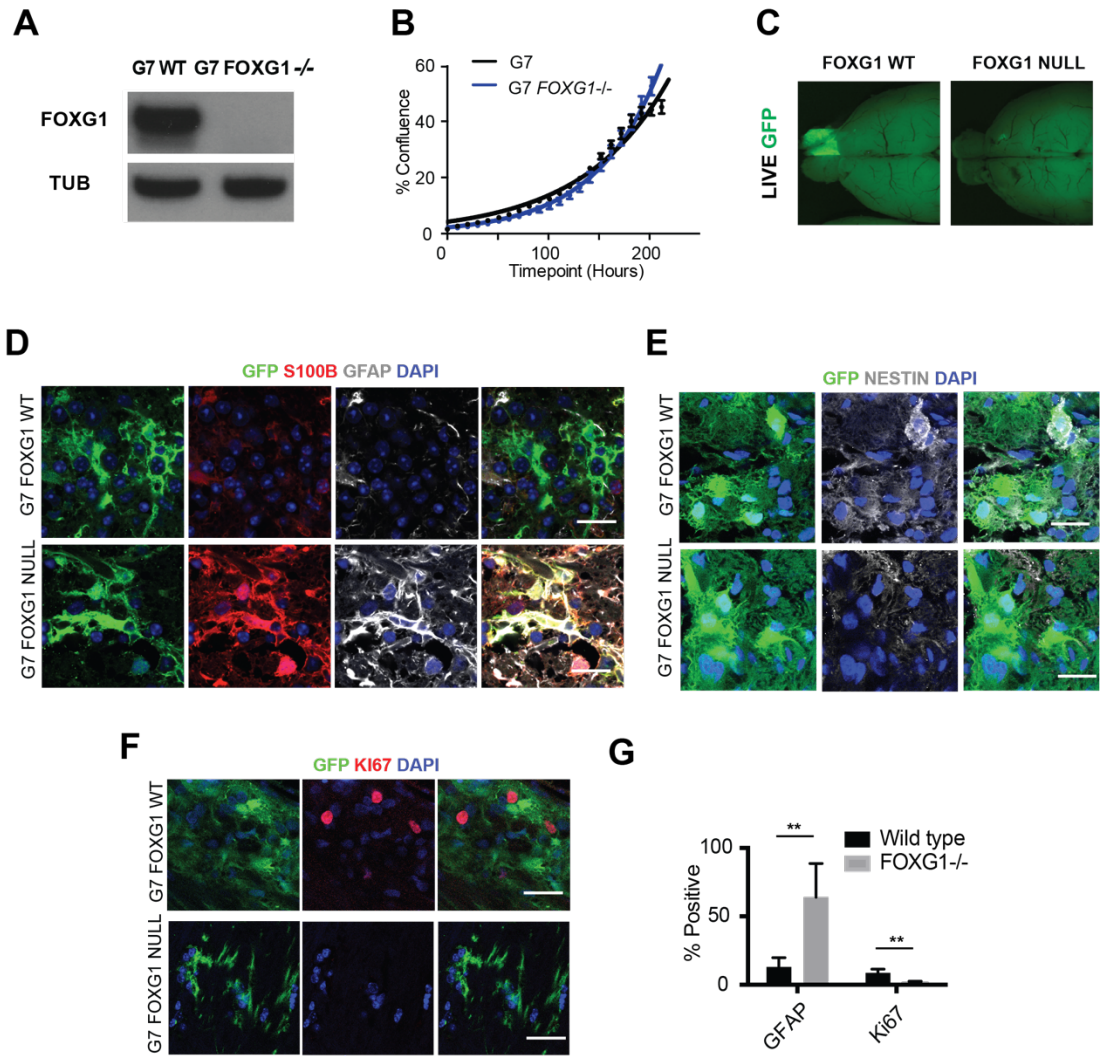

Figure 1-7 | CRISPR/Cas9-mediated ablation of *FOXG1* from human GBM cells inhibits tumour formation and increases astrocytic marker expression.

(A) Western blot confirmation of the absence of FOXG1 protein in G7 *FOXG1* null cell line. **(B)** Growth curve displaying percentage confluence over time, indicating wild-type and *FOXG1* null G7 cells display similar growth rates in EGF/FGF-2. **(C)** Upon xenotransplantation, wildtype G7 cells exhibit tumour formation, whereas *FOXG1* null cells fail to form tumours. n=4 for each cell line. Immunohistochemistry (IHC) analysis of xenografts reveals G7 *FOXG1* null cells show **(D)** higher levels of astrocyte markers, S100β and GFAP, **(E)** lower levels of the NSC marker NESTIN and **(F)** decreased Ki67 expression. **(G)** Quantification of IHC analysis, showing percentage of GFAP and Ki67 positive cells for each cell line. Scale bars: 10 μm. Students t-test, n =4; ** P < 0.005. Figure adapted from (Bulstrode *et al*, 2017).

Given FOXG1's clear role in GBM, understanding the signalling pathways through which it acts is of therapeutic interest. A role for FOXG1 in control of GBM cell proliferation in U87MG cells, via inhibition of TGFβ signalling, was first suggested by Seoane *et al.* (Seoane *et al*, 2004). Similarly, in medulloblastoma, the most common paediatric primary brain tumour, a decrease in FOXG1 levels is associated with increased survival in mice (Adesina *et al*, 2015) and high FOXG1 in tumours is reported to disrupt TGFβ signalling that normally controls neuronal differentiation (Adesina *et al*, 2007). However, more recent studies have shown that TGFβ signalling can have paradoxically oncogenic actions. The TGFβ ligand is often upregulated in malignant gliomas in which cells can selectively disable the tumour suppressor arm of TGFβ signalling, through either loss of $p15^{INK4b}$, inactivation of RB or PI3K hyperactivation. TGFβ can therefore stimulate the production of mitogens, such as platelet-derived growth factor β (PDGF-β), to drive glioma cell proliferation (Massagué, 2008; Peñuelas *et al*, 2009). There is therefore contrasting evidence for the connection of FOXG1 and TGFβ in GBM; FOXG1 may act to repress functional TGFβ signalling, or where the tumour suppressive arm is lost, cooperate with TGFβ to drive tumour growth. A recent study to uncover the transcriptional network controlled by FOXG1 and TLE-1, found the upregulation of two genes on *FOXG1* deletion, *EGR2* and *DMRTA1*, also identified as targets of FOXG1 in the developing neocortex of mice (Dali *et al*, 2018; Kumamoto *et al*, 2013). CHAC1, a pro-apoptotic factor, known to inhibit NOTCH signalling, was also upregulated, in keeping with FOXG1's role in promoting cell survival.

Thus, the functions of FOXG1 in development can provide clues as to how its dysregulated signalling acts in GBM; however, the key signalling pathways and downstream effectors through which it drives GSCs remain unclear.

1.5 *In vitro* models of glioblastoma

In recent years our ability to model GBM *in vitro* has greatly expanded owing to advancements in stem cell culture conditions and genetic engineering technologies. Here we will outline the *in vitro* models of GBM used throughout this thesis, highlighting the steps leading to their development and their advantages compared to prior modelling efforts.

1.5.1 Neural stem cells in mammalian brain development and adulthood

Given GBM is a disease of NSC-like cells, with a hierarchy recapitulating that of neural development, it follows that *in vitro* cultures of NSCs provide an invaluable system to explore 'normal' tissue stem cell counterparts (O'Duibhir *et al*, 2017). NSCs can be defined functionally as self-renewing cells with the ability to differentiate into both glial and neural cell types. Cultures can be derived from pluripotent stem cells (Zhang *et al*, 2001; Kelava & Lancaster, 2016), or as in this thesis, from primary foetal or adult brain tissue (Pollard & Conti, 2007). Distinct types of primary neural progenitor cells have been identified *in vivo* at various developmental stages; these produce specific types of neurons and glial cells, often through several divisions of fate-restricted progenitors (Kriegstein & Alvarez-Buylla, 2009). These regionally and temporally distinct neural stem/progenitor cells all share the same neuroepithelial-radial glia-astrocyte lineage (Alvarez-buylla *et al*, 2001).

During embryonic development, the earliest and most primitive form of NSCs are the neuroepithelium; these make up the neural plate in gastrulated embryos (embryonic day 7.5 (E7.5) in mice) which then forms the neural tube (E8.5) (Götz & Huttner, 2005). At the time of cortical neurogenesis (E9.5), neuroepithelium in the neural tube acquire features of glial cells and become radial glia (RG) or apical progenitors; these RG cells

maintain apico-basal polarity and undergo asymmetric division to maintain an NS cell pool and generate intermediate or transit-amplifying progenitor cells, which then generate glial and neuronal cell lineages. RG cells maintain contact with the ventricles throughout cortical development, following which they migrate to the cortical plate and transform into astrocytes. Inherently, much of our knowledge of mammalian brain development comes from studies in rodents; while many of these findings are applicable to humans, differences are expected due to variations in brain complexity. New populations of neural progenitors continue to be identified; for example, a population of outer RG cells in the expanded outer SVZ of humans are thought to lead to increased cortical complexity and size (Hansen *et al*, 2010; Johnson *et al*, 2015).

In adulthood, NSCs persist in restricted areas of the brain as type B astrocytes in the SVZ and radial astrocytes in the SGZ (Braun & Jessberger, 2014) (section 1.1.3). While a subset of RG cells remain neurogenic after birth in some species, such as songbirds, lizards and fish (Merkle & Alvarez-buylla, 2006), in mammals they disappear following birth, after giving rise to neural and glial progenitor cells and adult SVZ stem cells (Merkle *et al*, 2004). Type B cells retain epithelial properties by possessing apical and basal processes, that like the basal processes and branch contacts of RG cells, act to connect them to the brain surface and vasculature (Mirzadeh *et al*, 2008).

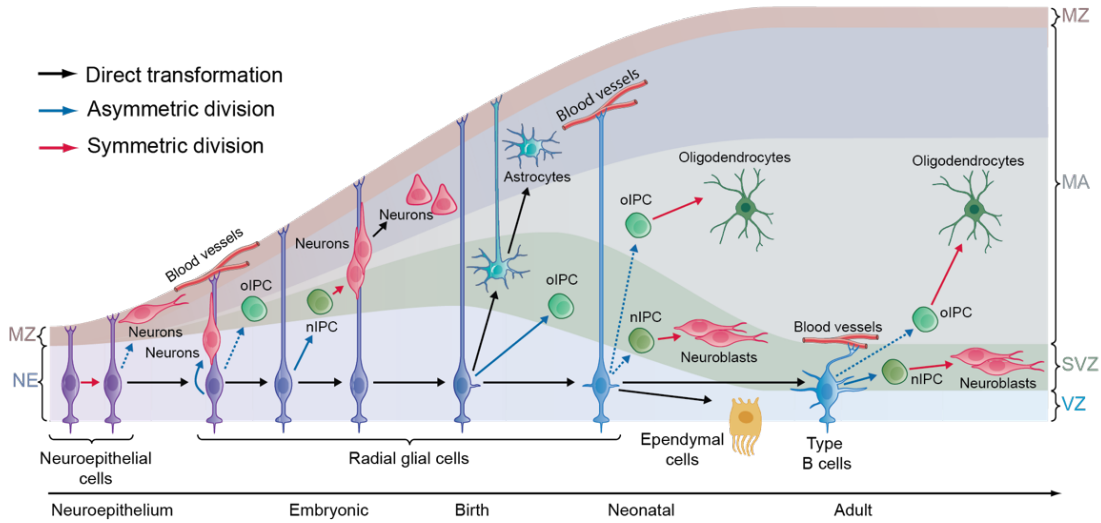

Figure 1-8 | Neural progenitor cells exist *in vivo* at various developmental stages along a continuous neuroepithelial-radial glia-astrocyte lineage.

Illustration depicting the continuous lineage of NS cells present in the developing and adult rodent brain. The earliest NS cells in development, the neuroepithelium, divide both symmetrically, to increase the progenitor pool, and asymmetrically, to generate early neurons. At the time of cortical neurogenesis, neuroepithelium in the neural tube elongate and acquire glial features to become radial glial (RG) cells. These cells have apico-basal polarity, via which they contact the ventricle surface (down) and the meninges, basal lamina and blood vessels (up). RG cells divide both symmetrically and asymmetrically to generate glial and neural cell types, such as oligodendrocytes and neurons, through intermediate progenitors (nIPCs and oIPCs). At the end of embryonic development, most RG cells migrate through the cortical plate and become astrocytes, possibly through an intermediate progenitor cell stage. A subset of RGs in the neonate continue to produce neurons and oligodendrocytes, as well as ependymal cells and type B cells. These type B cells function as SVZ NS cells into adulthood, maintaining contact with the vasculature and ventricle surface through their apico-basal polarity. They continue to produce glial and neural cells in the adult brain. Solid arrows are supported by experimental evidence; dashed arrows are hypothetical. MA, mantle; MZ, marginal zone; NE, neuroepithelium; SVZ, subventricular zone; VZ, ventricular zone. Figure adapted from (Kriegstein & Alvarez-Buylla, 2009), with permission from Annual Reviews.

1.5.2 *In vitro* culture of tissue-derived neural stem cells

The first *in vitro* culture of multipotent and clonogenic NSCs was reported in 1989 from the E13.5-E14.5 rat forebrain (Temple, 1989). Since then, isolation of NSCs from the developing and adult CNS has been intensely investigated (Kelava & Lancaster, 2016). While the earliest primitive neuroepithelial progenitors have proven evasive to capture, radial glia-like apical progenitors and adult SVZ NSCs can be cultured *in vitro* (Conti & Cattaneo, 2010). Expansion of multipotent neural progenitor cells from the adult mammalian brain (mouse foetal CNS) (Reynolds & Weiss, 1992) was first achieved as non-adherent free-floating aggregates, or neurospheres, using serum-free medium supplemented with epidermal growth factor (EGF). However, the spontaneous organisation of neurosphere cultures leads to heterogeneity and issues with reproducibility (Pollard & Conti, 2007; Pastrana *et al*, 2011). 3D organoid cultures that maintain tissue architecture have since been developed and are beneficial where experiments require accurate recapitulation of the *in vivo* niche structure. However, high-throughput studies exploring NS cell self-renewal and differentiation require culture homogeneity. 2D and 3D culture systems thus each have merits and drawbacks in terms of homogeneity and complexity (Kelava & Lancaster, 2016).

Expansion of homogeneous foetal and adult mouse NS cell cultures was achieved using the same conditions needed to expand human ESC-derived NSCs, an adherent substrate and the growth factors EGF and FGF-2 (Ying *et al*, 2003; Sun *et al*, 2008; Conti *et al*, 2005; Pollard *et al*, 2006). These adherent conditions enable the long-term expansion of homogeneous, highly pure cultures of NSCs, in which uniform access to growth factors prevents differentiation and cell death, and single cell behaviour can be easily monitored. Neurospheres can be derived from these monolayer cultures suggesting these cells are a pure population of the self-renewing fraction present in aggregate cultures (Conti *et al*,

2005). Adherent NS cell cultures, of foetal and adult derivation, display an identical RG-like phenotype, including bipolar morphology and expression of the NS progenitor/RG markers; Nestin, BLBP, GLAST, Sox2 and vimentin. Notably, adult cultures express TFs such Olig2 not seen in adult SVZ B cells *in vivo*, and do not express the type B cell markers GFAP and PDGFα. This suggests the *in vitro* culture conditions may impose a synthetic cell state driven by de-differentiation to a RG-state (Conti & Cattaneo, 2010; Pollard & Conti, 2007). It is therefore debatable whether *in vitro* adherent NSC cultures represent a direct *in vivo* NSC counterpart. Nevertheless, they share key functional properties and molecular apparatus of radial glia-like neural progenitors, namely self-renewal and differentiation potential, and can be termed RG-like NS cells.

1.5.3 Differentiation of neural stem cells *in vitro*

Adherent *in vitro* NS cell cultures provide a useful experimental system to explore the factors governing stem cell self-renewal and differentiation. Potent differentiation of rodent NSCs can be achieved using serum (Obayashi *et al*, 2009; Brunet *et al*, 2004), a component of which is bone-morphogenetic protein 4 (BMP4), known to play critical roles in NS cell fate and maturation during CNS development (Bond *et al*, 2012). Given issues with reproducibility and batch variations in serum, BMP4 is therefore a useful driver of mature astrocyte differentiation commitment (Bonaguidi *et al*, 2005). BMPs are signalling ligands belonging to the TGFβ superfamily; their tetramerisation and binding to BMP receptors leads to phosphorylation of R-SMADs, which associate with Co-SMADs and translocate to the nucleus to alter gene expression (Kretzschmar & Massague, 1998). In addition to promoting astrocytic maturation, SMAD signalling inhibits oligodendroglial lineage commitment through upregulation of Id2/4 proteins, which subsequently indirectly or directly sequester OLIG and E2A factors (Samanta & Kessler, 2004). Glial fibrillary acidic protein (Gfap) was the first, and is still the most widely used,

marker of mature astrocyte specification. However, evidence of Gfap-positive type B SVZ NSCs, Gfap-negative protoplasmic astrocytes and increasing knowledge of astrogliogenesis led to the identification of other markers, including S100β and Aqp4 (Molofsky *et al*, 2012; Bignami *et al*, 1972; Walz & Lang, 1998; Nielsen *et al*, 1997) . Currently we therefore rely on using a combination of astrocytic markers to denote a mature astrocytic state. Furthermore, quiescent NSCs, reminiscent of type B SVZ astrocytes, have been shown to be driven by the interaction between BMP4 and FGF signalling (Martynoga *et al*, 2013; Sun *et al*, 2011). These cells upregulate astrocyte markers however retain the ability to re-enter cell cycle upon re-exposure to growth factors. This state was also shown to be achieved in our lab using BMP4 at high plating densities (Bulstrode, 2015). Although being actively explored, definitive markers of these quiescent cells are currently lacking; therefore, they can be functionally distinguished from mature astrocytes by their ability to re-establish proliferation.

In vitro cell cultures of adult and foetal mouse NSCs and human foetal NSCs are now readily available. GBM is therefore one of the few cancers known to be organised in a hierarchical manner, in which the normal tissue stem cell counterparts can be cultured (O'Duibhir *et al*, 2017); however, access to adult human NSCs is more difficult. These cultures enable investigations into the normal mechanisms controlling human NSC self-renewal and differentiation, and the effects of individual gene aberrations on this process.

1.5.4 Human patient-derived GNS cells

Efforts to isolate and expand the GBM stem cell fraction driving brain tumours were initially achieved using neurosphere/suspension culture conditions developed for normal NSCs (serum-free media with EGF and FGF-2) (Galli *et al*, 2004; Singh *et al*, 2003). These cultures provide more disease-relevant models than previously established serum-cultured glioma cell lines and were shown to recapitulate parental tumour biology (Lee *et al*, 2006). However, the application of adherent culture conditions to primary GBM tumour samples enabled the derivation of a more homogeneous stem cell-like fraction with improved efficiency (Pollard *et al*, 2009). Following direct plating of glioma tissue samples and 2-3 passages, homogenous cultures sharing many properties of normal NSCs were derived. Hence these cultures were termed glioblastoma neural stem (GNS) cells. Unlike suspension cultures, these culture conditions enabled derivation of GNS cell lines from all tumour samples tested, that retained their tumorigenic potential following long-term expansion. While 3D 'tumourspheres' can better recapitulate features such as tumour hypoxia and invasion, 2D adherent models provide a uniform culture required to assess the behaviour and biochemistry of GSCs and undertake high-content phenotypic screening experiments (Heinrich *et al*, 2019; Linkous *et al*, 2019; O'Duibhir *et al*, 2017).

Using these improved culture conditions, efforts have increased to generate new patient-derived cell models of GBM (Xie *et al*, 2015). Recently the Cancer Research UK (CRUK)-funded Glioma Cellular Genetics Resource (GCGR) was established (www.gcgr.org.uk). The GCGR is led by the Pollard lab at the University of Edinburgh and is a collaboration with the CRUK University College London centre. This resource is generating a comprehensive collection of patient-derived GNS cell lines, alongside control human NS cell lines, each matched with tumour tissue samples that will be open to the research

community. Deep annotation of these cell lines and their associated tumour tissue, at the epigenomic, transcriptomic and genomic level, ensures that GNS cell lines are representative of the parental tumour, the importance of which has been highlighted by recent studies (Allen *et al*, 2016).

The GCGR therefore provides a set of well-annotated preclinical patient-derived models of GBM at early passages in culture, with matched tissue controls and traceable origins. This resource continues to be established and the tumour-initiating potential of these cell lines is being assessed. GNS cell lines made available through the GCGR provide a useful *in vitro* model of human GBM and are used in Chapters 4 and 5 of this thesis.

1.5.5 Genome engineering of mouse and human NS cells

In recent years, CRISPR/Cas9 technology has revolutionised our ability to genetically modify the genome of mammalian cells, in a much quicker and more reliable manner than previously. This technique adds an invaluable tool to our repertoire of genetic modification methods, expanding our ability to functionally annotate the human genome using targeted genetics; this will be useful for exploring the biology of GBM.

In addition to providing a tractable model to explore mechanisms controlling stem cell self-renewal and differentiation, *in vitro* cultured NSCs are genetically tractable allowing the effects of glioma-initiating genetic alterations on their biochemistry and behaviour to be investigated (Bressan *et al*, 2017). Normal mouse NSCs often provide a useful experimental system prior to pre-clinical validation in human cultures, due to their shorter doubling time and high conservation of many GBM-associated genes such as FOX factors. Novel GBM mouse model cell lines can now be produced with relative ease, especially when compared to the time-consuming and costly process of mouse breeding. For example, mouse NSCs can be transformed into GBM-initiating cell lines, with deletion

or overexpression of various tumour suppressors or oncogenes, using CRISPR/Cas9 technology and PiggyBac-mediated overexpression, respectively (E. Gangoso, manuscript in preparation). This allows the step-wise addition of driver mutations and analysis of the effects on downstream signalling pathways, in comparison to isogenic controls. The resulting cell lines also provide a tractable model to study the biology of GSCs due to their faster growth rate compared to patient-derived GNS cells. In addition to gene deletion, CRISPR/Cas9 can also be used to engineer numerous other sophisticated gene modifications, including somatic point mutations, specific insertions and deletions, modification of cis-regulatory elements and knock-in of gene reporters, to name a few (O'Duibhir *et al*, 2017).

CRISPR/Cas9 can also be used to engineer these modifications in normal human NS and GNS cell lines (Dewari *et al*, 2018), aiding investigations of endogenous protein function in patient-derived cells. CRISPR/Cas9 has also enabled genome-wide forward genetic screens to be performed, to identify core regulators of GSC fitness, as well as sensitivity to the chemotherapeutic TMZ (MacLeod *et al*, 2019). While we focus on direct genome editing in this thesis, the repurposing of Cas9 enzymes has extended CRISPR/Cas9 technologies to areas of gene regulation, epigenomic engineering and chromatin topology manipulation, highlighting the versatility of this technology and its transformative role in understanding gene function (Adli, 2018). In Chapters 4 and 5 we highlight the use of CRISPR/Cas9 technology to aid our investigations into FOXG1's mechanism in GSCs.

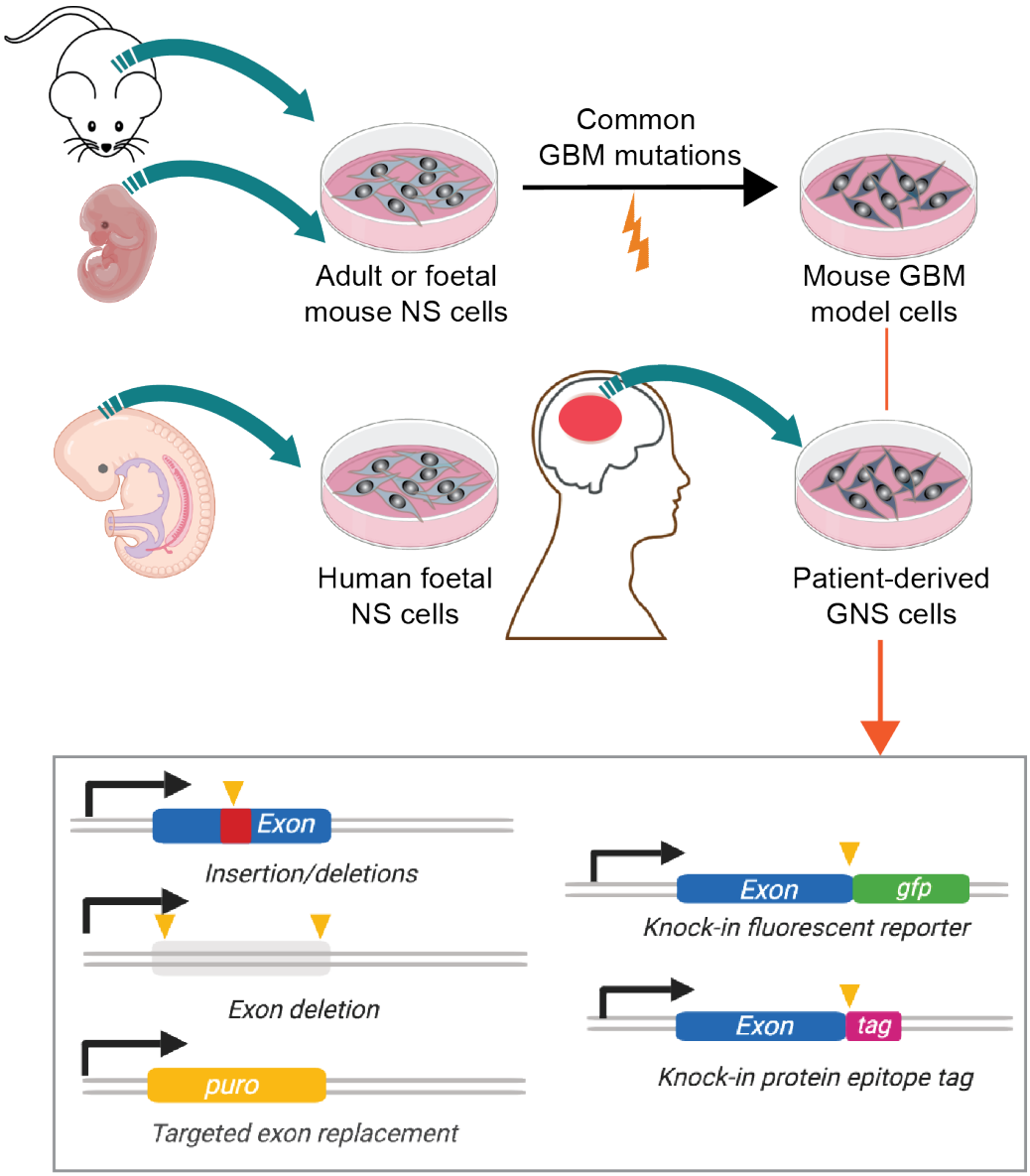

Figure 1-9 | GBM can be modelled *in vitro* using NS cell cultures and CRISPR/Cas9 genetic engineering.

Normal NSCs can be derived from adult or foetal mouse SVZ and human foetal SVZ. These can be cultured *in vitro* as an adherent monolayer in the presence of EGF/FGF-2 and laminin. Common GBM driver mutations can be genetically engineered into normal NSCs to generate model GSCs. GNS cells can be cultured directly from a patient's tumour under the same conditions (NS cell media with EGF/FGF-2). These normal and dysregulated NS and GNS cell lines are amenable to CRISPR/Cas9-mediated genetic engineering. This enables modifications to be introduced such as base insertions/deletions, whole exon deletions, whole exon targeting and replacement by reporter cassettes, and knock-in of fluorescent protein reporters or epitope tags.

1.6 Major aims and hypotheses

Evidence points to an important functional role of FOXG1 in driving the NS cell-like state of GSCs. The elevated FOXG1 levels found in GSCs may have multiple roles in influencing the GSC state. For example, high FOXG1 levels may be involved in the *de novo* initiation of NS-like cells, the reactivation of cells that have exited cell cycle and, most important therapeutically, the maintenance of the established proliferative GSC state by restricting differentiation commitment. We therefore hypothesise that FOXG1 is a key therapeutic target in GBM.

However, the activity of TFs such as FOXG1 is traditionally difficult to target using small molecule inhibitors. In order to realise its therapeutic potential, we must first better understand FOXG1's mode of action, and its downstream signalling pathways. The aims of this thesis are therefore two-fold: i) To further define the key transcriptional targets of FOXG1, and ii) Identify the key protein partners required for FOXG1's function in GBM.

Through these aims, our goal is to both improve our understanding of the fundamental mechanisms by which FOXG1 acts and uncover novel drug targets of potential therapeutic value.

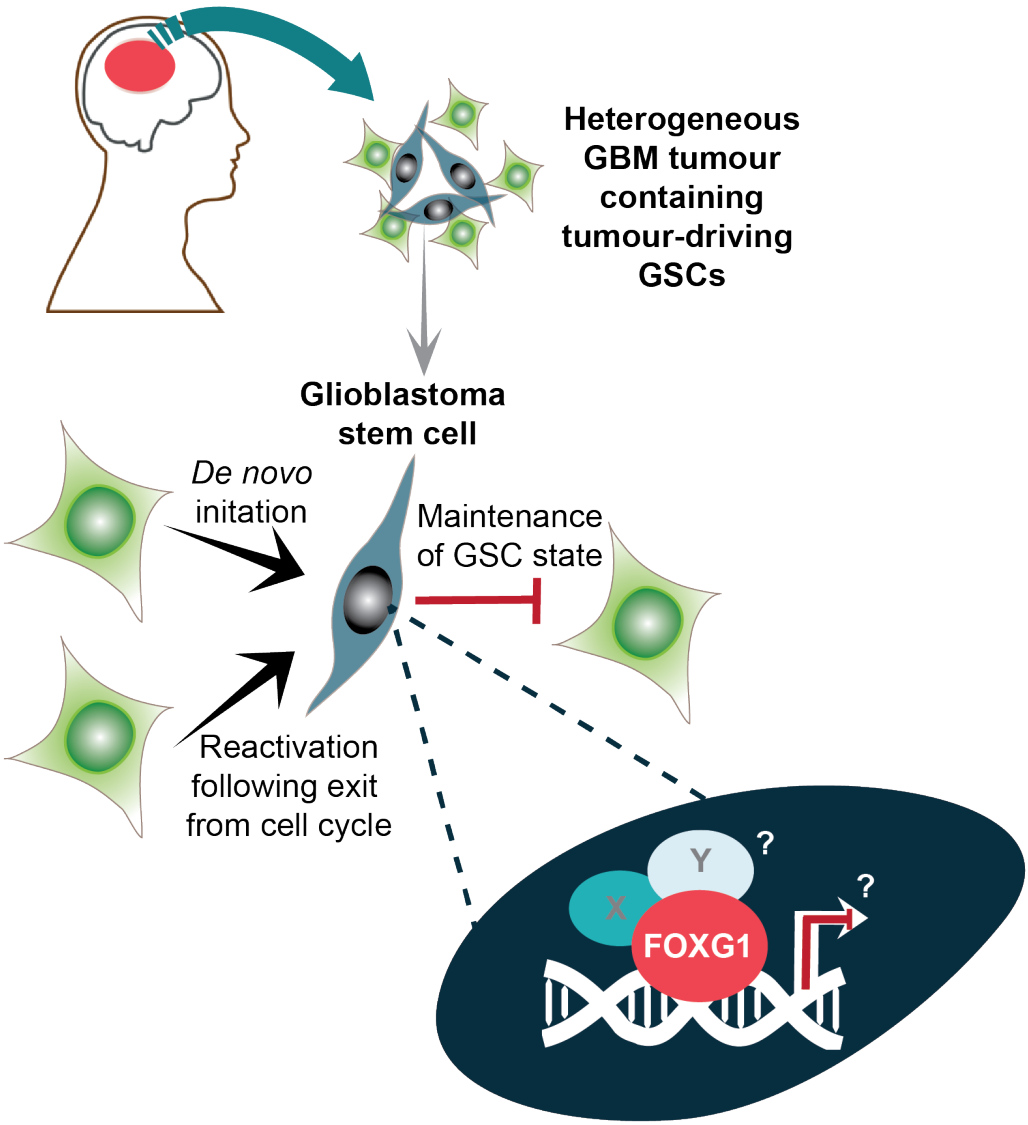

Figure 1-10 | The mechanism of FOXG1 is a key therapeutic target in GSCs.

We hypothesise that elevated FOXG1 levels found in tumour-derived GSCs may have multiple roles in maintaining and/or initiating the NS cell-like state of these cells. High FOXG1 levels may be involved in the *de novo* initiation of NS-like cells, the reactivation of cells that have exited cell cycle or maintenance of the GSC state by restricting differentiation commitment. To target FOXG1 we need to understand the protein-protein interactions and downstream transcriptional targets important for its function in GBM.

CHAPTER 2 Materials and Methods

2.1 Cell culture

2.1.1 Cell line maintenance

All cells, mouse and human, were cultured in an adherent monolayer on uncoated tissue culture plastics and incubated at 37°C with 5% CO_2. Media was exchanged every 3-4 days. Cells were dissociated once 70-80% confluency was reached using Accutase solution (Sigma). The frequency of passaging varied between cell lines. Mouse NS cell lines were passaged approximately 1:6 every 3-4 days. Human GNS cell lines were passaged approximately 1:4 every 5-7 days. Cells were grown under serum-free conditions in 'complete' NS cell media. This media consists of DMEM/HAMS-F12 (Sigma D8437) supplemented with N2 and B27 (Life Technologies/Gibco), penicillin-streptomycin (Gibco), BSA (Gibco), β-mercaptoethanol (Gibco), MEM NEAA (Gibco), 1 µg/ml Laminin (Sigma or Cultrex), 10 ng/ml mouse EGF and 10 ng/ml human FGF-2 (Peprotech). During passaging, cells were collected in wash media, consisting of DMEM/HAMS-F12 supplemented with Pen-Strep and BSA only. For cryo-preservation, cells were frozen at -80°C following resuspension of a cell pellet of approximately ½ million cells in DMEM-F12 wash media supplemented with 10% dimethylsulfoxide (DMSO), or by adding this freezing mixture directly to the cell culture plate. To reseed frozen cells, vials were quickly thawed at 37°C in a water bath and resuspended in 10 ml wash media, before pelleting and resuspension in NS cell media. Once cells had adhered to the plastic, NS cell media was changed to ensure removal of residual DMSO traces and dead cells. Prior to cell seeding, cells were counted using a haemocytometer.

2.1.2 Differentiation

In Figure 3-6, astroglial differentiation was induced by plating 1 x 10^4 cells in each well of a 24-well plate in NS cell media in the absence of EGF/FGF-2 and supplemented with BMP4 (10 ng/ml, Peprotech). Cells were fixed after 4 days. Neuronal differentiation was induced by plating 5 x 10^4 cells in each well of a 24-well plate in NS cell media in the absence of EGF, but supplemented with FGF-2 (10 ng/ml) (i.e. EGF withdrawal). After 24h, the media was exchanged fully with NS cell media supplemented with FGF-2 (5 ng/ml) and 1xB27 supplement. After 4-5 days, media was exchanged to NS cell media mixed with Neurobasal media (1:1) and supplemented with 0.5 x B27, but no growth factors. Cells with neuronal morphology were observed over the next 3-7 days, with half of the media replaced every 3-4 days. This protocol is described in (Pollard, 2013).

For all other figures, astroglial differentiation was induced by plating cells at a density of 10 cells/mm^2 in NS cell media in the absence of EGF/FGF-2 and supplemented with BMP4 (10 ng/ml, Peprotech). Cells were treated for 1 day or 3 days as indicated.

2.2 Design of reagents for genetically engineering cell lines

2.2.1 PiggyBac expression vectors for stable transgene integration

The Doxycycline-inducible *FOXG1*-V5 expression plasmid (SMP library ID: sp171) was previously constructed using Gateway cloning and verified using restriction digestion and Sanger sequencing by Dr Harry Bulstrode.

2.2.2 Guide RNA design for CRISPR/Cas9-mediated gene knock-out

CRISPR guide RNAs (gRNAs) were designed using the Optimised MIT CRISPR Design tool (http://crispr.mit.edu). gRNAs were selected based on their specificity to unique

genomic sites; this was determined based on a score, inverse to the likelihood of off-target binding. Off-target cleavage was deemed unlikely if similar genomic sequences contain mismatches of three or more nucleotides, with at least one in the PAM proximal region. Custom synthetic crRNAs, tracrRNAs and ssODNs were obtained from Integrated DNA Technologies (IDT). All designed gRNA and ssODN sequences used in this thesis are listed in Appendices I and II.

Deletion of *Foxg1* from IENS-GFP cells in Chapter 4 was achieved using plasmid-based gRNA delivery. gRNAs were previously designed to target the 5' and 3' ends of the *Foxg1* coding exon, by Dr Raul Bressan and Dr Maria Kalantsaki, respectively. Plasmid construction (sp322 and sp199) was previously performed by Dr Raul Bressan and Dr Maria Kalantsaki. Single-stranded oligonucleotides (ssODN) containing a 20 nt guide sequence and 4bp overhangs were annealed, phosphorylated and ligated into the BsaI site of a U6-sgRNA backbone plasmid containing the gRNA scaffold sequence (previously provided by S. Gerety, Sanger Institute, Cambridge, UK). A CAG promoter driven wild-type Cas9-2A-mCherry plasmid was previously obtained from the Chambers lab (sp404).

Genetic disruption of *FOXG1* from the human GNS cell line G313 was achieved using delivery of a pre-assembled Cas9 ribonucleoprotein (RNP) complex, made up of Cas9, crRNA and tracrRNA. The gRNA sequence was designed as above by Dr Raul Bardini Bressan, to target the 5' end of the *FOXG1* coding exon, as indel formation at the 5' end is most likely to disrupt synthesis of the full-length protein. The 36-mer crRNA contains this gene-specific 20-nt target sequence followed by a 16-nt sequence that base-pairs with the tracrRNA. The 67-nt tracrRNA contains the gRNA-scaffold region and 16-nt sequence complementary to the crRNA. The backbone and ends of both synthetic RNAs had been chemically modified by IDT to make them resistant to nuclease digestion, limit cellular immune responses and increase stability (Rahdar *et al*, 2015;

Kelley *et al*, 2016). Lyophilised crRNA and tracrRNA pellets were resuspended in Duplex buffer (IDT) to achieve a 100μM (100 pmol/μl) concentration and stored in aliquots at -80°C. Recombinant Cas9 protein was produced in-house by Dr Carla Blin (Pollard lab), as described in (Dewari *et al*, 2018).

2.2.3 Guide RNA and donor DNA design for CRISPR/Cas9-mediated gene tagging

For epitope-tagging of endogenous genes (*FoxO6, Foxg1* and *FOXG1*), gRNAs were designed to target the 3' end of the last coding exon (the second exon of *FoxO6* and only coding exon of *Foxg1/FOXG1*). gRNAs were chosen to cut 10-20 bp downstream of the stop codon in the 3' UTR to avoid disruption of the coding sequence. crRNAs and tracrRNAs were prepared and stored as above. For HA-tagging of *FoxO6* and V5-tagging of *Foxg1*/*FOXG1*, ~ 200bp ssODN donor DNAs were designed. ssODN sequences consisted of 77-bp 5' and 3' homology arms flanking the tag (tag inserted upstream of the stop codon). The PAM site was mutated from NGG to NGC/A/T to prevent cleavage of the repair template by Cas9. Ideally the PAM-strand (same strand as the chosen gRNA) was used for donor DNA synthesis, to prevent gRNA and ssODN annealing (Gasiunas *et al*, 2012; Dewari *et al*, 2018). ssODN donor DNAs were supplied as lyophilised pellets without modifications and resuspended in Duplex buffer (IDT) to achieve a 30 mM concentration. For 3xFLAG-HA-p2A-eGFP *FOXG1*-tagging, a gene fragment was designed containing the 3xFLAG-HA-p2A-eGFP tag (with the FLAG and HA tags preceded by a GS linker and the p2A peptide preceded by a GSG linker), flanked by 500 bp homology arms. These homology arms were longer, to account for lower HDR efficiencies with larger tag insertions and a dsDNA donor template. The gene fragment was ordered from GeneArt Gene Synthesis (Thermo Scientific), and supplied following sequence verification and cloning into a pMX series vector with kanamycin resistance. PCR amplification and

product purification was performed to obtain a high concentration of linear dsDNA donor template (primers in Appendix VI). SYBR Safe was used to visualise the PCR product. PCR product purification was performed using NucleoSpin™ Gel and PCR Clean-up Kit (Macherey-Nagel™), and eluted in 20-30 µl of elution buffer to achieve a concentration of approximately 200 ng/µl. Prior to transfection, formation of linear single-stranded DNA was promoted by incubating 300 ng of dsDNA donor template at 95°C for 5 min in 33% DMSO, followed by immediate cooling on ice.

2.3 Derivation of genetically engineered cell lines

2.3.1 Stable transgene integration using the PiggyBac system

This protocol was used to derive bulk populations of mouse NSCs with Dox-inducible overexpression of a V5-tagged *FOXG1* human transgene, as described in Chapters 4 and 5. Cells were transfected using the Amaxa 4D nucleofection system (Lonza) in 16-well cuvette strips, using the DN100 programme (pulsed once). 4×10^5 cells were transfected in 20 µl SG cell line transfection buffer with a total of 800 ng DNA, consisting of the CMV-PiggyBac transposase vector (PBase) (sp59), pCAG-Tet3G vector (sp169) (encoding the Tet-On 3G transactivator protein, rtTA) and the TetOn *FOXG1*_V5 expression vector (sp171) in a 2:1:1 ratio. Following recovery, cells were transferred from a 6 well plate to a T25 flask. Dox was added to the media (1000 ng/ml) for 24 h. Selection for integration of the *FOXG1*_V5 expression cassette was then commenced by supplementing NS cell media with Dox (1000 ng/ml) and blasticidin (5 µg/ml). All mock-transfected control cells died within seven days of selection. The surviving transfected population were then expanded in NS cell media and Dox-inducible FOXG1-V5 expression was confirmed by ICC and qRT-PCR. Due to difficulties with transgene silencing, cells were reselected for

stable transgene expression between independent experiments. The resulting populations were expanded for 3-4 days in NS cell media prior to functional assays, during which time existing FOXG1-V5 protein was degraded.

2.3.2 CRISPR/Cas9-mediated gene knockout

For deletion of *Foxg1* in mouse IENS-GFP, cells were transfected using the Amaxa 4D nucleofection system (Lonza) using 100 μl cuvettes and the DN100 programme (pulsed once). 1.5 million cells were transfected in 100 μl SG cell line transfection buffer with a total of 4 μg DNA, consisting of 2 μg sp404 (wild-type Cas9-2A-mCherry vector) and 1 μg of each sgRNA plasmid (sp322 and sp199). Transfected cells were plated in a 10 cm dish in NS cell media. Three days post-transfection, the Cas9-mCherry-expressing cells were isolated by fluorescence-activated cell sorting (FACS). Loss of FOXG1 was confirmed and the transfection efficiency estimated in the bulk sorted population by immunocytochemistry (ICC). For derivation of clonal cell lines, 300 cells were plated per 10 cm dish. After 10-15 days, discrete colonies were picked, expanded, and screened for successful disruption of *Foxg1* by PCR genotyping and ICC. Loss of FOXG1 protein expression was further validated by Western blotting.

For deletion of *FOXG1* in the human GNS cell line G313, cells were transfected using the Amaxa 4D nucleofection system (Lonza) in 16-well cuvette strips, using the EN138 programme (pulsed once). The Cas9 RNP complex was prepared immediately prior to transfection. 100 pmol of crRNA and tracrRNA were annealed using a gradual step-down cooling PCR programme (5 min at 95˚C, step cool-down from 95˚C to 25˚C at a ramp rate of 0.1˚C/s, then 25 ˚C-4˚C at a ramp rate of 0.5˚C/s). 10 μg of rCas9 protein was incubated with the annealed cr/tracrRNAs at room temperature for 10 min, then stored on ice.

2 x 10^5 cells were mixed with the Cas9 RNP mix and transfected in 20 µl SG cell line transfection buffer. Transfection was performed by a Masters student, Shruthi VijayKumar. Following recovery, loss of FOXG1 protein was assessed by ICC. For derivation of clonal cell lines, 400-500 cells were plated per well of a 6 well plate (performed by an undergraduate project student, Kanyarat Benjasupawan). After 5-7 weeks, discrete colonies were picked, expanded, and screened for successful disruption of *FOXG1* by ICC. Loss of FOXG1 protein expression was validated by Western blotting.

2.3.3 CRISPR/Cas9-mediated gene tagging

For HA tagging of *FoxO6* and V5 tagging of *Foxg1/FOXG1,* transfections were performed as above for G313 using 1-2 x 10^5 cells, but with the addition of 30 pmol ssODN donor template DNA to the Cas9 RNP complex prior to transfection. Amaxa 4D programmes EN138 (pulsed once) and DN100 (pulsed twice) were used for human and mouse cells, respectively. Clonal *Foxg1/FOXG1* V5-tagged cell lines were derived by FACS isolation of single cells into 96 well plates. After approximately two weeks (mouse) or four weeks (human), colonies were picked, expanded, and screened for successful V5 tag integration by PCR genotyping and ICC. For 3xFLAG-HA-p2A-eGFP tagging of *FOXG1*, 300 ng denatured dsDNA was included per transfection and the Amaxa 4D programme DN100 used. Transfected cells were expanded into T150 flasks and eGFP positive cells were isolated by FACS. Once recovered, the sorted cells were assessed for successful tag integration by PCR genotyping and ICC.

All cell lines and plasmids used in this thesis are detailed in Appendices III and IV.

2.4 DNA-based analyses

2.4.1 PCR-based genotyping of genetically engineered cell lines

Genomic DNA (gDNA) isolation from bulk transfected cells and clonal cell lines was performed using the DNeasy Blood and Tissue kit (Qiagen), according to the manufacturer's protocol. DNA concentrations were quantified using a NanoDrop™ spectrophotometer. All primers were designed using Primer3 software (http://primer3.ut.ee) and are listed in Appendix VI. To identify NHEJ-based indel formation, the region flanking the gRNA target site was amplified using gene-specific primers. In the case of *Foxg1* deletion from IENS-GFP, primers were designed flanking the 5' and 3' gRNA targeting sites. For validation of V5 tag knock-in, primers were designed flanking the tag, outside of the 77-bp 5' and 3' homology arms. For validation of HA tag knock-in at the bulk population level, one primer was designed outside of the 5' homology arm in a gene-specific region, with the other designed within the HA tag itself. For 3xFLAG-HA-p2A-eGFP tag knock-in, large 500 bp homology arms and the GC-rich nature of *FOXG1* made genotyping with both primers outside of the homology arms difficult. PCR genotyping was therefore performed with one primer outside of the 3' homology arm in a gene-specific region, and the other within the eGFP sequence. PCR products were analysed using 1-2.5% agarose gels with EtBr and GeneRuler™ 1kB plus DNA ladder (Thermo Scientific). Gels were imaged on a UV gel reader or Bio-Rad ChemiDoc™ Imager.

2.4.2 Reduced-representation bisulfite sequencing (RRBS)

RRBS was performed as described in (Bulstrode *et al*, 2017). Library preparation and sequencing were performed at the Edinburgh Clinical Research Facility. Analysis was

performed by Dr Duncan Sproul. gDNA was isolated from F6 cells (clonal ANS4 cells with Dox-inducible FOXG1-V5 expression) using the MasterPure™ Complete DNA purification kit (Epicentre) from three independent experiments and concentrated with the DNA Clean and Concentrator kit (Zymo Research) before being quantified using a Qubit® dsDNA broad-range assay kit (Thermo Scientific) and NanoDrop™ spectrophotometer. 85 ng of each purified gDNA sample was processed using the Ovation RRBS Methyl-Seq system kit (NuGEN Technologies). Unmethylated phage λ DNA (0.5 ng) was spiked into each sample to allow assessment of bisulfite conversion efficiency. Briefly, the methylation-insensitive restriction enzyme MspI was used to digest the gDNA, and digested fragments were ligated to adapters. Adapter-ligated fragments were then repaired before bisulfite conversion with the EZ DNA Methylation-Lightning kit (Zymo Research). Bisulfite-treated adapter-ligated fragments were amplified by 15 cycles of PCR and purified using Agencourt RNA Clean XP beads. Libraries were quantified using the Qubit dsDNA high-sensitivity assay (Thermo Scientific) and assessed for size and quality using the Agilent Bioanalyzer DNA high-sensitivity kit. Sequencing was performed using the NextSeq 500/550 high-output version 2 kit (150 cycles; Illumina) on the NextSeq 550 platform. Libraries were combined into equimolar pools and run across four flow cells.

2.5 Protein-based analyses

2.5.1 Immunocytochemistry

Cells were washed with PBS once before fixation using 4% paraformaldehyde (PFA) for 10 min at room temperature. The PFA was removed and cells were washed three times for 10 min in PBS to remove excessive fixative. Cells were then incubated in PBST (PBS

with 0.1% Triton) for 20 min for permeabilisation. Cells were incubated in blocking solution (PBST with 0.1% BSA and 3% goat serum) for 1 hr, before overnight incubation at 4°C, with primary antibody in blocking solution. Primary antibody was removed with three quick washes and three 10 min washes in PBST. Cells were incubated with the appropriate secondary antibody in blocking solution for 1 hr at room temperature. Wash steps were repeated as previously. Cells were then incubated in DAPI in PBST (1:10000 dilution) for 5 min for nuclear counter-staining then washed once in PBST. Imaging was performed using a Nikon TiE microscope and NIS-Elements software. Analysis was performed using FIJI (Image J) software. Quantification of immunopositive cells was performed using the Cell Counter plugin. Total cell number was determined by DAPI staining. Quantification of Gfap and Nestin staining in Chapter 3 and FOXG1-V5 staining in Chapter 4 was performed using PerkinElmer's Operetta High-content imaging system and Columbus software. A list of antibodies used for ICC and Western blotting are provided in Appendix V.

2.5.2 Western blotting

Cell pellets were resuspended in 70 ul of RIPA buffer (50 mM Tris-HCl pH 8.0, 150 mM NaCl, 1% NP-40, 0.5% deoxicholate, 0.1% SDS and protease inhibitors (Complete, Roche, 11697498001)). Following incubation for 5 min on ice, the resuspension was centrifuged at 13000 rpm for 10 min at 4 ˚C. The supernatant was collected in a clean tube and quantified using Thermo Scientific BCA kit (cat. 23227). 25% of the total volume of 4x Lithium dodecyl sulfate (LDS) buffer containing 10% 2-mercaptoethanol was added and samples were denatured at 95˚C for 10 min. Electrophoresis was performed using Tris-Bis-HCl buffered (pH 6.4) 4-12% polyacrylamide gels made by Dr Carla Blin, Pollard lab. Spectra Multicolour Broad Range Protein Ladder (Thermo Scientific) or BioRad Precision Plus Protein Dual Colour standards were used. Protein

bands were transferred to Immobilon-P PVDF membrane (Millipore) by wet electroblotting. Membranes were blocked in 5% milk in TBS-T (TBS + 0.1% Tween-20) for one hour at room temperature and incubated with primary antibody dilutions in 5% milk in TBS-T overnight at 4˚C with rocking. Following three 5 min washes in TBS-T at room temperature, membranes were incubated with species-specific horseradish peroxidase (HRP)-coupled secondary antibodies in 5% milk in TBS-T for 1 hr at room temperature with rocking. Following three 5 min washes in TBS-T, membranes were developed using homemade enhanced chemiluminescence (ECL) solution or Clarity ECL Western Blotting substrate (Bio-Rad) and imaged using X ray films or a Bio-Rad ChemiDoc™ Imager. A list of antibodies used for ICC and Western blotting are provided in Appendix V.

2.5.3 Co-immunoprecipitations

All cell pellets were washed with PBS following dissociation and collection in wash media, and frozen at - 80˚C. Once thawed, cell pellets were resuspended in 0.5-1 ml of lysis buffer depending on the pellet size (~5x volume of pellet) (Lysis buffer: 50 mM Tris-HCl pH 8.0, 150 mM NaCl, 0.5% NP-40, 5% glycerol, 1 mM DTT, 2 mM $MgCl_2$ and protease inhibitors (Complete, Roche, 11697498001)). 150 units/ml of benzonase (sigma, E1014) was added and samples were rocked for 30 min at 4 ˚C. Samples were then centrifuged at 13000 rpm for 10 min at 4˚C (centrifuge 5415D eppendorf). The supernatant was collected and 50 µl saved as the loading input (to which 12.5 ul of 4x LDS buffer was added). For each IP, 50 µl of protein G magnetic beads (Dynabeads, Novex, 10003D) or anti-V5-tag magnetic beads (MBL, M167-11) were washed once in 1x PBS + Tween-20 (0.02%) (PBS-T). Protein G magnetic beads were incubated with primary antibodies in PBS-T at room temperature with rocking for at least 30 min. For each antibody the amounts added were: ~ 10 µg of anti-FOXG1 (17B12 in glycerol), 10 µg of mouse IgG

(Sigma; I5381), 10 μg of anti-FOXG1 (ab18259), or 5 μg of anti-HA tag (ab9110). Cell extracts were quantified using the Thermo Scientific BCA kit (cat. 23227). Within each experiment, the same amount of protein extract was added to each IP. This varied between 800 ng – 2 μg. The beads with added extracts were rocked at 4 ˚C for 4.5 hours. Following removal of the supernatant, the beads were washed three times 1 min with lysis buffer. At the last wash, the Eppendorf was changed to avoid eluting proteins bound to the tube. The beads were resuspended in 50 μl of 2 x LDS buffer, boiled at 95˚C for 10 min and stored at -80˚C. For western blotting analysis, the input lysate was loaded alongside the IP, with the input loaded equating to ~2-5% of the IP extract. Blots were blocked overnight at 4˚C in 5% milk in TBS-T with 5% goat serum, to minimise detection of IgG heavy and light chains by the goat secondary antibodies.

2.5.4 Fluorescence-activated cell sorting (FACS)

For isolation of mCherry or eGFP positive cells, or single cell sorting into 96 well plates for clonal cell line derivation, cells were resuspended in FACS buffer (sterile PBS with 0.2 % BSA) to a concentration of ~2 million cells/ml and passed through a cell strainer. DAPI was added to cells at a 1:1000 dilution as a live/dead stain. Flow cytometry was performed on a BD FACS Aria II or BD FACS Fusion cell sorter by the SCRM Flow Cytometry Core Facility. FACSDiva software was used for data collection.

2.6 RNA-based analyses

2.6.1 qRT-PCR

RNA extraction was performed using the Masterpure™ RNA purification kit according to the manufacturer's instructions (Epicentre). DNase digestion was performed using RQ1

RNase-free DNase (Promega) or Masterpure™ RNase-free DNase I. RNA concentration was determined using the Qubit® RNA High Sensitivity kit (Thermo Scientific) or NanoDrop™ Spectrophotometer. Within each experiment, the same amount of RNA was inputted for cDNA synthesis. Reverse transcription was performed using Invitrogen Superscript III. RNA samples were made up to a volume of 11 µl in RNase-free water; to each sample, 1µl Oligo$(dT)_{18}$, 1µl dNTP mix and 0.5µl random hexamer primers (all Thermo Scientific) were added. The samples were incubated at 65˚C for 5 min, then cooled on ice for at least 1 min, before adding 4µl 5X FS buffer, 1µl 0.1M DTT, 0.5µl RNaseOUT and 0.5µl SuperScript™III Reverse Transcriptase (Life Technologies) (or RNase-free water for no-Reverse transcription (RT) controls). Samples were placed in a thermocycler at 25°C for 5 min, 50°C for 50 min, then 70°C for 15 min. cDNA was further diluted to the required volume using nuclease-free water. Quantitative RT-PCR (qRT-PCR) was performed using TaqMan Universal PCR Master Mix (Applied Biosystems) and TaqMan gene expression assays (Life Technologies) on a QuantStudio™7 Flex Real-Time PCR machine. For qRT-PCR analysis of *Jarid1B* expression, primers spanning exon 5-6 were used with SYBR® Green Master Mix (Thermo Scientific). No RT and water controls were run on each plate to ensure the absence of contamination. Technical replicates were run to ensure pipetting accuracy. Data were analysed using the ddCt method; this method assumes 100% PCR efficiency which is guaranteed with TaqMan assays. Replicate Ct values were averaged and normalised to the housekeeping gene, *Gapdh* (to give dCt). These values were then normalised to a calibrator sample (to give ddCt). Data are presented as $\log_2$(fold change) or - ddCt, where this value equals zero for the calibrator, as indicated in the figure legends. All TaqMan assays used in this thesis are listed in Appendix VII.

2.6.2 RNA-sequencing

GNS cell lines were generated by the Glioma Cellular Genetics Resource (GCGR) (www.gcgr.org.uk). RNA-seq data from glioma primary tissue and matched derived GSC lines was made available through the GCGR. A list of cell line names along with GCGR names is provided in Appendix VIII. RNA-seq data was analysed by Ben Southgate (Pollard lab). RNA-seq Fastq files were aligned to the hg38 transcriptome as defined by the TxDb.Hsapiens.UCSC.hg38.knownGene R package with the pseudo aligner kallisto. QC was completed on all samples using FASTQC and trimming was completed with Cutadapt. QC was adequate across all samples and summarised using MultiQC. Tximport was used to summarise read counts and subsequent normalisation was completed as per DESeq2. Gene wide FOXG1 correlation was completed following regularised logarithm transformation (rlog). FDR was calculated to account for multiple testing. This analysis was performed with reference to: (Soneson *et al*, 2016; Martin, 2011; Benjamini & Hochberg, 1995; Ewels *et al*, 2016; Bray *et al*, 2016; Love *et al*, 2014; Team BC, Maintainer BP, 2019). Supplementary RNA-seq figures and tables are provided in Appendix VIII.

2.7 Functional cell-based assays

2.7.1 Cell growth assay

Confluence analysis and growth curves were determined using the IncuCyte® live cell imaging system (Essen Bioscience). Cells were plated at ~25 cells/mm^2 in NS cell media with EGF/FGF-2 in triplicate wells and imaged periodically until confluence was reached.

2.7.2 EdU cell proliferation assay

For analysis of proliferation rates, cells were incubated in NS cell media with EGF/FGF-2, supplemented with 10 μM EdU for 24 h. Cells were then fixed in 4% PFA for 10 min at room temperature and stained with the Click-iT EdU Alexa Fluor 647 assay kit (Life Technologies) according to manufacturer's instructions. Imaging was performed using a Nikon TiE microscope and NIS-Elements software. For each condition, triplicate wells were analysed (4x4 10x stitched image per well). The total cell number was determined by DAPI staining. Quantification was performed using the Image thresholding and Particle Analysis functions on FIJI software.

2.7.3 Colony formation in NS cell media

Colony formation was assessed by plating cells in NS cell media in EGF/FGF-2 at a density of 1 cell/mm^2 (1000 cells per well of a 6 well plate, with 6 replicate wells). Media was changed every 3-4 days. Following 10 days, plates were fixed using 4% PFA for 10 min at room temperature. Colonies were stained using methylene blue for 30 min. Plates were washed gently with deionised water and allowed to dry. Plates were then imaged on a Celigo® Image Cytometer (Nexcelom Bioscience). Colonies were counted manually using the Cell Counter plugin on FIJI, or the % pixel area of the well covered by colonies was quantified using FIJI Image thresholding and Particle Analysis functions.

2.7.4 Colony formation following BMP4 treatment

Cells with Dox-inducible FOXG1-V5 overexpression were plated at a density of 10 cells/mm^2 (10,000 cells per well of a 6 well plate), in NS cell media in the absence of EGF/FGF-2 and supplemented with BMP4 (10 ng/ml). After 24 h, media was replaced fully with NS cell media containing EGF/FGF-2 with or without Dox (1000 ng/ml). Media

was then replaced every 3-4 days. Following 10-12 days, plates were fixed using 4% PFA for 10 min at room temperature. Colonies were stained using methylene blue for 30 min. Plates were washed gently with deionised water and allowed to dry. Plates were then imaged on a Celigo® Image Cytometer (Nexcelom Bioscience). Colonies were counted manually using the Cell Counter plugin on FIJI, or the % pixel area of the well covered by colonies quantified using FIJI Image thresholding and Particle Analysis functions. Three technical replicates were averaged to give the mean number of colonies per biological replicate.

2.8 Statistical analyses

Statistical analyses were performed in GraphPad Prism 7. Biological replicates were considered as different passage numbers of the same cell line plated in independent experiments. Mean and SEM or SD, and n numbers, are shown in the figure legends. Due to small sample sizes, tests for normality and distribution were of limited value. However, this was not considered to be an impediment to parametric analysis with small n numbers (de Winter, 2013). Statistical tests used are indicated in the figure legends. Where two-tailed one-sample t-tests are used, this is based on the null hypothesis that $\log_2$(FC)/-ddCt equals zero (i.e. equal to the calibrator sample). Paired Students t-tests were used where samples (e.g. wild-type and *Foxo6* KO cells) must be matched due to variation between biological replicates (e.g. growth analysis, colony assays following BMP4 treatment). Where significant, p values are indicated in Figures as asterisks, * $p \leq 0.05$, ** $p \leq 0.01$, *** $p \leq 0.001$, **** $p \leq 0.0001$.

CHAPTER 3

FOXG1 enforces an NS cell identity through transcriptional control of cell cycle and epigenetic regulators

3.1 Introduction

GBMs frequently overexpress FOXG1, the key forebrain neurodevelopmental transcription factor. The elevated levels of FOXG1, and other NS cell lineage-affiliated master regulators, are thought to regulate the NS cell-like identity of GSCs. However, the mechanisms by which they do this remain unclear. In this introduction I briefly describe data from the Pollard lab, generated by former PhD student Dr Harry Bulstrode. The results presented in this chapter build upon his initial findings.

To establish the role of the master regulators, FOXG1 and SOX2, on NSC fate, overexpression of both human *FOXG1-V5* and *SOX2* transgenes was performed in dormant quiescent mouse NSCs with astrocytic features (induced by BMP4 treatment of proliferative NSCs and removal of growth factors EGF and FGF-2). This resulted in the reactivation of cells to a proliferative radial glia-like NSC state. To begin to understand how this transition is driven, FOXG1-V5 ChIP-seq was performed and shared binding sites with SOX2 were identified (Lodato *et al*, 2013). In parallel, gene expression changes that accompany FOXG1/SOX2-induced quiescent NSC reactivation were assessed by RNA-seq. The intersection of these data sets led to the discovery of a set of candidate transcriptional target genes shared between FOXG1 and SOX2 (Figure 3-1). This set included enrichment of cell cycle regulators, chromatin modifiers and NS cell gene ontology (GO) categories. TaqMan arrays (TLDAs) for candidates from each category indicated that *FoxO3, FoxO6, Chd3* and *Tet3* were candidate targets of FOXG1/SOX2.

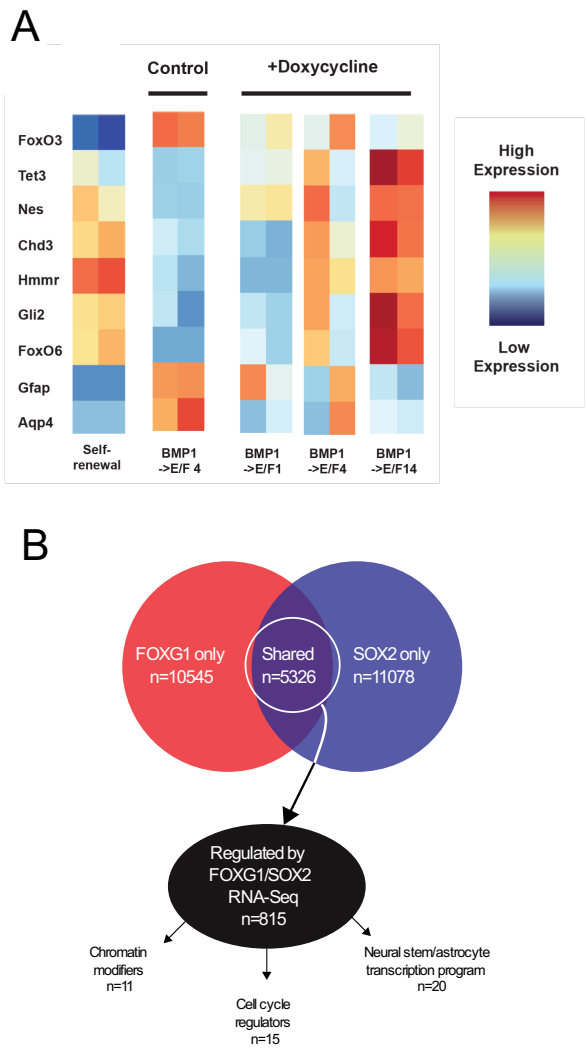

Figure 3-1 | Previously published studies have reported RNA-seq and ChIP-seq analyses that identify candidate FOXG1/SOX2-regulated target genes.

(A) RNA-seq analysis at timepoints during FOXG1/SOX2-induced reactivation of dormant quiescent mouse NSCs with astrocytic features. NS cells were treated with BMP4 for 24h and returned to NS cell media with EGF/FGF-2, with or without Dox-induced induction of *FOXG1/SOX2* human transgene expression (Bulstrode, 2015). **(B)** The intersection of FOXG1-V5 ChIP-Seq (red; in mouse NS cells with inducible *FOXG1* overexpression) with published mouse NSC Sox2 datasets (blue) (Lodato *et al*, 2013). Intersection with RNA-seq data from mouse NSCs with Dox-inducible *FOXG1/SOX2* overexpression revealed candidate transcriptional targets (black) (Adapted from (Bulstrode, 2015)).

In particular, the Forkhead factor and tumour suppressor, *FoxO3*, whose locus was bound by both FOXG1 and SOX2, was functionally validated as a downstream repressed target. Deletion of the FOXG1/SOX2-bound cis-regulatory region of *FoxO3* abolished FOXG1/SOX2-induced reactivation. However, loss of *FoxO3* itself was found to drive cell cycle re-entry but not reacquisition of an NS cell-like state. The loss of astrocytic markers and increased NSC marker expression was only achieved on inhibition of DNA methyltransferase activity by the nucleoside analogue 5-Azacytidine (5-Aza), indicating that cell cycle re-entry and epigenetic resetting can be uncoupled in the process of NS cell state reacquisition (Bulstrode *et al*, 2017; Mikkelsen *et al*, 2008; Chiu & Blau, 1985).

Given FOXG1 is the most frequently overexpressed gene in GSCs (Engstrom et al, 2012), we hypothesised it may be sufficient alone to drive an NSC identity. Based on promising preliminary data, we therefore decided to dissect its role when overexpressed alone, without combined SOX2 overexpression.

In this chapter, we therefore begin exploring FOXG1's function by testing whether overexpression of a human *FOXG1* transgene alone is sufficient to drive dormant quiescent mouse NSCs to a proliferative radial-glia-like NSC state. We assess the state of these reactivated cells following withdrawal of transgene induction. Based on a set of previously identified candidate targets, we then validate which of these targets are regulated by increased *FOXG1* alone during the reactivation process. Finally, we use reduced-representation bisulphite sequencing (RRBS) to determine changes in global DNA methylation during BMP4 treatment of adult mouse NS cells and subsequent FOXG1-induced reactivation. The overall goal was to define clear FOXG1 regulated target genes that may be functionally important during gliomagenesis.

3.2 Overexpression of FOXG1 in dormant quiescent NSCs

The ability of high FOXG1 levels alone to drive a proliferative NS cell-like state was scored quantitatively using an *in vitro* colony formation assay. Bone morphogenetic protein 4 (BMP4) was used to trigger a dormant quiescent NSC state in adult mouse NS cells. These quiescent NS cells were then returned to NS cell media containing the growth factors EGF and FGF-2, with or without Dox-induced *FOXG1* overexpression, to monitor conversion to the proliferative state. Colonies were scored 10 days later.

3.2.1 Mouse NS cells enter a dormant quiescent state with astrocytic features after 24 h BMP4 treatment

Adult mouse NS cells (ANS4, FS3) were plated at low density (10 cells/mm^2) and treated with BMP4 (10 ng/ml) for 24 h. Cells plated at the same density in either EGF/FGF-2 or BMP4 revealed strikingly distinct differences in morphology and marker expression. BMP4-treated cells displayed stellate, flattened morphology characteristic of astrocytes, whereas untreated NS cells had a bipolar phase-bright appearance (Figure 3-2 A). Immunocytochemistry (ICC) confirmed BMP4-induced downregulation of Nestin (a radial glia/NS cell marker), and upregulation of the astrocyte marker, Gfap (Figure 3-2 B). Quantification of the intensity of staining revealed a shift in distribution following BMP4 treatment, from high to low Nestin expression and low to high Gfap expression (Figure 3-2 C). qRT-PCR analysis confirmed a decrease in expression of the NS cell markers, *Nestin* and *Olig2*, and an increase in expression of astrocyte markers, *Gfap, Aqp4* and *S100β,* following BMP4 treatment (Figure 3-2 D). After re-exposure to EGF/FGF-2, the BMP4 treated cells did not re-enter cell cycle, as assessed by growth kinetics and EdU incorporation (Figure 3-3). 24 h BMP4 treatment therefore results in cells exiting the cell cycle and acquiring astrocytic features, in terms of morphology, marker expression and growth kinetics. As discussed in section 3.4 of this chapter, the exact state of these cells

is difficult to define due to NSCs existing in a continuum of states (Figure 1-2); however, recent findings from the Pollard lab suggest these BMP4-treated ANS4 cells are dormant quiescent NSCs (d-qNSCs), that are in a G0 state.

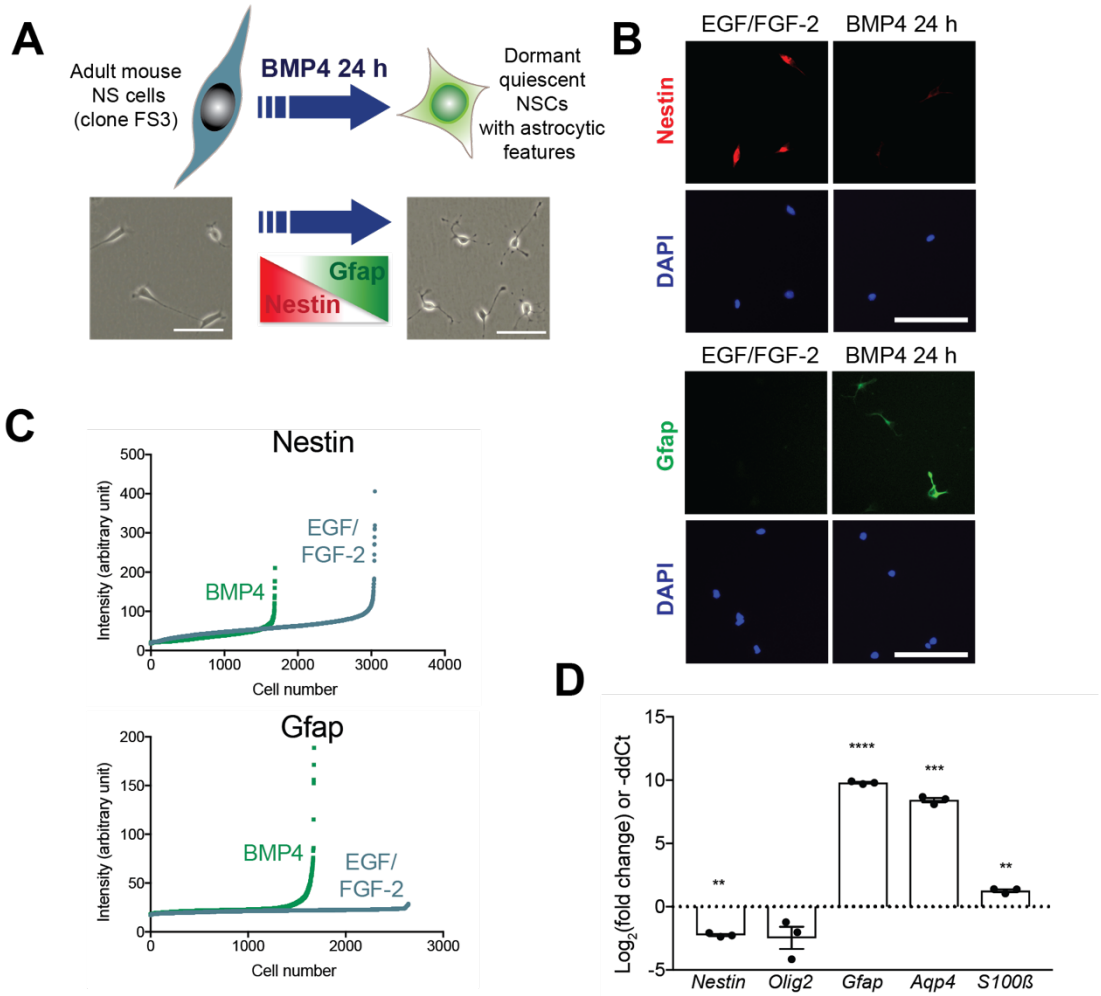

Figure 3-2 | 24 h BMP4 treatment of ANS4 cells (FS3) results in acquisition of astrocytic features.

(A) Representative phase-contrast images of ANS4 (adult mouse NS) cells (FS3 clone) plated at low density (10 cells/mm^2) in either NS cell media (EGF/FGF-2) or BMP4 (10 ng/ml) for 24 h. Scale bar: 100 µm. **(B)** ICC analysis of Nestin and Gfap expression in cells in EGF/FGF-2 or BMP4 for 24 h. **(C)** Quantification of the intensity of Nestin and Gfap ICC staining in cells in EGF/FGF-2 or BMP4 for 24 h. Each point represents one cell (number displayed on x axis and intensity (arbitrary units) displayed on y axis). **(D)** qRT-PCR analysis of *Nestin, Olig2, Gfap, Aqp4 and S100β* mRNA expression levels. Expression values were normalised to *Gapdh* and shown relative to the expression in EGF/FGF-2 (in which $\log_2$(FC) = 0). Y axis represents $\log_2$(Fold change), equivalent to -ddCt value. Graph shows Mean +/- SEM. n=3 independent experiments. Each data point shows the mean of one experiment, performed in technical duplicates. Statistics were calculated from ddCt values. Two-tailed one sample t-test. * P ≤ 0.05, ** P ≤ 0.01, *** P ≤ 0.001, **** P≤ 0.0001.

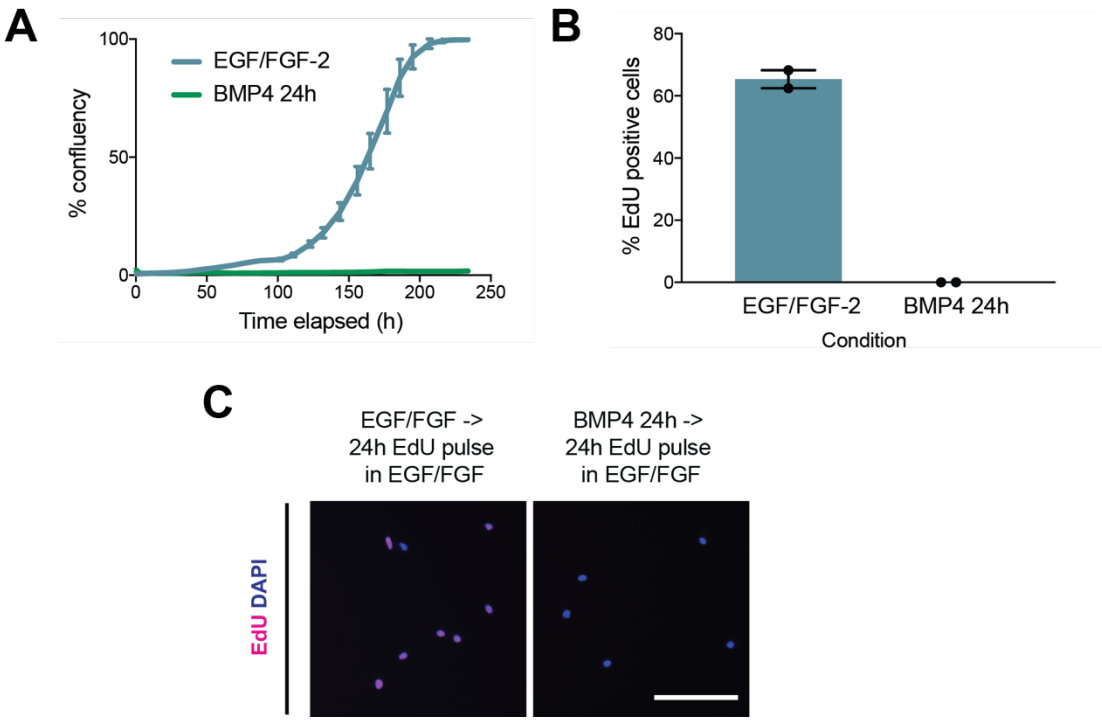

Figure 3-3 | 24 h BMP4 treatment of ANS4 cells (FS3) results in exit from the cell cycle.

(A) Growth curve displaying percentage confluence versus time. ANS4 (FS3) cells were plated at the same density then grown in NS cell media (EGF/FGF-2) (blue) or treated with BMP4 for 24 h then returned to NS cell media (green). Mean +/- SD, n=3 technical replicates. **(B)** Quantification of % EdU positive ANS4 (FS3) cells following plating at low density and treatment with EGF/FGF-2 (blue) or BMP4 for 24 h (green) followed by a 24 h EdU pulse in EGF/FGF-2. Mean +/- SEM. n=2 independent experiments. Each data point shows the mean of one experiment, performed in technical triplicates. **(C)** Representative fluorescent images of EdU incorporation following a 24 h pulse in EGF/FGF-2. Scale bar: 100 μm.

3.2.2 FOXG1 overexpression results in cell cycle re-entry, re-acquisition of an NS cell-like state and colony formation

To test whether FOXG1 overexpression in the absence of SOX2 is sufficient to drive d-qNSCs into a proliferative NSC-like state, we used an adult mouse NSC-derived cell line (termed 'F6'). This cell line was previously established by Dr Harry Bulstrode, and was engineered using the PiggyBac transposon system to stably express a Dox-inducible V5 epitope-tagged human *FOXG1* transgene (Figure 3-4 A and B). A Dox concentration of 1000 ng/ml was previously shown to induce a high level of transgene induction without negatively affecting cell proliferation in control proliferating NS cells (data not shown).

After plating at low density and treatment with BMP4 for 24 h, BMP4 was replaced with NS cell media (EGF/FGF-2) with and without Dox addition (Figure 3-4 C). Addition of Dox led to the overexpression of the human V5-tagged *FOXG1* transgene, as confirmed by ICC (Figure 3-5 A), and by day 4, a change in cell morphology was visible (Figure 3-4 B). Colony formation was assessed 10 days after replacement of BMP4 with EGF/FGF-2 +/- Dox. This confirmed cell cycle re-entry and colony formation occurred following FOXG1 overexpression, with minimal background colony formation observed in the no Dox controls (Figure 3-5 C-E). Upon withdrawal of Dox, the reactivated cells continued to divide and could be serially passaged. The expanded reactivated cells displayed a typical NS cell morphology (bipolar phase-bright appearance), and growth kinetics, marker expression and a differentiation potential similar to the parental NS cells (Figure 3-6). FOXG1 therefore drives d-qNSCs back into cell cycle and activates radial-glia/NS cell marker expression.

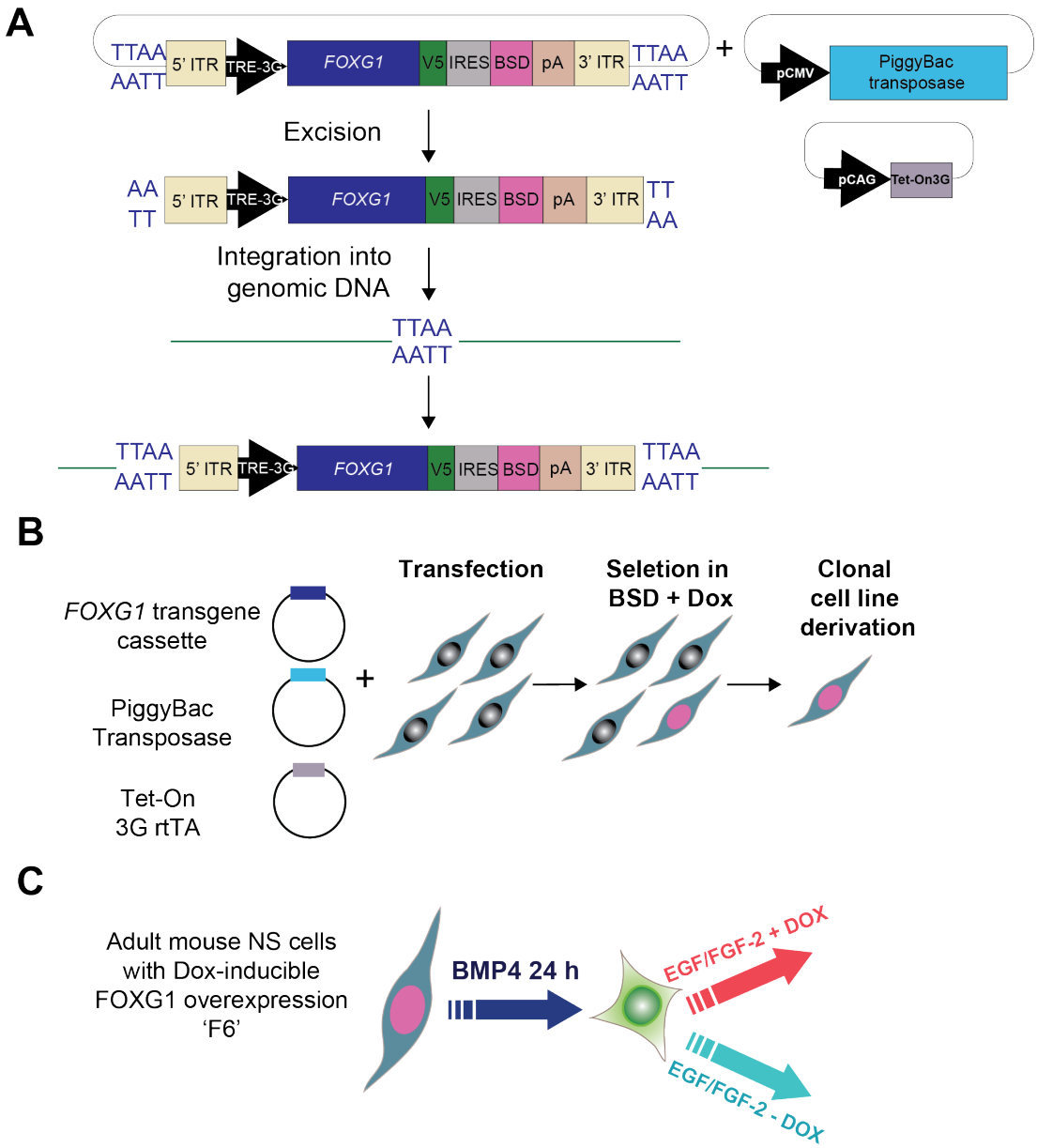

Figure 3-4 | Derivation of 'F6' ANS4 cell line with Dox-inducible overexpression of a human *FOXG1* transgene.

(A) and **(B)** Schematics of PiggyBac transposon strategy used by Harry Bulstrode to derive 'F6' cell line. ANS4 cells were transfected with three plasmids, containing the PiggyBac transposase, Tet-On 3G transactivator and Dox-inducible FOXG1-V5 expression cassette. The transposase binds to the ITRs of the transposon and frees it from the plasmid backbone. The transposase then locates TTAA sequences in genomic DNA and mediates insertion of the transposon, resulting in duplication of the TTAA so that it is found at both sides of the integrated transposon. This also results in stable integration of the sequence encoding the Tet3G transactivator needed for Dox-inducible expression from the TRE-3G promoter. ITR = inverted terminal repeat sequence, TRE = tetracycline response element, IRES = Internal ribosome entry site, BSD = Blasticidin resistance gene. pA = polyA signal **(C)** Schematic of treatment of F6 cells for the colony formation assay.

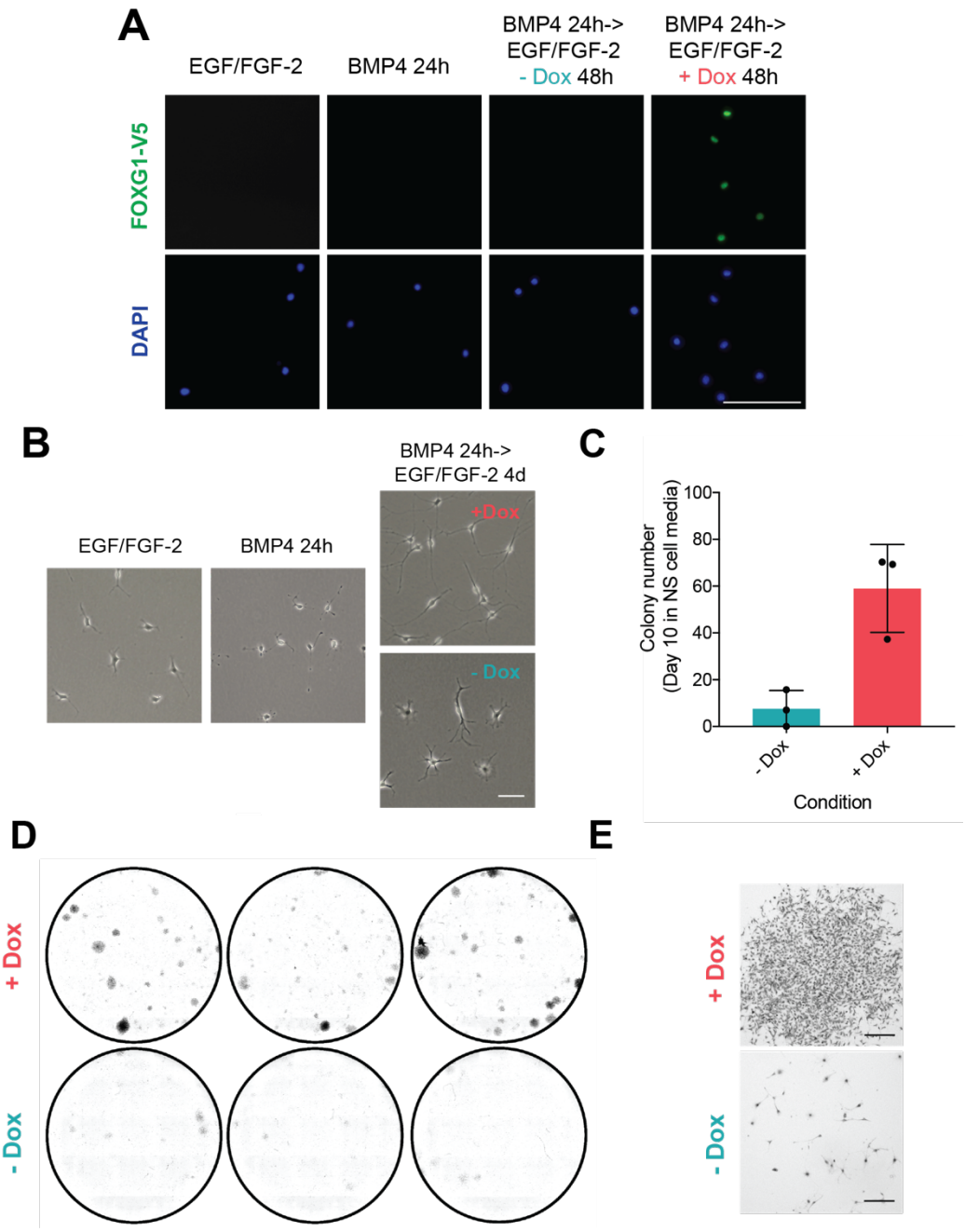

Figure 3-5 | FOXG1 overexpression in astrocytic d-qNSCs results in cell cycle re-entry and colony formation.

All experiments performed in ANS4 'F6' cell line. **(A)** ICC for V5, confirming FOXG1-V5 expression only on Dox addition (Scale bar: 100 μm). **(B)** Representative phase-contrast images showing changes in cell morphology on addition of Dox (Scale bar: 100 μm). **(C)** Number of colonies formed after 24 h BMP treatment and 10 days in EGF/FGF-2 , with or without Dox addition. Mean +/- SD, n=3 independent experiments. Each data point shows the mean of one experiment, performed in technical triplicates. **(D)** Colony formation in F6 cells after 24 h BMP treatment and 10 days in EGF/FGF-2, with or without Dox addition. 6 well plate stained with methylene blue after fixation. **(E)** Representative phase-contrast images of cells with or without Dox addition after 10 days, following fixation and methylene blue staining (Scale bar: 200 μm).

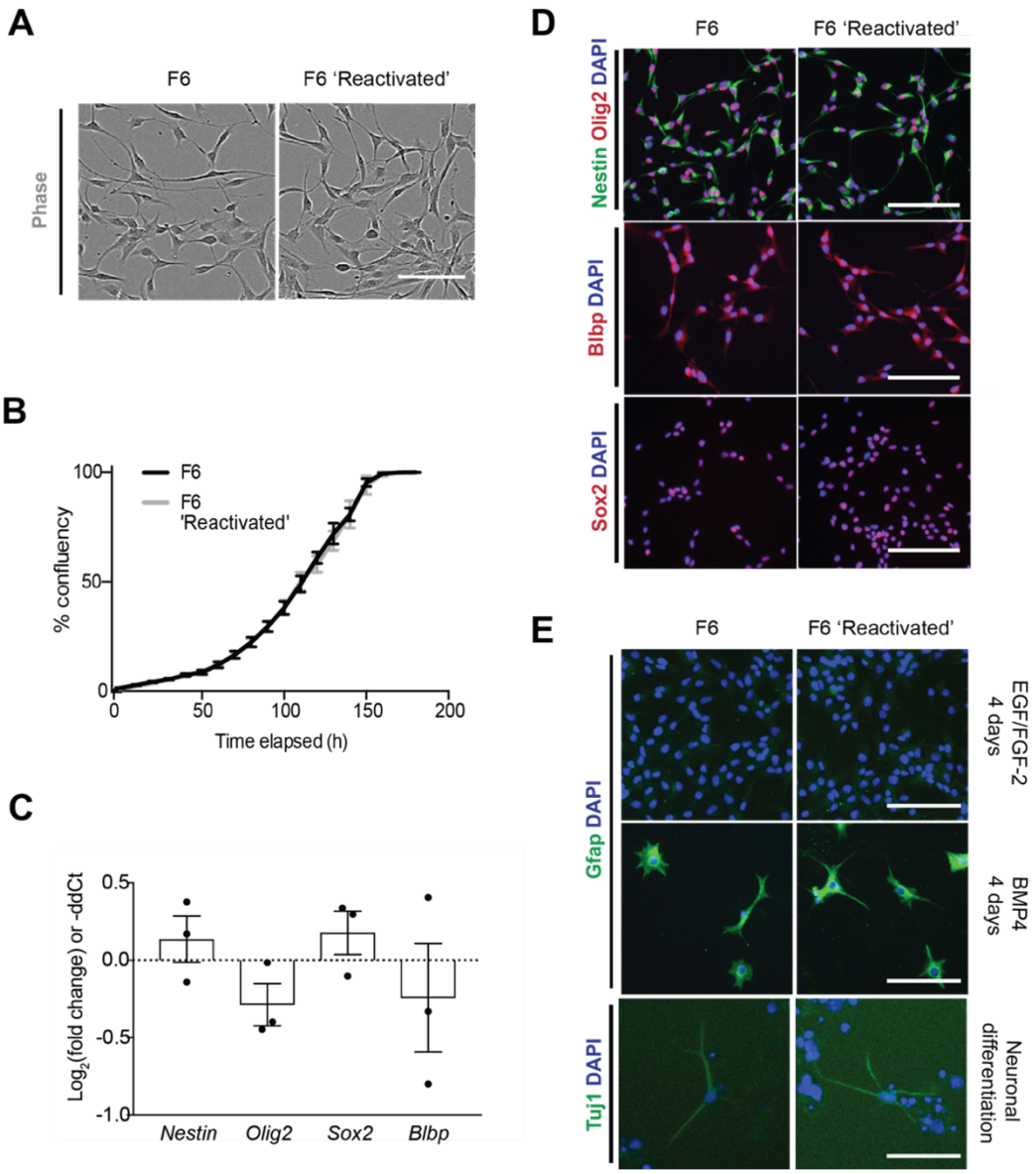

Figure 3-6 | 'Reactivated' NS cells show similar cell morphology, growth kinetics, marker expression and differentiation potentials to the parental F6 cells.

(A) Phase contrast images of parental F6 cells and 'reactivated' cells expanded after Dox withdrawal. **(B)** Growth curve showing percentage confluency versus time. Black = parental F6, grey = 'reactivated' F6 after Dox withdrawal. Mean +/- SD (n=3, technical replicates). **(C)** qRT-PCR analysis of common NS cell markers, *Nestin, Olig2, Sox2* and *Blbp* in 'reactivated' F6 cells. Expression values were normalised to *Gapdh* and shown relative to the expression in F6 parental cells (in which $\log_2$(FC) = 0). Y axis represents $\log_2$(Fold change), equivalent to -ddCt value. Mean +/- SEM. n=3 independent experiments. Each data point shows the mean of one experiment, performed in technical duplicates. Statistics were calculated from ddCt values. Two-tailed one sample t-test. **(D)** ICC images showing expression of Nestin, Olig2, Sox2 and Blbp, in parental F6 cells and 'reactivated' F6 after Dox withdrawal and expansion. **(E)** ICC images of Gfap expression after treatment with EGF/FGF-2 or BMP4 for 4 days. Tuj1 expression shows successful neuronal differentiation. Both parental and 'reactivated' F6 cells can differentiate to the glial and neural lineages. All scale bars: 100 μm.

3.3 FOXG1 transcriptionally controls cell cycle and epigenetic regulators

We next wanted to further explore the mechanism by which FOXG1 overexpression enforces a proliferative NS cell-like state on non-cycling astrocytic d-qNSCs. We focussed on testing this in the context of the 'reactivation' colony assay, as FOXG1 overexpression in already proliferating NSCs may fail to identify significant fold changes in its targets.

3.3.1 FOXG1 overexpression results in activation of cell cycle regulators

Based on the set of previously identified candidate targets of FOXG1/SOX2 (section 3.1), we first began by exploring the changes in expression of a panel of candidate cell cycle regulators. F6 cells were plated as described previously for the *in vitro* colony formation assay. RNA was extracted during a time-course following replacement of BMP4 with EGF/FGF-2, with and without Dox addition; gene expression levels were subsequently determined using TaqMan qRT-PCR assays (Figure 3-7 A). Assessment of human *FOXG1* mRNA levels confirmed significant induction of transgene overexpression upon Dox treatment, with a 235-fold upregulation in expression by day 1 in Dox (compared to EGF-FGF2 control, where $\log_2$(fold change) equals zero) (Figure 3-7 B). We noted that for the NS cell marker, *Nestin*, and the astrocyte marker, *Gfap*, EGF/FGF-2 alone alters their expression early in the time-course, and this was not significantly altered by Dox (Figure 3-7 C and D). We therefore focussed on changes in target gene expression that went beyond a media-induced change (with no Dox) at each point in the time-course.

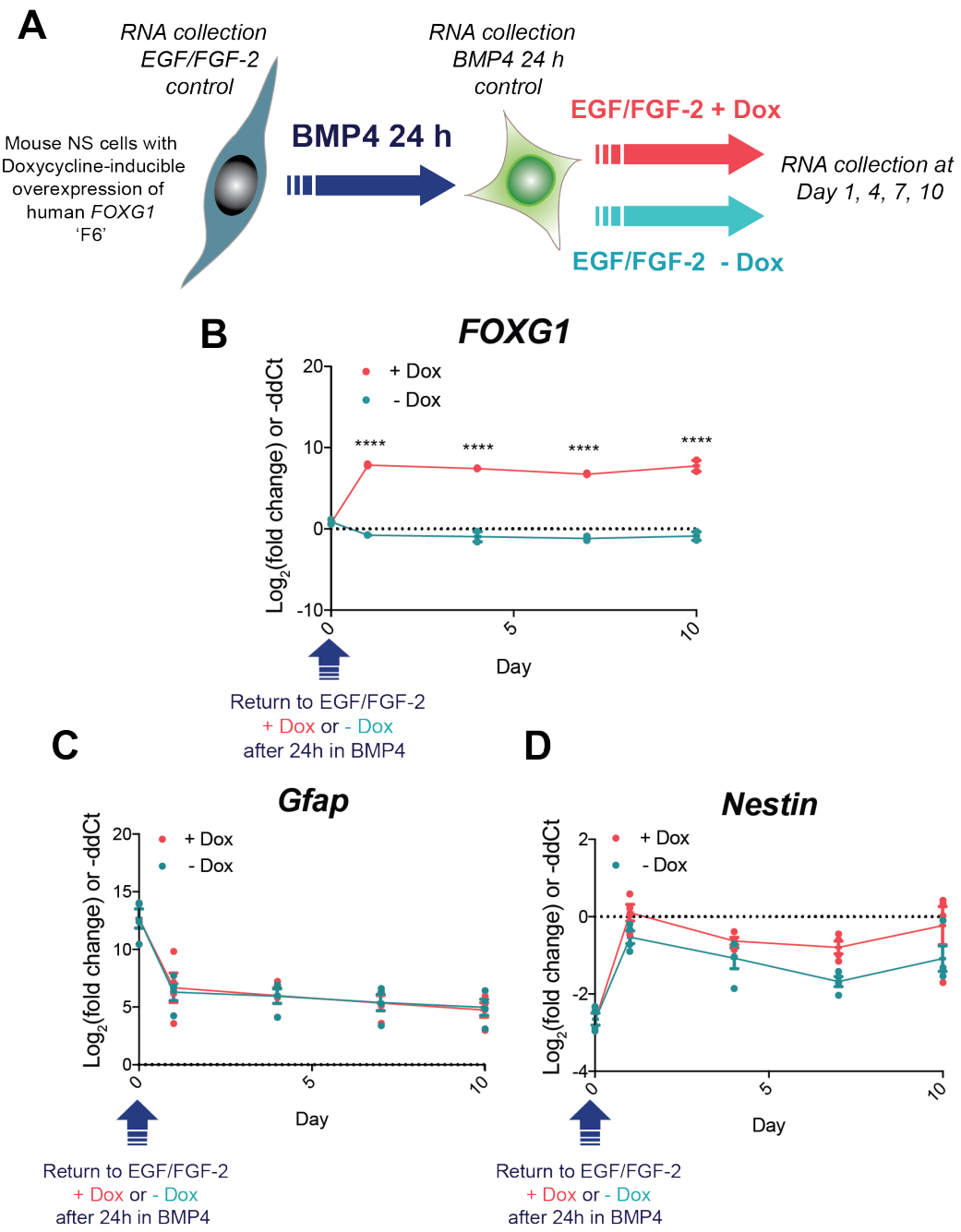

Figure 3-7 | *FOXG1* expression is significantly induced by Dox addition.

(A) Schematic describing RNA collection from F6 cells during the 'reactivation' colony assay. **(B)** mRNA expression of human *FOXG1* transgene during the reactivation time-course. Pink = + Dox addition, Blue = No Dox addition. Expression values were normalised to *Gapdh* and shown relative to the expression in EGF/FGF-2 control (in which $\log_2$(FC) = 0, marked by the dotted line). Time zero represents expression level after 24 h BMP4 treatment. Y axis represents $\log_2$(FC), equivalent to -ddCt value. Mean +/- SEM. n = 2 independent experiments. Each data point shows the mean of one experiment, performed in technical duplicates. Statistics calculated from ddCt values. **(C)** *Gfap* mRNA levels during the reactivation time-course. **(D)** *Nestin* mRNA levels during the reactivation time-course. Mean +/- SEM. (C) and (D) show n=4 independent experiments. * P ≤ 0.05, ** P ≤ 0.01, *** P ≤ 0.001, **** P≤ 0.0001. Two-way Anova with Sidak correction.

Polo-like kinase 1 (*Plk1*) is a crucial mitotic regulator involved in the G2/M transition. *NMyc*, is a well-known transcriptional regulator and oncogene. For both *Plk1* and *NMyc*, a significant upregulation in mRNA levels was identified in response to *FOXG1* overexpression (Figure 3-8 A and B). The Forkhead factor, *FoxO3*, a known tumour suppressor and previously reported target of FOXG1/SOX2 in the Bulstrode *et al*. study, did not show a significant change in expression on induction of FOXG1 (Figure 3-8 C). This suggests that either SOX2 may play an essential role in the regulation *FoxO3* expression, or that the switch to EGF/FGF-2 reduces *FoxO3* expression to a level at which further FOXG1-induced changes are no longer detectable. Importantly, another Forkhead factor, *FoxO6*, showed a dramatic upregulation in response to *FOXG1* induction. *FoxO6* levels showed a ~6.5-fold upregulation by day 1 in Dox (compared to EGF-FGF2 control), with levels at this timepoint ~16-fold higher than in the no Dox control (Figure 3-8 D). FoxO6 is the least well-described of the FoxO factors, however in contrast to the tumour suppressive functions of FoxO3, several studies suggest FoxO6 may act as a proto-oncogene (Qinyu *et al*, 2013; Rothenberg *et al*, 2015; Wang *et al*, 2017b; Lallemand *et al*, 2018; Li *et al*, 2019).

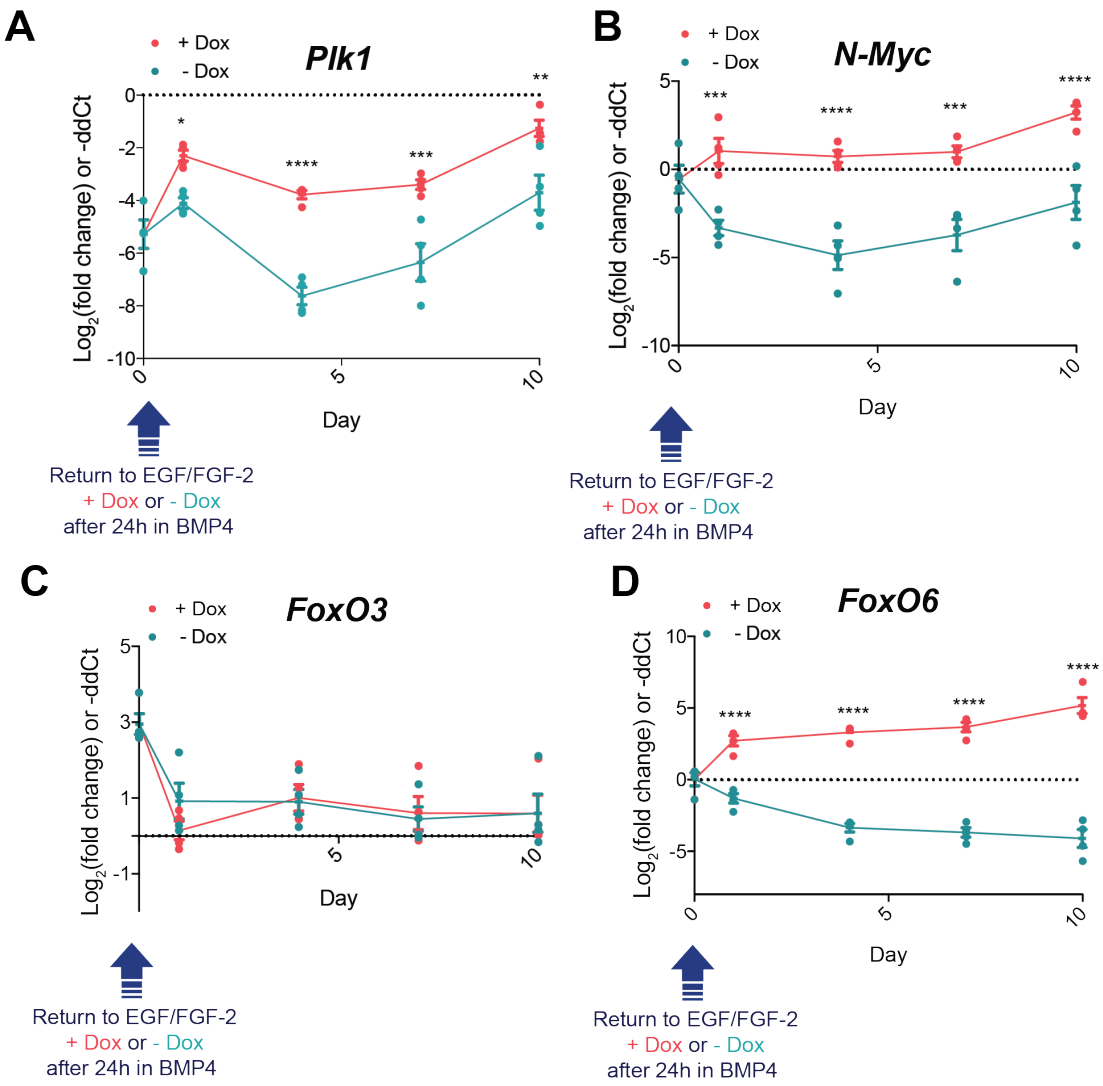

Figure 3-8 | FOXG1 overexpression results in activation of cell cycle regulators.

mRNA expression of **(A)** *Plk1*, **(B)** *NMyc*, **(C)** *FoxO3* and **(D)** *FoxO6,* during the reactivation time-course (F6 cells). Pink = + Dox addition, Blue = No Dox addition. Expression values were normalised to *Gapdh* and shown relative to the expression in EGF/FGF-2 control (in which $\log_2(FC) = 0$, shown by the dotted line). Time zero represents expression level after 24 h BMP4 treatment. Y axis represents $\log_2(FC)$, equivalent to -ddCt value. Mean +/- SEM. n=4 independent experiments. Each data point show the mean of one experiment, performed in technical duplicates. Statistics calculated from ddCt values. * $P \leq 0.05$, ** $P \leq 0.01$, *** $P \leq 0.001$, **** $P \leq 0.0001$. Two way Anova with Sidak correction.

3.3.2 FOXG1 overexpression results in activation of epigenetic regulators

As described earlier, previous work found that while *FoxO3* loss is sufficient to enable cell cycle re-entry, reacquisition of an NSC state can be driven only in combination with 5-Aza (Bulstrode *et al*, 2017). This indicated the importance of epigenetic resetting during re-acquisition of the NS cell state driven by FOXG1/SOX2 and suggested that cell cycle re-entry and epigenetic resetting are controlled by pathways that can be uncoupled.

We therefore searched for candidate epigenetic regulators that might be targets of FOXG1. We assessed a panel of six known epigenetic modifiers (*Dnmt1, Dnmt3b, Tet3, Hdac7, Ezh2* and *Chd3*), previously uncovered as candidate targets of FOXG1/SOX2. All factors analysed were confirmed as significantly upregulated in response to *FOXG1* transgene induction in F6 cells (Figure 3-9). These included regulators of DNA methylation: DNA methyltransferase 1 (*Dnmt1*) which is known for its role in maintenance of established methylation marks, DNA methyltransferase 3b (*Dnmt3b*) which catalyses *de novo* DNA methylation, and Tet methylcytosine dioxygenase 3 (*Tet3*) which catalyses oxidation of 5-methylcytosine leading to loss of methylation. In addition, proteins involved in chromatin remodelling were also upregulated: the histone deacetylase 7 (*Hdac7*), the histone methyltransferase component of PRC2, *Ezh2*, and most significantly, chromodomain helicase DNA binding protein 3 (*Chd3*), a component of the histone deacetylase NuRD complex which acts to remodel chromatin (Figure 3-9 F). *Chd3* levels showed a 2-fold upregulation by day 4 in Dox (compared to EGF-FGF2 control), with levels at this timepoint ~3-fold higher than in the no Dox control. By day 10 in Dox, *Chd3* levels showed a 4-fold upregulation, with levels ~7.4 fold higher than in the no Dox control (Figure 3-9 F).

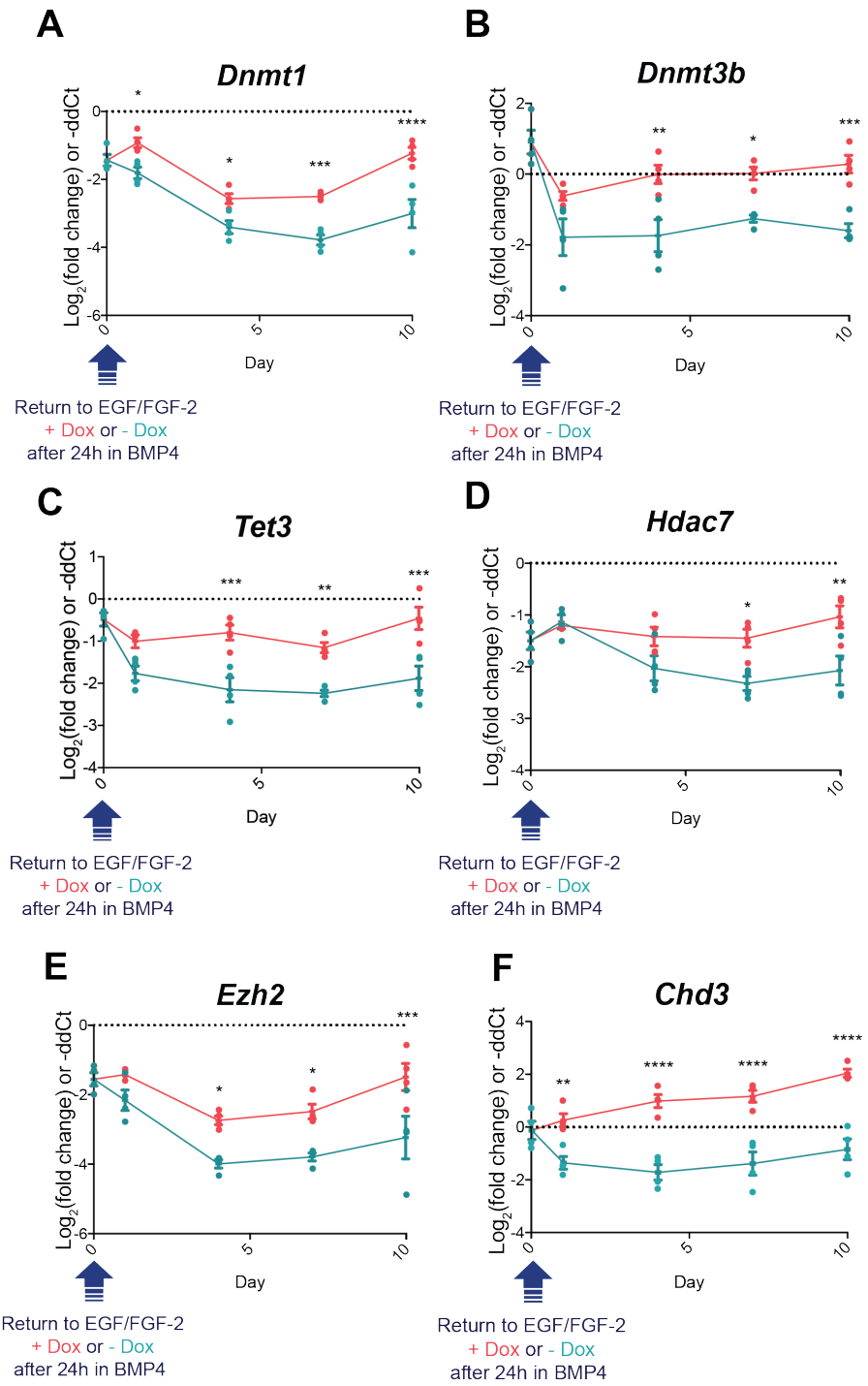

Figure 3-9 | FOXG1 overexpression results in activation of epigenetic regulators.

mRNA expression of **(A)** *Dnmt1*, **(B)** *Dnmt3b,* **(C)** *Tet3,* **(D)** *Hdac7,* **(E)** *Ezh2* and **(F)** *Chd3,* during the reactivation time-course (F6 cells). Pink = + Dox addition, Blue = No Dox addition. Expression values were normalised to *Gapdh* and shown relative to the expression in EGF/FGF-2 control (in which $\log_2(FC) = 0$, shown by the dotted line). Time zero represents expression level after 24 h BMP4 treatment. Mean +/- SEM. n=4 independent experiments. Each data point shows the mean of one experiment, performed in technical duplicates. Statistics calculated from ddCt values. * $P \leq 0.05$, ** $P \leq 0.01$, *** $P \leq 0.001$, **** $P \leq 0.0001$. Two way Anova with Sidak correction.

3.3.3 Activation of DNA methylation regulators by FOXG1 may affect key polycomb target genes

The activation of several epigenetic regulators by *FOXG1* overexpression, including those controlling DNA methylation, suggested that resetting of the epigenetic landscape may be an important aspect of FOXG1's ability to reactivate astrocytic d-qNSCs. To infer how these transcriptional changes could be leading to epigenetic resetting to an NS cell-like state, we next investigated the global DNA methylation changes that accompany both BMP4 treatment and FOXG1-induced reactivation.

Reduced representation bisulfite sequencing (RRBS) was performed on cells at various stages during the FOXG1-induced reactivation process (RRBS performed by WTCRF Edinburgh). Genomic DNA was collected from FOXG1-inducible (F6) adult mouse NS cells: in NS cell media (EGF/FGF-2), after treatment with BMP4 for 24 hr, 4 days or 10 days, and after treatment with BMP4 for 24 hr and return to EGF/FGF-2 for 4 days with or without Dox addition (Figure 3-10). The resulting methylation profiles were analysed by Dr Duncan Sproul, to identify the DNA methylation changes that accompany BMP4 treatment and FOXG1-induced reactivation.

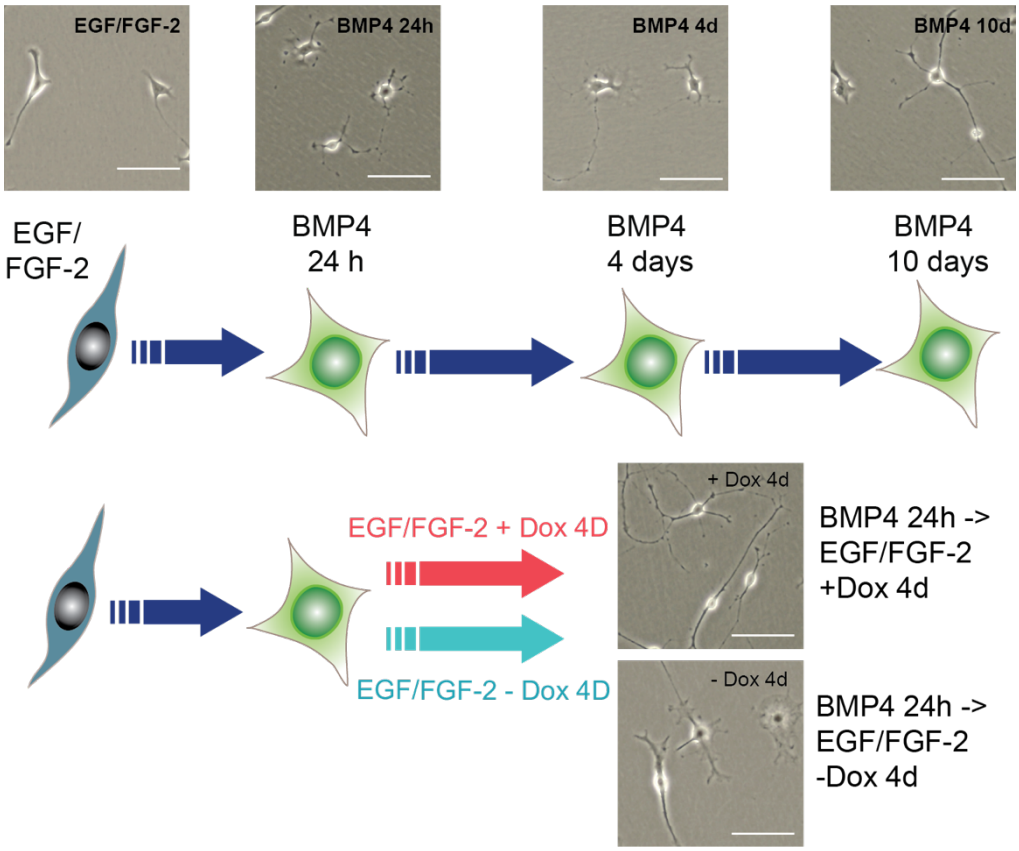

Figure 3-10 | Overview of genomic DNA collection for RRBS analysis.

Schematic describing the experimental set-up for genomic DNA collection. Genomic DNA was collected from FOXG1-inducible (F6) adult mouse NS cells: in NS cell media (EGF/FGF-2), after treatment with BMP4 for 24 hr, 4 days or 10 days, and after treatment with BMP4 for 24 hr and return to EGF/FGF-2 for 4 days with or without Dox addition. Representative phase-contrast images are shown of cells at each timepoint. Scale bar: 100 μm.

After 24 hr or 10 days of BMP4 treatment, 3231 significantly differentially methylated regions (DMRs) were identified compared to cells in EGF/FGF-2 (756 with reduced and 2475 with increased methylation). These were significantly enriched in the vicinity of developmental transcription factors (Figure 3-11 A and B), whose expression is known to be controlled by polycomb-repressive complexes (PRC). In keeping with this, DMRs were significantly enriched in the vicinity of PRC target genes previously reported in mouse NS cells, embryonic stem cells and brain tissue (Figure 3-12 A and B) (Meissner *et al*, 2008; Bulstrode *et al*, 2017). This included differential methylation near a Foxg1-binding site at the promoter of *FoxO3*, a known tumour suppressor and validated downstream transcriptional target of FOXG1/SOX2 (Figure 3-12 C), and also near the promoter of the developmental gene, *Pou3f1/Oct6* (data not shown). Unfortunately, significant differences in methylation profile were not observed following induction of FOXG1 overexpression for 4 days; this is most likely due to the low efficiency of reactivation, with only a small subset of cells returning to an NS cell state every 24 h.

These results suggested that through transcriptional activation of DNA methylation regulators, induction of high FOXG1 levels may aid the reconfiguration of the DNA methylation changes imposed during BMP4 treatment back to a proliferative NS cell-like state.

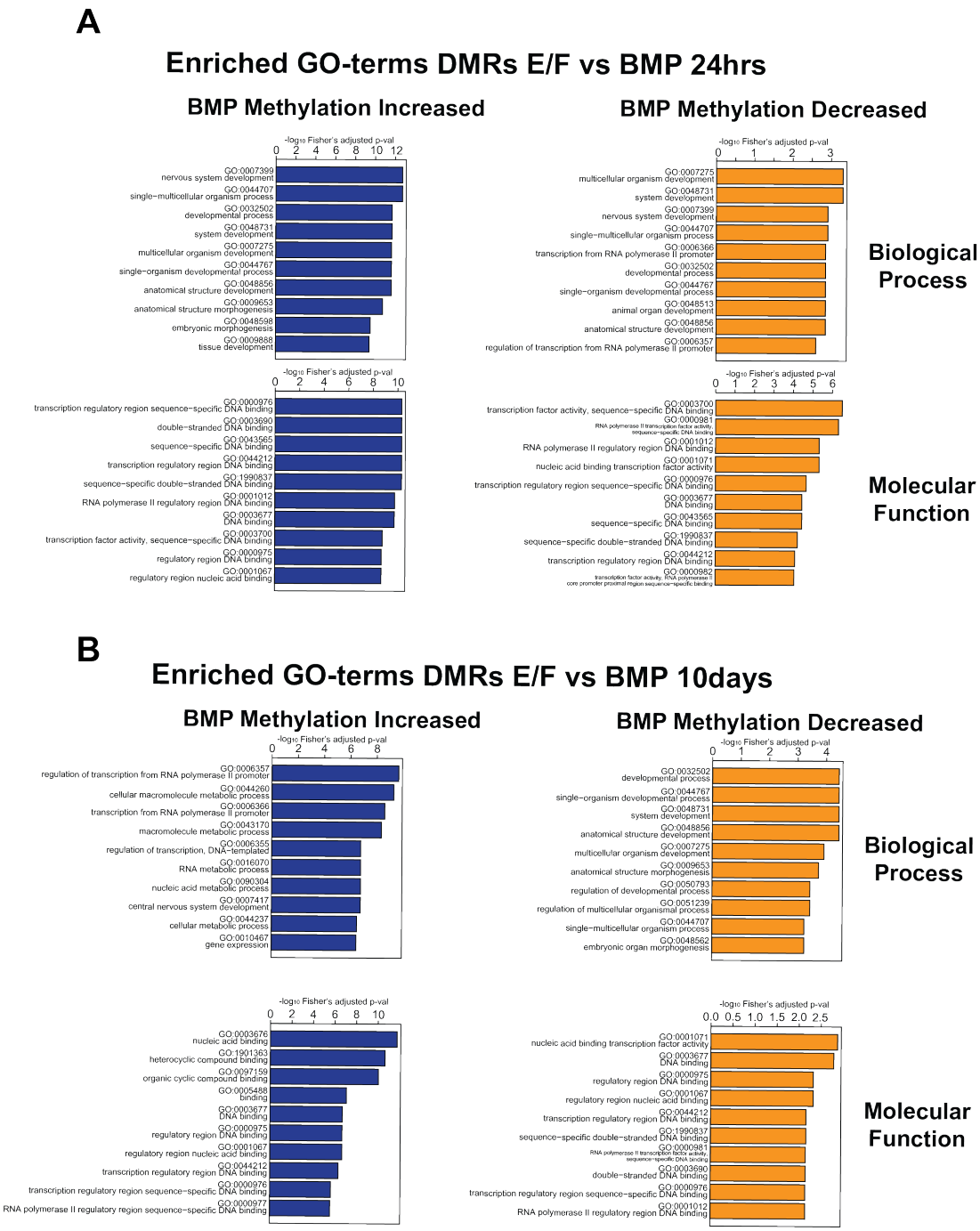

Figure 3-11 | RRBS reveals BMP4-induced DMRs are enriched in the vicinity of developmental transcription factors.

Analysis and figures by Dr Duncan Sproul. Published in Genes and Development (Bulstrode et al, 2017). Analysis of GO terms associated with genes located in the vicinity of differentially methylated regions (DMRs) identified by RRBS. Shown are the top 10 significantly enriched Biological Process and Molecular Function GO terms associated for BMP-induced DMRs after either **(A)** 24 h or **(B)** 10 days in differentiation conditions. Log_{10} Benjami-Hochberg adjusted p-values from Fisher's exact tests versus the background set are plotted. (Blue) BMP-increased methylation; (orange) BMP-decreased methylation.

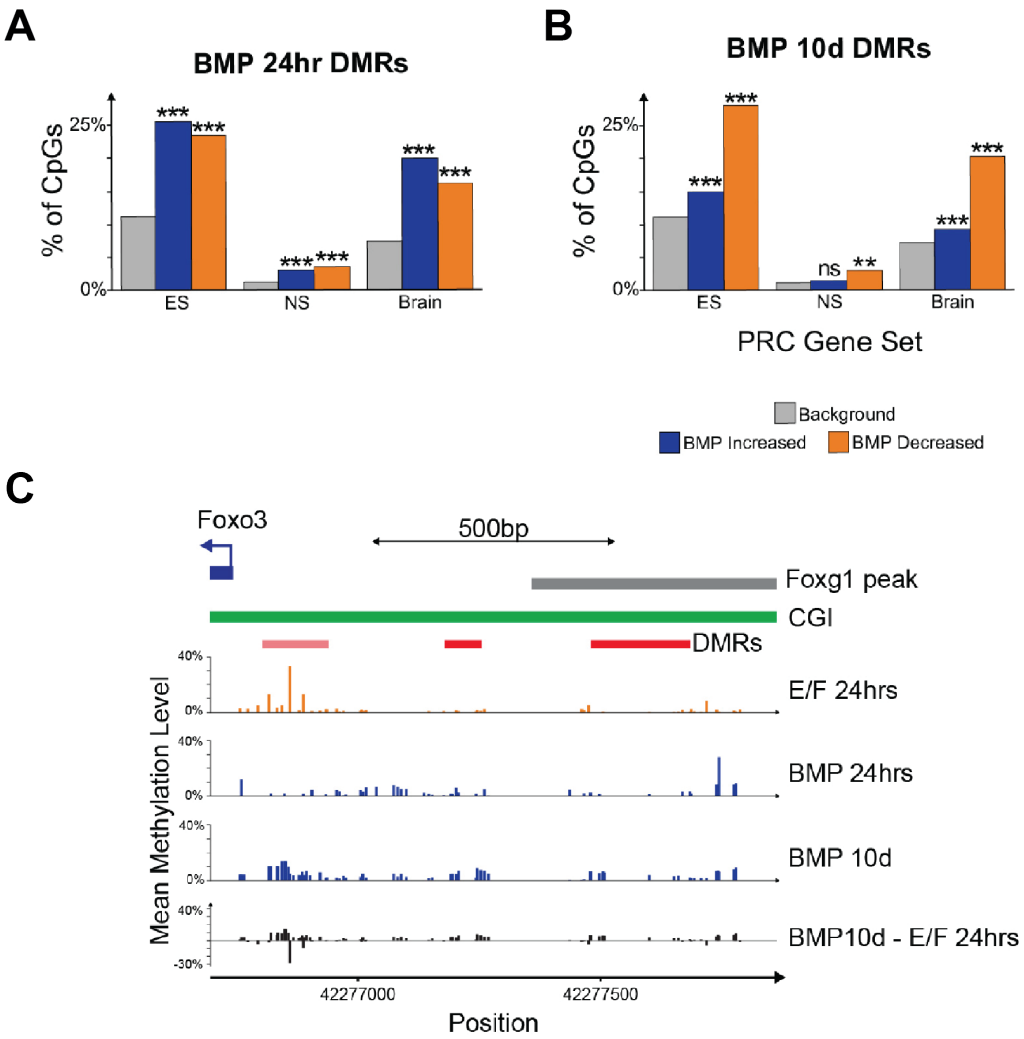

Figure 3-12 | RRBS reveals BMP4-induced DMRs are enriched in the vicinity of PRC target genes, including the FOXG1 target, *FoxO3*.

Analysis and figures Dr Duncan Sproul. Published in Genes and Development (Bulstrode et al, 2017). **(A and B)** Analysis of enrichment of RRBS identified DMRs near genes marked by polycomb in mouse embryonic stem (ES) cells, NS cells, and brains. Shown is the percentage of CpGs assayed by RRBS found near polycomb-marked genes (background, grey) compared with those in significant DMRs after either **(A)** 24 h or **(B)** 10 d of differentiation. Significance was assessed with Fisher's exact tests (**) $P < 0.01$; (***) $P < 0.001$. n = 3 biological replicates. **(C)** Mean methylation profiles observed by RRBS in the *FoxO3* promoter, including the locations of its CpG island (CGI) and *FOXG1* ChIP-seq peak. Significant DMRs are shown in red together with an additional DMR that did not reach statistical significance in all replicates of the experiment (pale red).

3.4 Discussion

In this chapter, we first investigated the ability of FOXG1 overexpression to drive reactivation of astrocytic d-qNSCs to a proliferative NS cell-like state, using a previously established colony formation assay.

After 24 h BMP4 treatment, we found that adult mouse NS cells: exit cell cycle, are growth factor unresponsive, obtain an astrocytic morphology, upregulate astrocytic markers such as Gfap and Aqp4, and downregulate radial glia/NS cell markers such as Nestin and Olig2 (Figures 3-2 and 3-3). We therefore initially viewed them as terminally differentiated. However, the exact state of these cells is difficult to define due to the lack of definitive markers and transcriptional differences that can distinguish terminally differentiated GFAP-expressing astrocytes from quiescent type B SVZ NS cells (which also express GFAP) (Bulstrode *et al*, 2017; Doetsch *et al*, 1999; Codega *et al*, 2014). Recent findings of the Pollard lab suggest some NS cell markers are maintained following BMP4 treatment and these cells can be forced back into cycle with combined Wnt/EGF signalling, or FGF/BMP signalling (Marqués-Torrejón *et al*, manuscript in preparation). This suggests *in vitro* NS cells may lie along a continuous spectrum of states from dormant quiescent, activated quiescent (primed for cell cycle re-entry) to actively proliferating, similar to that observed *in vivo* in the mouse SVZ (Figure 1-2B) (Dulken *et al*, 2017). Indeed, after 24 h BMP4 treatment, we observe a minimal level of colony formation in no Dox controls following 10 days of exposure to the growth factors EGF/FGF-2 (Figure 3-5). These non-cycling BMP4-induced astrocytic cells might therefore be better viewed as dormant quiescent NSCs and are hereafter described as d-qNSCs. The assay conditions used in this thesis differ to those of Marqués-Torrejón *et al*, in terms of density and length of BMP4 treatment; it is therefore likely that our BMP-treated cells are at different stages along the continuum between dormancy and primed

quiescent states. Importantly, regardless of the exact cell type induced by 24 h BMP4 treatment, we have considered the changes induced by FOXG1 overexpression, in comparison to the effect of NS cell media alone, and can therefore identify FOXG1-regulated target genes.

We found high levels of human FOXG1 are alone sufficient to drive cell cycle re-entry and reactivation of these d-qNSCs to a proliferative NS cell-like state, as assessed by colony formation 10 days following re-exposure to EGF/FGF-2 with or without Dox addition (Figure 3-5). Following FOXG1-induced reactivation, the resulting cells can be serially passaged on withdrawal of Dox. They also displayed similar characteristics to the original cells prior to BMP4 treatment, namely morphology, growth kinetics and NSC marker expression (Figure 3-6). This suggests that elevated FOXG1 levels drive q-dNSCs to stably re-acquire a proliferative radial-glia NS cell-like state. Thus, the key activity of FOXG1 seems to be to drive these cells back into cell cycle and re-activate radial glia-like marker expression.

Previous studies focused on investigating the role of elevated FOXG1 together with another master transcriptional regulator, SOX2, in GBM (Figure 3-1). While homozygous knock-out of *SOX2* has been shown by the Pollard lab and others to be incompatible with NS or GNS cell proliferation in EGF/FGF-2, loss of *FOXG1* is dispensable in this context (Gómez-López *et al*, 2011; Bulstrode *et al*, 2017). FOXG1 is however required for proliferation *in vivo*, where EGF/FGF-2 signals may be limited, and there are many pro-differentiation or cytostatic cues (Figure 1-7). In contrast SOX2 alone was previously found to be unable to drive an NSC-like phenotype (Bulstrode, 2015). We therefore concluded that, while SOX2 is essential for sustained proliferation of NS and GNS cell lines, FOXG1 is not; instead it has a key role in protecting the NS cell-like state and enabling exit from the dormant quiescent or differentiated state (Bulstrode *et al*, 2017).

To further explore the mechanism by which FOXG1 overexpression enforces a proliferative NS cell-like state, we analysed the changes in expression of a set of candidate target genes during FOXG1-induced d-qNSC reactivation. We found FOXG1's transcriptional targets to include numerous cell cycle regulators, such as *NMyc, Plk1* and *FoxO6*, highlighting a role for FOXG1 in driving cell cycle re-entry (Figure 3-8). These targets show a significant upregulation in expression at early time points, even following one day in EGF/FGF-2 with Dox, suggesting their expression changes are due to FOXG1 upregulation rather than a consequence of cell cycle re-entry.

Notably, in contrast to a previously validated FOXG1 target, the tumour suppressor *FoxO3*, these factors were upregulated in response to elevated FOXG1. FOXG1's role in inhibition of cytostatic TGFβ signalling and hence inhibition of *CDKN1A* ($p21^{Cip1}$) expression is well-described in the control of neural progenitor proliferation and cancer (Seoane *et al*, 2004; Vezzali *et al*, 2016; Chan *et al*, 2009; Adesina *et al*, 2007). This data provides evidence of an alternative role of FOXG1, in driving proto-oncogene expression compared to inhibition of cytostatic gene expression. Plk1 has been shown to bind and inhibit FoxO3 in HeLA cells; together with our results this suggests a possible indirect mechanism by which FOXG1 leads to FoxO3 repression (Bucur *et al*, 2014).

Previous work found reacquisition of an NS cell state could only be achieved with combined loss of the tumour suppressor, *FoxO3*, and addition of 5-Aza. This suggested an important role of FOXG1 in driving not just proliferation, but also epigenetic resetting to achieve an NS cell-like state. To delineate the mechanism by which FOXG1 leads to this change in epigenetic landscape, we analysed the expression changes of a candidate set of epigenetic regulators in response to FOXG1 induction. Enzymes controlling DNA methylation, such as *Dnmt3*b and *Tet3,* and chromatin modifiers, such as *Chd3,* all exhibited an upregulation in expression (Figure 3-9). Subsequent RRBS analysis on cells

before and after BMP4 treatment revealed global methylation changes, enriched in the vicinity of PRC target genes (Figures 3-11 and 3-12). This included differential methylation near a Foxg1-binding site at the promoter of *FoxO3*, a known target of Foxg1 (Figure 3-12 C). Together these results suggest that, through transcriptional activation of DNA methylation regulators, induction of high FOXG1 levels may aid the reconfiguration of DNA methylation changes imposed during BMP4 treatment back to an NS cell-like state. Indeed, this FOXG1-induced reactivation of d-qNSCs is analogous to direct cellular reprogramming *in vitro*, in which the re-establishment of an immature open chromatin state, through global resetting of histone and DNA modification patterns, is known to have critical roles in obtaining full cell fate conversion (Hochedlinger & Jaenisch, 2015; Hochedlinger & Plath, 2009; Mikkelsen *et al*, 2008).

Unfortunately, significant differences in methylation profile were not observed following induction of FOXG1 overexpression for 4 days; this is most likely due to the low efficiency of reactivation, with only a small subset (~0.15%) of cells returning to an NS cell state every 24 h (Bulstrode, 2015). These low reactivation efficiencies may also result in an underestimation of key transcriptional changes with underlying functions in driving proliferative NS cell-like colony formation. Addition of other factors to improve reactivation efficiency or methods to enrich for the reactivated population would enable the location of methylation changes associated with FOXG1 binding to be identified. For example, work by the Pollard lab has shown Wnt pathway activation, through addition of the GSK3 inhibitor Chiron, to enhance FOXG1-induced d-qNSC reactivation (F.Robertson, in preparation). However, caution would need to be taken to delineate changes due to FOXG1 or Wnt signalling. In addition, FOXG1 also has reported DNA binding-independent actions, therefore changes in methylation may not always coincide with TF binding. Alternatively, in future the generation of *FOXG1-ERT2* fusion transgenes

may provide a more reliable way to identify direct FOXG1-induced changes in gene expression, through direct control of FOXG1's nuclear localisation and hence increased efficiency of reactivation.

The results in this chapter led us to conclude that the high levels of FOXG1 found in GSCs enforce an NS cell identity and facilitate cell cycle re-entry, at least in part, through the transcriptional control of both cell cycle and epigenetic regulators (Figure 3-13). This suggests FOXG1 is functionally important in sustaining a proliferative state with an immature stem cell-like epigenetic profile, and may explain observations that high FOXG1 is a recurrent feature of many GBMs. The findings presented in this Chapter were published in 2017 in Genes and Development, alongside the original observations and RNA-seq/ChIP-seq data from Harry Bulstrode (Bulstrode *et al*, 2017).

In the next chapter, I focus on exploring the functional importance of two of FOXG1's transcriptional targets identified here: the Forkhead factor and potential proto-oncogene, *FoxO6*, and the histone modifier, *Chd3*.

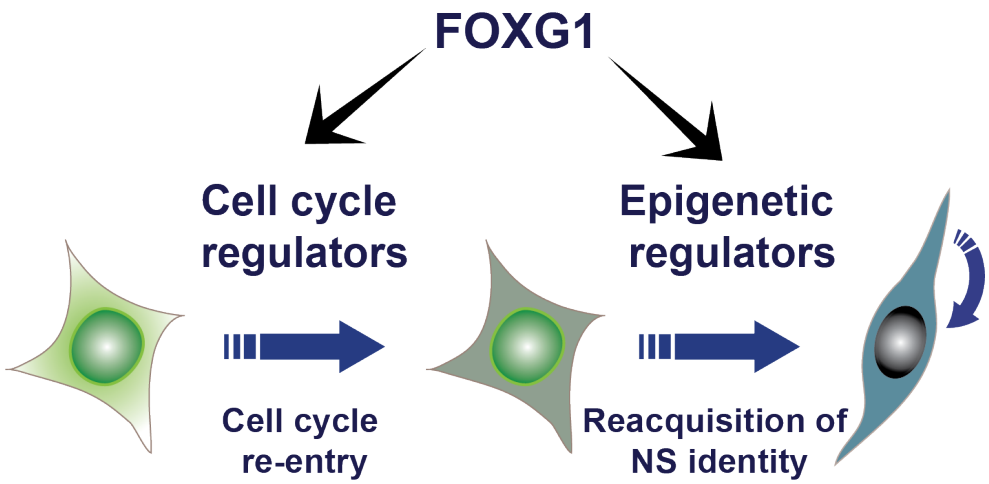

Figure 3-13 | FOXG1 enforces an NS cell identity through transcriptional control of cell cycle and epigenetic regulators.

Working model for FOXG1 function in GSCs (adapted from Bulstrode *et al*, 2017.). Green =astrocytic d-qNSC, blue = radial glia-like proliferative NS cell.

CHAPTER 4

FoxO6 is a functionally important transcriptional target of FOXG1

4.1 Introduction

In the previous chapter, two genes were identified as candidate transcriptional targets of FOXG1: the Forkhead factor, *FoxO6*, and the histone modifier, *Chd3*, showed the most dramatic transcript upregulation. In this chapter we further explore the roles of these two genes and use genetic knockout to identify FoxO6 as a functionally important target of FOXG1.

In mammals, the FoxO protein subclass consists of four members: FoxO1, FoxO3, FoxO4 and FoxO6. These factors have pleiotropic roles in proliferation, metabolism, differentiation and apoptosis; they have hence been implicated in ageing and cancer. However, FoxO6 is the most recently identified FoxO gene and the least well-studied. It also has some distinct characteristics compared to its other family members. While the activity of all FoxO family members is regulated by growth factor signalling via PKB-mediated phosphorylation, unlike the other family members phosphorylation status does not regulate FoxO6 nuclear-cytoplasmic shuttling. FoxO6 remains localised constitutively to the nucleus, even in the inactive form (van der Heide *et al*, 2005; Jacobs *et al*, 2003).

In addition, while other FoxO factors are relatively ubiquitously expressed, FoxO6 is predominantly expressed in the CNS of mammals (Salih *et al*, 2012; Hoekman *et al*, 2006). Similarly to FOXG1, FoxO6 is expressed at high levels in the developing foetal

brain, in a spatial and temporal pattern that suggests an important role in specifying cellular differentiation (Hoekman *et al*, 2006; Paap *et al*, 2016). In the adult brain, FoxO6 has been shown to have roles in both promoting memory consolidation and modulating synaptic functions in the hippocampus (Salih *et al*, 2012) and establishing polarity of neuronal processes (de la Torre-Ubieta *et al*, 2010). In other tissues, FoxO6 has reported metabolic roles, controlling hepatic glucose homeostasis (Kim *et al*, 2013) and oxidative metabolism in skeletal muscle (Chung *et al*, 2013). Furthermore, changes in FoxO6 expression are reported to regulate childhood facial development via Hippo signalling (Sun *et al*, 2018), and dendritic cell maturation (Kim *et al*, 2019).

Whilst emerging evidence suggests FoxO factors can have context-dependent roles in supporting cellular resilience of cancer cells, they are most well-known for their tumour suppressive functions (Hornsveld *et al*, 2018; Dansen & Burgering, 2008). For example, FoxO3 has been well-described in preserving quiescence and preventing premature differentiation of NS cells (Renault *et al*, 2009). The clinical relevance of FoxO6 in cancer biology is not fully understood; however, its levels have been shown to be upregulated in various cancer types, suggesting an oncogenic role. For example, FoxO6 has been reported to promote proliferation and regulate *c-Myc* expression in gastric cancer cells (Qinyu *et al*, 2013), whereas in lung cancer it has been reported to induce Sox2 expression in EGFR-inhibitor resistant cells (Rothenberg *et al*, 2015). More recent studies have implicated elevated FoxO6 with progression and poor prognosis in gastric cancer (Wang *et al*, 2017a) and breast cancer carcinogenesis (Lallemand *et al*, 2018). It is evident that FoxO6 has potentially important, yet underexplored, roles in development and cancer biology.

Chd3 is a component of the NuRD (nucleosome remodelling and histone deacetylase) complex, and has ATP-dependent chromatin remodelling activity (Lai & Wade, 2011). As

with other chromatin remodellers, the NuRD complex has been implicated in regulating transcriptional events vital to cancer progression. Chd3 itself was found to be one of 60 genes significantly associated with overall survival in GBM (Bao *et al*, 2013; Li *et al*, 2016). Both Chd3 and another core component of the NuRD complex, Chd4, can interact with transcription factors. For example, the co-repressor NAB2 can bind to the C-terminal domain of Chd3 to co-repress trans-activators involved in prostate cancer progression (Srinivasan *et al*, 2006). Association of Chd4 to the transcription factor ZFHX4 has been implicated in maintenance of tumour-initiating cells in GBM by transcriptional regulation of targets such as Myc, PDGFRβ and tumour suppressors such as SPRY1 (Chudnovsky *et al*, 2014).

As described in section 1.3.5, epigenetic modifications have been widely implicated in GBM tumorigenesis. In light of the 'epigenetic progenitor' hypothesis of tumour progression, epigenetic changes may occur early in tumorigenesis (Feinberg *et al*, 2006; Stricker & Pollard, 2014). However, since these epigenetic changes may be reversible and may also have roles in CSC maintenance, they pose interesting therapeutic targets. For example, there is interest in the use of demethylating agents and HDAC inhibitors to reactivate tumour suppressors and other transcription factors aberrantly silenced in cancer (Safa *et al*, 2016). Furthermore, addition of inhibitors of epigenetic modifiers to DNA damaging agents has been shown to enhance their effectiveness, possibly by enhancing access by creating a more open chromatin landscape (Carén *et al*, 2013).

Given this literature, we therefore wanted to further investigate the roles of FoxO6 and Chd3 in GBM in relation to FOXG1. In this chapter, we use some of the *in vitro* mouse and human models of GBM described in the introduction, along with CRISPR/Cas9 technology, to validate whether *FoxO6* and *Chd3* are downstream targets of FOXG1 in alternative contexts.

4.2 Validation of *FoxO6* as a downstream target of FOXG1

4.2.1 *FoxO6* mRNA expression increases in response to elevated FOXG1 in proliferating NSCs

While reactivation of astrocytic d-qNSCs provides a convenient system to identify FOXG1's transcriptional targets, it is also important to ascertain whether these transcriptional targets are regulated in alternative contexts. For example, does FOXG1 also regulate FoxO6 in proliferating NS cells? If so, this may suggest a role in both initiating and maintaining a proliferative NS cell state. To answer this question, *FoxO6* mRNA levels were assessed following Dox-induced FOXG1 overexpression in proliferating NS cells (cultured in EGF and FGF-2). Two independent FOXG1-inducible clonal adult mouse NS cell lines were assessed (F6 and F11-19). We found a significant increase in *FoxO6* expression for both cell lines, of ~17-fold and ~4-fold in F6 and F11-19, respectively (Figure 4-1). While F6 and F11-19 exhibited similar fold-increases in *FOXG1* expression with Dox, the absolute normalised expression was higher in F6, possibly leading to increased *FoxO6* activation. *FoxO6* is therefore a transcriptional target of FOXG1 in both proliferating NSCs, as well as during d-qNSC reactivation.

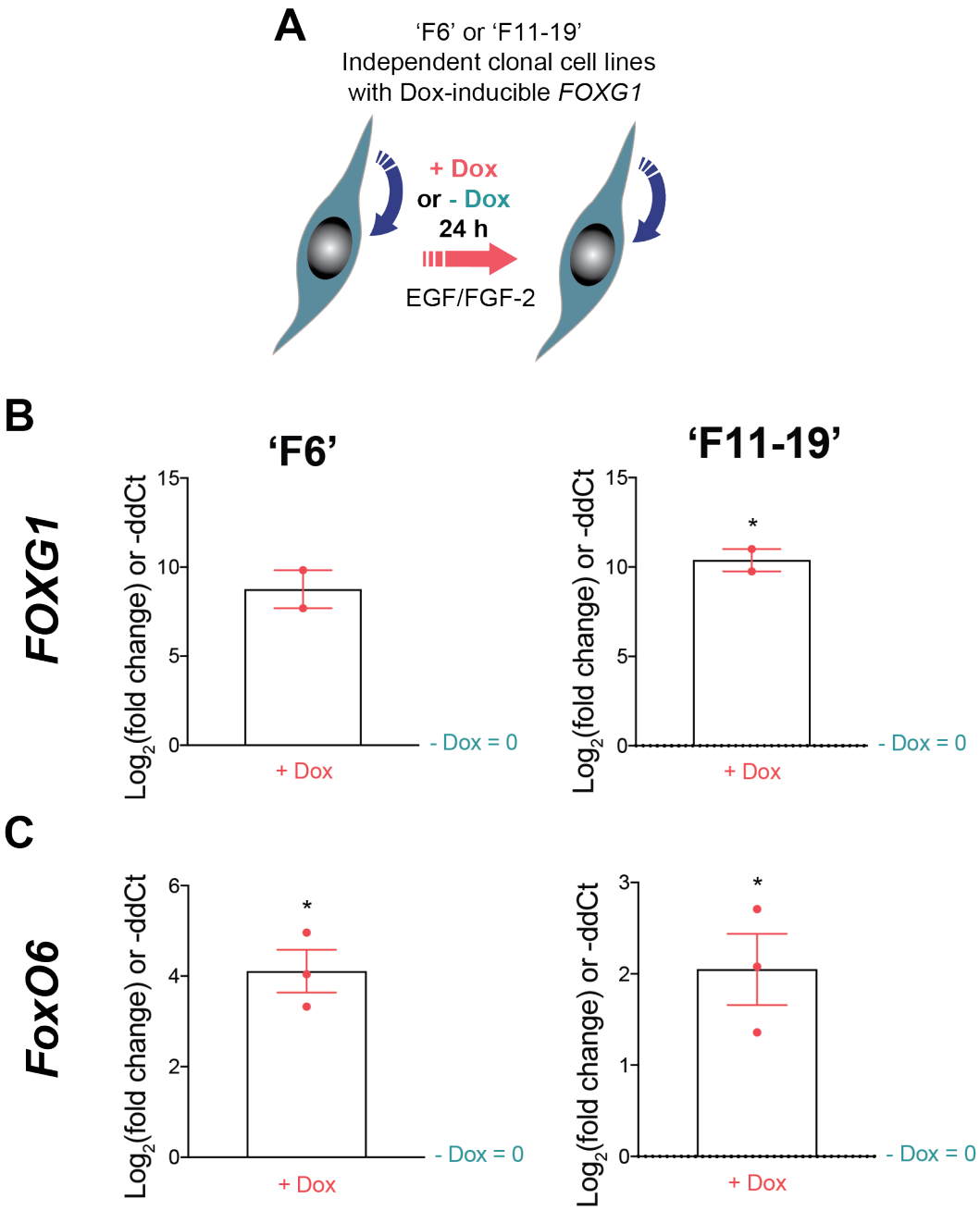

Figure 4-1 | *FoxO6* mRNA levels are increased in response to FOXG1 overexpression in proliferating NSCs.

(A) Schematic of experimental set-up: adult mouse NS cell lines ('F6' and 'F11-19') with Dox-inducible *FOXG1* expression were grown in NS cell media (EGF/FGF-2) with or without Dox for 24h. **(B)** qRT-PCR analysis of *FOXG1* mRNA levels in F6 and F11-19. n=2 independent experiments. Each data point shows the mean of one experiment, performed in technical duplicates. **(C)** qRT-PCR analysis of *FoxO6* mRNA levels in F6 and F11-19. n=3 independent experiments. Each data point shows the mean of one experiment, performed in technical duplicates. Expression values were normalised to *Gapdh* and shown relative to the expression in EGF/FGF-2 -Dox (in which $\log_2(FC) = 0$). Y axis represents $\log_2$(Fold change), equivalent to -ddCt value. Graph shows Mean +/- SEM. Statistics were calculated from ddCt values. Two-tailed one sample t-test. * $P \leq 0.05$.

4.2.2 FOXO6 protein levels increase in response to elevated FOXG1

To validate that FOXG1 overexpression leads to upregulation of FOXO6 at the protein level, several anti-FOXO6 antibodies were tested by ICC and Western blotting. Unfortunately, out of three commercial antibodies tested, none showed specific staining by ICC, nor a specific band at the correct molecular weight (~70 kDa) by Western blotting. It was therefore necessary to knock-in an epitope-tag to enable monitoring of FOXO6 protein levels and localisation. This was achieved using a CRISPR/Cas9 method optimised by Raul Bressan and Pooran Dewari in the Pollard lab, and described later in Chapter 5 (Bressan *et al*, 2017; Dewari *et al*, 2018).

The epitope tag was introduced in F6 cells at the 3' end of *FoxO6* using a pre-assembled Cas9/ cr/tracrRNA ribonucleoprotein (RNP) complex that cuts close to stop codon. The resulting double-strand break (DSB) was repaired by homology-directed repair (HDR) using a co-transfected single-stranded oligonucleotide donor DNA template (Figure 4-2 A). We chose an HA tag, which is commonly used for biochemical and ICC studies. Successful insertion of the HA tag was confirmed using PCR genotyping of the bulk transfected population (Figure 4-2 B). FOXO6-HA expression was not visible by ICC or Western blotting in proliferating NS cells, consistent with the lower levels of mRNA detected by qRT-PCR (Figure 4-1). However, following addition of Dox and hence induction of *FOXG1* transgene expression in the bulk transfected population, a clear increase in FOXO6-HA protein level was observed (Figure 4-2 C-E).

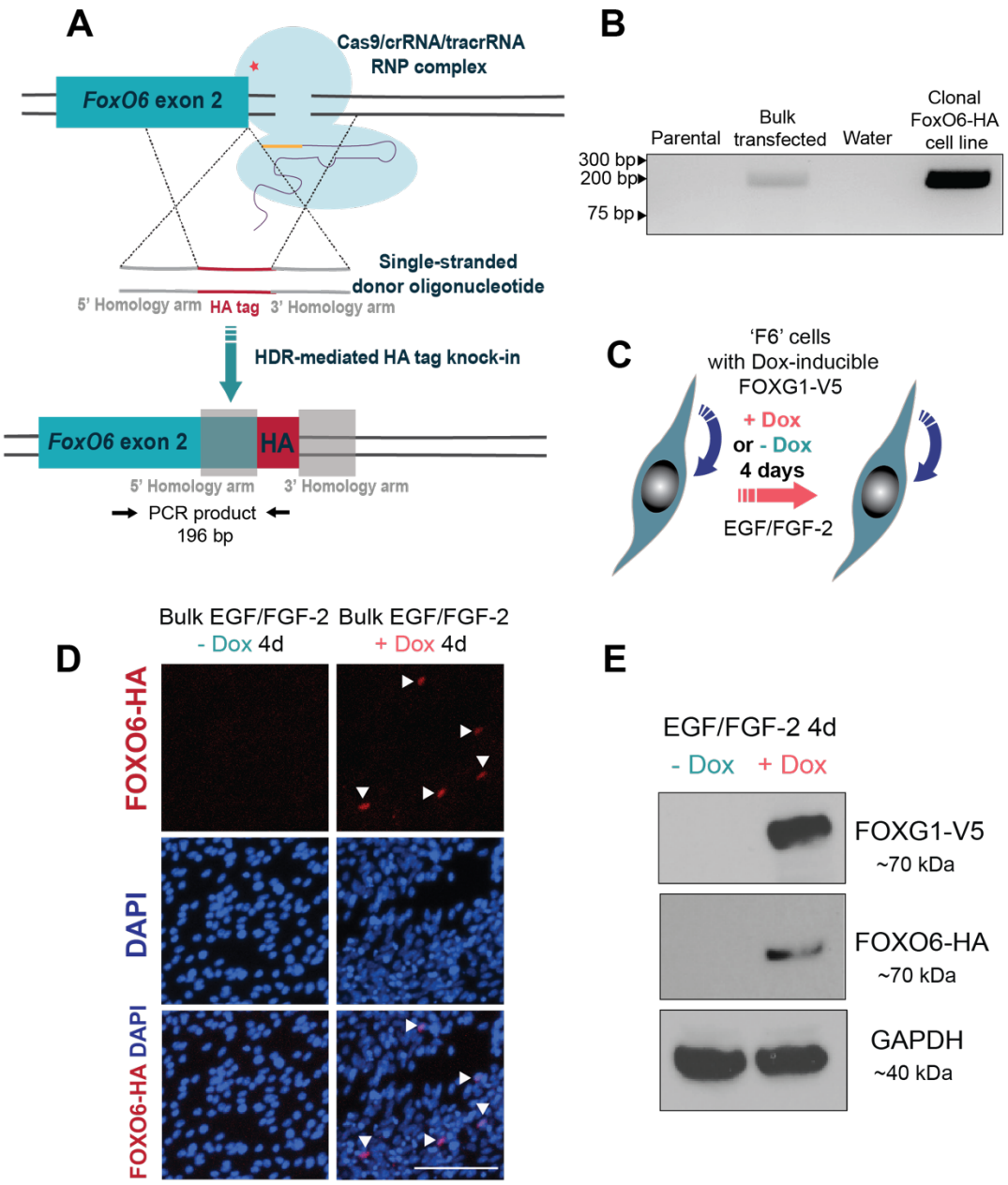

Figure 4-2 | FOXO6 protein levels increase in response to elevated FOXG1.

(A) Schematic of HDR-mediated knock-in of an HA epitope tag at the 3' end of the second, and last, *FoxO6* coding exon in F6 cells. Cells are transfected with a pre-assembled Cas9/cr/tracrRNA ribonucleoprotein (RNP) complex and a single-stranded oligonucleotide donor containing the epitope tag flanked by 3' and 5' homology arms. **(B)** PCR genotyping of the bulk transfected F6 cell population revealed a 196 bp product, indicating the presence of cells with insertion of the HA tag at the 3' end of *FoxO6*. Clonal F6 FoxO6-HA cell line shown as positive control. **(C)** Schematic describing treatment of F6 *FoxO6*-HA bulk population for assessment of FOXO6 protein levels following FOXG1 induction. **(D)** ICC images of F6 *FoxO6*-HA bulk population with and without Dox addition for 4 days. Scale bar: 100 µm. **(E)** Western blot analysis of FOXG1-V5 and FOXO6-HA protein levels in the F6 *FoxO6*-HA bulk population with and without Dox addition for 4 days. GAPDH was used as a loading control. Performed by C. Blin (Pollard lab).

4.2.3 *FoxO6* mRNA is reduced following *Foxg1* knock-out in mouse GSCs

Following the validation that FoxO6 levels increase in response FOXG1 overexpression, we next investigated how FoxO6 levels change in response to FOXG1 downregulation. An available mouse glioma-initiating cell line, IENS, provided a useful model to explore this (a gift from Prof M. Lohuizen). IENS are derived from cortical astrocytes of postnatal day 7 *Cdk2na*$^{-/-}$ mice, and therefore lack *Ink4a/ARF*; these cells were then transduced with EGFRvIII retrovirus (Bruggeman *et al*, 2007). They therefore possess two common GBM genetic aberrations. IENS cells express FOXG1 at higher levels than normal adult mouse NS cells and are tumorigenic upon xenotransplantation (Bulstrode *et al*, 2017). CRISPR/Cas9 technology has been shown to provide a useful tool for bi-allelic knock-out of neurodevelopmental genes in NS cells (Bressan *et al*, 2017). We therefore engineered IENS cells with bi-allelic deletion of *Foxg1* (Figure 4-3 A). This was performed in IENS cells with constitutive GFP expression, termed 'IENS-GFP'.

Single guide RNA (sgRNA)-encoding plasmids, targeting the 5' and 3' ends of the mouse *Foxg1* coding exon, had previously been designed and cloned into expression vectors under control of a U6 promoter (R. Bressan and M. Kalantsaki, respectively). Alongside a wild-type Cas9-2A-mCherry expression vector, these sgRNAs were transiently delivered into IENS-GFP by nucleofection. Successful transfectants were isolated using FACS for mCherry expression (Figure 4-3 B). ICC analysis confirmed the presence of *Foxg1*$^{-/-}$ cells in the sorted population. Clonal cell lines were derived by plating the sorted cells at clonal density. Clonal cell lines were assessed for FOXG1 protein expression by ICC. Successful transfection would result in two DSBs at the sgRNA cutting sites at the 5' and 3' end of the coding exon; indel formation and non-homologous end-joining (NHEJ) of the two resulting ends would result in the loss of approximately 1.3 kb of coding sequence and most likely a frameshift. Out of 60 clones analysed, 15 showed evidence of

Foxg1 disruption in at least one allele. Three clonal cell lines (54, 58 and 59) were selected for further analysis. PCR genotyping revealed both 58 and 59 showed a single band at ~1.3 kb less than the wild-type 2.6 kb PCR product (Figure 4-3 C). These lines were confirmed to have bi-allelic deletion of *Foxg1* by ICC and Western blotting (Figure 4-3 D and E).

An independent mouse GBM model cell line with the same mutations as IENS (EGFRvIII overexpression and *Ink4a/Arf* deletion) was created in the lab by Dr Ester Gangoso (Figure 4-3 F). This transformed cell line, termed FF-IEK, was derived from adult mouse NS cell line 'FF', derived from the SVZ of homozygous adult *Foxg1*$^{fl/fl}$ mice by H.Bulstrode (mice provided V. Fotaki; originally produced by the Fischell lab, (Miyoshi & Fishell, 2012). Addition of Cre recombinase to these cells resulted in deletion of *Foxg1*, as confirmed by Western blotting (Figure 4-3 G).

qRT-PCR analysis was performed in these two independent cell lines (IENS-GFP and FF-IEK) alongside their respective *Foxg1* knockout clones. In both cases, this revealed a trend for downregulation of *FoxO6* mRNA levels upon *Foxg1* deletion (Figure 4-4). IENS-GFP *Foxg1* KO cell lines 58 and 59 showed a mean 6-7-fold (84-86%) decrease in *FoxO6* mRNA levels, whereas FF-IEK *Foxg1*$^{-/-}$ cells showed an ~1.5-fold (~30%) reduction. These data confirm that FOXG1 is necessary to sustain *FoxO6* expression.

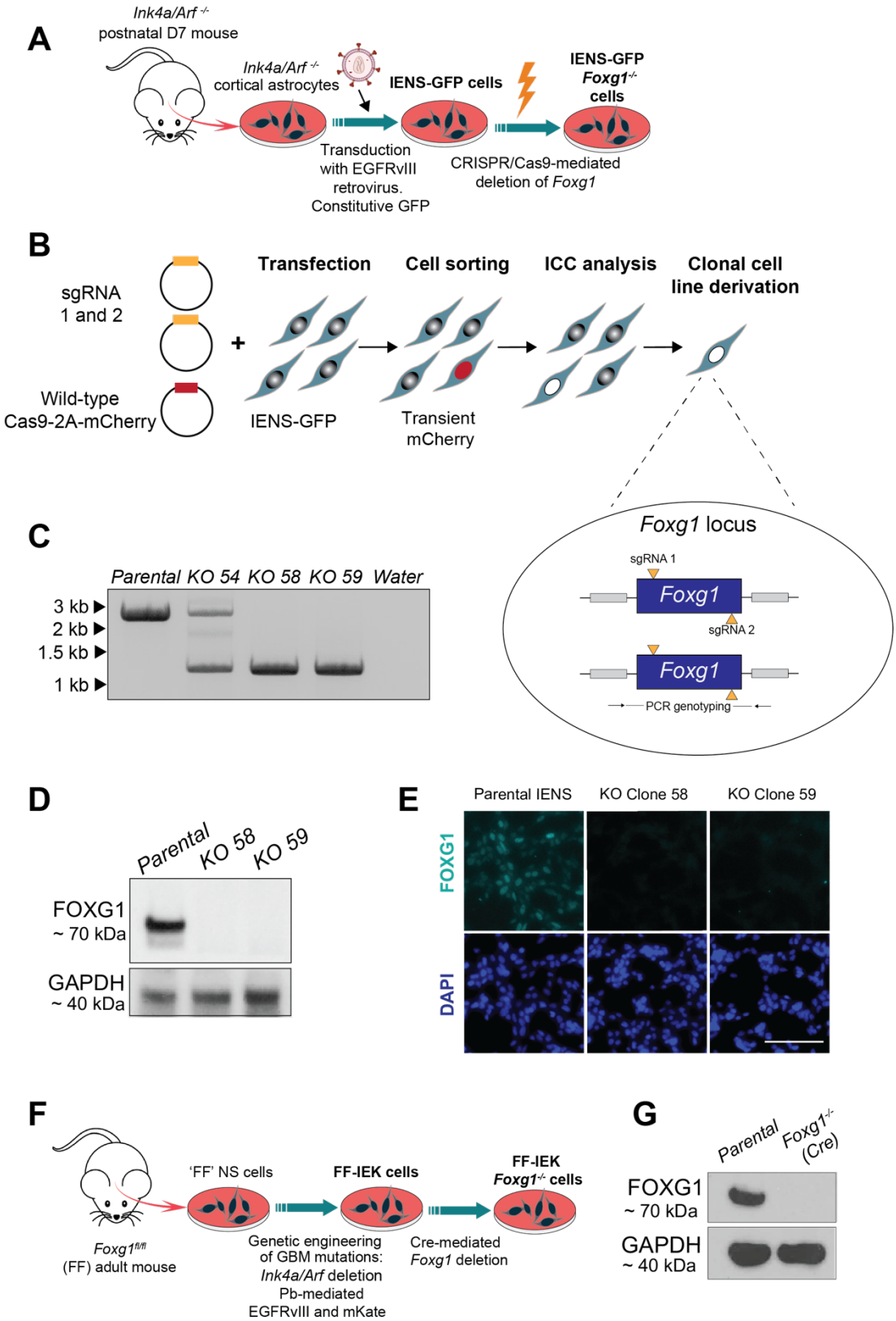

Figure 4-3 | *Foxg1* knockout in mouse GSC line, IENS, via CRISPR/Cas9-induced NHEJ.

(A) Schematic describing derivation of *Foxg1* $^{-/-}$ mouse GBM model IENS cells. **(B)** Experimental strategy for *Foxg1* deletion in IENS-GFP cells. *Figure legend continued overleaf.*

Yellow triangles show the target sites of the sgRNAs at either the 5' or 3' end of the coding exon. **(C)** PCR genotyping of parental IENS-GFP cells and *Foxg1* KO clonal cell lines, 54, 58 and 59. Wild-type PCR product ~2.6 kb, knockout PCR product ~1.3 kb. **(D)** Western blot analysis confirms loss of FOXG1 protein expression in IENS-GFP *Foxg1* KO 58 and 59 (performed by Carla Blin). **(E)** ICC analysis confirms loss of FOXG1 protein expression in IENS-GFP *Foxg1* KO 58 and 59. Scale bar: 100 μm. **(F)** Schematic describing derivation of *Foxg1*$^{-/-}$ mouse GSC line 'FF-IEK' (by Dr Ester Gangoso). **(G)** Western blot analysis confirms loss of FOXG1 protein expression on Cre addition to FF-IEK cells.

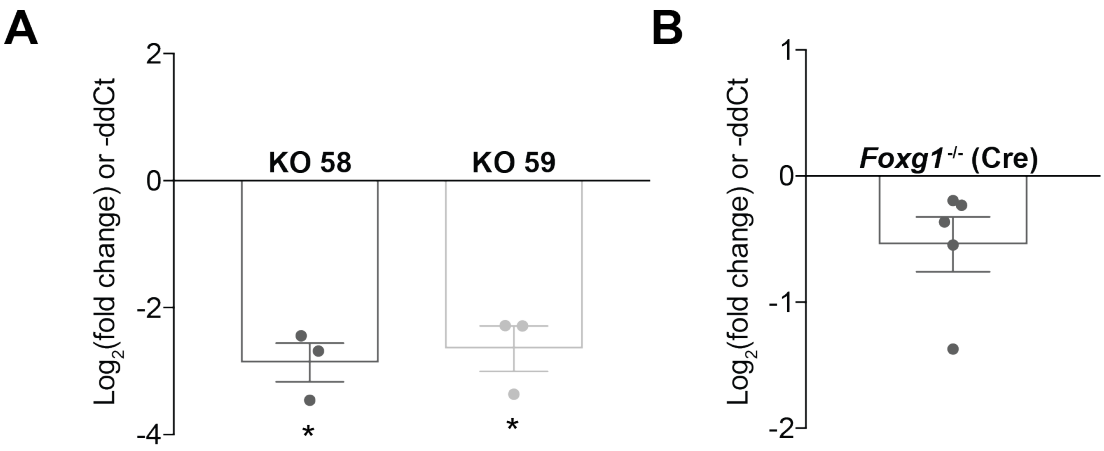

Figure 4-4 | *FoxO6* mRNA is reduced following *Foxg1* knock-out in mouse GSCs.

(A) qRT-PCR analysis of *FoxO6* mRNA levels in IENS-GFP *Foxg1* KO clonal cell lines 58 and 59, compared to parental IENS-GFP (in which in which log_2(FC) = 0). Expression values were normalised to *Gapdh*. Y axis represents log_2(Fold change), equivalent to -ddCt value. Mean +/- SEM. n=3 independent experiments. Each data point shows the mean of one experiment, performed in technical duplicates. **(B)** qRT-PCR analysis of *FoxO6* mRNA levels in FF-IEK *Foxg1*$^{-/-}$ cells (Cre addition), compared to parental 'FF-IEK' (in which in which log_2(FC) = 0). n=5 independent experiments. Each data point shows the mean of one experiment, performed in technical duplicates. Mean +/- SEM. Statistics were calculated from ddCt values. Two-tailed one sample t-test. * $P \leq 0.05$.

4.2.4 FoxO6 is not essential for NS cell proliferation in EGF/FGF-2 or response to BMP4 signalling.

Following validation that FoxO6 is a downstream target of FOXG1 in multiple contexts, we next wanted to define whether these elevated levels are necessary to enforce a proliferative NS-cell like identity. Gene targeting to delete *FoxO6* from adult mouse NS (ANS4) cells was previously performed by Claudia Garcia-Diaz using a CRISPR/Cas9 strategy described in Bressan *et al.* (2017). A clonal *FoxO6* knockout cell line was derived (clone 53). In one allele, exon 1 of *FoxO6* is replaced by an EF1α-puromycin cassette, whereas the remaining allele is targeted by a sgRNA resulting in NHEJ and indel formation. Previous analysis confirmed correct targeting of the EF1α-puromycin cassette and a 178 bp deletion across the start codon of *FoxO6* in the remaining allele (Figure 4-5 A). PCR genotyping was repeated on both parental ANS4 and *FoxO6* KO 53 cells; this showed a single band, approximately ~178 bp smaller in size than the wild-type PCR product, confirming clone 53 contains no wild-type *FoxO6* sequence (Figure 4-5 B). Due to the lack of available FOXO6-specific commercial antibodies, protein analysis could not be performed. qRT-PCR analysis confirmed negligible *FoxO6* expression in comparison to the parental control (Figure 4-5 C); *FoxO6* KO clone 53 showed an ~ 55-fold (98%) decrease in expression.

Analysis of the growth kinetics of *FoxO6* KO cells in EGF/FGF-2 showed a modest decrease in proliferation compared to parental ANS4 cells (Figure 4-6 A). This was assessed by measuring the slope of the linear portion of the logistic growth curve (% confluence over time in hrs) (Figure 4-6 B). EdU incorporation after a 24 h pulse at day 3 of the growth analysis, however, did not show any significant difference in proliferation (Figure 4-6 C and D). The ability of *FoxO6* KO cells to form colonies was also assessed after 10 days in NS cell media (EGF/FGF-2) following plating at low density (1000 cells

per 6 well). This revealed that *FoxO6* KO cells are able to form typical NS cell colonies (Figure 4-6 E). Parental ANS4 cells showed inconsistent results between independent replicates, therefore it was not possible to conclude whether deletion of *FoxO6* significantly alters the efficiency of colony formation (Figure 4-6 F). These results indicate that *FoxO6* is not essential for proliferation or colony formation of NSCs in EGF/FGF-2.

Next we assessed the ability of *FoxO6* KO cells to respond to BMP4 signalling. ICC analysis revealed both parental ANS4 and *FoxO6* KO 53 cells show a decrease in Nestin and increase in Gfap expression after 3 days of BMP4 treatment (Figure 4-7 A and B). Similarly, qRT-PCR analysis showed that both cell lines decrease *Nestin* and *Olig2* mRNA levels and increase *Gfap* and *Aqp4* mRNA levels on treatment with BMP4 for 1 day. No significant differences in expression levels of *Olig2, Gfap* or *Aqp4* were found between parental ANS4 and *FoxO6* KO cells after BMP4 treatment (Figure 4-7 C and D), although *Nestin* levels were slightly lower in *FoxO6* KO cells. Finally, assessment of EdU incorporation following BMP4 treatment for 1 day and a 24h EdU pulse in EGF/FGF-2 revealed no significant difference between the cell lines, with both showing negligible EdU incorporation following BMP4 treatment. 24h of EdU pulse was chosen as this is the typical doubling time of mouse NS cells. While negligible, it was noted that a couple of EdU positive ANS4 cells (<1%) were observed, but none for *FoxO6* KO cells. Thus, FoxO6 is not required for proliferative NSCs to exit the cell cycle and upregulate astrocytic markers in response to BMP4 signalling.

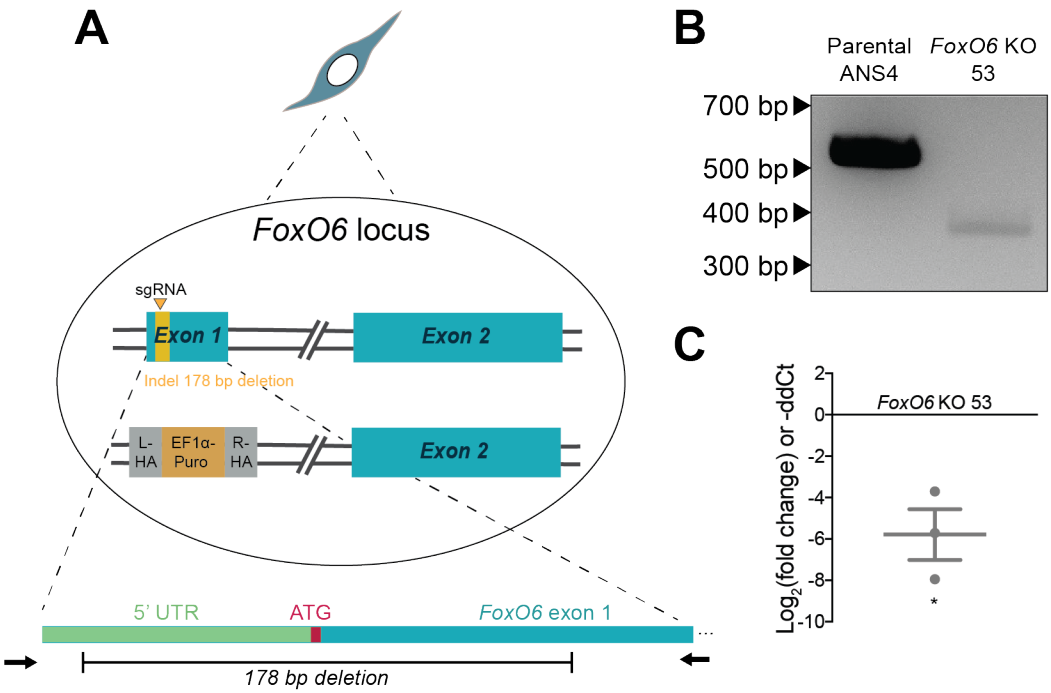

Figure 4-5 | *FoxO6* knockout in adult mouse NS cells.

FoxO6 knockout from ANS4 cells performed by Claudia Garcia-Diaz. **(A)** Schematic of *FoxO6* locus following CRISPR/Cas9-mediated knockout strategy. Yellow triangle shows the target site of the sgRNA, resulting in a 178 bp deletion in allele 1 in *FoxO6* knockout clone 53. Exon 1 of allele 2 is replaced by an EF1α-puromycin cassette (strategy as described in (Bressan *et al*, 2017). **(B)** PCR genotyping of parental ANS4 and *FoxO6* KO 53 cells. WT band = 565 bp, knockout band = 387 bp. **(C)** qRT-PCR analysis of *FoxO6* mRNA levels in *FoxO6* KO 53 cells, compared to ANS4 parental cells (in which $\log_2$(FC) = 0). Expression values were normalised to *Gapdh*. Y axis represents $\log_2$(Fold change), equivalent to -ddCt value. Mean +/- SEM. n=3 independent experiments. Each data point shows the mean of one experiment, performed in technical duplicates. Statistics were calculated from ddCt values. Two-tailed one sample t-test. * $P \leq 0.05$.

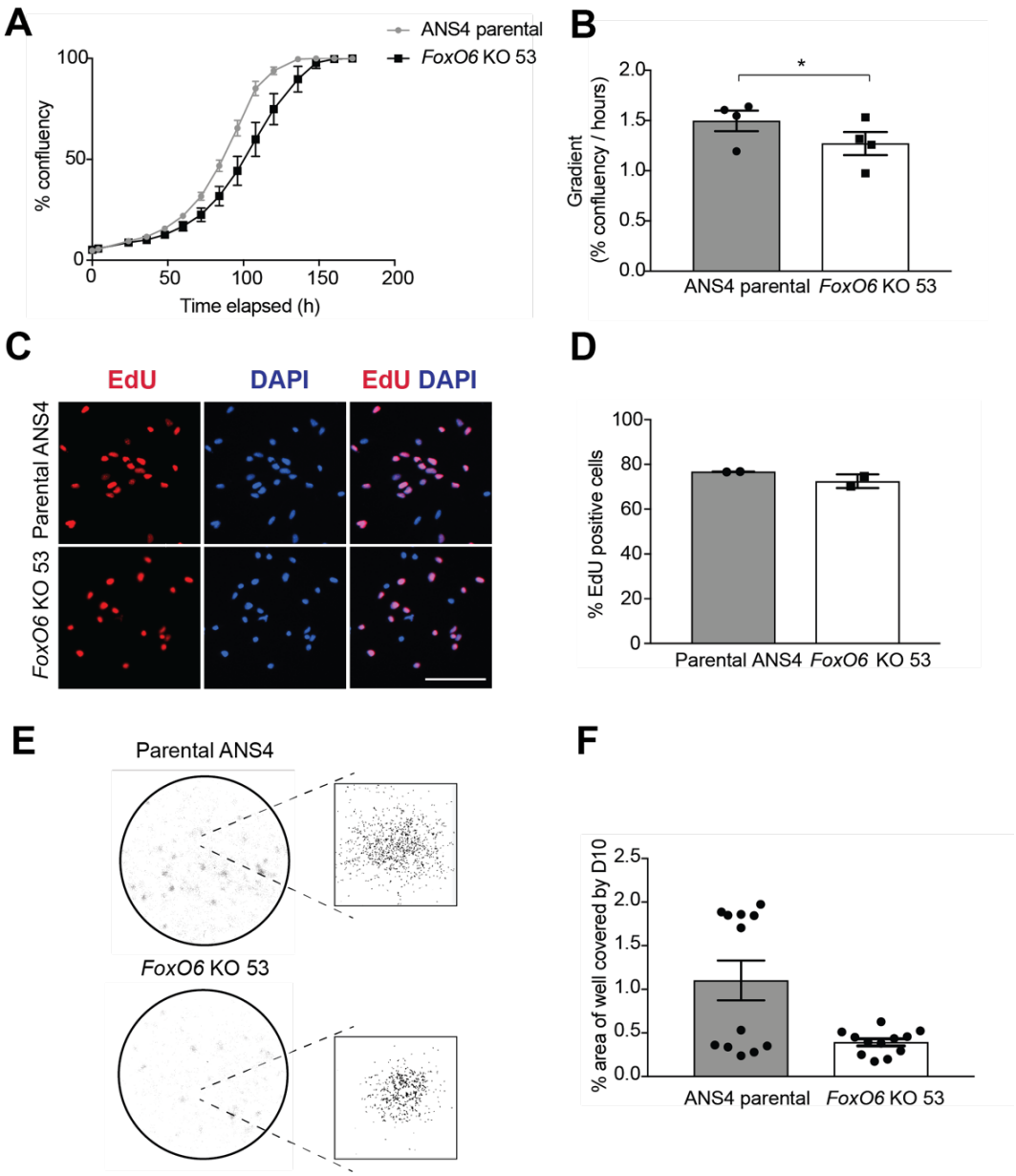

Figure 4-6 | *FoxO6* is not essential for NSC proliferation or colony formation in EGF/FGF-2.

(A) Growth curve displaying percentage confluence versus time in EGF/FGF-2. Light grey = ANS4 parental, black = *FoxO6* KO 53. Mean +/- SD, n=3 technical replicates. Representative of n=4 independent experiments. **(B)** Bar graph showing the gradient of the linear portion of the logistic growth curve (%/h). Mean +/- SEM, n=4 independent experiments. Each data point shows the mean of one experiment. Two-tailed paired Student's t-test. (* $P \leq 0.05$). **(C)** Representative fluorescent images of EdU incorporation after 24 h pulse on day 3 of growth analysis (ANS4 parental and *FoxO6* KO 53 cells). Scale bar: 100 µm. **(D)** Quantification of % EdU positive cells after 24 h pulse on day 3 of growth analysis. Mean +/- SEM, n=2 independent experiments. Each data point shows the mean of one experiment, performed in technical triplicates. **(E)** Representative images of colony formation by parental ANS4 or *FoxO6* KO 53 cells 10 days after plating at low density. Plates stained with methylene blue. **(F)** Quantification of percentage of the well area covered by cells after 10 days (pixel area). Mean +/- SEM. n=2 independent experiments, each with 6 technical replicates. Each data point represents one technical replicate.

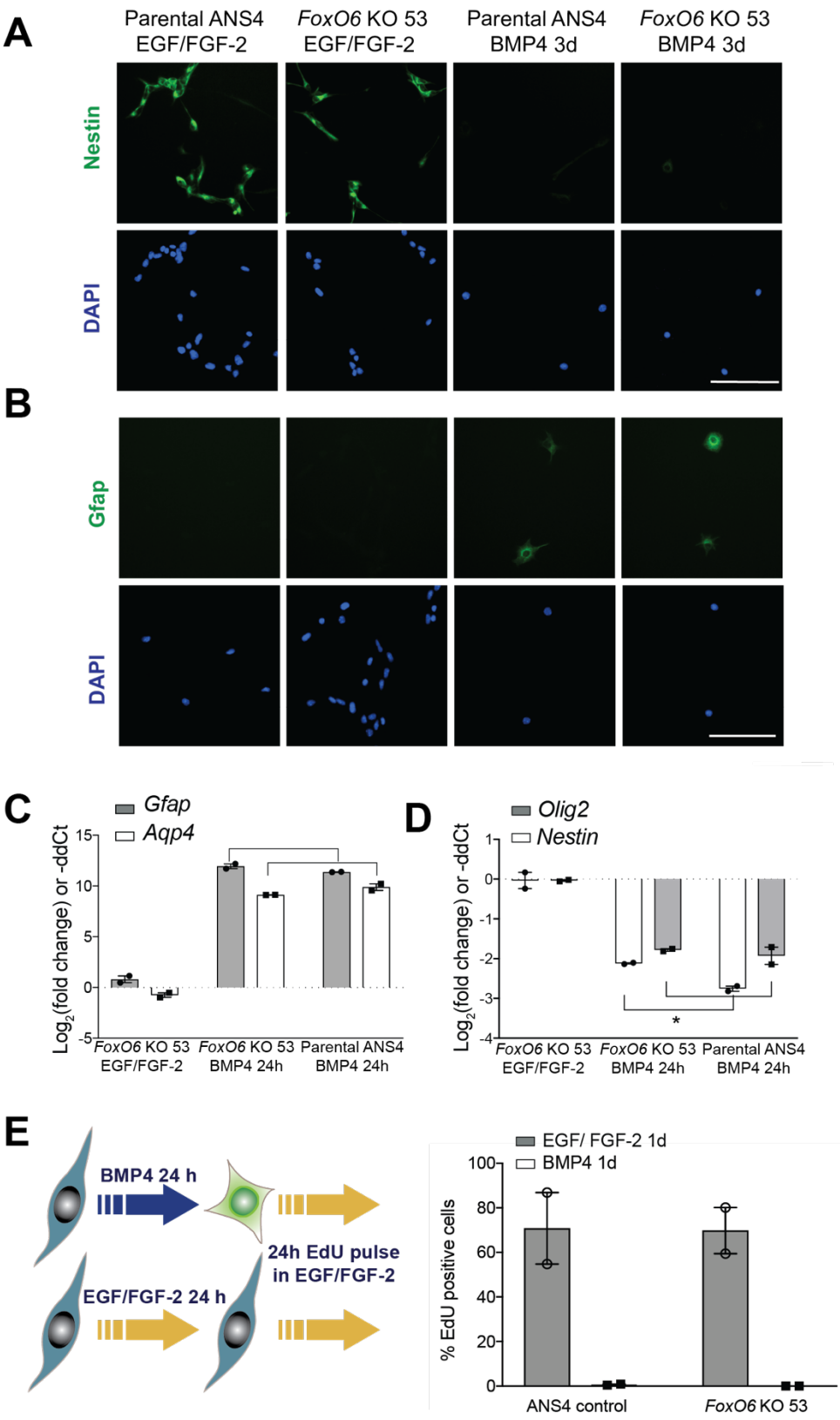

Figure 4-7 | *FoxO6* is not required for proliferative NSCs to exit the cell cycle and upregulate astrocytic markers in response to BMP4 signalling. *Figure legend continued overleaf.*

Immunofluorescent images showing **(A)** Nestin and **(B)** Gfap expression in parental ANS4 or *FoxO6* KO 53 cells after treatment with EGF/FGF-2 or BMP4 for 3 days. Scale bar: 100 μm. **(C)** qRT-PCR analysis of mRNA expression levels of *Gfap* and *Aqp4,* **(D)** *Nestin* and *Olig2*, in parental ANS4 or *FoxO6* KO 53 cells after treatment with EGF/FGF-2 or BMP4 for 3 days. Expression values were normalised to *Gapdh* and shown relative to the expression in parental ANS4 cells in EGF/FGF-2 (in which $\log_2$(FC) = 0, shown by the dotted line). Y axis represents $\log_2$(Fold change), equivalent to -ddCt value. Graph shows Mean +/- SEM. n=2 independent experiments. Each data point shows the mean of one experiment, performed in technical duplicates. Statistics were calculated from ddCt values. Two-tailed Student's t-test. * $P \leq 0.05$ **(E)** Quantification of % cells with EdU incorporation after treatment with BMP4 or EGF/FGF-2 for 1d, followed by a 24 h EdU pulse in EGF/FGF-2 (ANS4 parental and *FoxO6* KO 53). Mean +/- SEM. n=2 independent experiments. Each data point shows the mean of one experiment, performed in technical triplicates.

4.2.5 FOXG1-induced reactivation of dormant quiescent NSCs is inhibited in *FoxO6* null cells

With the knowledge that *FoxO6* loss does not have a significant negative effect on proliferation in EGF/FGF-2 or BMP4 induction of an astrocytic d-qNSC state, we next set out to determine if loss of *FoxO6* affects the efficiency of FOXG1-induced colony formation. Both ANS4 and *FoxO6*-null mouse NS cells (clone 53) were transfected with expression vectors encoding the PiggyBac transposase, Tet-On 3G transactivator and Dox-inducible FOXG1-V5 expression cassette, as previously described in Figure 3-4 (Figure 4-8 A). Following antibiotic selection for 7 days (in which all mock-transfected control cells died), the remaining cells were expanded, resulting in a mixed population of cells harbouring varying copy numbers of the *FOXG1* transgene. These cells (ANS4 and *FoxO6* KO 53, with inducible FOXG1-V5 overexpression) were each re-plated in BMP4 to assess the efficiency of FOXG1-induced colony formation, as in section 3.2.2.

The level of transgene induction was monitored in both cell lines by qRT-PCR analysis of *FOXG1* mRNA levels (Figure 4-8 B) and ICC for FOXG1-V5 expression (Figure 4-8 C and D). Parental ANS4 cells showed slightly lower, but statistically insignificant, levels of V5 positive cells and *FOXG1* mRNA after four days in EGF/FGF-2 with Dox, compared to the FoxO6 KO cells. Assessment of colony formation revealed that parental ANS4 cells were able to form colonies upon induction of FOXG1. However, *FoxO6*-null cells showed significantly reduced colony formation, despite their slightly higher levels of *FOXG1* transgene induction (Figure 4-8 E-G). This result indicates that *FoxO6* may be a key downstream effector of FOXG1 in driving d-qNSCs back into cycle.

ICC analysis confirmed that, unlike ANS4, levels of Nestin were not highly upregulated in the *FoxO6* KO cells on addition of Dox (compared to no Dox control) (Figure 4-9 A). However, the *FoxO6* KO cells did show a change in morphology on induction of FOXG1,

from a fried-egg, stellate astrocytic morphology, to an elongated spindle shape (Figure 4-9 A and C). In addition, some *FoxO6* KO cells with high Ki67 expression were visible on addition of Dox (Figure 4-9 C). Assessment after an extended period in EGF/FGF-2 +Dox (25 days) revealed evidence of some colony formation by the *FoxO6* KO cells. (Figure 4-9 D). Indeed, in one replicate an average of 9 colonies per well formed in *FoxO6* KO cells, compared to ~72 in ANS4 wild-type after 10 days (Figure 4-8 F). This suggests that while *FoxO6* KO cells are able to respond in some form to *FOXG1* overexpression, FoxO6 expression is required for BMP4 treated cells to transition to a highly proliferative NS cell-like state.

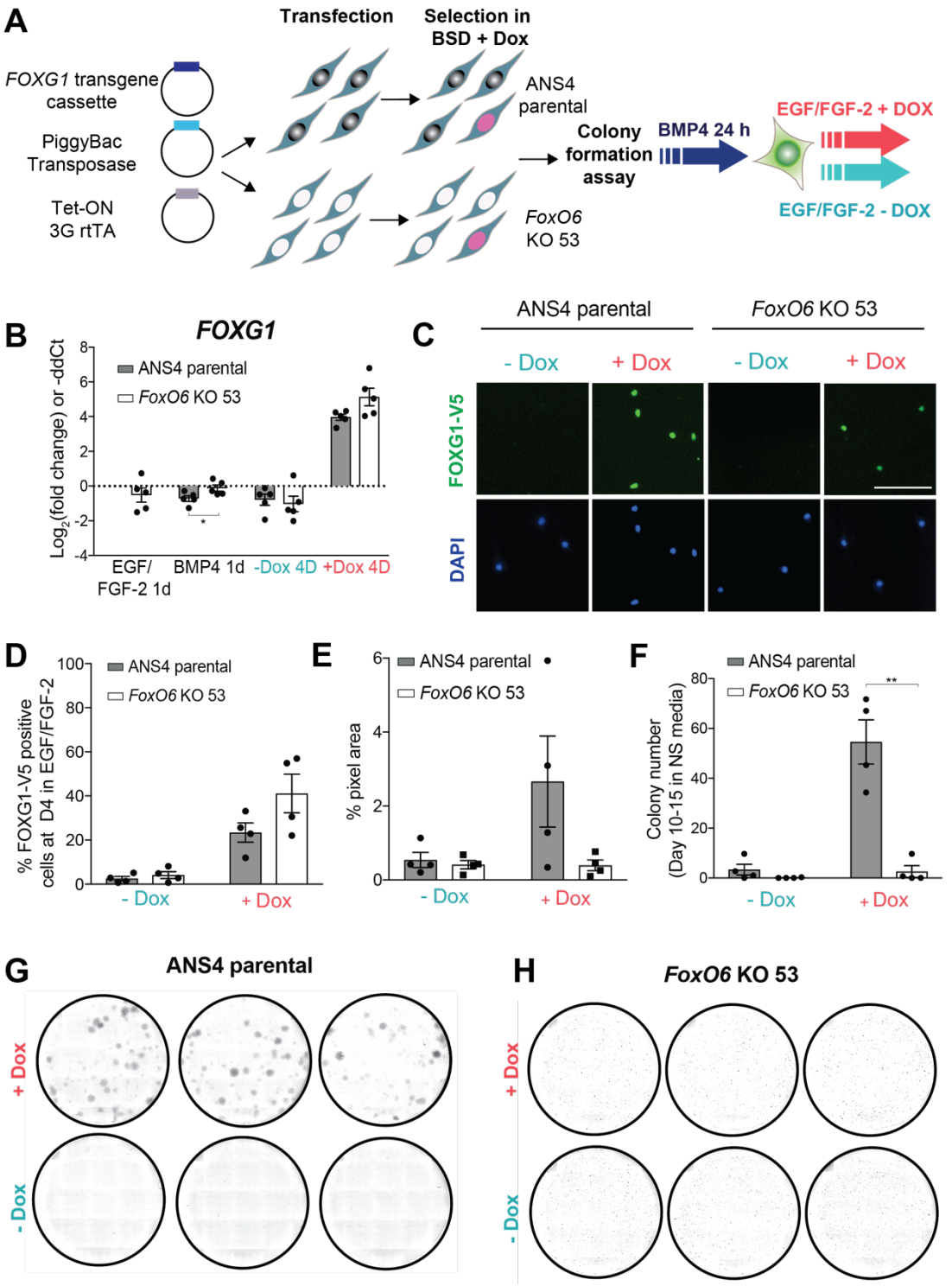

Figure 4-8 | Deletion of *FoxO6* restricts the ability of FOXG1 to drive exit from quiescence.

(A) Schematic of PiggyBac transposon strategy used to derive ANS4 parental and *FoxO6* KO 53 cells with Dox-inducible FOXG1 expression (as shown in Figure 3-4). In panels (B)-(H) ANS4 parental and *FoxO6* KO 53 refer to transfected cell populations with Dox-inducible FOXG1-V5 overexpression. *Figure legend continued overleaf.*

(B) qRT-PCR analysis of mRNA expression levels of human *FOXG1* in parental ANS4 or *FoxO6* KO 53 cells, at time points during the colony formation assay. Expression values were normalised to *Gapdh* and shown relative to the expression in ANS4 EGF/FGF-2 control (in which $\log_2(FC) = 0$). Y axis represents $\log_2$(Fold change), equivalent to -ddCt value. Graph shows Mean +/- SEM. n=5 independent experiments. Each data point shows the mean of one experiment, performed in technical duplicates. Statistics were calculated from ddCt values. Two-tailed paired t-test. **(C)** Representative ICC images showing FOXG1-V5 expression at Day 4 in NS cell media (EGF/FGF-2) with or without Dox addition in both transfected parental ANS4 and *FoxO6* KO 53 cells (following 24 h BMP4 treatment). Scale bar: 100 μm**. (D)** Quantification of percentage of ANS4 parental or *FoxO6* KO 53 cells expressing FOXG1-V5 (assessed by ICC) after 4 days in NS cell media (EGF/FGF-2) with or without Dox (following 24 h BMP4 treatment). Graph shows Mean +/- SEM. n = 4 independent experiments. Each data point shows the mean of one experiment, performed in technical triplicates. Two-tailed paired t-test. **(E)** Quantification of percentage of the well area covered by cells after 24 h BMP4 treatment and return to NS cell media with or without Dox for 10-15 days (ANS4 parental or *FoxO6* KO 53). Mean +/- SEM. n=4 independent experiments. Each data point shows the mean of one experiment, performed in technical triplicates. **(F)** Numbers of colonies formed after 24 h BMP4 treatment and return to NS cell media with or without Dox for 10-15 days (ANS4 parental or *FoxO6* KO 53). Graph shows Mean +/- SEM, n= 4 independent experiments. Each data point shows the mean of one experiment, performed in technical triplicates. Two-tailed paired Student's t-tests. (* $P \leq 0.05$, ** $P \leq 0.01$). **(G)** Example ANS4 colony assay at day 10 in EGF/FGF-2, with or without Dox. Plate fixed and stained with methylene blue. **(H)** Example *FoxO6* KO clone 53 colony assay at day 10 in EGF/FGF-2, with or without Dox. Plate fixed and stained with methylene blue.

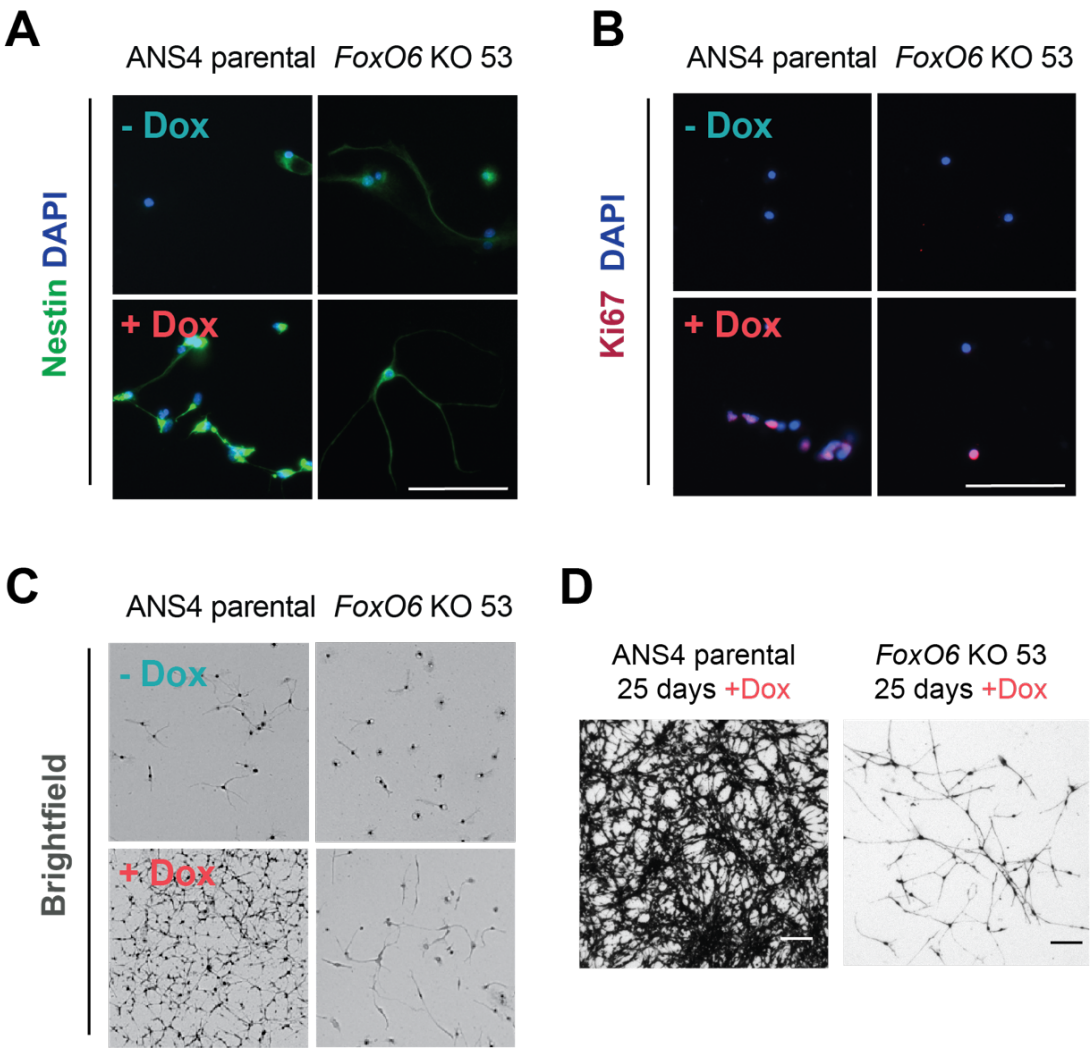

Figure 4-9 | *FoxO6* KO cells show some evidence of response to *FOXG1* overexpression.

In panels (A)-(D) ANS4 parental and *FoxO6* KO 53 refer to transfected cell populations with Dox-inducible FOXG1-V5 overexpression. **(A)** ICC images showing Nestin expression at Day 10 in NS media with or without Dox addition (following 24 h BMP4 treatment) in both transfected parental ANS4 and *FoxO6* KO 53 cells. **(B)** ICC images showing Ki67 expression at Day 10 in NS media with or without Dox addition (following 24 h BMP4 treatment) in both transfected parental ANS4 and *FoxO6* KO 53 cells. **(C)** Brightfield images following fixation of colony assay plate and staining with methylene blue. **(D)** Brightfield images of parental and *FoxO6* KO 53 colonies after 25 days in NS cell media + Dox. Scale bars: 100 μm.

4.2.6 Analysis of *FOXO6* expression in patient-derived GNS cells

Following the validation of a functional role for FoxO6 in quiescent mouse NSCs, we wanted to explore its role in human GBM using patient-derived GNS cells. As detailed in the introduction, GNS cells can be grown *in vitro* under NSC culture conditions, consistently express high levels of FOXG1 (Bulstrode *et al*, 2017), and are amenable to genetic engineering using CRISPR/Cas9. They therefore provided a useful model for us to disrupt *FOXG1* and analyse the effect on *FOXO6* expression in a human context.

Through the Cancer Research UK Glioma Cellular Genetics Resource (GCGR) (www.gcgr.org.uk), a series of new patient-derived GNS cell lines were available (Figure 4-10 A), each of which had been profiled alongside its parental tumour tissue to ensure no transcriptional or karyotypical corruptions during culture. Firstly, using Western blotting we confirmed that FOXG1 protein levels were elevated in GNS cells (G7, G301-B, G313, G317, G325, G326, G327, G328 and G330), compared to normal human foetal NS cell lines (CB152 and CB11130) (Figure 4-10 B). ICC and qRT-PCR analysis then showed that each cell line had variable levels of FOXG1 expression, compared to an established and widely used GNS cell line, G7 (Figure 4-10 C and D).

A *FOXG1* null cell line, derived from G7, had been previously engineered by Dr Raul Bressan (G7 FOXG1$^{-/-}$) (Bulstrode *et al*, 2017). Given the availability of one *FOXG1* null line from a single patient, we set out to derive another. G313 was chosen due to similar levels of FOXG1 expression as G7. CRISPR/Cas9-mediated gene deletion was achieved using a Cas9 RNP method with a crRNA previously designed by R. Bressan, targeting the 5' end of the *FOXG1* exon close to the start codon. This method is similar to that used in Figure 4-2, except a repair DNA template is not supplied, leading to repair of the DSB by NHEJ and hence indel formation in the targeted alleles (Figure 4-11 A). In contrast to the plasmid-based method used for *Foxg1* deletion in mouse IENS cells (Figure 4-3), this

Cas9 RNP method was later adopted due to high transfection efficiencies and quicker 'on' and 'off' rates, as well as no requirement for plasmid construction. Following transfection, the cells were plated at clonal density and approximately 80 resulting colonies were screened for FOXG1 expression by ICC. Three G313 *FOXG1* knock-out cell lines (42, 44 and 47) were derived and validated by ICC and Western blotting (Figure 4-11 B and C).

Using these G7 and G313 *FOXG1* null cell lines, we assessed the effect of *FOXG1* deletion on *FOXO6* expression in EGF/FGF-2. By qRT-PCR, basal *FOXO6* expression levels were found to be low, therefore large amounts of RNA were reverse-transcribed to enable the fluorescence level to reach the threshold within 40 PCR cycles. In both G7 and G313, we saw a trend for *FOXO6* levels to decrease upon deletion of *FOXG1* (Figure 4-11 D and E). For G313, *FOXO6* Ct values were close to the limit of detection due to lower starting RNA quantities; higher RNA yields are needed to increase confidence in these results.

Finally, RNA-seq was performed on a panel of GNS cell lines and their matched tissue samples by the GCGR. Analysis by Ben Southgate (Pollard lab) revealed no significant correlation between *FOXG1* and *FOXO6* expression levels across all tissue and cell line samples (Figure 4-12). Relatively small differences in *FOXG1* expression between cell lines or culture in proliferative conditions with EGF/FGF-2 may explain this lack of correlation.

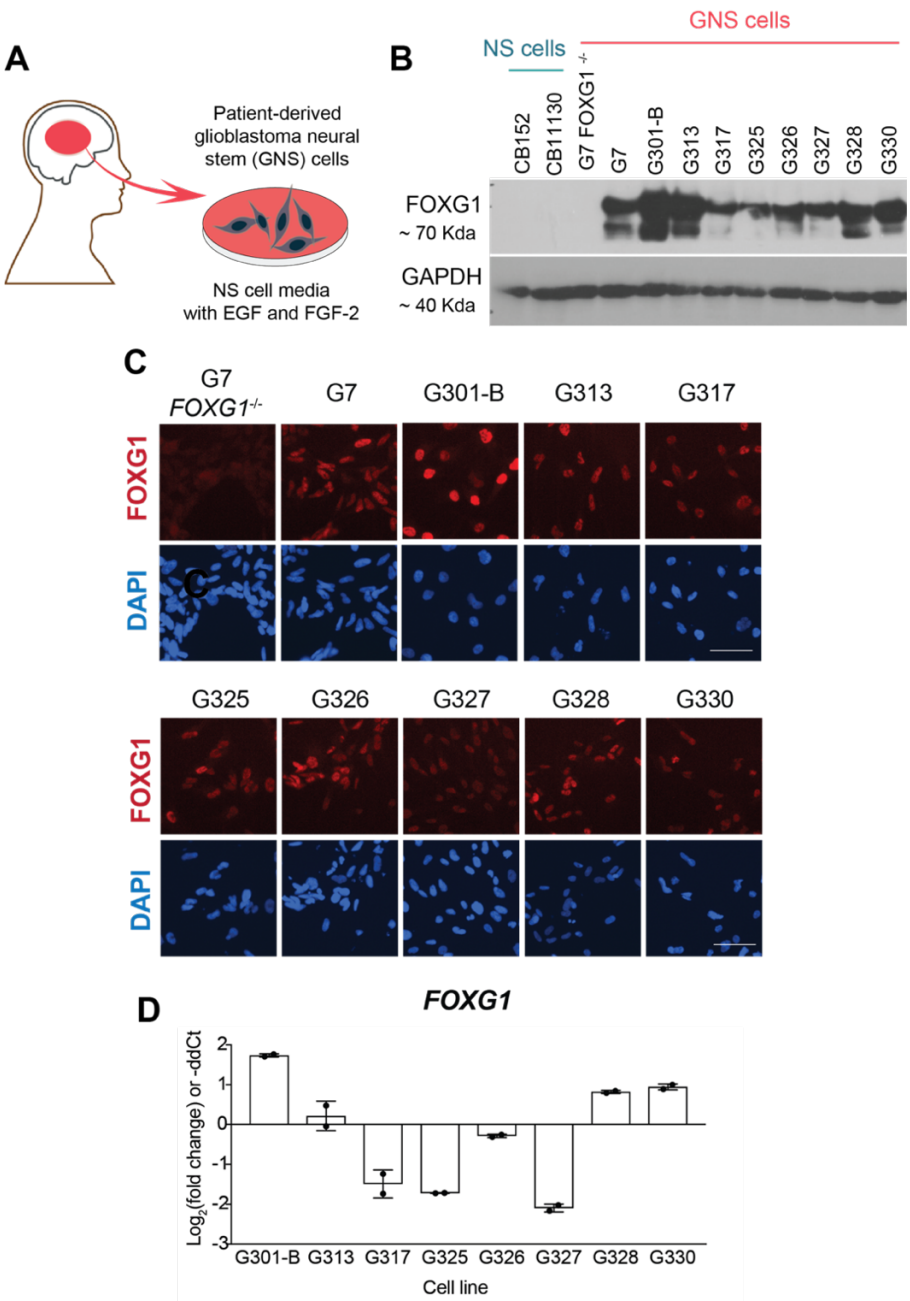

Figure 4-10 | FOXG1 is consistently overexpressed in human GNS cell lines.

(A) Schematic for derivation of human GNS cells from patient tumours. **(B)** Western blot analysis of FOXG1 expression in normal foetal NS cell lines (CB152 and CB11130) and a panel of patient-derived GNS cell lines from the GCGR (G7, G301-B, G313, G317, G325, G326, G327, G328 and G330). G7 *FOXG1* $^{-/-}$ is included as a negative control. GAPDH was used as a loading control (C.Blin and S. ViyayKumar). **(C)** ICC analysis of FOXG1 expression in the panel of human GNS cell lines. G7 *FOXG1* $^{-/-}$ is included as a negative control. Scale bar: 100 µm. **(D)** qRT-PCR analysis of *FOXG1* mRNA levels in a panel of human GNS cell lines. Expression values were normalised to *GAPDH* and shown relative to the expression in G7 (in which $\log_2$(FC) = 0). Y axis represents $\log_2$(Fold change), equivalent to -ddCt value. Graph shows Mean +/- SD of one experiment performed in technical duplicates. Each data point shows one technical replicate. Experiments in (C) and (D) performed by S. ViyayKumar.

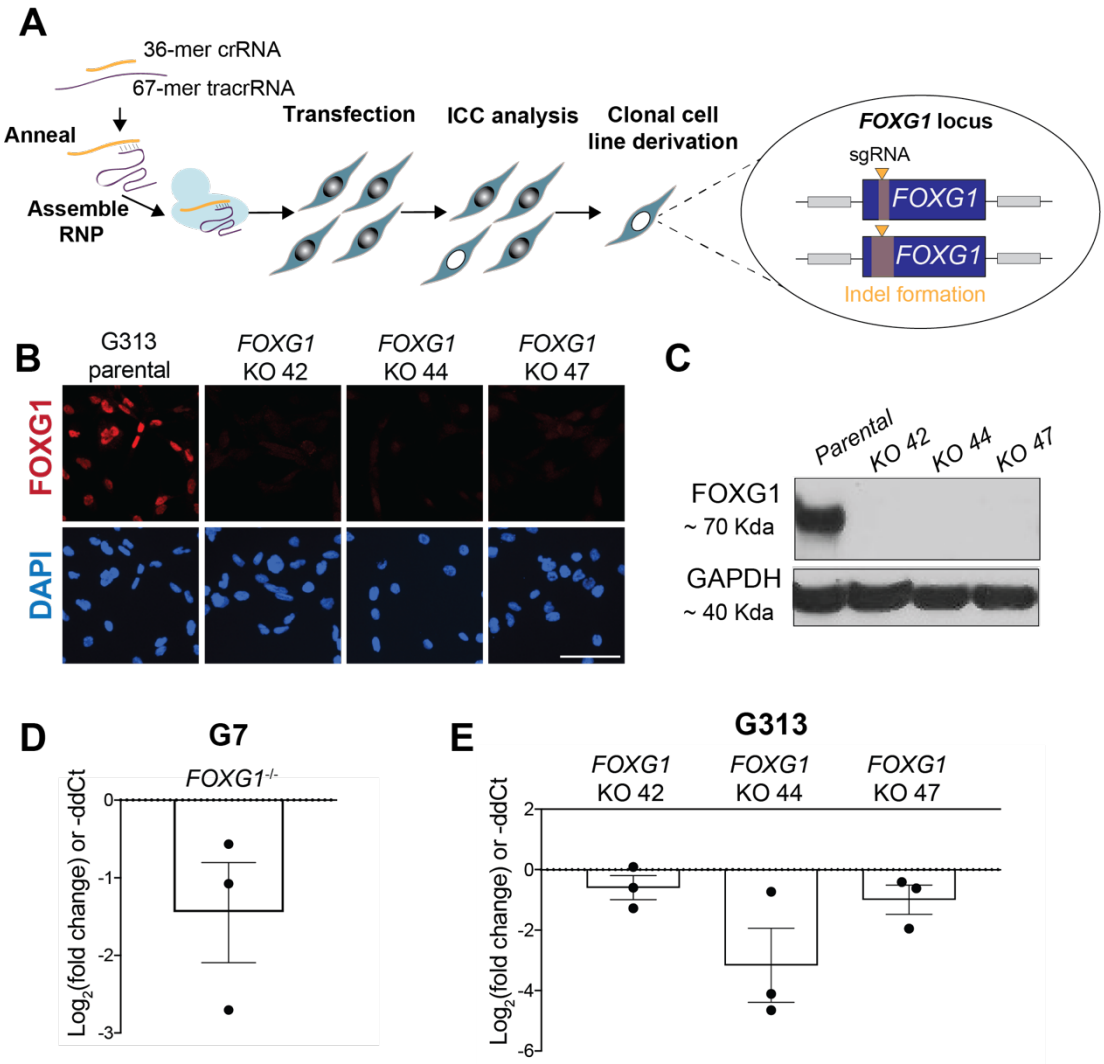

Figure 4-11 | *FOXO6* mRNA levels decrease on deletion of *FOXG1* from human GNS cells

(A) Experimental strategy for FOXG1 deletion in human GNS G313 cells using a Cas9 ribonucleoprotein complex. Transfection performed by S. VijayKumar. Cells plated for colony formation by K. Benjasupawan. **(B)** Representative ICC images of FOXG1 expression in parental G313 and *FOXG1* KO clonal lines 42, 44 and 47. Scale bar: 100 µm. **(C)** Western blot analysis to confirm loss of FOXG1 protein expression in G313 *FOXG1* KO clonal lines 42, 44 and 47. GAPDH was used as a loading control. **(D)** qRT-PCR analysis of mRNA expression levels of *FOXO6* in parental G7 or *FOXG1* KO clonal line. **(E)** qRT-PCR analysis of mRNA expression levels of *FOXO6* in parental G313 or *FOXG1* KO clonal lines (42, 44 and 47). Expression values were normalised to *GAPDH* and shown relative to the expression in control cells (in which $\log_2(FC) = 0$). Y axis represents $\log_2$(Fold change), equivalent to -ddCt value. Graph shows Mean +/- SEM. n=3 independent experiments. Each data point shows the mean of one experiment, performed in technical duplicates. Statistics were calculated from ddCt values. Two-tailed one sample t-test.

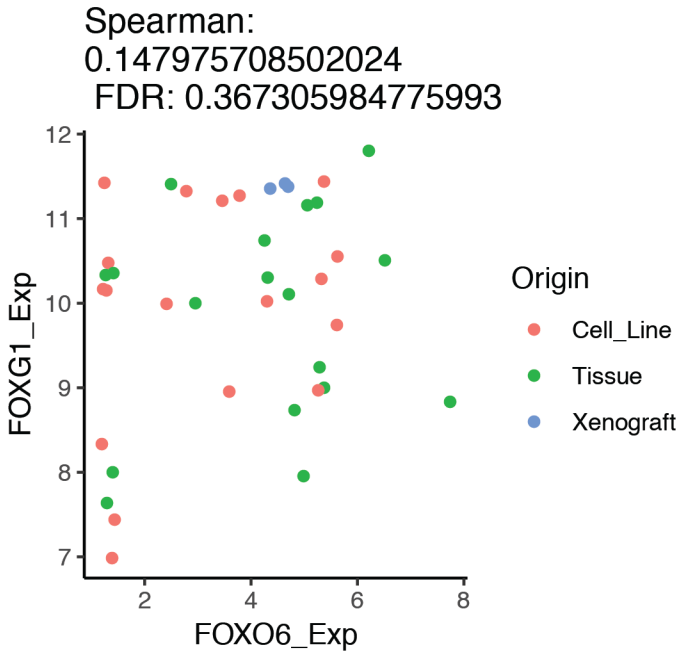

Figure 4-12 | No correlation is found between *FOXG1* and *FOXO6* expression levels in patient-derived GNS cell lines and matched tissue samples.

RNA-seq data for glioma primary tissue, matched GNS cell lines and three lines derived from xenograft tissue was made available through the GCGR. Analysis was performed by Ben Southgate (Pollard lab). Expression values are log2 normalised counts as processed by DESeq2. A graph with labelled data points is provided in the Appendix VIII.

4.3 Validation of *Chd3* as a downstream target of FOXG1

4.3.1 *Chd3* expression increases in response to elevated FOXG1 in proliferating NSCs

To confirm if *Chd3* is a downstream transcriptional target of FOXG1, identical experiments were performed as for FoxO6 in sections 4.2.1, 4.2.3 and 4.2.5. mRNA levels of *Chd3* and the other epigenetic regulators monitored in section 3.3.2 were assessed in two independent mouse NS cell lines (F6 and F11-19) with Dox-inducible *FOXG1* in NS cell media (EGF/FGF-2). The DNA methylation regulators, *Dnmt1/3a/3b*, showed inconsistent changes in expression on addition of Dox, suggesting they may only be FOXG1 targets during reactivation to a proliferative NS cell-like state. However, *Tet3* and more notably *Chd3* expression levels increased consistently on addition of Dox in both cell lines (Figure 4-13). A mean fold increase in *Chd3* of ~2 and ~1.6-fold was observed in F6 and F11-19, respectively. This suggests that, like *FoxO6, Chd3* is a transcriptional target of FOXG1 in both proliferating NSCs, as well as during reactivation of d-qNSCs.

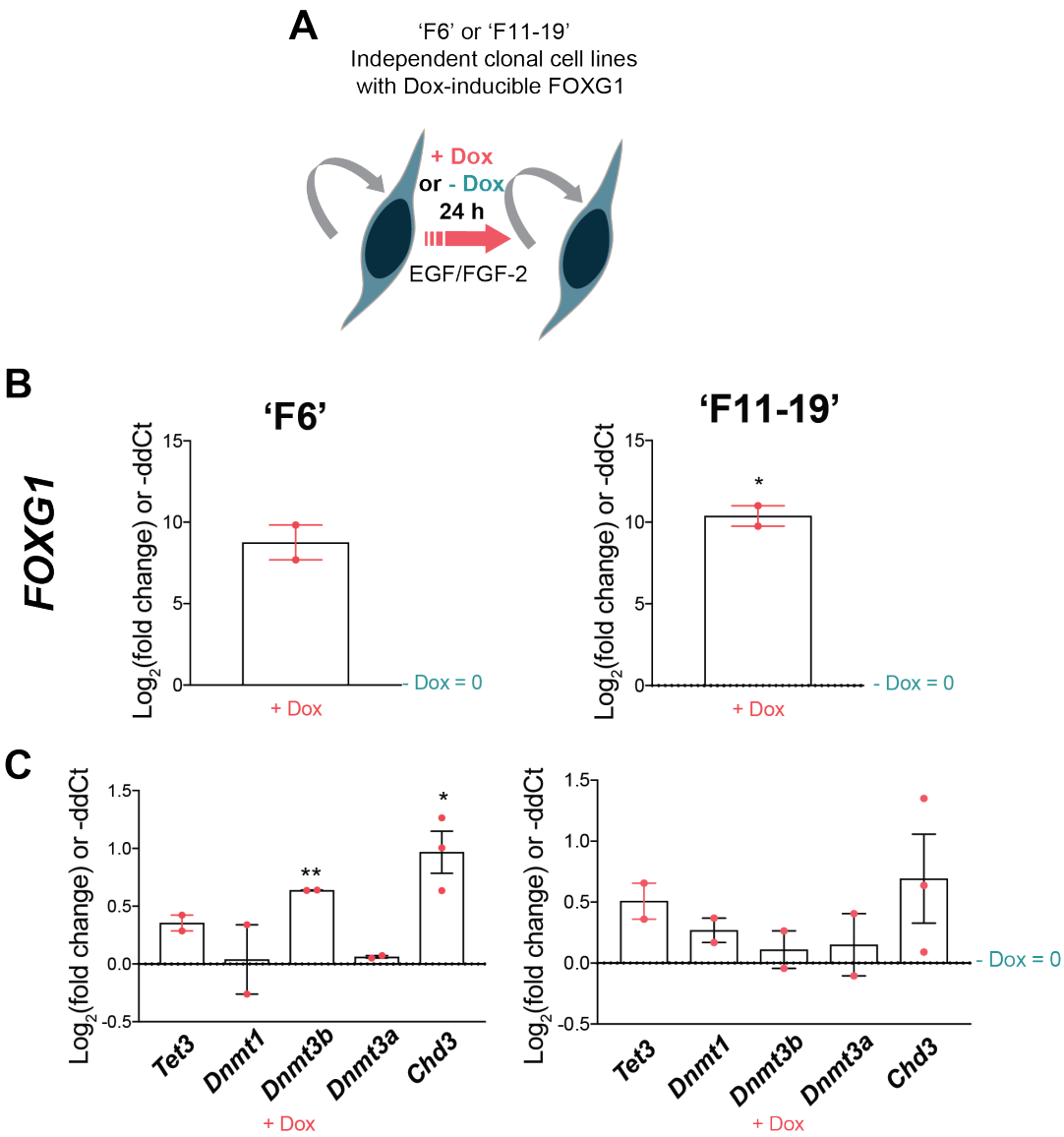

Figure 4-13 | *Chd3* mRNA levels are increased in response to FOXG1 overexpression in proliferating NSCs.

(A) Schematic of experimental set-up: adult mouse NS cell lines ('F6' and 'F11-19') with Dox-inducible *FOXG1* overexpression were grown in NS cell media (EGF/FGF-2) with or without Dox for 24 h. **(B)** qRT-PCR analysis of *FOXG1* mRNA levels in F6 and F11-19. n=2 independent experiments. Each data point shows the mean of one experiment, performed in technical duplicates. **(C)** qRT-PCR analysis of *Chd3, Tet3, Dnmt1, Dnmt3b and Dnmt3a* mRNA levels in F6 and F11-19. n=2 or 3 independent experiments. Each data point shows the mean of one experiment, performed in technical duplicates. All expression values were normalised to *Gapdh* and shown relative to the expression in EGF/FGF-2 -Dox (in which $\log_2(FC) = 0$). Y axis represents $\log_2$(Fold change), equivalent to -ddCt value. Graph shows Mean +/- SEM. Statistics were calculated from ddCt values. Two-tailed one-sample Student's t-test. * $P \leq 0.05$, ** $P \leq 0.01$).

4.3.2 *Chd3* mRNA is reduced following *Foxg1* knockout in mouse GSCs

To further validate *Chd3* as a transcriptional target of FOXG1, qRT-PCR analysis of *Chd3* mRNA levels, alongside other epigenetic regulators, was performed in the two independent mouse GBM model cell lines shown in Figure 4-3 (IENS-GFP and FF-IEK). While *Tet3* levels were not altered upon *Foxg1* deletion from IENS cells, *Chd3* mRNA levels were significantly downregulated in both clonal *Foxg1* null cell lines (Figure 4-14). In clone 58 and clone 59, *Chd3* levels decreased by ~4-fold (~73%) and ~8.5-fold (~88%), respectively. However, these results were less consistent in the 'FF-IEK' model, with FF-IEK *Foxg1*$^{-/-}$ cells showing an ~1.1-fold (10%) decrease in *Chd3* mRNA levels. The 'FF-IEK' and 'IENS' cell lines were derived independently from mice of different ages (adult or postnatal), using different methods for *Ink4a/Arf* deletion (CRISPR/Cas9-mediated deletion versus Cre-mediated excision of floxed sequence) and EGFRvIII overexpression (PiggyBac-mediated versus retroviral transduction). It is possible these variations in age and methodology lead to this difference in results between the two cell lines.

4.3.3 Analysis of *CHD3* expression in patient-derived GNS cells

Using the *FOXG1* null human GNS cell lines in Figure 4-11, the effect of *FOXG1* deletion on *CHD3* expression was assessed. *CHD3* expression levels where higher than those of *FOXO6*, therefore RNA yields were not limiting in this case. While *FOXG1* deletion in G7 cells led to a decrease in *CHD3* levels, this was not consistent in the G313 *FOXG1* null cell lines (Figure 4-15). The RNA-seq analysis described in section 4.2.6 revealed no correlation between *FOXG1* and *CHD3* levels in a panel of patient-derived GNS cell lines and matched tissue samples (Figure 4-16).

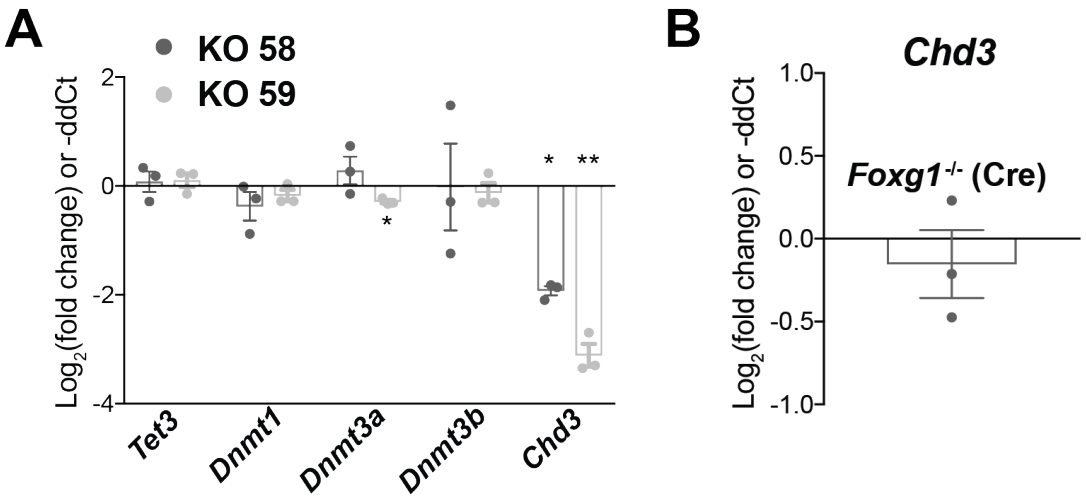

Figure 4-14 | *Chd3* mRNA is reduced following *Foxg1* knock-out from IENS cells.

(A) qRT-PCR analysis of *Chd3, Tet3, Dnmt1, Dnmt3b and Dnmt3a* mRNA levels in IENS-GFP *Foxg1* KO clonal cell lines 58 and 59, compared to parental IENS-GFP (in which $\log_2(FC) = 0$). Expression values were normalised to *Gapdh*. Y axis represents $\log_2$(Fold change), equivalent to -ddCt value. Mean +/- SEM. n=3 independent experiments. Each data point shows the mean of one experiment, performed in technical duplicates. **(B)** qRT-PCR analysis of *Chd3, Tet3, Dnmt1, Dnmt3b and Dnmt3a* mRNA levels in FF-IEK *Foxg1*$^{-/-}$cells (Cre addition), compared to parental 'FF-IEK' (in which $\log_2(FC) = 0$). n=3 independent experiments. Each data point shows the mean of one experiment, performed in technical duplicates. Mean +/- SEM. Statistics were calculated from ddCt values. Two-tailed one sample Student's t-test. * $P \leq 0.05$, ** $P \leq 0.01$.

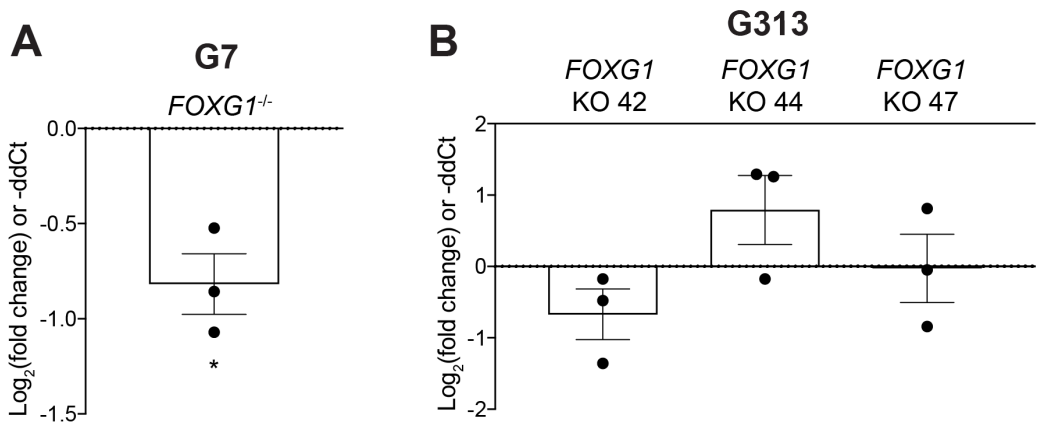

Figure 4-15 | *CHD3* mRNA is reduced on genetic knockout of *FOXG1* from human GNS cell line G7.

(A) qRT-PCR analysis of *CHD3* mRNA levels in G7 *FOXG1*$^{-/-}$ cells, compared to parental G7 (in which $\log_2$(FC) = 0). Expression values were normalised to *GAPDH*. Y axis represents $\log_2$(Fold change), equivalent to -ddCt value. Mean +/- SEM. n=3 independent experiments. Each data point shows the mean of one experiment, performed in technical duplicates. **(B)** qRT-PCR analysis of *CHD3* mRNA levels in G313 *FOXG1* KO clonal lines, compared to parental G313 (in which $\log_2$(FC) = 0). n=3 independent experiments. Each data point shows the mean of one experiment, performed in technical duplicates. Mean +/- SEM. Statistics were calculated from ddCt values. Two-tailed one sample Student's t-test. * $P \leq 0.05$.

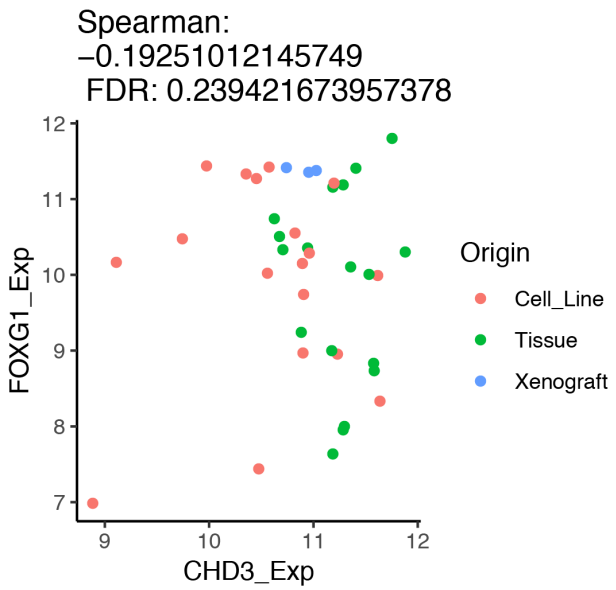

Figure 4-16 | No correlation is found between *FOXG1* and *CHD3* expression levels in patient-derived GNS cell lines and matched tissue samples.

RNA-seq data for glioma primary tissue, matched GNS cell lines and three lines derived from xenograft tissue was made available through the GCGR. Analysis was performed by Ben Southgate (Pollard lab). Expression values are log2 normalised counts as processed by DESeq2. A graph with labelled data points is provided in the Appendix VIII.

4.4 Discussion

In this chapter, we have found *FoxO6* and *Chd3* to act as downstream transcriptional targets of FOXG1 in multiple contexts. *FoxO6* showed significant fold changes, with consistent upregulation when FOXG1 was overexpressed (Figures 4-1 and 4-2), and downregulation when *FOXG1* was deleted, across both mouse and human models of GBM (Figures 4-4 and 4-11).

The low efficiency of FOXG1-induced reactivation of d-qNSCs, discussed in Chapter 3, limited our ability to monitor changes in expression at the protein level in this context. FoxO6 analyses were further limited by the lack of commercially available protein-specific antibodies. However, increased protein levels upon induction of FOXG1 in proliferating mouse NS cells was confirmed with the aid of CRISPR/Cas9-mediated gene epitope tagging (Figure 4-2), a technology I discuss in greater depth in the next chapter. These promising results led us to investigate whether FoxO6 is required for FOXG1's function in driving the reactivation of astrocytic d-qNSCs. This revealed that *FoxO6* KO cells show significantly defective colony formation, despite similar levels of *FOXG1* transgene expression as their wild-type counterparts (Figure 4-8). ICC analysis reveals *FoxO6* KO cells alter their morphology in response to FOXG1 overexpression and show some evidence of Ki67 positive cells but do not show a significant upregulation in levels of the NS cell marker, Nestin (Figure 4-9). While *FoxO6* KO cells displayed a slight decrease in proliferation in EGF/FGF-2 compared to wild-type cells (Figure 4-6), this is unlikely to account for this dramatic loss of colony formation. This indicates that *FoxO6* is a functionally important target of FOXG1, with loss of *FoxO6* inhibiting reacquisition of a highly proliferative NS cell-like state. Reproducibility in an independent clonal *FoxO6* KO cell line would further support our findings.

It is possible that *FoxO6* loss affects either the initial response to BMP4 signalling or the transition out of dormancy. Analysis of the response of wild-type ANS4 and *FoxO6* KO cells to BMP4 treatment showed no significant differences under our experimental conditions (Figure 4-7). While not statistically significant, a couple of EdU-positive ANS4 cells were noted following 24 h BMP4 treatment and return to EGF/FGF-2, compared to none in the *FoxO6* KO cells (Figure 4-7 E). *FoxO6* KO cells also showed slightly lower levels of *Nestin* mRNA after 24h BMP4 treatment (Figure 4-7 D). It is possible that high FoxO6 levels act to restrict differentiation commitment, and deletion of *FoxO6* results in a 'deeper' dormant quiescent state. However, this is difficult to establish due to the current lack of markers distinguishing quiescent NS cells and mature astrocytes. Further markers or prolonged EdU exposure may help to establish if *FoxO6* loss positively regulates the acquisition of dormant astrocytic features. While the patterns of FoxO6 expression in development suggest a role in controlling neural precursor specification, this role has yet to be clarified (Hoekman *et al*, 2006; Paap *et al*, 2016; Salih *et al*, 2012).

Alternatively, *FoxO6* loss may affect cell cycle re-entry and re-acquisition of an NS cell-like state, a more likely possibility in the context of the FoxO6 literature. Several studies suggest a role of elevated FOXO6 in driving cancer cell proliferation and progression (Qinyu *et al*, 2013; Rothenberg *et al*, 2015; Wang *et al*, 2017a; Lallemand *et al*, 2018). In EGF/FGF-2 we observed only a small proliferation defect on *FoxO6* deletion from ANS4 cells (Figure 4-6 A-D). However, basal *FoxO6* levels are low in these conditions; we therefore cannot discount a role for high FOXO6 in driving cell cycle re-entry of dormant quiescent NSCs or in maintaining a proliferative state in the presence of pro-differentiation cues.

FoxO6 also has reported metabolic roles in the liver and skeletal muscle (Kim *et al*, 2011a; Chung *et al*, 2013); it is therefore plausible that high FoxO6 levels may aid re-

acquisition of a proliferative NS cell-like state through altering cell metabolism. Indeed deregulation of cellular energetics is one of the hallmarks of cancer proposed by Hanahan and Weinburg (Hanahan & Weinberg, 2011) and a switch to aerobic glycolysis is considered a typical feature of tumorigenesis (Liberti & Locasale, 2016). FoxO3 is known to protect NS cells against oxidative stress (Yeo *et al*, 2013) and control their glucose metabolism to ensure continued optimal self-renewal (Renault *et al*, 2009); this is achieved in part through inhibition of Myc, one of the most-studied proto-oncogenes in cancer whose overexpression drives cell cycle progression and several metabolic changes (Peck *et al*, 2013).

In contrast, FoxO6 has been reported to promote cell proliferation in gastric cancer through induction of c-Myc expression (Qinyu *et al*, 2013). Notably, in Chapter 3 we observed FOXG1-induced upregulation of *N-Myc* in d-qNSCs (Figure 3-8 B). We therefore speculate that, in comparison to FoxO3, FoxO6 may have oncogenic roles in altering cell metabolism, perhaps controlling a shift between oxidative and glycolytic metabolism needed to transition to a highly proliferative state. A shift towards glycolytic metabolism has recently been suggested to play a pivotal role in acquisition of cancer stemness (Menendez & Alarcon, 2014). Silencing of *FoxO6* has recently been shown to inhibit proliferation and glycolysis in colorectal cancer cells (Li *et al*, 2019). This was accompanied by loss of activation of PI3K/Akt/mTor signalling; furthermore mTOR signalling has been shown to control glycolytic metabolism in GBM through inhibition of HDACs, leading to acetylation of FoxO1/3 and subsequent derepression of *c-Myc* expression (Masui *et al*, 2013). FOXG1 itself has been implicated in regulating mitochondrial functions (Pancrazi *et al*, 2015), suggesting a potential role for FoxO6 in altering cell metabolism should be further explored.

Unlike other epigenetic regulators identified in Chapter 3, mRNA levels of *Chd3* were

found to: i) increase with *FOXG1* overexpression in mouse NS cells in EGF/FGF-2 (Figure 4-13), and ii) decrease on deletion of *Foxg1* from the mouse GSC line, IENS (Figure 4-14 A). Furthermore, levels of *Chd3* significantly decreased on deletion of *FOXG1* from the human GNS cell line, G7 (Figure 4-15 A). These results were not consistent in an additional mouse GSC line, 'FF-IEK' or the human GNS cell line, G313 (Figures 4-14 B and 4-15 B); such differences may be due to inherent genetic differences between patient-derived cell lines and age or methodology-related differences in the mouse GBM models. Our results suggest that the majority of epigenetic regulators analysed are targets of FOXG1 in a context-dependent manner, during the cell fate transition from a dormant quiescent to a proliferative radial-glia-like NS cell state. In agreement, chromatin and DNA methylation-related drivers have been implicated in driving CSC initiation in numerous malignancies (Wainwright & Scaffidi, 2017). However, epigenetic remodelling is also important for the maintenance of self-renewal during cancer progression, enabling adaptation in the presence of environmental cues that threaten the CSC state. Our data suggest *Chd3* is a downstream target of FOXG1 in driving reacquisition of an NS cell-like state and, in contrast to other investigated epigenetic regulators, has a possible role in GSC maintenance.

The transcriptional changes in both *FoxO6* and *Chd3*, when FOXG1 is upregulated or deleted from proliferating GSC models, suggest a potential role for both in maintaining the GSC state. While neither showed a significant correlation with FOXG1 levels in patient tissue samples and cell lines (Figures 4-12 and 4-16), these studies were limited to proliferation in EGF/FGF-2. It would be interesting to explore potential roles of these targets in initiating and/or maintaining GNS cells under conditions which may more accurately mimic the situation *in vivo,* where cells are in a more quiescent and/or differentiating state.

In addition to advancing our understanding of FOXG1's mechanism in driving the GSC state, *FoxO6* and *Chd3* provide useful readouts of FOXG1 function in mouse NSCs. In the next chapter, we focus on defining the key protein partners of FOXG1. We will explore both the relevance of the candidate partner, H3K4 demethylase JARID1B to FOXG1's functions, and new genetic technologies to aid the discovery of novel protein-protein interactions. Understanding the protein interactors of FOXG1, alongside its transcriptional targets, will allow us to build a more complete picture of how this master regulator may function in GBM and hence could reveal a potential pathway for therapeutic intervention.

CHAPTER 5

Defining the critical protein partners of FOXG1

5.1 Introduction

In Chapter 4 we identified the Forkhead factor, FoxO6, as a clear transcriptional target of FOXG1 in mouse NSCs and GSCs. The early induction of *FoxO6* suggests this might be via a direct mechanism, but this is paradoxical given FOXG1 is best described as a transcriptional repressor. The binding of co-factors is one aspect that determines the regulatory properties of TFs. We therefore surmised that understanding FOXG1's key protein partners may provide further clues into its mechanism of action in activating target genes. This was of interest, both in terms of improving our understanding of FOXG1's mechanism of action, and the potential therapeutic interventions which could come from this knowledge.

FOXG1 is a multi-domain transcription factor, with three published domains: a DNA-binding Forkhead domain, a Groucho/TLE-1 binding domain and a JARID1B binding domain (Figure 1-6). While both TLE-1 and JARID1B have been shown to play important roles in development, currently most studies have focussed on the FOXG1-TLE-1 interaction in GSCs.

Like TLE-1, JARID1B is a transcriptional co-repressor, acting primarily through its histone demethylase activity. Indeed, identification of a FOXG1-JARID1B interaction was accompanied by the finding that the transcriptional repression activity of FOXG1 is enhanced by co-expression of *JARID1B*, and mutation of the interaction motif in *FOXG1* abolishes this co-repression (Tan *et al*, 2003). However, there are also reports of

JARID1B acting as a transcriptional co-activator in other contexts (Xiang *et al*, 2007; Zhang *et al*, 2014; Secombe *et al*, 2007). The studies by Tan *et al*. were carried out using luciferase reporter assays in HEK cells following plasmid-based gene co-expression. We therefore wanted to investigate the functional importance of FOXG1's interaction with JARID1B in NSCs.

We speculated that FOXG1's interaction with JARID1B may facilitate transcriptional activation in several ways (Figure 5-1). FOXG1 has been reported to have a dose-dependent dual activity in two studies of *Xenopus* neural development (Hardcastle & Papalopulu, 2000; Bourguignon *et al*, 1998); for example injection of Xenopus embryos with a high dose of *FoxG1* RNA in the posterior neural plate results in suppression of the cell cycle inhibitor $p27^{XIC1}$ and increased proliferation, whereas a low dose results in $p27^{XIC1}$ activation. In this context, co-injection of FOXG1 with SOX3 was shown to convert a low-dose phenotype to a high-dose one, suggesting that protein-protein interactions may act to switch FOXG1's regulatory mechanism (Hardcastle & Papalopulu, 2000). It is therefore possible that FOXG1's interactions with proteins such as JARID1B could lead, in some contexts, to a switch in its function. For example, binding of FOXG1 to JARID1B may be required to recruit co-activators or result in higher order complexes (Figure 5-1 A).

We also considered that the elevated levels of FOXG1 found in GSCs may lead to gene activation through a DNA binding-independent mechanism. FOXG1 has been shown to have DNA binding-independent functions in several studies, for example through control of neural progenitor cell proliferation via sequestration of FoxO-SMAD complexes (Seoane *et al*, 2004; Obendorf *et al*, 2007; Hanashima *et al*, 2002). We therefore hypothesised that elevated FOXG1 may act to sequester its co-activators or co-repressors, such as JARID1B, in a manner termed 'regulatory squelching' (Cahill *et al*,

1994). In this way, excess FOXG1 may regulate *in trans* the activity of promoters to which it doesn't bind, leading to 'de-repression' of normally repressed genes (Figure 5-1 B).

Uncovering additional critical protein partners of FOXG1 could also provide new insights into its mechanism of action. Following the recent developments in CRISPR/Cas9 technology, our laboratory has optimised a method to tag endogenous genes in both mouse and human NS cells (Dewari *et al*, 2018; Bressan *et al*, 2017); this provides an invaluable tool to investigate protein interactions using immunoprecipitation when commercial antibodies are not available or of poor quality.

In this chapter, we explore the relevance of JARID1B to FOXG1's function, including its role as a transcriptional activator. Our results do not suggest a critical role for JARID1B in FOXG1-driven d-qNSC reactivation or transcriptional activation of *FoxO6/Chd3*. We then demonstrate the use of CRISPR/Cas9 technology to tag endogenous *FOXG1* in mouse and human models of GBM. We further optimise this method in patient-derived GNS cells to circumvent low tagging efficiencies. This provides possibilities in future studies to fully define FOXG1's interactome.

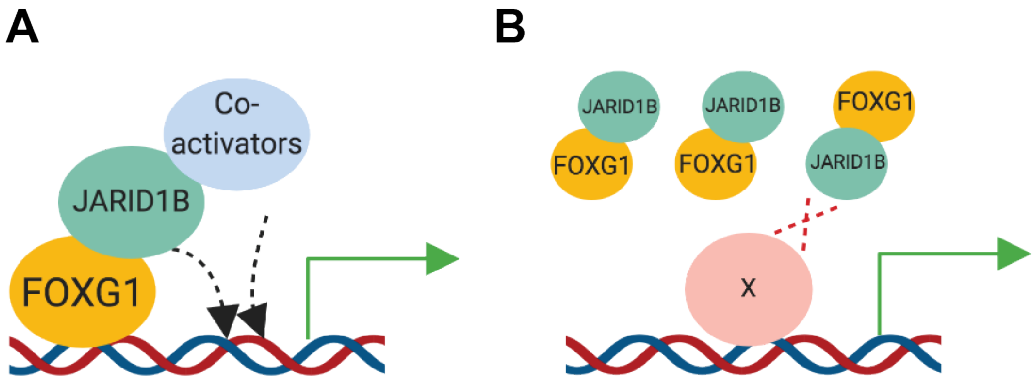

Figure 5-1 | Hypotheses of how FOXG1 acts as a transcriptional activator via JARID1B binding

(A) Binding of FOXG1 to JARID1B may result in a switch to transcriptional activation, for example through recruitment of co-activators. **(B)** Elevated levels of FOXG1 may sequester co-repressors, such as JARID1B, in a manner termed 'regulatory squelching' (Cahill *et al*, 1994).

5.2 Investigating the importance of JARID1B to FOXG1's function

5.2.1 Co-immunoprecipitation experiments suggest an interaction between FOXG1 and JARID1B in mouse NS and human GNS cells

FOXG1 has been reported to interact with the co-repressor JARID1B via a sequence termed the VP motif (Tan *et al*, 2003). We first set out to validate this interaction in both mouse NS and human GNS cells. Immunoprecipitations (IPs) were performed using our own anti-FOXG1 monoclonal hybridoma antibody (17B12). These experiments were performed with research technician, Carla Blin and Master's student, Shruthi VijayKumar. This antibody was generated to target a tertiary structural motif of the highly conserved Forkhead binding domain and detects both mouse and human FOXG1.

Native IP of FOXG1 in ANS4 mouse NS cell lysates was successful and showed an enrichment of FOXG1 in the IP versus the input lane (Figure 5-2 A). Co-immunoprecipitation (co-IP) of JARID1B was observed, with a band at ~175 kDa. An IgG isotype control was clean (used to show any non-specific background signal due to binding by the protein G Dynabeads™ or antibody). Heavy and light IgG chains (~50 kDa and 25 kDa, respectively) were visible in IPs due to the elution being carried out under denaturing conditions (Figure 5-2 A). Native IP of FOXG1 was then performed in three human GNS cell lines (G313, G326 and G328), profiled in Figure 4-10. These were chosen as they displayed a range of FOXG1 levels above and below those of the widely used line, G7. Western blotting revealed a large enrichment of FOXG1 in the IP versus input for all lines and co-IP of JARID1B with FOXG1, more weakly in G313. Based on these results, we decided to further explore the role of the FOXG1-JARID1B interaction in FOXG1's function.

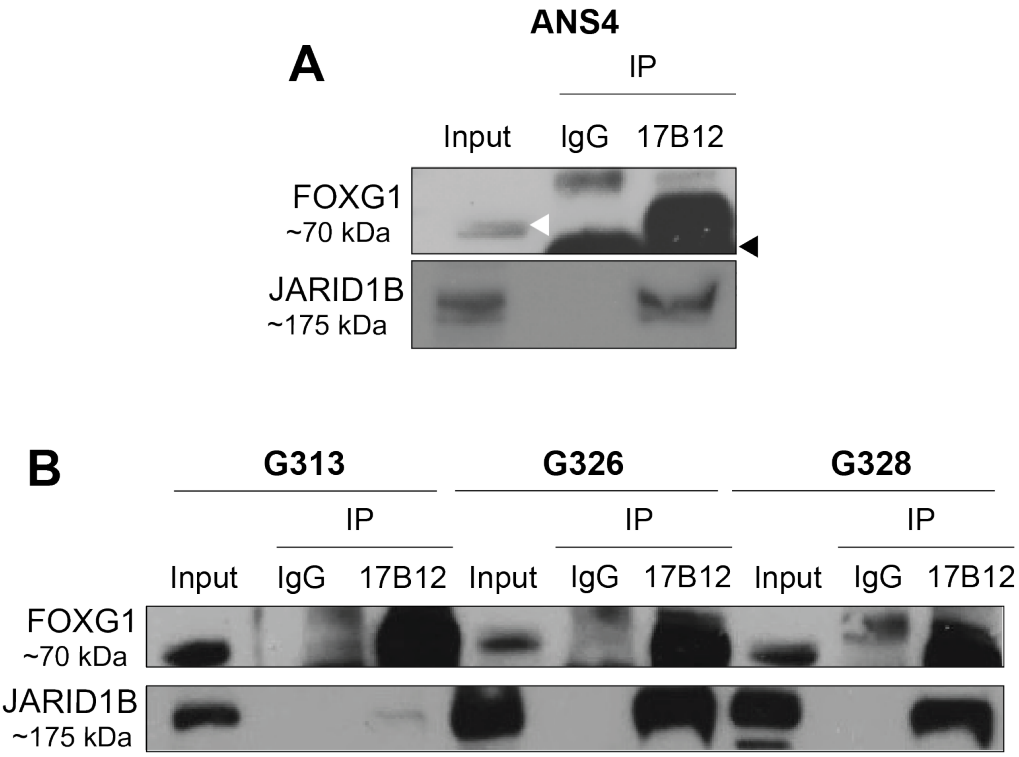

Figure 5-2 | Co-immunoprecipitation of FOXG1 with JARID1B.

(A) Western blot analysis of native IP of FOXG1 in ANS4 adult mouse NS cells. ~2-5 % of the IP lysate was loaded in the input lane. IgG control shows IP performed with mouse IgG antibody (by Carla Blin). White arrow indicates FOXG1 band of ~70 kDa. Black arrow indicates the heavy chain of the IgG antibody at ~50 kDa. **(B)** Western blot analysis of native IP of FOXG1 in human GNS cell lines, G313, G326 and G328 (by S. VijayKumar). IP performed using anti-FOXG1 17B12 antibody. Blots probed with anti-FOXG1 17B12 and anti-JARID1B (Novus Biologicals, NBP1-84352).

5.2.2 JARID1B is not required for NS cell proliferation or colony formation in EGF/FGF-2

In order use the mouse colony assay described in section 3.4 to explore the importance of JARID1B to FOXG1's function, it was first necessary to characterise the role of JARID1B in NSCs. We obtained conditional targeted *Jarid1b* NSCs, derived from the cerebral cortex of E12.5 *Jarid1b*$^{F/F}$; *Rosa26*::*CreERT2* mouse embryos, from the Kristian Helin lab (Schmitz *et al*, 2011). In these cells (*Jarid1b*$^{F/F}$; *Rosa26*::*CreERT2*), the *Jarid1b* exon 6 is flanked by *loxP* sites (Figure 5-3 A); administration of 4-hydroxytamoxifen (4OHT) leads to Cre recombinase expression and subsequent Cre-mediated frameshift and formation of a premature termination mutation specifically in both alleles of *Jarid1b* (Figure 5-3 B). These cell lines were provided with and without prior 4OHT treatment. We cultured both cell lines in NS cell media (EGF/FGF-2) but hereinafter describe them as -4OHT and +4OHT, with regards to their previous treatment.

PCR genotyping confirmed the presence of *Rosa26::CreERT2* in both cell lines (Figure 5-3 C) and the absence of *Jarid1b* exon 6 in the +4OHT treated cells (Figure 5-3 D). qRT-PCR analysis using primers spanning exons 5 and 6 showed no amplification in +4OHT treated cells, confirming removal of full-length *Jarid1b* expression (Figure 5-3 E) (Ct values of 40 were assigned, resulting in a downregulation of >99% compared to -OHT cells). Western blot analysis revealed loss of a band of the predicted size (~175 kDa) (Figure 5-3 F). The anti-JARID1B DAIN78 antibody used to assess protein expression was gifted by the Helin lab. This antibody was raised against amino acids 1395–1418 of JARID1B, a C-terminal region with little homology to other JARID1 family members, and therefore would not detect truncated protein forms. However, this deletion strategy was previously validated to ensure that splice variants or truncated proteins, if at all present, should be at very low levels (Schmitz *et al*, 2011; Albert *et al*, 2013). In addition, the

catalytic core of JARID1B has been shown to extend beyond exon 6, with important functional and protein binding domains, such as JmjC and PHD domains lying downstream (Kristensen *et al*, 2012). Based on our validation that full-length *Jarid1b* expression is lost at the mRNA and protein level, and previous validations by Schmitz *et al.*, we hereon refer to these E12.5 mouse NS cells as *Jarid1b*$^{F/F}$ (-4OHT) and *Jarid1b*$^{-/-}$ (+4OHT), respectively.

Analysis of the growth kinetics of *Jarid1b*$^{-/-}$ (+4OHT) cells in NS cell media (EGF/FGF-2) showed a modest but statistically insignificant increase in proliferation compared to *Jarid1b*$^{F/F}$ (-4OHT) cells (Figure 5-4 A, B, D). This was assessed by measuring the slope of the linear portion of the logistic growth curve (% confluence over time in hours) (Figure 5-4 B) and EdU incorporation after a 24 h pulse at day 3 of the growth analysis (Figure 5-4 C and D). Both cell types (*Jarid1b*$^{F/F}$ (-4OHT) and *Jarid1b*$^{-/-}$ (+4OHT)) were also plated at low density (1000 cells per 6 well) to assess their ability to form colonies in EGF/FGF-2. This revealed inconsistent results between independent replicates, with both *Jarid1b*$^{F/F}$ and *Jarid1b*$^{-/-}$ cells able to form typical NS cell colonies with varying efficiencies (Figure 5-4 E and F). These results indicate that JARID1B is not essential for NSC proliferation or colony formation in EGF/FGF-2, and that JARID1B depletion provides a modest growth advantage.

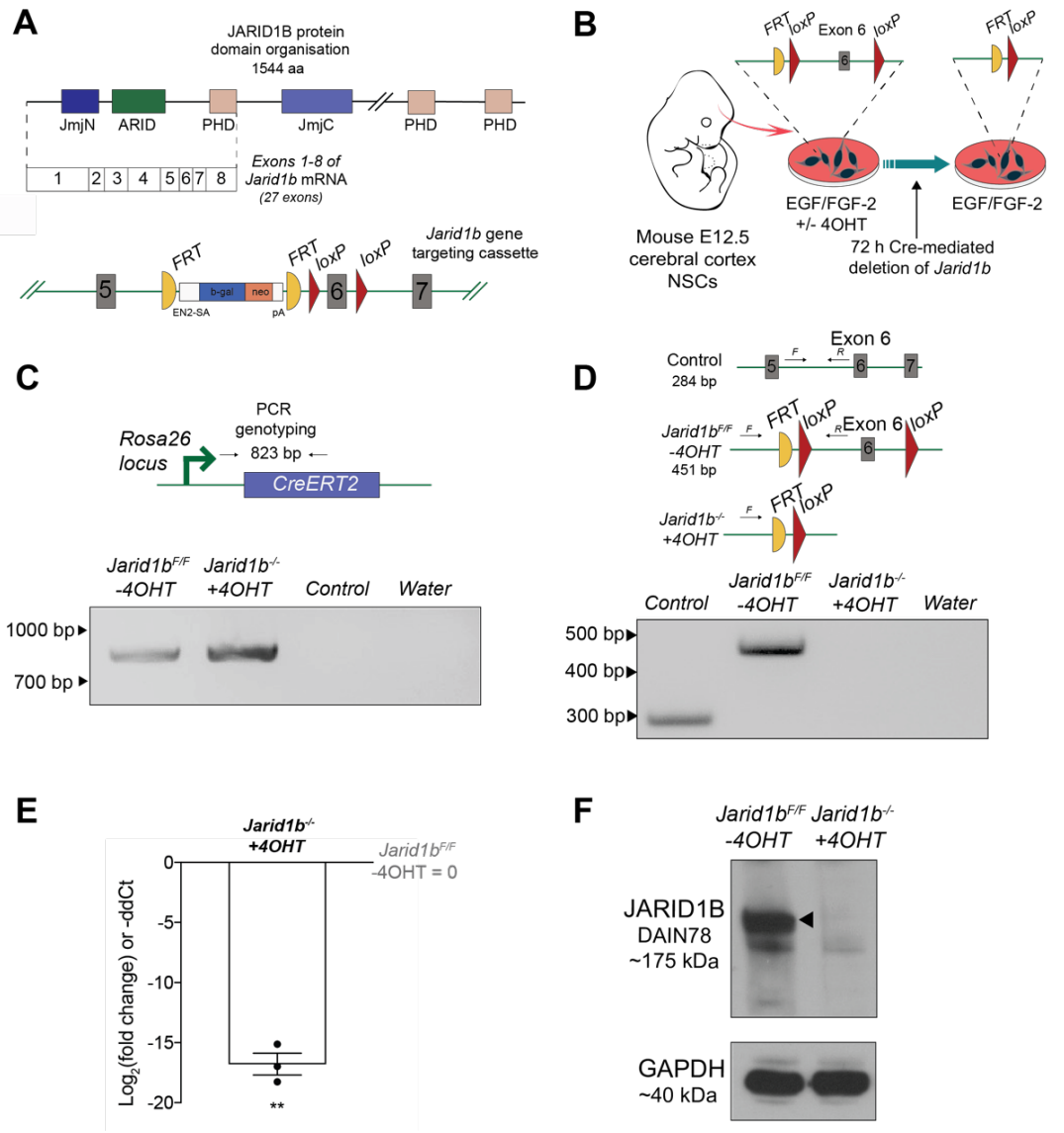

Figure 5-3 | Deletion of *Jarid1b* exon 6 in E12.5 mouse NSCs.

Jarid1b$^{F/F}$ (-4OHT) and *Jarid1b*$^{-/-}$ (+4OHT) E12.5 mouse NS cells were supplied by the Kristian Helin lab (Schmitz *et al*, 2011). **(A)** Schematic of JARID1B protein domain organisation and the position of the gene targeting cassette for deletion of exon 6 in the *Jarid1b* locus (27 exons). Adapted from (Schmitz *et al*, 2011). **(B)** Overview of experimental strategy used to delete *Jarid1b* exon 6 from mouse E12.5 NSCs. Adapted from (Schmitz *et al*, 2011). **(C)** PCR genotyping to confirm presence of *CreERT2* at the *Rosa26* locus in both *Jarid1b*$^{F/F}$ (-4OHT) and *Jarid1b*$^{-/-}$ (+4OHT) cells. **(D)** PCR genotyping to confirm deletion of *Jarid1b* exon 6 in +4OHT treated cells. **(E)** qRT-PCR analysis of *Jarid1B* mRNA levels in *Jarid1b*$^{F/F}$ (-4OHT) and *Jarid1b*$^{-/-}$ (+4OHT) cells, using primers spanning exons 5 and 6. n=3 independent experiments. Each data point shows the mean of one experiment, performed in technical duplicates. Expression values were normalised to *Gapdh* and shown relative to the expression in *Jarid1b*$^{F/F}$ (-4OHT) cells (in which $\log_2$(FC) = 0). Y axis represents $\log_2$(Fold change), equivalent to -ddCt value. Graph shows Mean +/- SEM. Statistics were calculated from ddCt values. Two-tailed one sample Student's t-test. ** P ≤ 0.01. **(F)** Western blot analysis of JARID1B expression in *Jarid1b*$^{F/F}$ (-4OHT) and *Jarid1b*$^{-/-}$ (+4OHT) cells using DAIN78 antibody. JARID1B band at ~175 kDa is indicated by the arrow. GAPDH was used as a housekeeping loading control.

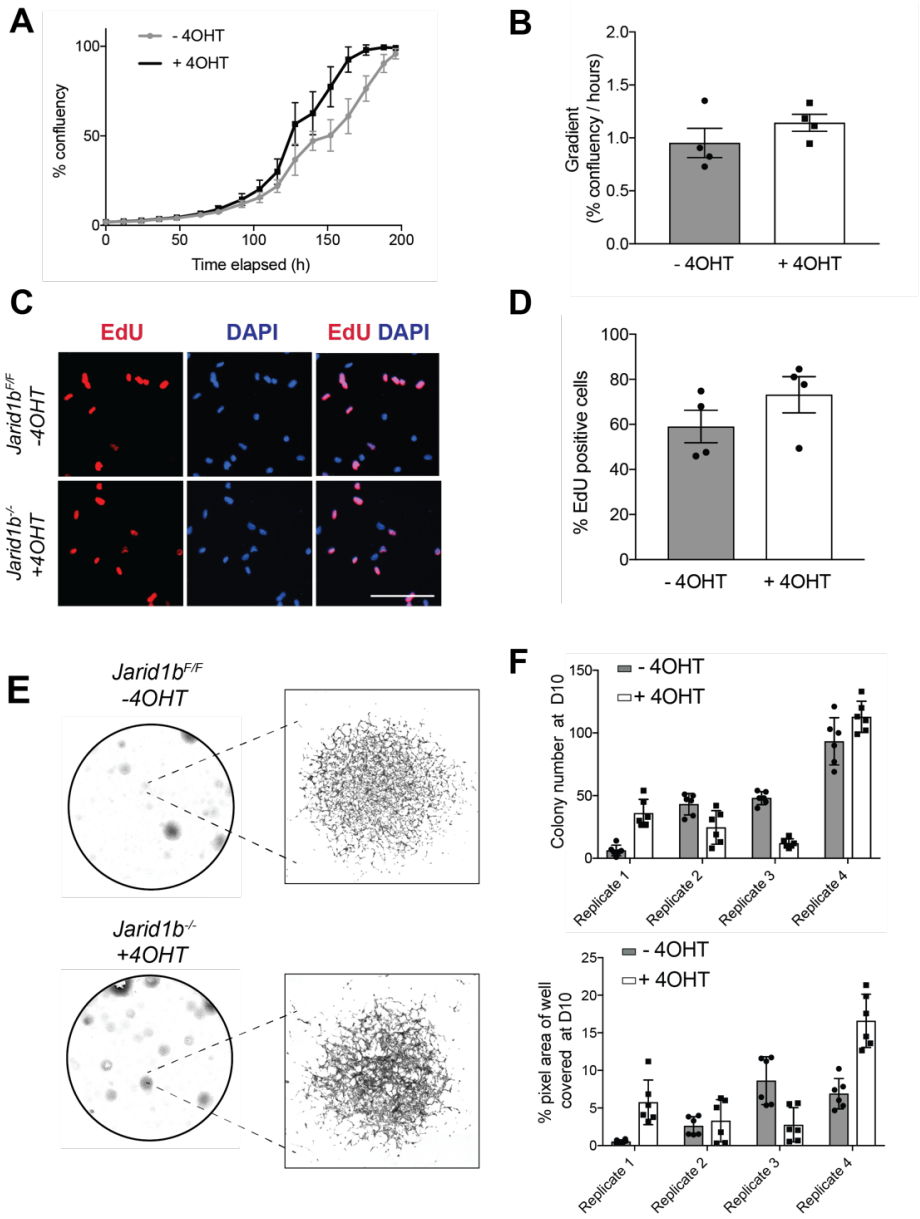

Figure 5-4 | JARID1B is not essential for NSC proliferation or colony formation in EGF/FGF-2.

(A) Example growth curve displaying percentage confluence versus time (hours) in EGF/FGF-2. Light grey = *Jarid1b*$^{F/F}$ (-4OHT), black = *Jarid1b*$^{-/-}$ (+4OHT). Mean +/- SD, n=3 technical replicates. **(B)** Graph showing the gradient of the linear portion of the logistic growth curve (%/h). Mean +/- SEM. n=4 independent experiments, shown by each data point. Two-tailed paired Student's t-test. **(C)** Representative fluorescent images of EdU incorporation after 24 h pulse on day 3 of growth analysis (*Jarid1b*$^{F/F}$ (-4OHT) and *Jarid1b*$^{-/-}$ (+4OHT) cells). Scale bar: 100 µm. **(D)** Quantification of % EdU positive cells after 24 h pulse on day 3 of growth analysis. Mean +/- SEM, n=4 independent experiments. Each data point shows the mean of one experiment, performed in technical triplicates. **(E)** Images of colony formation by *Jarid1b*$^{F/F}$ (-4OHT) and *Jarid1b*$^{-/-}$ (+4OHT) cells 10 days after plating at low density in EGF/FGF-2. Plates fixed and stained with methylene blue. **(F)** Quantification of percentage of the well pixel area covered by cells or colony number after 10 days. 4 independent experiments are shown, each with n=6 technical replicates, shown by each data point. Mean +/- SD.

5.2.3 *Jarid1b* $^{-/-}$ NSCs are able to respond to BMP4 signalling

Next we assessed the ability of *Jarid1b*$^{-/-}$ (+4OHT) cells to exit cell cycle and upregulate astrocytic markers on treatment with BMP4. ICC analysis revealed both *Jarid1b*$^{F/F}$ and *Jarid1b*$^{-/-}$ cells show a decrease in NESTIN and increase in GFAP expression after 3 days of BMP4 treatment (Figure 5-5 A and B). Similarly, qRT-PCR analysis showed that both cell lines decrease *Nestin* and *Olig2* mRNA levels and increase *Gfap* and *Aqp4* mRNA levels on treatment with BMP4 for 1 day. No significant differences in expression levels of these markers were found between *Jarid1b*$^{F/F}$ and *Jarid1b*$^{-/-}$ cells in EGF/FGF-2 or after BMP4 treatment (Figure 5-5 C and D). Finally, assessment of EdU incorporation following BMP4 treatment for 1 day and a 24 h EdU pulse in EGF/FGF-2 revealed that both cell lines exited cell cycle, with negligible EdU incorporation following BMP4 treatment (Figure 5-5 E).

While statistically insignificant with both lines showing <5% EdU incorporation, it was noted that more EdU positive *Jarid1b*$^{-/-}$ (+4OHT) cells were observed than *Jarid1b*$^{F/F}$ (-4OHT) cells following return to EGF/FGF-2. This indicates that *Jarid1b* depletion could cause a modest decrease in response to BMP4, however this cannot be concluded from the current data. These results therefore suggest that JARID1B is not necessary and has no significant negative impact on the cytostatic BMP4 response of mouse NSCs. As described in section 3.4, we term these BMP4-treated NSCs as d-qNSCs.

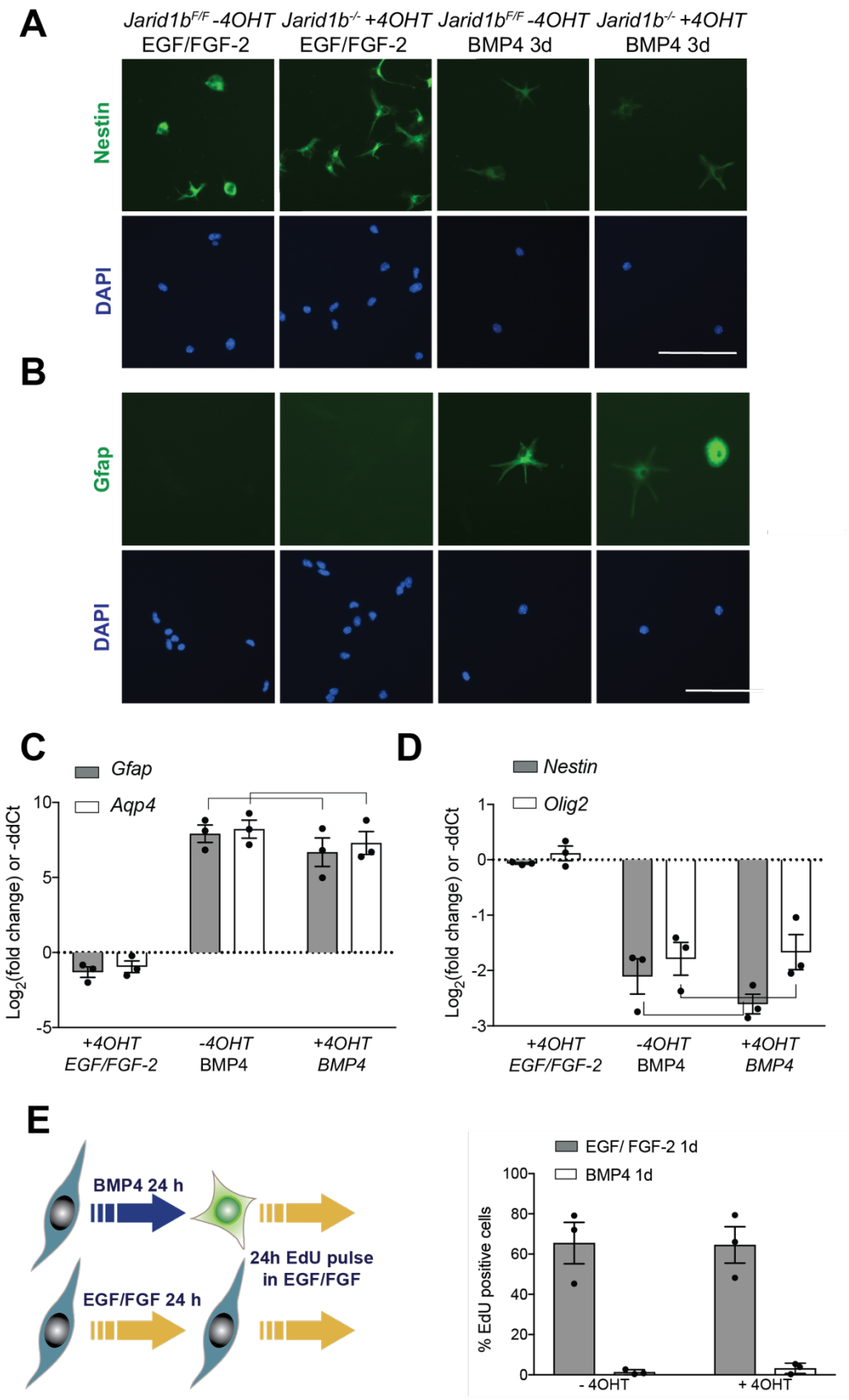

(Figure legend overleaf)

Figure 5-5 | JARID1B is not required for proliferative NSCs to exit cell cycle and upregulate astrocytic markers in response to BMP4 signalling.

Immunofluorescent images showing **(A)** NESTIN and **(B)** GFAP expression in *Jarid1b*$^{F/F}$ (-4OHT) and *Jarid1b*$^{-/-}$ (+4OHT) cells after treatment with EGF/FGF-2 or BMP4 for 3 days. Scale bar: 100 μm. Representative of n=2 independent experiments. **(C)** qRT-PCR analysis of mRNA expression levels of *Gfap, Aqp4*, **(D)** *Nestin* and *Olig2,* in *Jarid1b*$^{F/F}$ (-4OHT) and *Jarid1b*$^{-/-}$ (+4OHT) cells after treatment with EGF/FGF-2 or BMP4 for 24 h. Expression values were normalised to *Gapdh* and shown relative to the expression in *Jarid1b*$^{F/F}$ (-4OHT) cells in EGF/FGF-2 (in which $\log_2$(FC) = 0, shown by the dotted line). Y axis represents $\log_2$(Fold change), equivalent to -ddCt value. Graph shows Mean +/- SEM. n=3 independent experiments. Each data point shows the mean of one experiment, performed in technical duplicates. Statistics were calculated from ddCt values. **(E)** Quantification of % cells with EdU incorporation after treatment with BMP4 or EGF/FGF-2 for 1d, followed by a 24 h EdU pulse in EGF/FGF-2 (*Jarid1b*$^{F/F}$ (-4OHT) and *Jarid1b*$^{-/-}$ (+4OHT) cells). Mean +/- SEM. n=3 independent experiments. Each data point shows the mean of one experiment, performed in technical triplicates. Two-tailed Student's t-tests.

5.2.4 The presence of JARID1B is not required for FOXG1-induced reactivation of d-qNSCs and *Jarid1b* loss alone is not sufficient to drive reactivation

To investigate the effect of *Jarid1b* loss on FOXG1's ability to drive the proliferative NS cell state, we used the same experimental set-up as in Figure 4-8. Both *Jarid1b*$^{F/F}$ (-4OHT) and *Jarid1b*$^{-/-}$ (+4OHT) cells were transfected with expression vectors encoding the PiggyBac transposase, Tet-On 3G transactivator and Dox-inducible FOXG1-V5 expression cassette (Figure 5-6 A). Following antibiotic selection for 7 days (in which all mock-transfected control cells died), the remaining cells were expanded, resulting in a mixed population of cells with different numbers of transgene copies. These cells were then simultaneously plated at 10 cells/mm^2 density in BMP4 to assess FOXG1-induced colony formation, as in sections 3.2.2 and 4.2.5.

qRT-PCR analysis confirmed Dox-inducible expression of the *FOXG1* transgene in both populations. However, this also revealed that the *Jarid1b*$^{-/-}$ (+4OHT) cells had a higher background level of *FOXG1* expression in no Dox controls, and thus a higher absolute level of *FOXG1* expression (Figure 5-6 B and C). While *Jarid1b*$^{F/F}$ (-4OHT) cells showed an ~25-fold increase in *FOXG1* expression with Dox (compared to EGF/FGF-2 control), they did not show significant colony formation in the time frame of the assay (Figure 5-6 D and E). This was likely due to the lower absolute *FOXG1* expression levels. Due to these differences, we could not directly compare the efficiency of colony formation between *Jarid1b*$^{F/F}$ (-4OHT) and *Jarid1b*$^{-/-}$ (+4OHT) cells.

However, upon addition of Dox to *Jarid1b*$^{-/-}$ (+4OHT) cells, the induction of high FOXG1 levels was able to drive reactivation to a highly proliferative NS cell-like state. As seen previously in wildtype mouse NSCs, this resulted in the formation of colonies of NS-like cells, displaying high FOXG1-V5, Nestin and Ki67 expression (Figure 5-7 D and E). We

therefore conclude that JARID1B is not absolutely required for FOXG1-induced reactivation of astrocytic d-qNSCs. In addition, we noted that loss of JARID1B alone is not sufficient to drive reactivation to an NSC-like state, as no colonies formed in the absence of Dox.

Unfortunately, in the *Jarid1b*$^{-/-}$ (+4OHT) cells we noted that the *FOXG1* transgene background expression increased over time, complicating our analysis and conclusions. However, the first experimental replicate showed evidence of equal transgene induction in both cell types (Figure 5-7 A and B), accompanied by increased colony formation in *Jarid1b*$^{-/-}$ (+4OHT) cells after 10 days (Figure 5-7 C). This suggests that loss of *Jarid1b* may increase the efficiency of colony formation, however further repetition is required.

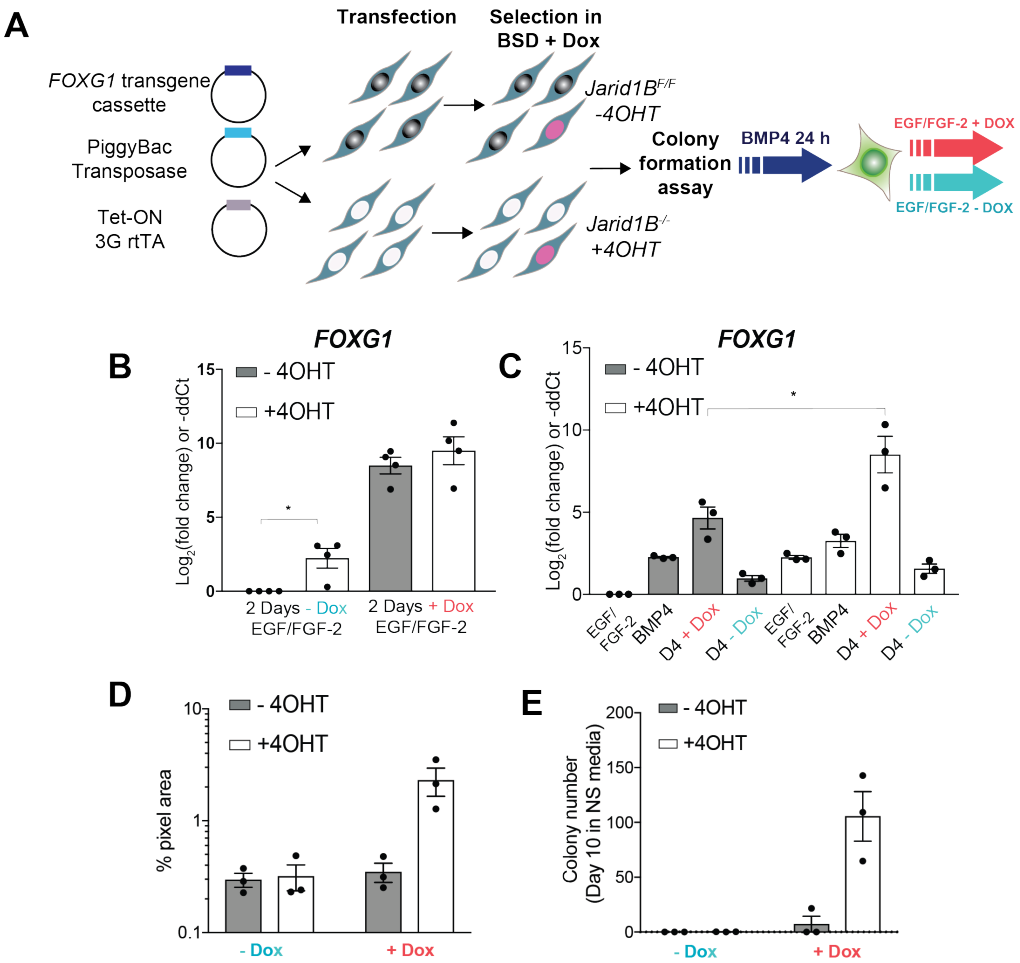

Figure 5-6 | FOXG1 overexpression in BMP4-induced d-qNSCs with or without JARID1B. **(A)** Schematic of PiggyBac transposon strategy used to derive *Jarid1b*$^{F/F}$ (-4OHT) and *Jarid1b*$^{-/-}$ (+4OHT) cells with Dox-inducible expression of a *FOXG1* transgene. In panels (B)-(E), -4OHT and +4OHT refer to transfected cell populations with Dox-inducible FOXG1-V5 overexpression. **(B)** qRT-PCR analysis of *FOXG1* mRNA expression levels in *Jarid1b*$^{F/F}$ (-4OHT) and *Jarid1b*$^{-/-}$ (+4OHT) cells in NS cell media with or without Dox for 2 days. Expression values were normalised to *Gapdh* and shown relative to the expression in *Jarid1b*$^{F/F}$ (-4OHT) cells in EGF/FGF-2 -Dox (in which $\log_2$(FC) = 0). Y axis represents $\log_2$(Fold change), equivalent to -ddCt value. Mean +/- SEM, n=4 independent experiments. Each data point shows the mean of one experiment, performed in technical duplicates. Two-tailed paired t-test. * P ≤ 0.05. **(C)** qRT-PCR analysis of *FOXG1* mRNA expression in *Jarid1b*$^{F/F}$ (-4OHT) and *Jarid1b*$^{-/-}$ (+4OHT) cells after treatment with EGF/FGF-2 or BMP4 for 24h and return to EGF/FGF-2 with or without Dox addition for 4 days. Expression values were normalised to *Gapdh* and shown relative to the expression in *Jarid1b*$^{F/F}$ (-4OHT) cells in EGF/FGF-2 (in which $\log_2$(FC) = 0). Y axis represents $\log_2$(Fold change), equivalent to -ddCt value. Graph shows Mean +/- SEM. n=3 independent experiments. Each data point shows the mean of one experiment, performed in technical duplicates. Two-tailed paired t-test. * P ≤ 0.05. **(D)** Quantification of percentage of the well pixel area covered by cells after 24 h BMP4 treatment and return to NS cell media with or without Dox for 10 days. Mean +/- SEM. n=3 independent experiments. Each data point shows the mean of one experiment, performed in technical triplicates. **(E)** Colony number after 24 h BMP4 treatment and 10 days in NS cell media, with or without Dox addition. Mean +/- SEM, n=3 independent experiments. Each data point shows the mean of one experiment, performed in technical triplicates.

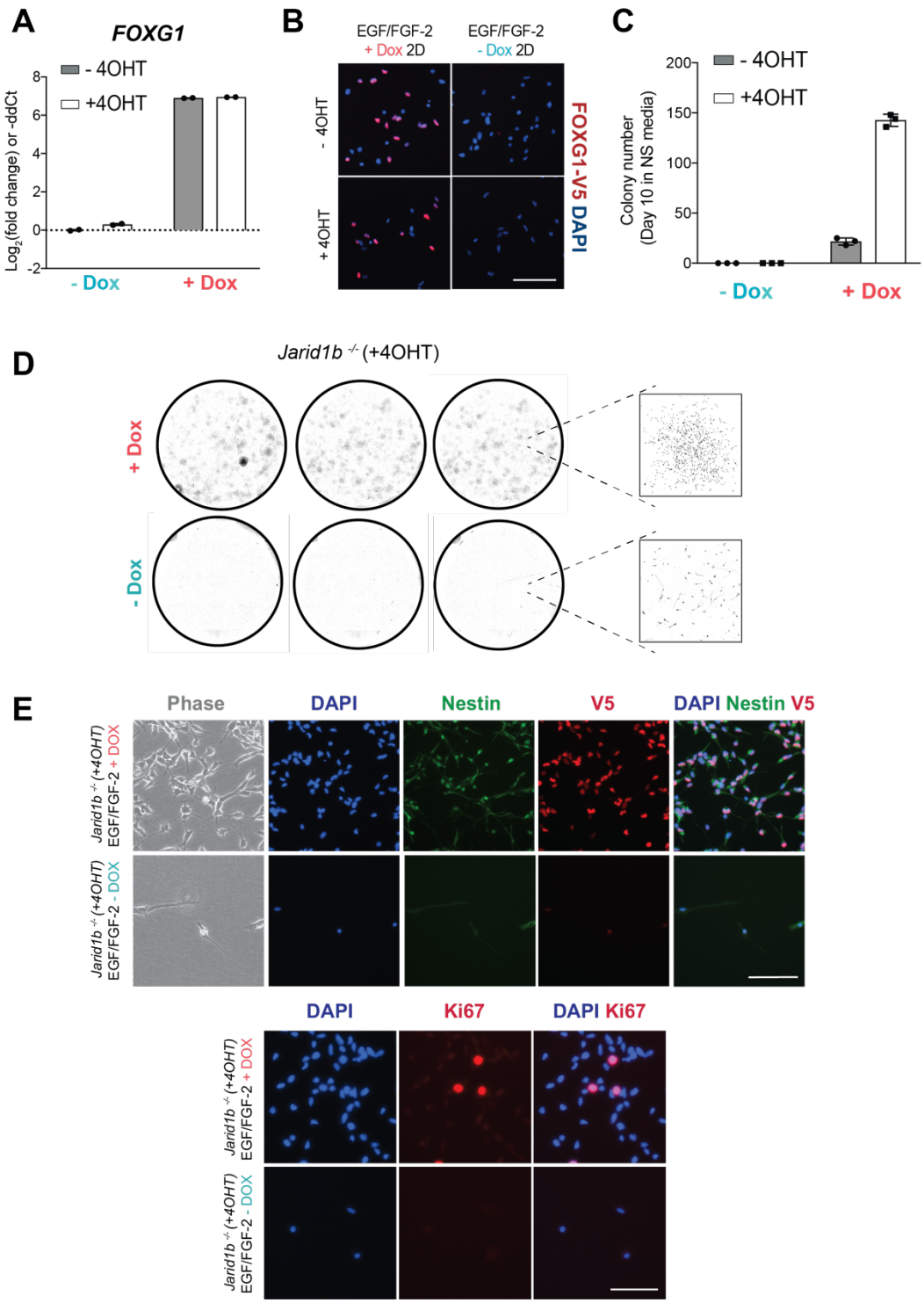

Figure 5-7 | The presence of JARID1B is not required for FOXG1-induced reactivation of d-qNSCs and *Jarid1b* loss alone is not sufficient to drive reactivation.
In panels (A)-(E), *Jarid1b*$^{F/F}$ (-4OHT) and *Jarid1b*$^{-/-}$ (+4OHT) refer to transfected cell populations with Dox-inducible FOXG1-V5 overexpression. **(A)** qRT-PCR analysis of mRNA expression levels of FOXG1 in *Jarid1b*$^{F/F}$ (-4OHT) and *Jarid1b*$^{-/-}$ (+4OHT) NS cells in NS cell media with or without Dox for 2 days. *Figure legend continued overleaf.*

Expression values were normalised to *Gapdh* and shown relative to the expression in *Jarid1b*$^{F/F}$ (-4OHT) cells in EGF/FGF-2 -Dox (in which $\log_2$(FC) = 0, shown by the dotted line). Y axis represents $\log_2$(Fold change), equivalent to -ddCt value. Graph shows Mean +/- SD. One experiment, n=2 technical replicates. **(B)** Immunofluorescent images showing FOXG1-V5 expression in *Jarid1b*$^{F/F}$ (-4OHT) and *Jarid1b*$^{-/-}$ (+4OHT) cells in NS cell media with or without Dox for 2 days. Scale bar: 100 μm. **(C)** Colony number after 24 h BMP treatment and 10 days in NS cell media with EGF/FGF-2, with or without Dox addition. Mean +/- SD, n=3 technical replicates. **(D)** Representative image of colony formation in *Jarid1b*$^{-/-}$ (+4OHT) cells after 24 h BMP4 treatment and 10 days in media with EGF/FGF-2, with or without Dox addition. 6 well plate stained with methylene blue after fixation. **(E)** Phase-contrast and immunofluorescent images showing FOXG1-V5, Nestin and Ki67 expression in parental *Jarid1b*$^{-/-}$ (+4OHT) cells after 24 h BMP4 treatment and 10 days in NS cell media with EGF/FGF-2, with or without Dox addition. Scale bar: 100 μm.

5.2.5 The presence of JARID1B is not required for FOXG1-induced activation of *FoxO6* or *Chd3* expression and *Jarid1b* loss alone is not sufficient to drive their activation

In parallel to assessing colony formation on induction of FOXG1 expression, mRNA was collected to investigate whether JARID1B was required for transcriptional activation by FOXG1. In the *Jarid1b*$^{-/-}$ (+4OHT) cells with inducible FOXG1-V5 overexpression, an upregulation in *FoxO6* and *Chd3* levels was observed on addition of Dox, indicating JARID1B is not required for FOXG1-induced activation of these genes (Figure 5-8 A, B E and F). In addition, *Jarid1b* loss alone does not result in *FoxO6* or *Chd3* activation. Again, due to unequal levels of *FOXG1* transgene expression we could not make any firm conclusions regarding the relative effects of *Jarid1b* loss on activation of these targets. However, the first experimental replicate, which showed evidence of equal transgene induction in both cell types (Figure 5-7 A and B), suggests that loss of *Jarid1b* does not affect the magnitude of *FoxO6* or *Chd3* upregulation by FOXG1 (not shown). mRNA collected during the colony assays conducted for *Jarid1b*$^{F/F}$ (-4OHT) cells showed no significant upregulation of *FoxO6* nor *Chd3* on addition of Dox (Figure 5-8 C and D). In summary, altogether our results suggest that JARID1B does not play a critical role in enabling FOXG1-induced reactivation of d-qNSCs, nor transcriptional activation of *FoxO6* or *Chd3.*

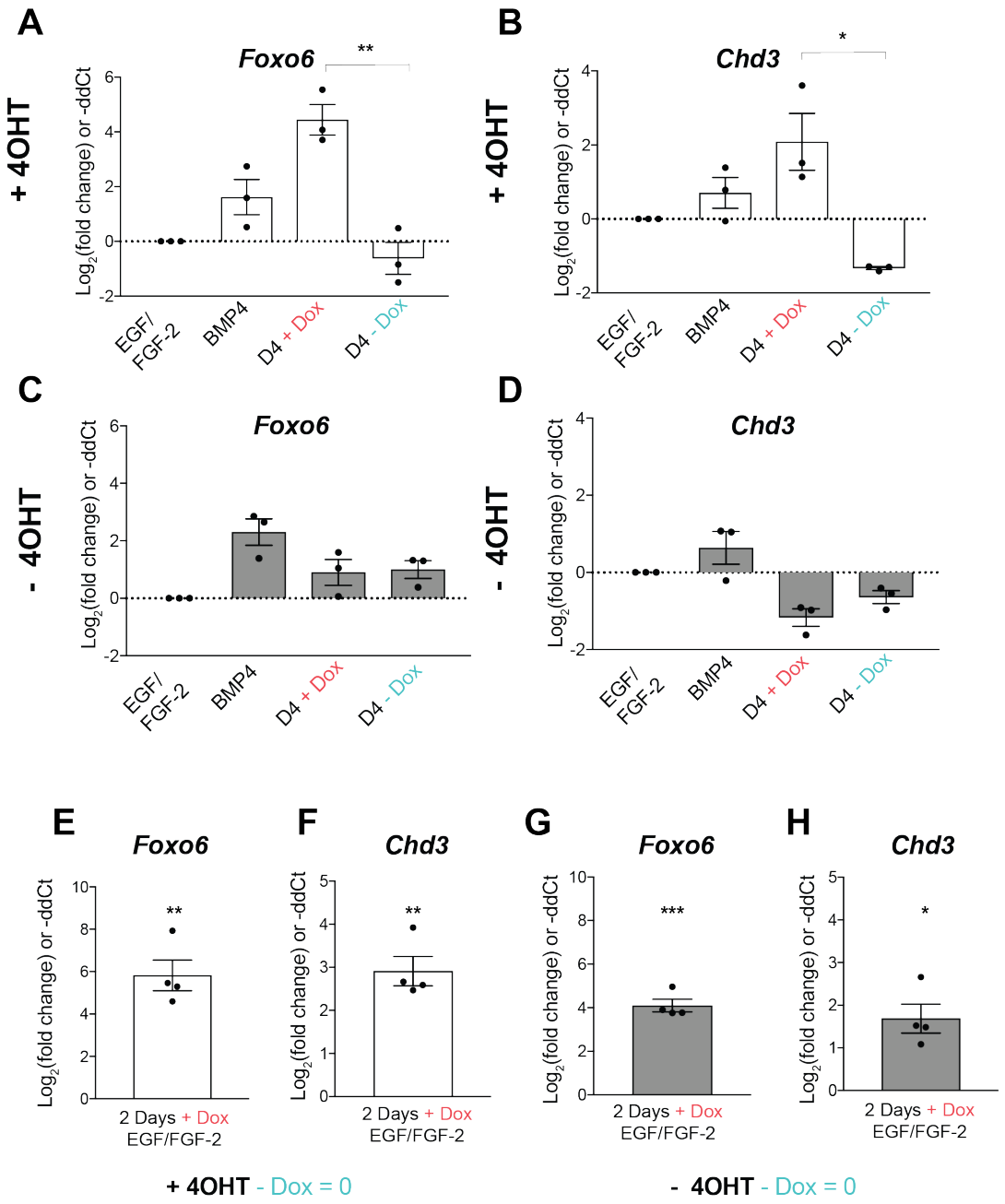

Figure 5-8 | The presence of JARID1B is not required for FOXG1-induced activation of *FoxO6* or *Chd3* expression and *Jarid1b* loss alone is not sufficient to drive their activation.

In panels (A)-(H), *Jarid1b*$^{F/F}$ (-4OHT) and *Jarid1b*$^{-/-}$ (+4OHT) refer to transfected cell populations with Dox-inducible FOXG1-V5 overexpression. **(A and B)** qRT-PCR analysis of mRNA expression levels of **(A)** *FoxO6* or **(B)** *Chd3* in *Jarid1b*$^{-/-}$ (+4OHT) cells after treatment with EGF/FGF-2 or BMP4 for 24h and return to EGF/FGF-2 with or without Dox addition for 4 days. Expression values were normalised to *Gapdh* and shown relative to the expression in *Jarid1b*$^{-/-}$ (+4OHT) cells in EGF/FGF-2 (in which $\log_2(FC) = 0$, shown by the dotted line). Y axis represents $\log_2$(Fold change), equivalent to -ddCt value. Graph shows Mean +/- SEM. n=3 independent experiments. Each data point shows the mean of one experiment, performed in technical duplicates. *Figure legend continued overleaf.*

(C and D) qRT-PCR analysis of mRNA expression levels of **(C)** *FoxO6* or **(D)** *Chd3* in *Jarid1b*$^{F/F}$ (-4OHT) cells after treatment with EGF/FGF-2 or BMP4 for 24h and return to EGF/FGF-2 with or without Dox addition for 4 days. Expression values were normalised to *Gapdh* and shown relative to the expression in *Jarid1b*$^{F/F}$ (-4OHT) cells in EGF/FGF-2 (in which $\log_2$(FC) = 0, shown by the dotted line). n=3 independent experiments. Each data point shows the mean of one experiment, performed in technical duplicates. Two-tailed Student's t-tests. * P ≤ 0.05, ** P ≤ 0.01. **(E and F)** qRT-PCR analysis of mRNA expression levels of **(E)** *FoxO6* or **(F)** *Chd3* in *Jarid1b*$^{-/-}$ (+4OHT) cells in NS cell media with or without Dox for 2 days. Expression values shown relative to the expression in *Jarid1b*$^{-/-}$ (+4OHT) cells in EGF/FGF-2 -Dox (in which $\log_2$(FC) = 0). Graph shows Mean +/- SEM. n=4 independent experiments. Each data point shows the mean of one experiment, performed in technical duplicates. **(G and H)** qRT-PCR analysis of mRNA expression levels of **(G)** *FoxO6* or **(H)** *Chd3* in *Jarid1b*$^{F/F}$ (-4OHT) cells in NS cell media with or without Dox for 2 days. Expression values shown relative to the expression in *Jarid1b*$^{F/F}$ (-4OHT) cells in EGF/FGF-2 -Dox (in which $\log_2$(FC) = 0). n=4 independent experiments. Each data point shows the mean of one experiment, performed in technical duplicates. Two-tailed one sample t-tests. * P ≤ 0.05, ** P ≤ 0.01, *** P ≤ 0.001.

5.2.6 Available FOXG1 antibodies are sub-optimal for immunoprecipitation

Following the derivation of additional *FOXG1* knock-out mouse and human GBM model cell lines, described in sections 4.2.3 and 4.2.6, we decided to validate the co-IP of FOXG1 and JARID1B using these as additional negative controls. Although isotype controls matching the class and type of the primary antibody used for IP are standard practice, knockout cell lines provide the most robust negative control, as any background observed in an IP with a knock-out cell line is due to unspecific binding by the exact antibody used for the test IP.

Native FOXG1 IPs using the 17B12 monoclonal antibody were performed in the mouse GSC line, IENS, and human GNS cell lines, G7 and G313, alongside their respective *FOXG1* null controls. Again, this showed a successful enrichment of FOXG1 in the IP versus the input lane for each parental cell line, with no FOXG1 expression in the null control. However, surprisingly, we also observed a band at the expected size of JARID1B, of similar intensities, in both IPs with the wild-type and *FOXG1* null cell lines (Figure 5-9 A and B).

To validate this result, G7 and G7 *FOXG1* null cells were re-cultured and the FOXG1 IP repeated with an additional IgG isotype control (Figure 5-9 C). A different anti-human JARID1B antibody (CST 3273 instead of NBP1-84352) was used to probe for JARID1B co-IP. This again showed co-IP of JARID1B in the *FOXG1* null cell line and confirmed the previous result was not due to non-specificity of the Novus Biologicals anti-JARID1B antibody. The IgG control showed no non-specific binding by the beads or antibody, other than bands we considered to be degradation products of the antibody itself. For example, a band at approximately 90 kDa was visible in all IPs (IgG and 17B12) which could be due to incomplete antibody denaturation. If due to unspecific binding, this

contamination did not lead to co-IP of JARID1B. In addition, the mouse IENS blots were re-probed with the knockout validated anti-JARID1B DAIN78 antibody (Figure 5-9 B), again confirming the co-IP of JARID1B with FOXG1 in *Foxg1* null cells.

While the anti-FOXG1 17B12 antibody has been shown to be specific for FOXG1 by ICC and Western blotting (Figures 4-3 and 4-11), these results suggest that, by IP, 17B12 is binding another factor non-specifically. It is possible that the epitope that 17B12 was raised against also leads to binding to another Forkhead factor which interacts with JARID1B. As the specific epitope sequence is not available, we were unable to formally test this hypothesis.

This result raised questions regarding our initial result (Figure 5-2) that JARID1B is pulled down with FOXG1. While FOXG1 is clearly enriched in the IP versus control, the presence of a JARID1B band of similar intensities in the IPs on wildtype and *FOXG1* null cell lysates indicates this is due to poor specificity of 17B12 in the context of IPs. We next tested a commercial anti-FOXG1 ChIP-grade antibody (ab18259); this revealed a pull-down of FOXG1 but poor enrichment compared to the input lane, and no co-IP with JARID1B (Figure 5-9 D and E). These experiments highlight both the importance of knockout controls for IPs, and potential problems with native antibodies, both in terms of specificity and suitability for desired applications. Together with the functional data, we therefore do not view JARID1B as a strong candidate partner controlling the activity of FOXG1 in NSCs.

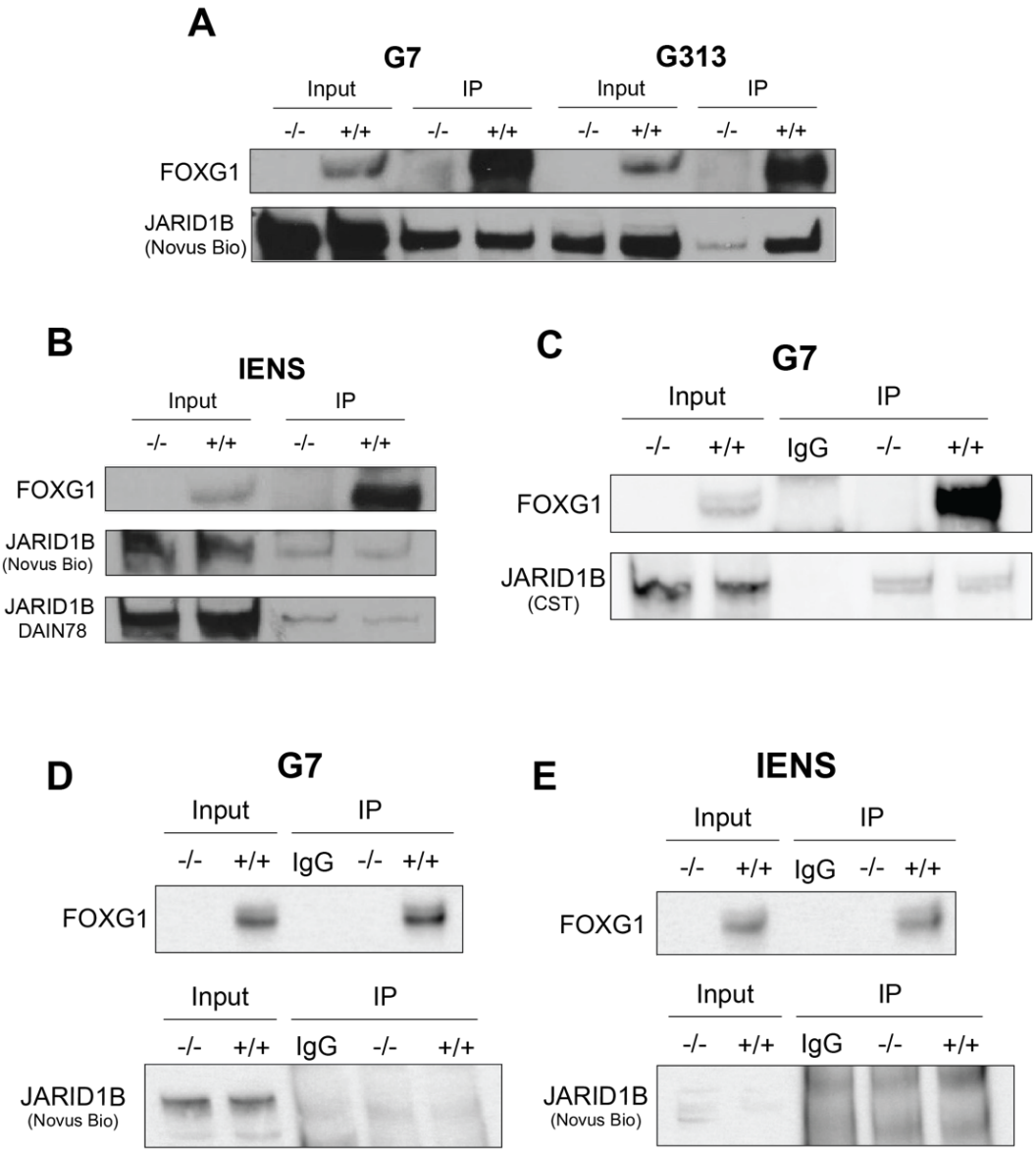

Figure 5-9 | Available anti-FOXG1 antibodies are sub-optimal for immunoprecipitation.

(A) 17B12 FOXG1 IP in human GNS cell lines: G7, G7 *FOXG1* null clonal line, G313 and G313 *FOXG1* null clonal line 42. Blots probed with FOXG1 17B12 and anti-JARID1B antibodies (Novus Biologicals, NBP1-84352). **(B)** 17B12 FOXG1 IP in mouse GSC line IENS and IENS *Foxg1* null clonal line 58 (all cells IENS-GFP). Blots probed with FOXG1 17B12 and anti-JARID1B antibodies (Novus Biologicals, NBP1-84352 and DAIN78 (Helin lab)). **(C)** 17B12 FOXG1 IP in human GNS cell line G7 and G7 *FOXG1* null clonal line. Blots probed with FOXG1 17B12 and anti-JARID1B antibodies (CST, 3273). **(D)** FOXG1 Abcam (ab18259) IP in human GNS cell line G7 and G7 *FOXG1* null clonal line. Blots probed with FOXG1 17B12 and anti-JARID1B antibodies (Novus Biologicals, NBP1-84352). **(E)** FOXG1 Abcam (ab18259) IP in mouse GSC line IENS and IENS *Foxg1* null clonal line 58 (all cells IENS-GFP). Blots probed with FOXG1 17B12 and anti-JARID1B antibodies (Novus Biologicals, NBP1-84352). All FOXG1 bands are at ~70 kDa, all JARID1B bands are at ~175 kDa.

5.3 CRISPR/Cas9-mediated gene tagging as a tool to aid exploration of protein-protein interactions

The results in section 5.2.6 highlight the difficulties with reliance on native antibodies for applications such as immunoprecipitation. Our results show that isotype controls are not always sufficient to guarantee the specificity of an antibody. The advent of CRISPR/Cas9 technology has meant the derivation of knockout controls has become more accessible, but these may not be available for every protein of interest. In addition, it is time-consuming and costly to search for commercial antibodies suitable for each desired application and polyclonal antibodies can show batch-to-batch variation.

In this section, we therefore explored the use of CRISPR/Cas9 technology to epitope tag the endogenous *FOXG1* gene in models of GBM (an approach also used to tag *FoxO6* in section 4.2.2). The fusion of small universal peptide tags (e.g. V5, FLAG, HA) to proteins generally does not disrupt their native structure or function and means that validated high-quality antibodies are available for any application. A single validated antibody can then be used to explore many proteins of interest.

Previously, epitope tagging in mammalian cell lines was limited to transgenes ectopically expressed at non-physiological levels. The development of CRISPR/Cas9 facilitated tagging of endogenous genes for the first time in ES cells and cancer cell lines, importantly allowing studies on the gene of question at native levels (Savic *et al*, 2015; Yang *et al*, 2013; Bressan *et al*, 2017). Recently, a protocol was developed by our lab for the knock-in of epitope tags to endogenous genes in mouse NS cells (Bressan *et al*, 2017). To facilitate scale-up, this method was later modified to incorporate a modified two-part synthetic cr/tracrRNA system (Dewari *et al*, 2018), with further gains in efficiency.

5.3.1 Epitope tagging *Foxg1* with a V5 tag in mouse and human GNS cells

Highly efficient epitope tagging of endogenous genes in NS cells can be achieved without the requirement of selectable markers, cell sorting or plasmid delivery (Dewari *et al*, 2018). These studies included the V5 tag, a 42 bp epitope derived from the paramyxovirus of the simian virus 5 family. This is a widely used epitope tag in our laboratory and does not impair the production of functional FOXG1 protein or its activity (the transgene used in Chapter 3 was V5-tagged, and functional). This method was therefore used to V5 tag the endogenous *Foxg1* gene in both mouse (IENS) and human (G7) models of GBM, with reagents designed separately for each.

Firstly, a CRISPR gRNA was designed to cut proximal to the stop codon in the 3' UTR of *Foxg1*, with minimal predicted off-target cleavage. Tagging at the C terminus was chosen to avoid disruption of the endogenous gene-coding sequence by gRNA cutting. A two-part RNA complex was then formed by annealing this short, chemically synthesised, target-specific crRNA with a longer universal tracrRNA (Anderson *et al*, 2015; Jacobi *et al*, 2017) (Figure 5-10 A). This dual cr/tracrRNA (obtained from IDT) was then incubated with rCas9 protein to form a Cas9 ribonucleoprotein complex (RNP). This pre-assembled Cas9 RNP was then co-delivered into cells alongside a single-stranded ~200 bp long oligodeoxynucleotide (ssODN) that acts as a repair template. This ssODN was designed to comprise the 45 bp V5 tag sequence, flanked by 70 bp homology arms, with the protospacer adjacent motif (PAM) mutated from NGG to NGC to prevent re-cutting of the edited alleles. This resulted in a DSB produced by the Cas9 RNP which is repaired by homology-directed repair (HDR) to incorporate the V5 tag directly upstream of the stop codon (Figure 5-10 B). The bulk transfected

population was assessed by ICC for successful integration of the V5 tag, revealing a high knock-in frequency (~10% in IENS and ~8% in G7). Clonal cell lines were then derived and assessed for FOXG1-V5 expression by ICC and tag integration confirmed by PCR genotyping (Figure 5-11 A-C). Sequencing of the PCR product confirmed successful targeting, shown for an IENS tagged clonal line. This resulted in the successful recovery of biallelic-tagged clonal lines in both mouse IENS cells and human G7 cells (both constitutively expressing GFP).

V5-IPs were performed in both mouse IENS and human G7 cells (by C. Blin and S. VijayKumar). While in IENS FOXG1-V5 cells this showed a good enrichment of FOXG1-V5 in the IP versus input (Figure 5-12 C), the enrichment in G7 FOXG1-V5 clone 50 was poorer (Figure 5-12 A). This was repeated in additional G7 clonal tagged lines, showing an enrichment in all lines but still lower than in IENS (Figure 5-12 B). It was noted that co-IP of JARID1B was not observed in any of the IPs.

In order to validate protein partners of FOXG1 in GBM, it is necessary to confirm their interaction in multiple cell lines derived from different patients. We therefore tested this tagging strategy in additional human GNS cell lines from the GCGR, such as G313 and G328 (by S. VijayKumar). This revealed variations in tagging efficiency between the cell lines, with G313 and G328 showing approximate efficiencies of 7% and 0.47%, respectively (Figure 5-12 D). While the former is amenable to recovery of bi-allelic knock-in clonal lines without prior selection, an efficiency of less than 1% is not compatible with this method and further compounded by slow colony formation by human GNS cell lines (6 weeks or longer). Sequencing around the gRNA cutting site was performed to ensure the absence of polymorphisms that could decrease knock-in efficiencies (Figure 5-12 E). Alternative strategies would therefore be required to recover successfully tagged cells.

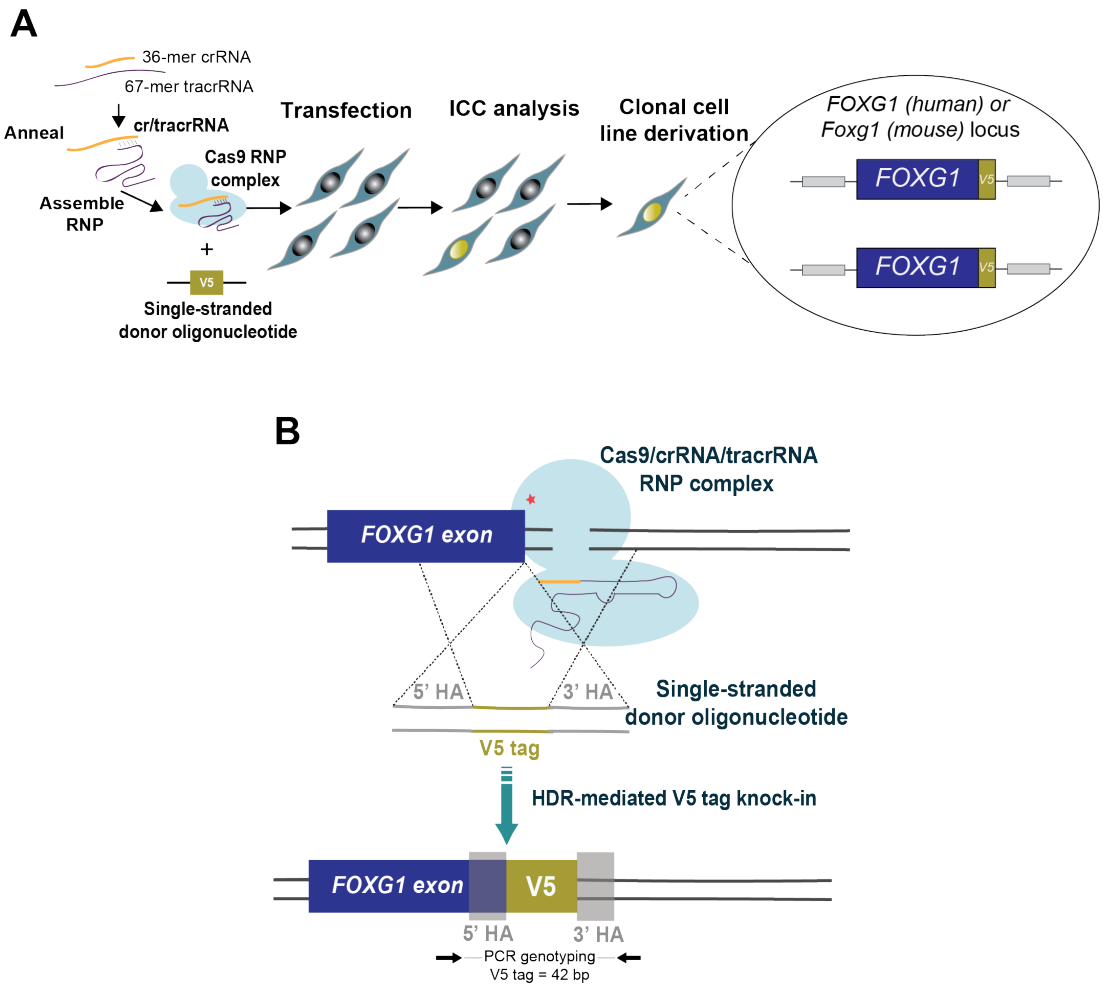

Figure 5-10 | Overview of CRISPR/Cas9-mediated V5 epitope tagging of endogenous *FOXG1*.

(A) Experimental strategy used to V5 epitope-tag endogenous *Foxg1/FOXG1* gene in mouse GSC line, IENS, and human GNS cell line, G7. **(B)** Schematic describing epitope-tagging knock-in strategy. Stop codon is indicated by red asterisk. Following formation of a double-strand break by the Cas9 RNP complex, HDR using the ssODN repair template results in V5 tag knock-in at the 3' end of the FOXG1 coding exon. Approximate location of PCR genotyping primers indicated. HA = homology arm.

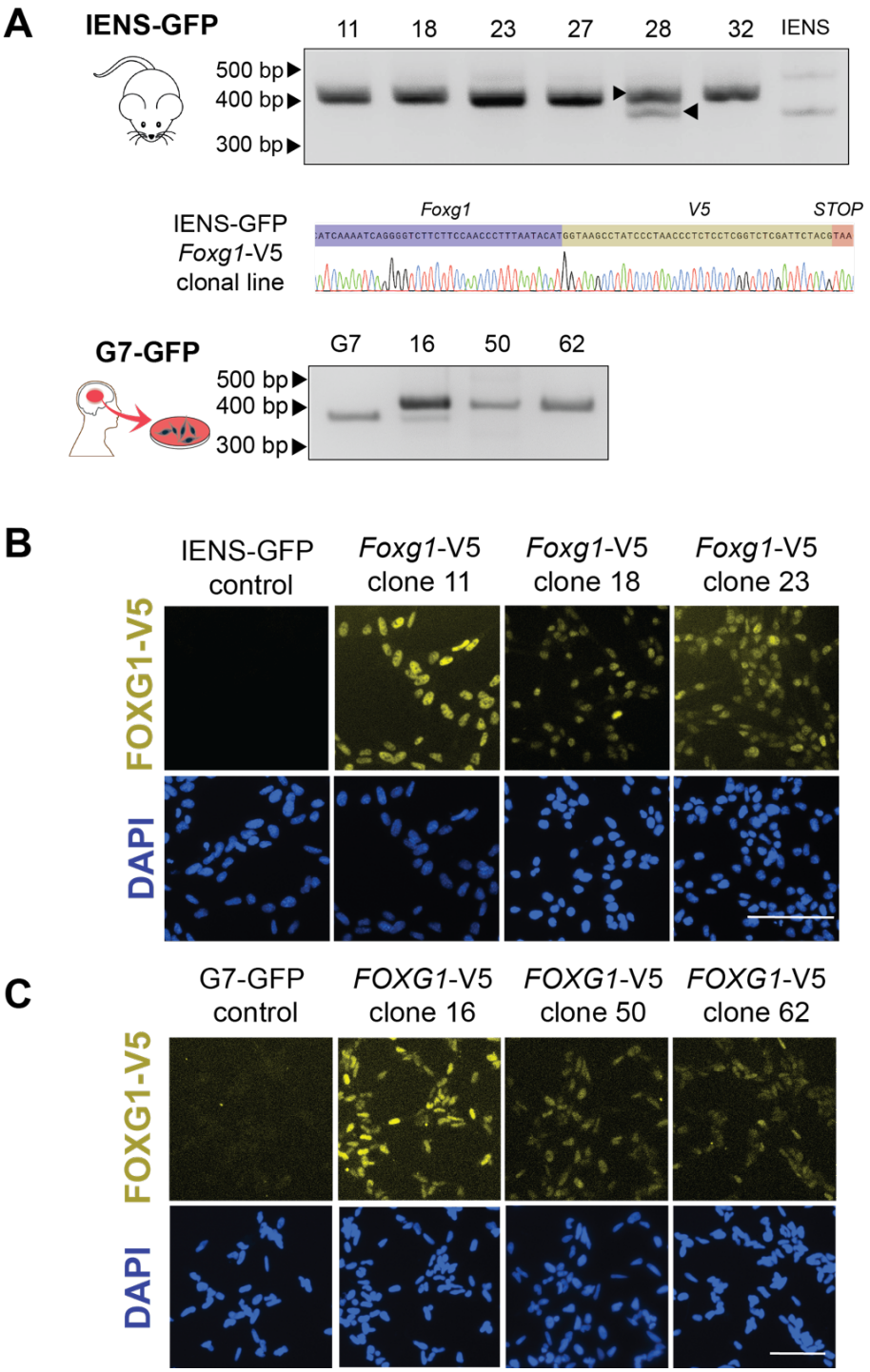

Figure 5-11 | V5 epitope tagging of FOXG1 in mouse GSCs (IENS cells) and human GNS cells (G7).

(A) PCR genotyping of IENS-GFP and G7-GFP clonal cell lines to verify insertion of the V5 tag at the 3' end of *Foxg1/FOXG1*. Correct insertion verified by a 42 bp increase in PCR product size. Example sequencing trace of an IENS-GFP FOXG1-V5 clonal line is shown. Upper arrow indicates tag insertion, lower arrow indicates wild-type sequence. **(B and C)** ICC analysis of FOXG1-V5 expression in **(B)** IENS parental cells, and *Foxg1*-V5 clonal lines 11, 18 and 23, **(C)** G7 parental cells, and *FOXG1*-V5 clonal lines 16, 50 and 62. Scale bars: 100 μm.

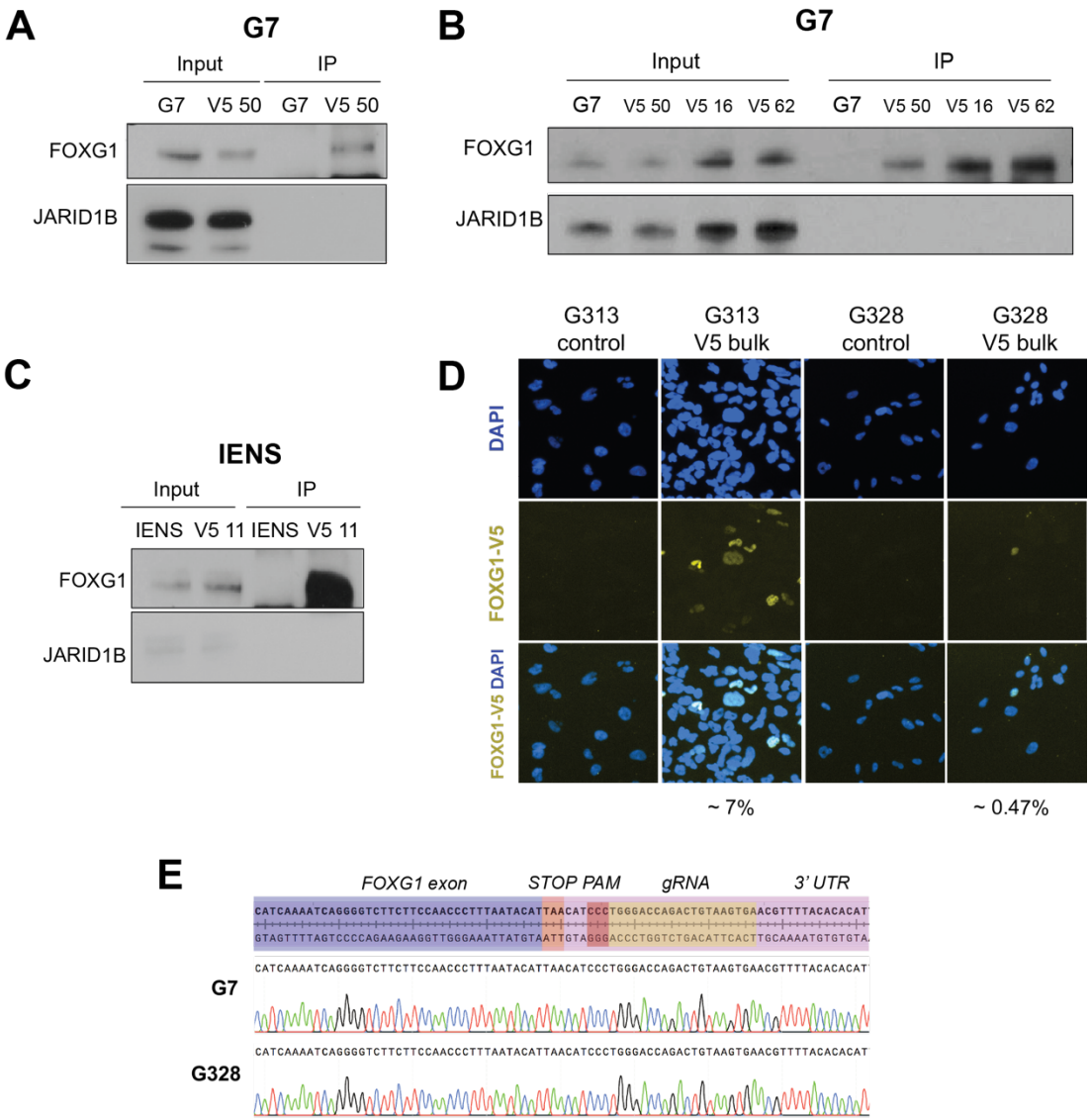

Figure 5-12 | V5-IPs in *FOXG1*-tagged IENS and G7 cells, and epitope tagging of *FOXG1* in additional human GNS cell lines.

(A) V5-IP in human GNS cell lines G7 and G7 FOXG1-V5 clone 50. **(B)** V5-IPs in human GNS cell lines G7 and G7 FOXG1-V5 clones 50, 16 and 62. **(C)** V5-IP in mouse GSC lines IENS and IENS FOXG1-V5 clone 11. Blots probed with anti-FOXG1 (17B12) and anti-JARID1B (Novus Biologicals) antibodies. **(D)** ICC analysis of human GNS G313 and G328 populations following transfection for FOXG1-V5 tagging. Number indicates approximate tagging efficiency. Scale bar: 100 μm. **(E)** Sanger sequencing of G7 and G328 at region of the *FOXG1* gene around the gRNA cutting site. Regions of interest are highlighted, including *FOXG1* exon sequence (purple), STOP codon (orange), PAM site (red), gRNA annealing site (yellow) and *FOXG1* 3' UTR (pink). A-C performed by C. Blin and S. VijayKumar. D-E performed by S. VijayKumar.

5.3.2 Enrichment of epitope-tagged population using self-cleaving p2A peptide

We next adapted the method by including a fluorescent reporter linked via a self-cleaving p2A peptide, as this would allow the enrichment of successfully tagged cells by FACS. The dual cr/tracrRNA Cas9 RNP method described has been previously used to successfully knock-in fluorescent reporters in NS cells using a double-stranded donor DNA repair template (Dewari *et al*, 2018). However, the addition of a large protein tag to a coding sequence poses an increased risk of disrupting the native protein folding or function. To mitigate this risk, a strategy was designed in collaboration with Dr Pooran Dewari in the Pollard lab to incorporate a C terminal epitope tag, followed by a self-cleaving peptide and fluorescent marker.

We chose to employ the p2A peptide, as it is reported to be the most efficiently cleaved 2A peptide (Kim *et al*, 2011b). This peptide was preceded by a GSG linker to further increase cleavage efficiency (Wang *et al*, 2015) and followed by an upstream eGFP sequence, recognised by available anti-GFP antibodies. Following translation of the FOXG1 protein, the p2A peptide would be cleaved, leaving the C-terminal epitope tag and a small portion of the p2A peptide at the C terminus of FOXG1. The fluorescent eGFP tag would be released, leading to all cells with successful tag insertion being marked by positive eGFP expression.

Following a report that dual tagging with 3xFLAG and HA achieves the highest IP efficiency (direct communication Olivier Ayrault, (Forget *et al*, 2014)), a gene fragment was ordered from GeneArt, which was sequence verified and cloned into a pMX series vector (Figure 5-13 A). This gene fragment consisted of the 3xFLAG-HA-p2A-eGFP tag (with the FLAG and HA tags preceded by a GS linker and the p2A peptide preceded by a GSG linker), flanked by 500 bp homology arms. These homology arms

were larger than described in section 5.3.1, as HDR efficiency is lower with larger tag insertions and a dsDNA donor template.

Following PCR amplification of the dsDNA fragment from the received plasmid, the 1888 bp product was purified by gel extraction and amplified again by PCR to yield enough dsDNA for transfections (Figure 5-13 A). Prior to co-delivery with the cr/tracrRNA Cas9 RNP complex by transfection, the dsDNA PCR product was purified and denatured by treatment with DMSO at 95°C for 5 minutes to promote ssDNA formation.

This transfection was performed in human GNS cell lines, G7 and G313, as proof of principle of the tagging strategy (Figure 5-13 B). Following recovery of the transfected cells, FACS was performed to enrich for the GFP positive population (Figure 5-13 C). PCR genotyping of the sorted populations showed successful tag integration (Figure 5-13 D). ICC analysis revealed expression of FLAG and HA in both sorted populations. No defect in FOXG1 expression was observed as a result of the tag insertion (Figure 5-13 E and F). Quantification of the HA positive cells revealed ~57% and ~92% in the G7 and G313 sorted populations, respectively. This is likely due to the stringency of the GFP gates when sorting and should be optimised to achieve 100%. Although this strategy results in a large reduction in the initial transfection efficiency (compared to the V5 tag alone), this is not detrimental to the final outcome as FACS enables isolation of even very small cell numbers, side-stepping lengthy colony screening.

HA-IPs using these sorted populations confirmed successful pull-down of the tagged FOXG1 protein in both G7 and G313 (Figure 5-14). As expected, in the tagged sorted populations, the input lane shows two bands for FOXG1, at approximately 70 and 76 kDa; this indicated remaining untagged FOXG1 protein due to the presence of a mixed population of heterozygous or homozygous tagged cells. Tagged-FOXG1 was modestly

enriched in the IP versus the input. It was noted that co-IP of JARID1B was not seen in either cell line. These tagged GNS cell lines will be useful in further studies, such as IP-Mass spectrometry, to characterise FOXG1 interaction partners.

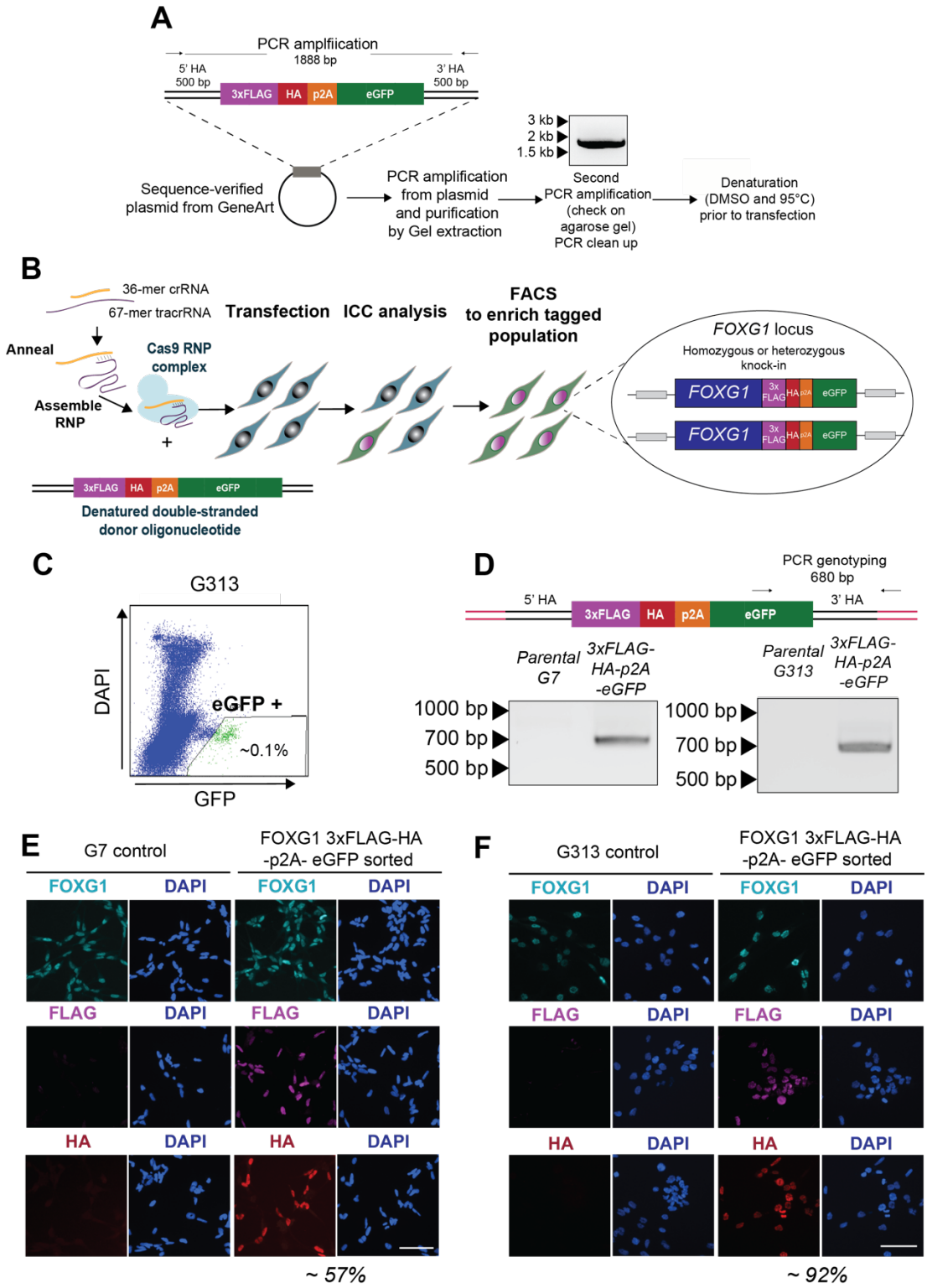

Figure 5-13 | Enrichment of epitope-tagged population using self-cleaving p2A peptide.

(Figure legend continued overleaf)

(A) Schematic describing preparation of dsDNA repair template. **(B)** Experimental strategy using cr/tracrRNA Cas9 RNP complex and denatured dsDNA repair template to derive a population enriched for tagged cells. **(C)** FACS was performed to collect GFP positive G313 population following transfection (Note: parental G7 and G313 cell lines do not express GFP). **(D)** PCR genotyping to confirm successful integration of tag at the 3' end of *FOXG1* in human GNS cell lines G7 and G313. 3xFLAG-HA-p2A-eGFP represents the sorted GFP positive population. **(E)** ICC analysis of FOXG1, FLAG and HA expression in parental G7 and 3xFLAG-HA-p2A-eGFP GFP positive sorted population. Scale bar: 100 μm. **(F)** ICC analysis of FOXG1, FLAG and HA expression in parental G313 and 3xFLAG-HA-p2A-eGFP GFP positive sorted population. Scale bar: 100 μm. Number indicates approximate % of HA tagged cells in the sorted population.

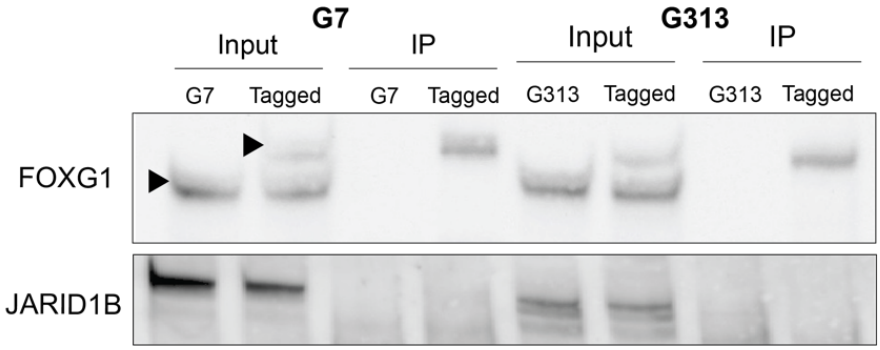

Figure 5-14 | HA IP in 3xFLAG-HA-p2A-eGFP *FOXG1* tagged human GNS cells (G7 and G313)

HA IP in G7 and G313 parental cells, alongside 3xFLAG-HA-p2A-eGFP sorted populations. Arrows indicate the untagged wild-type and tagged forms of FOXG1, at approximately 70 kDa and 76 kDa, respectively. Approximately 2-5 % of the IP lysate was loaded in the input lane. Blot probed with 17B12 anti-FOXG1 antibody (upper panel) or anti-JARID1B antibody (Novus Biologicals, lower panel).

5.4 Discussion

In this chapter, we first explored the importance of the H3K4 demethylase JARID1B to the function of FOXG1. We reasoned that binding of FOXG1 to JARID1B off DNA might limit its ability to repress gene expression, and thereby explain FOXG1 driven activation of *FoxO6* (Figure 5-1 B). However, we did not find any indication of a critical role for JARID1B in explaining FOXG1 activity. Furthermore, we did not validate an interaction between these factors.

Our loss-of-function experiments involved overexpression of a human *FOXG1* transgene in mouse NSCs with and without a Cre-mediated frameshift in *Jarid1b.* This experimental system therefore investigated the role of an interaction between human FOXG1 and mouse JARID1B. Both mouse and human *Foxg1* sequences contain a conserved JARID1B-binding VP motif. While the motif through which JARID1B binds FOXG1 has not been mapped, mouse and human proteins display 94% protein sequence homology. We therefore considered the FOXG1-JARID1B interacting regions would most likely be conserved between mouse and human proteins. Deletion of *Jarid1b* was previously shown to have no effect on the expression of other *Jarid1*-family members (Schmitz *et al*, 2011); furthermore while JARID1 proteins show high sequence homology, domain differences in their C terminals are thought to lead to the formation of diverse protein complexes, with only JARID1B reported to bind to FOXG1 (Catchpole *et al*, 2011). Therefore, we also considered it unlikely that loss of *Jarid1b* would be replaced by redundant functions of other Jarid1 members. Based on our validation that full-length JARID1B expression is absent at the mRNA and protein level in +4OHT treated cells (Figure 5-3 E and F) and previous validation of this deletion strategy by Schmitz *et al.,* we reasoned these cells could be termed *Jarid1b*$^{-/-}$. Due to the lack of available antibodies against the N-terminus of JARID1B it was not possible to confirm the absence of

truncated forms, although if present these are likely to be at low levels (Schmitz *et al*, 2011).

Our results suggest that the presence of JARID1B is not required for FOXG1's ability to induce reactivation of astrocytic BMP4-induced d-qNSCs (Figures 5-6 and 5-7), or for the transcriptional activation of *FoxO6* and *Chd3* (Figure 5-8). In light of our initial hypotheses, these findings suggest that an interaction between FOXG1 and JARID1B is not required to lead to FOXG1-mediated transcriptional activation.

While we cannot exclude a role of a FOXG1-JARID1B interaction in activation or repression of other genes, the ability of FOXG1 overexpression to drive a proliferative NS cell-like state in the absence of JARID1B suggests that any genes regulated via FOXG1-JARID1B are not determining factors of this cell fate transition. In addition, the loss of JARID1B alone was not sufficient to drive cells into a proliferative state or lead to upregulation of *FoxO6* or *Chd3* (Figures 5-6, 5-7 and 5-8). This suggests *FoxO6* and *Chd3* are not upregulated through a mechanism by which excess FOXG1 sequesters JARID1B leading to *in trans* gene 'de-repression'.

We note that we cannot rule out a positive or negative impact of JARID1B loss on the efficiency of FOXG1-induced d-qNSC reactivation; for this stable induction of equal levels of *FOXG1* transgene are needed in *Jarid1b*$^{F/F}$ (-4OHT) and *Jarid1b*$^{-/-}$ (+4OHT) cell lines. JARID1B loss itself did not significantly affect NSC proliferation in EGF/FGF-2 (Figure 5-4) or response to BMP4 signalling (Figure 5-5). Indeed, while JARID1B is essential in controlling ES cell differentiation by epigenetically silencing developmental genes, it was shown to be dispensable for neuronal differentiation of NSCs (Schmitz *et al*, 2011). However, Schmitz *et al* did find *Jarid1b* knockout NSCs to show a slightly delayed downregulation of the NS cell marker, Nestin; this suggests

that while JARID1B is not a determining factor, it may support differentiation of NSCs. While the binding sites of JARID1B in NS cells are unknown, we observed a transcriptional upregulation of *Pax9* in *Jarid1b*$^{-/-}$ (+4OHT) cells; such transcriptional changes may have functional consequences in determining cell fate in response to BMP4. However again, the lack of markers to distinguish cell states along the continuum between mature astrocytes and proliferative NSCs makes subtle differences difficult to define. In such a scenario where JARID1B has a mild effect in positively regulating NSC differentiation, loss of JARID1B function at its target genes (genetically or through protein sequestration) though alone not sufficient to induce the NSC state may be expected to 'prime' cells. This would lead to increased FOXG1-induced colony formation, as hinted by our initial replicate (Figure 5-7 A-C). We therefore cannot rule out a contributing factor of JARID1B in increasing efficiency of FOXG1-induced colony formation, irrespective of *FoxO6* and *Chd3*, and further exploration is needed.

Although the unequal levels of *FOXG1* transgene induction hampered our conclusions, this was accompanied by an interesting observation. Despite an ~25-fold upregulation in *FOXG1* mRNA expression in *Jarid1b*$^{F/F}$ (-4OHT) cells in Dox, NS cell-like colonies did not form (Figure 5-6 C-E) and neither *FoxO6* nor *Chd3* expression levels were upregulated (Figure 5-8 C-D). This would correlate with our data suggesting FoxO6 is an important target in driving a proliferative NS cell-like phenotype. Moreover, it suggests FOXG1 could function as a transcriptional activator in a concentration-dependent manner. These experiments were performed using 'bulk' populations of cells, in which different transgene copy numbers exist; using clonal cell lines, it would therefore be interesting to now investigate if a threshold FOXG1 concentration exists above which *FoxO6/Chd3* expression is activated.

In this chapter we also performed FOXG1-IPs in mouse and human GBM models, to confirm its interaction with JARID1B. While our initial results suggested an interaction between FOXG1 and JARID1B (Figure 5-2), repetition with newly-derived *FOXG1* null cell lines as additional negative controls revealed potential non-specific binding of the 17B12 FOXG1 antibody (Figure 5-9). Subsequent epitope tag-IPs in cells lines with tagged FOXG1 also did not show co-IP of FOXG1 with JARID1B (Figures 5-12 A-C and 5-14). From these experiments we therefore have not validated an interaction between FOXG1 and JARID1B. However, there are multiple reasons why this interaction may have not been observed. For example, due to the high levels of FOXG1 in GBM models, it is possible that only a small proportion of FOXG1 is bound to JARID1B. In most cases, we observed a sub-optimal enrichment of FOXG1 in the IP versus input; a greater FOXG1 enrichment could reveal such a small proportion of JARID1B-bound FOXG1. Alternatively, a reverse co-IP could reveal if FOXG1 is pulled down with JARID1B. It is also plausible that an alternative buffer composition is needed to capture this interaction; a mild non-denaturing lysis buffer containing NP-40 was used for all IPs to maintain protein complexes in their native conformations, however a different salt concentration, divalent cation concentration or pH could be investigated.

Protein-protein interactions may also be dependent on PTMs not conserved during cell lysis. While FOXG1 has two known conserved phosphorylation sites (Regad *et al*, 2007), co-IP of JARID1B was also not observed on addition of the phosphatase inhibitors, sodium orthovandate and β-glycerophosphate, to the lysis buffer (data not shown); it is therefore unlikely that phosphorylation controls this interaction, however there may be other as yet undiscovered functional PTMs of FOXG1.

We performed native IPs to enable us to observe interactions relevant to both DNA binding-dependent and -independent functions of FOXG1. However, FOXG1's interaction

with JARID1B may be transient and not captured in a native cell lysate. P. Dewari in the Pollard lab has recently optimised a method to identify on-chromatin partners of SOX TFs in GNS cells using RIME (Rapid Immunoprecipitation Mass-spectrometry of Endogenous proteins) (Mohammed *et al*, 2013, 2016). This protocol involves an initial two-step crosslinking procedure using disuccinimidyl glutarate and formaldehyde to conserve both protein-DNA and protein-protein interactions (Papachristou *et al*, 2018; direct communication from Soufi lab). While FOXG1 may exist in distinct chromatin-bound and soluble transcription complexes (Li *et al*, 2015), this protocol could reveal chromatin-bound partners which are otherwise difficult to capture.

Finally, we have demonstrated the power of CRISPR/Cas9 to tag endogenous *Foxg1* in both mouse and human models of GBM (Figure 5-10 and 5-11). Epitope-tagging reduces our reliance on the availability of good quality protein-specific antibodies, a problem highlighted by the FOXG1-IPs performed in this chapter.

Here, we show how this method can be modified to account for variable HDR efficiencies in different GNS cell lines (Figure 5-12 D), by introduction of a self-cleaving fluorescent tag (Figure 5-13). This strategy could be used in multiple cell lines, independent of HDR efficiency, to derive sorted populations with a high proportion of tagged cells. To increase the efficiency of FOXG1 bait enrichment, the use of sequential FLAG/HA tandem affinity purification should be explored (Forget *et al*, 2014). Use of 'bulk' sorted populations in downstream IPs would allow the cellular heterogeneity to be conserved as is present in the tumour; this avoids the risks associated with clonalisation, which is particularly problematic in heterogeneous cultures such as patient-derived GNS cell lines. Alternatively, multiple clonal cell lines could be efficiently derived from the sorted population and validated for homozygous tag insertion. FOXG1 expression was shown by ICC to be unaltered by

this tagging strategy (Figure 5-13 E-F); a flexible GS linker was inserted prior to the FLAG/HA tags to avoid disruption to protein folding. Functional studies should also be performed to confirm the action of FOXG1 is not altered. Once further optimised, these cell lines could be used to both validate FOXG1's candidate protein partners and discover new partners through IP-Mass spectrometry studies.

In conclusion, in this chapter we have found that JARID1B is not required for FOXG1's functions in driving a proliferative NS cell-like state and transcriptional activation of *FoxO6* and *Chd3*. We have highlighted the difficulties in relying on available protein-specific antibodies for IP studies and developed a new approach using a CRISPR/Cas9-based method for epitope-tagging *FOXG1* in patient-derived GNS cell lines, to aid the future search for key protein partners.

CHAPTER 6

General Discussion

In this thesis we present work that improves our understanding of the key downstream transcriptional targets and protein interactions of FOXG1 in GBM. In this General Discussion I will discuss the key themes highlighted by our findings and current conclusions, and how these relate to the current literature. Within each section I will highlight areas of future research.

6.1 FOXG1 drives an NS cell identity through transcriptional control of cell cycle and epigenetic regulators

FOXG1 is widely known for its roles in brain development, with functional roles including control of neural progenitor proliferation and differentiation, ventral telencephalon patterning and the survival of post-mitotic neurons (Hanashima *et al*, 2002; Xuan *et al*, 1995; Dastidar *et al*, 2011). These studies all convey an important role for FOXG1 as a master regulator in determining neural cell fate. Furthermore, FOXG1 has been reported to have activity as an *in vitro* reprogramming factor, facilitating the direct conversion of differentiated cells into tripotent neural precursors (Lujan *et al*, 2012; Raciti *et al*, 2013). In a manner analogous to *in vitro* cell reprogramming, we show that high levels of FOXG1 are able to drive cell cycle re-entry and re-acquisition of radial glia marker expression in d-qNSCs (Figures 3-5 and 3-6); it is therefore important in driving the exit from quiescence, but, in contrast to SOX2, is not required to sustain proliferative NSCs.

To elucidate how FOXG1 is functioning to mediate this cell fate transition and drive an immature identity, we next investigated the gene expression changes accompanying this

'FOXG1-induced reactivation'. The explored targets were based on a set of candidates previously identified by our lab to be both bound by and transcriptionally altered in response to overexpression of *FOXG1/SOX2* human transgenes (Figure 3-1). This revealed that FOXG1 drives the upregulation of key cell cycle regulators and known proto-oncogenes, including *NMyc, Plk1* and *FoxO6* (Figure 3-8). FOXG1 has been reported to control the proliferation of neural progenitor cells via a DNA binding-independent mechanism, namely through sequestration of FoxO-SMAD complexes preventing their transcriptional activation of cell cycle inhibitors such as $p21^{cip1}$ (Seoane *et al*, 2004). A further study of this pathway also found FOXG1 to directly regulate the transcription of *FoxO1* and *Tgfβ* (Vezzali *et al*, 2016). Our results also suggest that in addition to possible DNA-independent interactions, FOXG1 directly activates the transcription of genes controlling the cell cycle. Further work is needed to explore FOXG1's regulation of cell cycle inhibitors, such as *p21* and *p27* in this context.

FOXG1 may also control pathways involving epigenetic resetting. We therefore next analysed a set of six candidate genes associated with DNA methylation and chromatin regulation: *Dnmt1, Dnmt3b, Tet3, Hdac7, Ezh2* and *Chd3*. Our results confirmed that the expression levels of all six factors were significantly upregulated in response to FOXG1 overexpression and therefore may contribute to FOXG1-induced epigenetic resetting (Figure 3-9). RRBS analysis of cells before and after BMP4 treatment revealed significantly DMRs in the vicinity of developmental PRC target genes, including near a FOXG1 binding site at the promoter of *FoxO3* (Figures 3-10, 3-11 and 3-12). While directions of transcriptional change are difficult to predict based on acquisition or loss of DNA methylation, these results suggest that high FOXG1 levels reconfigure DNA methylation patterns to a stem-like state through transcriptional activation of DNA methylation regulators. FOXG1 therefore drives an NS cell identity both through driving

cells into a proliferative state and facilitating epigenetic resetting.

This is in agreement with previous reports that FOXG1 has distinct roles in controlling cell proliferation and neural cell fate in development and cancer. For example, while overexpression of the cell cycle inhibitor *p27^{xic1}* in *Xenopus* embryos was sufficient to inhibit proliferation of neuroectodermal cells, it did not fully recapitulate the effects that *FoxG1* RNA injection had on both proliferation and differentiation (Hardcastle & Papalopulu, 2000). Furthermore, a recent analysis of gene expression changes following *FOXG1* deletion in patient-derived GSC 'tumourspheres' revealed an enrichment in gene ontology categories such as 'nervous system development', 'cell proliferation' and 'cell differentiation' (Dali *et al*, 2018).

Epigenetic resetting, specifically, is known to play vital roles in *in vitro* cell reprogramming; in iPSC reprogramming, acquisition of a unique open chromatin state in pluripotent cells enables suppression of differentiation genes and activation of a stem cell transcriptional programme (Orkin & Hochedlinger, 2011). Such epigenetic rewiring is also thought to be recapitulated in cellular transformations leading to cancer (Suvà *et al*, 2013). Our results are in fitting with FOXG1 driving changes in the epigenetic landscape that facilitate the acquisition of a proliferative radial glia-like NSC phenotype.

Expression of the chromatin modifier, *Chd3*, a component of the NuRD complex, was further found to be upregulated in response to FOXG1 induction in mouse NS cells under proliferating conditions (Figure 4-13) or downregulated in response to *Foxg1* deletion from mouse GSCs (Figure 4-14); this suggests of a role for this factor, in not just initiating, but maintaining the GSC state. Indeed, overexpression of developmental master regulators in GNS cell lines has been suggested to restrict their differentiation commitment by inhibiting appropriate chromatin remodelling at gene regulatory

regions; for example analysis of the chromatin regions that failed to close on BMP4 treatment of GNS cells revealed an enrichment in developmental TF binding motifs, including Forkhead factors (Carén *et al*, 2015). Furthermore, ATAC-seq analysis performed by the Pollard lab in GNS and NS cells suggested FOXG1 target genes are persistently 'open' in the GNS cell state. High FOXG1 levels in GSCs may therefore regulate the expression of chromatin remodellers, such as *Chd3*, which in turn ensure an open chromatin landscape to enable FOXG1 binding to regulatory elements. Another NuRD component, Chd4, has been shown to modulate GSC gene expression directed by the TF ZFHX4 (Chudnovsky *et al*, 2014).

We note, however, that we did not observe a significant correlation between *FOXG1* levels and *CHD3*, nor *FOXO6*, expression in patient-derived GNS cell lines or tissue samples (Figures 4-12 and 4-16). The tissue samples in these studies however do not capture the GSC population alone and the GNS cell lines were cultured in EGF/FGF-2. We therefore cannot rule out a role of *FOXO6/CHD3* in maintaining the GSC state in the presence of pro-differentiation cues, a topic which we would like to further explore. As GNS cell lines are known to resist BMP4-induced differentiation commitment (Caren et al 2015), we are investigating the use of serum, as used by Suvà *et al.*, (2014), to generate 'differentiated' GNS cells that are growth factor unresponsive. Such conditions would assist us in determining whether GNS cells are more susceptible to serum-induced differentiation and/or re-entry into cell cycle on misexpression of *FOXG1/FOXO6/CHD3.*

6.2 FoxO6 is a transcriptional target of FOXG1

Our studies identified the Forkhead factor *FoxO6* as a key target downstream of FOXG1. Although the least well-studied of the FoxO factors, a number of recent studies have

implicated FoxO6 and alterations in its expression in a diverse range of processes, most notably cell proliferation and metabolism. Although FoxO6 itself is a TF and therefore difficult to drug, delineating the role of FoxO6 with respect to controlling the proliferation, differentiation and metabolism of GSCs may further our understanding of the processes underlying GSC self-renewal and exit from quiescence. While the downstream targets of FoxO6 in NS cells are unknown, FoxO6 has been implicated in leading to transcriptional changes in various cell contexts. For example, analysis of the genes downregulated in hippocampal neurons of *FoxO6* null mice following learning experiments identified p53 pathway genes and a co-occurrence of binding sites for FoxO6 and STAT TFs (Salih *et al*, 2012). In lung cancer, upregulation of FOXO6 in response to EGFR-inhibition is reported to lead to elevated SOX2 levels (Rothenberg *et al*, 2015). Subtle changes in *Foxo6* expression are also reported to control postnatal facial development through control of the Hippo signalling pathway (Sun *et al*, 2018). SOX2, STAT3 and Hippo signalling are all thought to play vital roles in controlling GSC proliferation (Ganguly *et al*, 2018; Yang *et al*, 2016; Bulstrode *et al*, 2017). It would be interesting to reveal if FoxO6's role in any of these signalling pathways is conserved in GSCs.

The seemingly opposing functions of FoxO6 and FoxO3 downstream of FOXG1 also raise the possibility of a 'Forkhead factor competition model' in GBM. Could a Forkhead TF competition exist in GSCs, whereby FOXG1 acts to antagonise FOXO3, which in turn antagonises FOXO6? Several Forkhead factors have been shown to act antagonistically; for example FOXO3 antagonises FOXM1 transcriptional activity through several mechanisms (Lam & Gomes, 2014). FOXG1 itself has been shown to sequester FOXO1/3-SMAD complexes as well as directly repress *FoxO1/3* expression in neural progenitors (Vezzali *et al*, 2016; Bulstrode *et al*, 2017). Furthermore, at a later stage of cortical

differentiation, FOXO1-SMAD complexes themselves drive FOXG1 expression to allow integration of differentiating neurons into the cortical plate (Vezzali *et al*, 2016; Miyoshi & Fishell, 2012).

While FoxO3 is known to protect cells from oxidative stress through Myc inhibition, FoxO6 has been shown to induce c-Myc expression in gastric cancer. In colorectal cancer, FoxO6 is implicated in activating mTOR signalling, leading to a glycolytic switch in cell metabolism; such a change in metabolism could drive the transition from dormancy into a proliferative state. It is possible these mechanisms could be brought together in GBM, where mTORC2 signalling has been shown to control glycolytic metabolism through inhibition of HDACs, leading to acetylation of FoxO1/3 and subsequent de-repression of c-Myc expression (Masui *et al*, 2013). The interconnectivity of these three factors is an interesting topic for further exploration.

6.3 FOXG1 can act as a transcriptional activator and repressor

In contrast to FoxO3, which is downregulated in response to elevated FOXG1 levels (Busltrode 2017), we have found that *FoxO6* expression is activated by high levels of FOXG1 (Figures 3-8 D, 4-1 and 4-2). FOXG1 was discovered as a transcriptional repressor and is most well-known for its repressive functions. However, there are reports of FOXG1 acting as a transcriptional activator. The first suggestion of a dual activity of FOXG1 came from studies of neurogenesis patterning in the *Xenopus* ectoderm; while injection of *FoxG1* RNA fused to a repressor domain mimicked most the wild-type functions, suppression of endogenous levels of the neuron marker *N-Tubulin*, was only achieved when *FoxG1* was fused to an activator domain. This suggested that while predominantly repressive, high FOXG1 levels also have some activating functions in inhibiting

endogenous neuronal differentiation, presumably by activating an inhibitor of differentiation (Bourguignon *et al*, 1998). While the repressive activity of FOXG1 was mapped mainly to the C terminus, an N terminal transactivation domain was suggested based on sequence similarities with an activating region of HNF3 (Bourguignon *et al*, 1998). More recently, analysis of the transcriptional programme through which FOXG1 controls neocortical projection neuron production in the cerebral cortex of mice revealed several immediately upregulated transcripts amongst a predominantly repressive transcriptional programme (Kumamoto 2013). FOXG1 overexpression in rat hippocampal neural precursor cells also showed an immediate upregulation of several transcripts (Nam *et al*, 2010). Furthermore, Dali *et al* found that 89% of the 150 differentially expressed genes identified upon *FOXG1* deletion in GSCs were upregulated, indicating the remaining 11% are activated targets of FOXG1. Together with our findings, there is evidence to support an under-explored role of FOXG1 as an activator of transcription.

How does FOXG1 achieve this activation? Forkhead factors are known to display diverse regulatory properties owing to their differences in tissue-specific expression, protein domains, protein-protein interactions and PTMs. While they generally act as activators or repressors of gene expression, it is therefore possible that they act in a context-dependent manner through modification of these features. For example, co-activators or co-repressors may bind to a TF in different cellular contexts, for example dependent on the phosphorylation status of the TF. Examples of context-dependent functions exist within the Forkhead family, with FoxP1 reported to have tumour suppressive functions in some types of cancer but oncogenic roles in B cell lymphoma, possibly owing to transactivation of genes involved in B cell development (Fox *et al*, 2008; Aster & Kutok, 2009; Hu *et al*, 2006). Within individual cells, the TF GATA-1 has been shown to form

distinct protein complexes during different stages of erythroid differentiation to activate or repress different subsets of genes (Rodriguez *et al*, 2005). To begin to understand the mechanism by which FOXG1 leads to transcriptional activation, we explored the role of a published binding partner, JARID1B, in this function; we hypothesised that JARID1B could recruit co-activators or that elevated FOXG1 levels could act to sequester the repressive functions of JARID1B, leading to *in trans* gene derepression (Figure 5-1). While we cannot rule out that loss of JARID1B (or sequestration by FOXG1) affects the efficiency of FOXG1-induced d-qNSC reactivation, from our data we can conclude that the FOXG1:JARID1B interaction is not a determining factor in driving *FoxO6*/*Chd3* activation (Figure 5-8) or reacquisition of an NSC-like state (Figures 5-6 and 5-7). Additionally, our IP studies did not validate a FOXG1:JARID1B interaction (Figures 5-9, 5-12 and 5-14). Further studies are therefore needed to explore this interaction.

Nevertheless, 'regulatory squelching', whereby the elevated FOXG1 levels found in GSCs sequester a protein partner preventing transcriptional co-repression, is an appealing hypothesis for further investigation (Figure 5-1 B). FOXG1 has known DNA-binding independent functions through which it indirectly leads to transcriptional repression (Hanashima *et al*, 2002; Seoane *et al*, 2004; Li *et al*, 2013), therefore it is plausible that an analogous mechanism may exist to facilitate transcriptional activation. In breast cancer, FOXG1 has been proposed to act as a short-range repressor, acting to quench an activating transcription complex at the AIB1 promoter (Li *et al*, 2013). It is tempting to think that FOXG1 could also act to quench a repressive transcription complex. Secondly, several studies indicate a concentration-dependent mechanism of action of FOXG1 (Bourguignon *et al*, 1998; Hardcastle & Papalopulu, 2000; Shen *et al*, 2006). Furthermore, while further exploration is needed, from our data we speculate that a FOXG1 threshold may exist above which activation of *FoxO6*/ *Chd3* expression occurs.

The interaction between FOXG1 and TLE-1, a transcriptional co-repressor of Wnt signalling, has been reported to have a functional role in driving the GSC state (Dali *et al*, 2018; Verginelli *et al*, 2013). Recent work by the Pollard lab suggests a potent functional synergy between FOXG1 and Wnt signalling in driving an NSC identity (F. Robertson, in preparation). It is possible that high FOXG1 levels may act to sequester TLE-1, preventing binding to TCF/LEF and enabling Wnt target transcription. We are currently investigating whether *FoxO6* is a Wnt target gene; initial experiments suggest that indeed, FoxO6 may be activated by Chiron (a small molecule stimulator of Wnt signalling). Following this we would, in future, like to investigate the effect of deleting the Forkhead or Groucho/TLE-1-binding domains of *FOXG1* on transcriptional activation.

A concentration-dependent dual activity has also been seen in other developmental TFs, such as *Drosophila* Krüppel and vertebrate Pax3 (Sauer & Jackie, 1991; Hong & Saint-Jeannet, 2007; Bourguignon *et al*, 1998) and may also lead to a switch in activity by other mechanisms. For example, a high FOXG1 concentration could lead to novel co-factor interactions; an increased affinity for FOXG1 binding to the co-repressor Hes1 at high concentrations was suggested to explain its inability to inhibit neuronal differentiation at low doses (Yao *et al*, 2001; Bourguignon *et al*, 1998). High concentrations could also lead to a switch in activity by facilitating dimerisation; for example Krüppel acts bimodally as a monomer and dimer through different interactions with transcription initiation factors (Sauer & Jackie, 1991; Sauer *et al*, 1995) and homo- or heterodimerisation of FoxP1 with FoxP2/4 is required for co-factor interactions and transcriptional repression (Li *et al*, 2004). A concentration-dependent basis of FOXG1's transcriptional activities is clearly of interest for further exploration in GSCs.

6.4 Defining the key protein partners important to FOXG1's function and therapeutic implications

Uncovering the protein partners of FOXG1 is key to deciphering its role in driving the GSC state and might reveal ways to block its activity as a GBM therapeutic. In light of our above discussions, it would also be interesting to explore whether FOXG1 forms different protein complexes in a concentration-dependent manner, and whether these correlate with changes in cell behaviour; such concentration-dependent protein-protein interactions could present GSC-specific therapeutic targets. Given FOXG1's abilities to act in both DNA binding-dependent and -independent manners, it would also be important to delineate whether these interactions occur on or off chromatin. Furthermore, it would be of interest to identify whether any of FOXG1's candidate transcriptional targets, such as *Chd3*, also exist as protein partners. Another reprogramming transcription factor Sox2, and the chromatin remodelling-ATPase Chd7, have been shown to physically interact and cooperatively activate target genes (Engelen *et al*, 2011). Both Chd3 and Chd4 have also been shown to interact with transcription factors in prostate cancer and GBM, respectively (Srinivasan *et al*, 2006; Chudnovsky *et al*, 2014).

We have presented a CRISPR/Cas9 epitope-tagging method which could be used to tag FOXG1 in multiple patient-derived GNS cell lines (Figure 5-13). This opens up possibilities for performing downstream protein-protein interaction studies to further decipher FOXG1's interactome. This methodology could be further used to tag FOXG1 in non-tumorigenic human foetal NS cell lines, enabling comparison of FOXG1's protein partners in a normal versus malignant state by IP-Mass spectrometry. Furthermore, this technology could be used to iteratively tag and validate subsequently identified candidate protein interactors without the reliance on good quality protein-specific antibodies. This would enable the use of a single antibody in protein analysis studies of

multiple candidate interactors, by Western blotting, ICC or IP. Moreover, the Pollard lab's recent development of the Extensible Mammalian Modular Assembly (EMMA) toolkit (Martella *et al*, 2017) would enable rapid and efficient assembly of vectors containing the repair template sequence. This system consists of a standardised library of genetic parts from which plasmids can be constructed in a single-step Golden Gate reaction, and its use would avoid the need for *in vitro* synthesis of dsDNA gene fragments.

Modulation of identified functional protein-protein interactions (PPIs) may present a promising therapeutic avenue to alter the activity of 'undruggable' FOXG1 (Fontaine *et al*, 2015; Berg, 2003; Koehler, 2010; Inamoto & Shin, 2018). Identification of binding sites between proteins can be achieved using peptide array technology (Katz *et al*, 2011); these consist of a library of spotted, immobilised peptides which, following incubation with a purified protein partner of interest, identify putative binding sites as positive dark spots (Frank, 2002; Kramer and Schneider-Mergener, 1998). Key amino acids or a minimal binding sequence can be further identified by alanine scanning or N/C terminus truncation, and cell-permeable protein-protein interaction disruptor (PPID) peptides or small molecules can be synthesised and screened for their ability to block the PPI. Numerous PPIDs have been published and several have entered clinical trials, highlighting the possibility of targeting PPIs to treat diseases including cancer (Ivanov *et al*, 2014; Mabonga & Kappo, 2020).

6.5 Concluding remarks

GBM is a currently incurable, aggressive adult brain tumour, thought to be driven by a population of NS cell-like GSCs. There is an urgent need for new treatments to target these cells and prevent patient relapse following surgery and chemo/radiotherapy.

FOXG1 presents a target of importance as it supports both the proliferative GSC identity and exit from quiescence. Here, using *in vitro* models of GBM we have advanced our understanding of the key downstream transcriptional targets and protein interactions through which FOXG1 functions. While clearly much further research is needed to pin together these pieces, our findings highlight the importance of FOXG1 in driving GBM and bring us one step closer to elucidating a unified molecular mechanism by which FOXG1 drives the GSC state.

REFERENCES

Abbaszadegan MR, Bagheri V, Razavi MS, Momtazi AA, Sahebkar A & Gholamin M (2017) Isolation, identification, and characterization of cancer stem cells: A review. *J Cell Physiol* 232: 2008–2018

Adesina AM, Nguyen Y, Mehta V, Takei H, Stangeby P, Crabtree S, Chintagumpala M & Humerlock MK (2007) FOXG1 dysregulation is a frequent event in medulloblastoma. *J Neurooncol* 85: 111–122

Adesina AM, Veo BL, Courteau G, Mehta V, Wu X, Pang K, Liu Z, Li X, Li XN & Peters L (2015) FOXG1 expression shows correlation with neuronal differentiation in cerebellar development , aggressive phenotype in medulloblastomas and survival in a xenograft. *Hum Pathol* 46: 1859–1871

Adli M (2018) The CRISPR tool kit for genome editing and beyond. *Nat Commun* 9: 1911

Al-Hajj M, Wicha MS, Benito-Hernandez A, Morrison SJ & Clarke MF (2003) Prospective identification of tumorigenic breast cancer cells. *PNAS* 100: 3983-3988

Albert M, Schmitz SU, Kooistra SM, Malatesta M, Morales Torres C, Rekling JC, Johansen J V., Abarrategui I & Helin K (2013) The Histone Demethylase Jarid1b Ensures Faithful Mouse Development by Protecting Developmental Genes from Aberrant H3K4me3. *PLoS Genet* 9: e1003461

Alcantara Llaguno SR & Parada LF (2016) Cell of origin of glioma: Biological and clinical implications. *Br J Cancer* 115: 1445–1450

Alcantara Llaguno S, Sun D, Pedraza AM, Vera E, Wang Z, Burns DK & Parada LF (2019) Cell-of-origin susceptibility to glioblastoma formation declines with neural lineage restriction. *Nat Neurosci* 22: 545–555

Aldape K, Brindle KM, Chesler L, Chopra R, Gajjar A, Gilbert MR, Gottardo N, Gutmann DH, Hargrave D, Holland EC, *et al* (2019) Challenges to curing primary brain tumours. *Nat Rev Clin Oncol* 16: 509-520

Allen M, Bjerke M, Edlund H, Nelander S & Westermark B (2016) Origin of the U87MG glioma cell line: Good news and bad news. *Sci Transl Med* 8: 354re3

Allfrey G, Faulkner R & Mirsky AE (1964) Acetylation and Methylation of histones and their possible role in the regulation of RNA synthesis. *Proc Natl Acad Sci* 51: 786–794

Alvarez-Buylla A, García-Verdugo JM & Tramontin AD (2001) A unified hypothesis on the lineage of neural stem cells. *Nat Rev Neurosci* 2: 287–293

Alvarez-Buylla A, Seri B & Doetsch F (2002) Identification of neural stem cells in the adult vertebrate brain. *Brain Res Bull* 57: 751–758

Anderson EM, Haupt A, Schiel JA, Chou E, Machado HB, Strezoska Z, Lenger S, McClelland S, Birmingham A, Vermeulen A *et al* (2015) Systematic analysis of CRISPR-Cas9 mismatch tolerance reveals low levels of off-target activity. *J Biotechnol* 211: 56-65

Apostolou E & Stadtfeld M (2018) Cellular trajectories and molecular mechanisms of iPSC reprogramming. *Curr Opin Genet De* 52: 77–85

Ariani F, Hayek G, Rondinella D, Artuso R, Mencarelli MA, Spanhol-Rosseto A, Pollazzon M, Buoni S, Spiga O, Ricciardi S *et al* (2008) FOXG1 Is Responsible for the Congenital Variant of Rett Syndrome. *Am J Hum Genet* 83: 89–93

Arnold K, Sarkar A, Yram MA, Polo JM, Bronson R, Sengupta S, Seandel M, Geijsen N & Hochedlinger K (2011) Sox2 + adult stem and progenitor cells are important for tissue regeneration and survival of mice. *Cell Stem Cell* 9: 317–329

Artene SA, Tuţă C, Dragoi A, Alexandru O, Stefana Oana P, Tache DE, Dănciulescu MM, Boldeanu MV, Siloşi

CA & Dricu A (2018) Current and emerging EGFR therapies for glioblastoma. *J Immunoass Immunochem* 39: 1–11

Ashby LS, Smith KA & Stea B (2016) Gliadel wafer implantation combined with standard radiotherapy and concurrent followed by adjuvant temozolomide for treatment of newly diagnosed high-grade glioma: A systematic literature review. *World J Surg Oncol* 14: 1–15

Assanah M, Lochhead R, Ogden A, Bruce J, Goldman J & Canoll P (2006) Glial Progenitors in Adult White Matter Are Driven to Form Malignant Gliomas by Platelet-Derived Growth Factor-Expressing Retroviruses. *J Neurosci* 26: 6781–6790

Aster J & Kutok J (2009) Complexity made simple in diffuse large B-cell lymphoma. *Clin Cancer Res* 15: 5291–5293

Azzarelli R, Simons BD & Philpott A (2018) The developmental origin of brain tumours: a cellular and molecular framework. *Development* 145: 1–12

Bachoo RM, Maher EA, Ligon KL, Sharpless NE, Chan SS, You MJ, Tang Y, DeFrances J, Stover E, Weissleder R *et al* (2002) Epidermal growth factor receptor and Ink4a/Arf: governing terminal differentiation and transformation stem cell to astrocyte axis. *Cancer Cell* 1: 269–77.

Baek ST, Copeland B, Yun E, Kwon S, Guemez-Gamboa A, Schaffer AE, Kim S, Kang H, Song S, Mathern GW *et al* (2015) An AKT3-FOXG1-reelin network underlies defective migration in human focal malformations of cortical development. *Nat Med* 21: 1445–1454

Bao S, Wu Q, McLendon RE, Hao Y, Shi Q, Hjelmeland AB, Dewhirst MW, Bigner DD & Rich JN (2006) Glioma stem cells promote radioresistance by preferential activation of the DNA damage response. *Nature* 444: 756–760

Bao ZS, Zhang CB, Wang HJ, Yan W, Liu YW, Li MY & Zhang W (2013) Whole-Genome mRNA Expression Profiling Identifies Functional and Prognostic Signatures in Patients with Mesenchymal Glioblastoma Multiforme. *CNS Neurosci Ther* 19: 714–720

Barrett A, Santangelo S, Tan K, Catchpole S, Roberts K, Spencer-Dene B, Hall D, Scibetta A, Burchell J, Verdin E *et al* (2007) Breast cancer associated transcriptional repressor PLU-1/JARID1B interacts directly with histone deacetylases. *Int J Cancer* 121: 265–275

Basta J & Rauchman M (2009) The nucleosome remodeling deacetylase (NuRD) complex in Development and Disease. *Transl Res* 165: 36–47

Beier D, Hau P, Proescholdt M, Lohmeier A, Wischhusen J, Oefner PJ, Aigner L, Brawanski A, Bogdahn U & Beier CP (2007) CD133+ and CD133- glioblastoma-derived cancer stem cells show differential growth characteristics and molecular profiles. *Cancer Res* 67: 4010–4015

Benayoun A, Caburet S & Veitia RA (2011) Forkhead transcription factors : key players in health and disease. *Trends Genet* 27: 224–232

Benevolenskaya E V., Murray HL, Branton P, Young RA & Kaelin WG (2005) Binding of pRB to the PHD protein RBP2 promotes cellular differentiation. *Mo. Cell* 18: 623–635

Benjamini Y & Hochberg Y (1995) Controlling the False Discovery Rate: A Practical and Powerful Approach to Multiple Testing. *J R Stat Soc Ser B* 57: 289–300

Berg T (2003) Modulation of protein-protein interactions with small organic molecules. *Angew Chemie - Int Ed* 42: 2462–2481

van den Bent MJ, Brandes AA, Rampling R, Kouwenhoven MC, Kros JM, Carpentier AF, Clement PM, Frenay M, Campone M, Baurain JF *et al* (2009) Randomized phase II trial of erlotinib versus temozolomide or carmustine in recurrent glioblastoma: EORTC brain tumor group study 26034. *J Clin Oncol* 27: 1268–1274

Bhat KPL, Balasubramaniyan V, Vaillant B, Ezhilarasan R, Hummelink K, Hollingsworth F, Wani K, Heathcock L, James JD, Goodman LD *et al* (2013) Mesenchymal Differentiation Mediated by NF-κB Promotes Radiation Resistance in Glioblastoma. *Cancer Cell* 24: 331–346

Bignami A, Eng LF, Dahl D & Uyeda CT (1972) Localisation of the glial fibrillary acidic protein in astrocytes by immunofluorescence. *Brain Res* 43: 429–435

Bird A (2002) DNA methylation patterns and epigenetic memory. *Genes Dev* 16: 16–21

Blount AL, Schmidt K, Justice NJ, Vale WW, Fischer WH & Bilezikjian LM (2009) FoxL2 and Smad3 coordinately regulate follistatin gene transcription. *J Biol Chem* 284: 7631–7645

Bonaguidi MA, Mcguire T, Hu M, Kan L, Samanta J & Kessler JA (2005) LIF and BMP signaling generate separate and discrete types of GFAP-expressing cells. *Development* 132: 5503–5514

Bond AM, Bhalala OG & Kessler JA (2012) The Dynamic Role of Bone Morphogenetic Proteins in Neural Stem Cell Fate and Maturation. *Dev Neurobiol* 72: 1068–1084

Bond AM, Ming G & Song H (2015) Review Adult Mammalian Neural Stem Cells and Neurogenesis : Five Decades Later. *Stem Cell* 17: 385–395

Bottardi S, Ghiam AF, Bergeron F & Milot E (2007) Lineage-specific transcription factors in multipotent hematopoietic progenitors: A little bit goes a long way. *Cell Cycle* 6: 1035–1039

Bourguignon C, Papalopulu N & Li J (1998) XBF-1, a winged helix transcription factor with dual activity, has a role in positioning neurogenesis in Xenopus competent ectoderm. *Development* 125: 4889–4900

Bracken AP, Brien GL & Verrijzer CP (2019) Dangerous liaisons: interplay between SWI/SNF, NuRD, and Polycomb in chromatin regulation and cancer. *Genes Dev* 33: 936-959.

Bradshaw A, Wickremsekera A, Tan ST, Peng L, Davis PF & Itinteang T (2016) Cancer Stem Cell Hierarchy in Glioblastoma Multiforme. *Front Surg* 3: 1–15

Branter J, Basu S & Smith S (2018) Tumour treating fields in a combinational therapeutic approach. *Oncotarget* 9: 36631–36644

Braun SMG & Jessberger S (2014) Adult neurogenesis : mechanisms and functional significance. *Development* 141: 1983–1986

Bray NL, Pimentel H, Melsted P & Pachter L (2016) Near-optimal probabilistic RNA-seq quantification. *Nat. Biotechnol* 34: 525–527

Bredenkamp N, Seoighe C & Illing N (2007) Comparative evolutionary analysis of the FoxG1 transcription factor from diverse vertebrates identifies conserved recognition sites for microRNA regulation. *Dev. Genes Evo* 217: 227–233

Brennan C, Momota H, Hambardzumyan D, Ozawa T, Tandon A, Pedraza A & Holland E (2009) Glioblastoma subclasses can be defined by activity among signal transduction pathways and associated genomic alterations. *PLoS One* 4: e7752

Brennan CW, Verhaak RG, McKenna A, Campos B, Noushmehr H, Salama SR, Zheng S, Chakravarty D, Sanborn JZ, Berman SH *et al* (2013) The somatic genomic landscape of glioblastoma. *Cell* 155: 462-477

Bressan RB, Dewari PS, Kalantzaki M, Gangoso E, Matjusaitis M, Garcia-Diaz C, Blin C, Grant V, Bulstrode H, Gogolok S *et al* (2017) Efficient CRISPR/Cas9-assisted gene targeting enables rapid and precise genetic manipulation of mammalian neural stem cells. *Development* 144: 635–648

Brier AB, Loft A, Madsen JGS, Rosengren T, Nielsen R, Schmidt SF, Liu Z, Yan Q, Gronemeyer H & Mandrup S (2017) The KDM5 family is required for activation of pro-proliferative cell cycle genes during adipocyte differentiation. *Nucleic Acids Res* 45: 1743–1759

Bruggeman SW, Hulsman D, Tanger E, Buckle T, Blom M, Zevenhoven J, van Tellingen O & van Lohuizen M (2007) Bmi1 Controls Tumor Development in an Ink4a/Arf-Independent Manner in a Mouse Model for Glioma. *Cancer Cell* 12: 328–341

Brunet A, Bonni A, Zigmond MJ, Lin MZ, Juo P, Hu LS, Anderson MJ, Arden KC, Blenis J & Greenberg ME (1999) Akt Promotes Cell Survival by Phosphorylating and Inhibiting a Forkhead Transcription Factor. *Cell* 96: 857–868

Brunet J, Grollimund L, Chatton JY, Lengacher S, Magistretti P, Villemure J & Pellerin L (2004) Early Acquisition of Typical Metabolic Features upon Differentiation of Mouse Neural Stem Cells into astrocytes. *Glia* 46: 8–17

Brunetti-Pierri N, Paciorkowski AR, Ciccone R, Della Mina E, Bonaglia MC, Borgatti R, Schaaf CP, Sutton VR, Xia Z, Jelluma N *et al* (2011) Duplications of FOXG1 in 14q12 are associated with developmental epilepsy, mental retardation, and severe speech impairment. *Eur J Hum Genet* 19: 102–107

Bucur O, Stancu AL, Muraru MS, Melet A, Petrescu SM, Khosravi-Far R (2014) PLK1 is a binding partner and a negative regulator of FOXO3 tumor suppressor. *Discoveries (Craiova)* 2: pii:e16

Bulstrode H, Johnstone E, Marques-Torrejon MA, Ferguson KM, Bressan RB, Blin C, Grant V, Gogolok S, Gangoso E, Gagrica S *et al* (2017) Elevated FOXG1 and SOX2 in glioblastoma enforces neural stem cell identity through transcriptional control of cell cycle and epigenetic regulators. *Genes Dev* 31: 757–773

Bulstrode HJCJ (2015) Dissecting the function and targets of FOXG1 in glioblastoma. University of Edinburgh

Buscarlet M, Perin A, Laing A, Brickman JM & Stifani S (2008) Inhibition of Cortical Neuron Differentiation by Groucho / TLE1 Requires Interaction with WRPW , but Not Eh1 , Repressor Peptides. *J Biol Chem* 283: 24881–24888

Cahill MA, Ernst WH, Janknecht R & Nordheim A (1994) Regulatory squelching. *FEBS Lett* 344: 105–108

Cahoy JD, Emery B, Kaushal A, Foo LC, Zamanian JL, Christopherson KS, Xing Y, Lubischer JL, Krieg PA, Krupenko SA *et al* (2008) A Transcriptome Database for Astrocytes, Neurons, and Oligodendrocytes: A New Resource for Understanding Brain Development and Function. *J Neurosci* 28: 264–278

Carén H, Pollard SM & Beck S (2013) The good, the bad and the ugly: Epigenetic mechanisms in glioblastoma. *Mol Aspects Med* 34: 849–862

Carén H, Stricker SH, Bulstrode H, Gagrica S, Johnstone E, Bartlett TE, Feber A, Wilson G, Teschendorff AE, Bertone P *et al* (2015) Glioblastoma stem cells respond to differentiation cues but fail to undergo commitment and terminal cell-cycle arrest. *Stem Cell Reports* 5: 829–842

Cargnin F, Kwon JS, Katzman S, Chen B, Lee JW & Lee SK (2018) FOXG1 Orchestrates Neocortical Organization and Cortico-Cortical Connections. *Neuron* 100: 1083-1096.e5

Carroll JS, Liu XS, Brodsky AS, Li W, Meyer CA, Szary AJ, Eeckhoute J, Shao W, Hestermann EV, Geistlinger TR *et al* (2005) Chromosome-wide mapping of estrogen receptor binding reveals long-range regulation requiring the forkhead protein FoxA1. *Cell* 122: 33–43

Catchpole S, Spencer-Dene B, Hall D, Santangelo S, Rosewell I, Guenatri M, Beatson R, Scibetta AG, Burchell JM & Taylor-Papadimitriou J (2011) PLU-1/JARID1B/KDM5B is required for embryonic survival and contributes to cell proliferation in the mammary gland and in ER+ breast cancer cells. *Int J Oncol* 38: 1267–1277

Chan DW, Liu VW, To RM, Chiu PM, Lee WY, Yao KM, Cheung AN & Ngan HY (2009) Overexpression of FOXG1 contributes to TGF- b resistance through inhibition of p21 WAF1 / CIP1 expression in ovarian cancer. *Br J Cancer* 101: 1433–1443

Chan SW & Hong W (2001) Retinoblastoma-binding Protein 2 (Rbp2) Potentiates Nuclear Hormone Receptor-mediated Transcription. *J Biol Chem* 276: 28402–28412

Chen J, Li Y, Yu TS, McKay RM, Burns DK, Kernie SG & Parada LF (2012) A restricted cell population propagates glioblastoma growth after chemotherapy. *Nature* 488: 522–526

Chen J, Wu X, Xing Z, Ma C, Xiong W, Zhu X & He X (2018a) FOXG1 Expression Is Elevated in Glioma and Inhibits Glioma Cell Apoptosis. *J Cancer* 9: 778–783

Chen S, Le T, Harley BAC & Imoukhuede PI (2018b) Characterizing Glioblastoma Heterogeneity via Single-Cell Receptor Quantification. *Front Bioeng Biotechnol* 6: 92

Chen Y & Xu R (2016) Drug repurposing for glioblastoma based on molecular subtypes. *J Biomed Inform* 64: 131–138

Chittock EC, Latwiel S, Miller TC & Müller CW (2017) Molecular architecture of polycomb repressive complexes. *Biochem Soc Trans* 45: 193–205

Chiu CP & Blau HM (1985) 5-Azacytidine Permits Gene Activation in a Previously Noninducible Cell Type. *Cell* 40: 417–424

Chokas AL, Trivedi CM, Lu MM, Tucker PW, Li S, Epstein JA & Morrisey EE (2010) Foxp1/2/4-NuRD interactions regulate gene expression and epithelial injury response in the lung via regulation of interleukin. *J Biol Chem* 285: 13304–13313

Chowdhary SA, Ryken T & Newton HB (2015) Survival outcomes and safety of carmustine wafers in the treatment of high-grade gliomas: a meta-analysis. *J Neurooncol* 122: 367–382

Chudnovsky Y, Kim D, Zheng S, Whyte WA, Bansal M, Bray MA, Gopal S, Theisen MA, Bilodeau S, Thiru P *et al* (2014) ZFHX4 Interacts with the NuRD core member CHD4 and regulates the glioblastoma tumor-initiating cell state. *Cell Rep* 6: 313–324

Chung SY, Huang WC, Su CW, Lee KW, Chi HC, Tao C, Chen S, Huang KM, Tsai MS, Yu HP *et al* (2013) FoxO6 and PGC-1 α form a regulatory loop in myogenic cells. *Bioscience Reports* 33: e00045

Cirillo LA & Zaret KS (2007) Specific Interactions of the Wing Domains of FOXA1 Transcription Factor with DNA. *J Mol Biol* 366: 720–724

Claes A, Idema AJ & Wesseling P (2007) Diffuse glioma growth: A guerilla war. *Acta Neuropathol* 114(5): 443–458

Clark KL, Halay ED, Lai E & Burley SK (1993) Co-crystal structure of the HNF-3/fork head DNA-recognition motif resembles histone H5. *Nature* 364: 412–420

Clarke MF, Dick JE, Dirks PB, Eaves CJ, Jamieson CH, Jones DL, Visvader J, Weissman IL & Wahl GM (2006) Cancer stem cells - Perspectives on current status and future directions: AACR workshop on cancer stem cells. *Cancer Res* 66: 9339–9344

Codega P, Silva-Vargas V, Paul A, Maldonado-Soto AR, Deleo AM, Pastrana E & Doetsch F (2014) Prospective Identification and Purification of Quiescent Adult Neural Stem Cells from Their In Vivo Niche. *Neuron* 82: 545–559

Conti L & Cattaneo E (2010) Neural stem cell systems : physiological players or in vitro entities ? *Nat Rev Neurosci* 11: 176–187

Conti L, Pollard SM, Gorba T, Reitano E, Toselli M, Biella G, Sun Y, Sanzone S, Ying QL, Cattaneo E *et al* (2005) Niche-independent symmetrical self-renewal of a mammalian tissue stem cell. *PLoS Biol* 3: e283

Corrò C & Moch H (2018) Biomarker discovery for renal cancer stem cells. *J Pathol Clin Res* 4: 3–18

Couturier CP, Ayyadhury S, Le PU, Monlong J, Riva G, Allache R, Baig S, Yan X, Bourgey M, Lee C *et al* (2018) Single-cell RNA-seq reveals that glioblastoma recapitulates normal brain development. *bioRxiv* doi: 10.1101/449439

Dali R, Verginelli F, Pramatarova A, Sladek R & Stifani S (2018) Characterization of a FOXG1 : TLE1 transcriptional network in glioblastoma-initiating cells. *Mol Oncol* 12: 775–787

Danesin C, Peres JN, Johansson M, Snowden V, Cording A, Papalopulu N & Houart C (2009) Integration of Telencephalic Wnt and Hedgehog Signaling Center Activities by Foxg1. *Dev Cell* 16: 576–587

Dansen TB & Burgering BM (2008) Unravelling the tumor-suppressive functions of FOXO proteins. *Trends Cell Biol* 18: 421–429

Dastidar SG, Landrieu PM & & D'Mello SR (2011) FoxG1 Promotes the Survival of Postmitotic Neurons. *J Neurosci* 31: 402–413

Dastidar SG, Narayanan S, Stifani S & D'Mello SR (2012) Transducin-like enhancer of split-1 (TLE1) combines with Forkhead box protein G1 (FoxG1) to promote neuronal survival. *J Biol Chem* 287: 14749–14759

Davis RL, Weintraub H & Lassar AB (1987) Expression of a single transfected cDNA converts fibroblasts to myoblasts. *Cell* 51: 987–1000

Dawson MRL, Polito A, Levine JM & Reynolds R (2003) NG2-expressing glial progenitor cells: An abundant and widespread population of cycling cells in the adult rat CNS. *Mol Cell Neurosci* 24: 476–488

de la Torre-Ubieta, Gaudillière B, Yang Y, Ikeuchi Y, Yamada T, DiBacco S, Stegmüller U, Salih DA, Rowitch D, Brunet A *et al* (2010) A FOXO – Pak1 transcriptional pathway controls neuronal polarity. *Genes Dev* 24: 799–813

Deleyrolle LP, Harding A, Cato K, Siebzehnrubl FA, Rahman M, Azari H, Olson S, Gabrielli B, Osborne G, Vescovi A *et al* (2011) Evidence for label-retaining tumour-initiating cells in human glioblastoma. *Brain* 134: 1331–1343

Dewari PS, Southgate B, Mccarten K, Monogarov G, O'Duibhir E, Quinn N, Tyrer A, Leitner MC, Plumb C, Kalantzaki M *et al* (2018) An efficient and scalable pipeline for epitope tagging in mammalian stem cells using Cas9 ribonucleoprotein. *Elife* 7: e35069

Dey BK, Stalker L, Schnerch A, Bhatia M, Taylor-Papidimitriou J & Wynder C (2008) The Histone Demethylase KDM5b / JARID1b Plays a Role in Cell Fate Decisions by Blocking Terminal Differentiation. *Mol Cell Biol* 28: 5312–5327

Dick JE (2009) Looking ahead in cancer stem cell research. *Nat Biotechnol* 27: 44-46

Dimou L, Simon C, Kirchhoff F, Takebayashi H & Gotz M (2008) Progeny of Olig2-Expressing Progenitors in the Gray and White Matter of the Adult Mouse Cerebral Cortex. *J Neurosci* 28: 10434–10442

Meyer M, Reimand J, Lan X, Head R, Zhu X, Kushida M, Bayani J, Pressey JC, Lionel A, Clarke ID *et al* (2014) Single Cell Derived Clonal Analysis of Human Glioblastoma Links Functional and Genomic Heterogeneity. *Proc Natl Acad Sci* 112: 851-856

Doetsch F, Caille I, Lim DA, Garcı JM & Alvarez-Buylla A (1999) Subventricular Zone Astrocytes Are Neural Stem Cells in the Adult Mammalian Brain. *Cell* 97: 703–716

Dou C, Lee J, Liu B, Liu F, Massague J, Xuan S & Lai E (2000) BF-1 Interferes with Transforming Growth Factor beta Signaling by Associating with Smad Partners. *Mol Cell Biol* 20: 6201–6211

Dou C, Li S & Lai E (1999) Dual Role of Brain Factor-1 in Regulating Growth and Patterning of the Cerebral Hemispheres. *Cerebral* 9: 543–550

Down CF, Millour J, Lam EW & Watson RJ (2012) Binding of FoxM1 to G2/M gene promoters is dependent upon B-Myb. *Biochim Biophys Acta - Gene Regul Mech* 1819: 855–862

Dulken BW, Leeman DS, Boutet C, Hebestreit K, Brunet A, Boutet C, Hebestreit K & Brunet A (2017) Single-Cell Transcriptomic Analysis Defines Heterogeneity and Transcriptional Dynamics in the Adult Neural Stem Cell Lineage. *Cell Rep* 18: 777–790

Eijkelenboom A & Burgering BM (2013) FOXOs : signalling integrators for homeostasis maintenance. *Nat Rev Mol Cell Biol* 14: 83–97

Elsen GE, Bedogni F, Hodge RD, Bammler TK, MacDonald JW, Lindtner S, Rubenstein JLR & Hevner RF (2018) The epigenetic factor landscape of developing neocortex is regulated by transcription factors Pax6→ Tbr2→ Tbr1. *Front Neurosci* 12:571, 1-22

Engelen E, Akinci U, Bryne JC, Hou J, Gontan C, Moen M, Szumska D, Kockx C, van Ijcken W, Dekkers DH *et al* (2011) Sox2 cooperates with Chd7 to regulate genes that are mutated in human syndromes. *Nat Genet* 43: 607–611

Engström PG, Tommei D, Stricker SH, Ender C, Pollard SM & Bertone P (2012) Digital transcriptome profiling of normal and glioblastoma-derived neural stem cells identifies genes associated with patient survival. *Genome Med* 4: 76

Ewels P, Magnusson M, Lundin S & Käller M (2016) MultiQC: Summarize analysis results for multiple tools and samples in a single report. *Bioinformatics* 32: 3047–3048

Feinberg AP, Ohlsson R & Henikoff S (2006) The epigenetic progenitor origin of human cancer. *Nat Rev Genet* 7: 21–33

De Filippis R, Pancrazi L, Bjørgo K, Rosseto A, Kleefstra T, Grillo E, Panighini A, Cardarelli F, Meloni I, Ariani F *et al* (2011) Expanding the phenotype associated with FOXG1 mutations and in vivo FoxG1 chromatin-binding dynamics. *Clin Genet* 82: 395–403

Fischer JJ, Toedling J, Krueger T, Schueler M, Huber W & Sperling S (2008) Combinatorial effects of four histone modifications in transcription and differentiation. *Genomics* 91: 41–51

Fong AP & Tapscott SJ (2013) Skeletal muscle programming and re-programming. *Curr Opin Genet Dev* 23: 568–573

Fontaine F, Overman J & François M (2015) Pharmacological manipulation of transcription factor protein-protein interactions : opportunities and obstacles. *Cell Regen* 4:2

Forget A, Bihannic L, Cigna SM, Lefevre C, Remke M, Barnat M, Dodier S, Shirvani H, Mercier A, Mensah A *et al* (2014) Shh Signaling Protects Atoh1 from Degradation Mediated by the E3Ubiquitin Ligase Huwe1 in Neural Precursors. *Dev Cell* 29: 649–661

Fox SB, Brown P, Han C, Ashe S, Leek RD, Harris AL & Banham AH (2008) Expression of the forkhead transcription factor FOXP1 is associated with that of estrogen receptorβ in primary invasive breast carcinomas. *Breast Cancer Res Treat* 111: 453–459

Frank R (2002) The SPOT-synthesis technique. Synthetic peptide arrays on membrane supports - principles and applications. *J Immunol Methods* 267: 13–26

Freije WA, Castro-Vargas FE, Fang Z, Horvath S, Cloughesy T, Liau LM, Mischel PS & Nelson SF (2004) Gene expression profiling of gliomas strongly predicts survival. *Cancer Res* 64: 6503–6510

Frietze S & Farnham PJ (2011). Transcription factor effector domains. In: Hughes T. (eds) A Handbook of Transcription factors. *Subcellular Biochemistry,* vol 52. Springer, Dordrecht.

Frullanti E, Amabile S, Lolli MG, Bartolini A, Livide G, Landucci E, Mari F, Vaccarino FM, Ariani F, Massimino L *et al* (2016) Altered expression of neuropeptides in FoxG1-null heterozygous mutant mice. *Eur J Hum Genet* 24: 252–257

Fuentealba LC, Obernier K & Alvarez-Buylla A (2012) Adult neural stem cells bridge their niche. *Cell Stem Cell* 10: 698–708

Furnari FB, Fenton T, Bachoo RM, Mukasa A, Stommel JM, Stegh A, Hahn WC, Ligon KL, Louis DN, Brennan C *et al* (2007) Malignant astrocytic glioma: Genetics, biology, and paths to treatment. *Genes Dev* 21: 2683–2710

Gage FH (2000) Mammalian Neural Stem Cells. *Science* 287: 1433–1438

Galli R, Binda E, Orfanelli U, Cipelletti B, Gritti A, De Vitis S, Fiocco R, Foroni C, Dimeco F & Vescovi A (2004) Isolation and Characterization of Tumorigenic, Stem-like Neural Precursors from Human Glioblastoma. *Cancer Res* 64: 7011–7021

Gallo M, Ho J, Coutinho FJ, Vanner R, Lee L, Head R, Ling EK, Clarke ID & Dirks PB (2012) A tumorigenic MLL-homeobox network in human glioblastoma stem cells. *Cancer Res* 73: 417–427

Gangemi RM, Griffero F, Marubbi D, Perera M, Capra MC, Malatesta P, Ravetti GL, Zona GL, Daga A & Corte G (2009) SOX2 Silencing in Glioblastoma Tumor-Initiating Cells Causes Stop of Proliferation and Loss of Tumorigenicity. *Stem Cells* 27: 40–48

Ganguly D, Fan M, Yang CH, Zbytek B, Finkelstein D, Roussel MF & Pfeffer LM (2018) The critical role that STAT3 plays in glioma-initiating cells: STAT3 addiction in glioma. *Oncotarget* 9: 22095–22112

Garcia I, Aldaregia J, Marjanovic Vicentic J, Aldaz P, Moreno-Cugnon L, Torres-Bayona S, Carrasco-Garcia E, Garros-Regulez L, Egaña L, Rubio A *et al* (2017) Oncogenic activity of SOX1 in glioblastoma. *Sci Rep* 7:46575

Gargiulo G, Cesaroni M, Serresi M, de Vries N, Hulsman D, Bruggeman SW, Lancini C & van Lohuizen M (2013) In vivo RNAi Screen for BMI1 Targets Identifies TGF-β/BMP-ER Stress Pathways as Key Regulators of Neural- and Malignant Glioma-Stem Cell Homeostasis. *Cancer Cell* 23: 660–676

Gasiunas G, Barrangou R, Horvath P & Siksnys V (2012) Cas9-crRNA ribonucleoprotein complex mediates specific DNA cleavage for adaptive immunity in bacteria. *Proc Natl Acad Sci* 109: E2579–E2586

Gervais L, van den Beek M, Josserand M, Sallé J, Stefanutti M, Perdigoto CN, Skorski P, Mazouni K, Marshall OJ, Brand AH *et al* (2019) Stem Cell Proliferation Is Kept in Check by the Chromatin Regulators Kismet/CHD7/CHD8 and Trr/MLL3/4. *Dev Cell* 49: 556-573.e6

Ghosh D, Nandi S & Bhattacharjee S (2018) Combination therapy to checkmate Glioblastoma: clinical challenges and advances. *Clin Transl Med* 7: 33

Golson ML & Kaestner KH (2016) Fox transcription factors: from development to disease. *Development* 143: 4558–4570

Gómez-López S, Wiskow O, Favaro R, Nicolis SK, Price DJ, Pollard SM & Smith A (2011) Sox2 and Pax6 maintain the proliferative and developmental potential of gliogenic neural stem cells in vitro. *Glia* 59: 1588–1599

Götz M & Huttner WB (2005) The Cell Biology of Neurogenesis. *Nat Rev Mol Cell Biol* 6: 777–788

Graham V, Khudyakov J, Ellis P, Pevny L (2003) SOX2 Functions to Maintain Neural Progenitor Identity. *Neuron* 39: 749–765

Greer EL, Oskoui PR, Banko MR, Maniar JM, Gygi MP, Gygi SP & Brunet A (2007) The energy sensor AMP-activated protein kinase directly regulates the mammalian FOXO3 transcription factor. *J Biol Chem* 282: 30107–30119

Guen T Le, Fichou Y, Nectoux J, Bahi-Buisson N, Rivier F, Boddaert N, Diebold B, Héron D, Chelly J & Bienvenu T (2011) A missense mutation within the fork-head domain of the forkhead box G1 Gene (FOXG1) affects its nuclear localization. *Hum Mutat* 32: 2026–2035

Guo Y, Liu S, Wang P, Zhao S, Wang F, Bing L, Zhang Y, Ling EA, Gao J & Hao A (2011) Expression profile of embryonic stem cell-associated genes Oct4, Sox2 and Nanog in human gliomas. *Histopathology* 59: 763–775

Hagenbuchner J & Ausserlechner MJ (2016) Targeting transcription factors by small compounds - Current strategies and future implications. *Biochem Pharmacol* 107: 1–13

Hanahan D & Weinberg RA (2011) Hallmarks of cancer: The next generation. *Cell* 144: 646–674

Hanashima C, Li SC, Shen L, Lai E & Fischell G (2004) Foxg1 Suppresses Early Cortical Cell Fate. *Science* 303: 56–59

Hanashima C, Shen L, Li SC & Lai E (2002) Brain Factor-1 Controls the Proliferation and Differentiation of Neocortical Progenitor Cells through Independent Mechanisms. *J Neurosci* 22: 6526–6536

Hansen D V, Lui JH, Parker PR & Kriegstein AR (2010) Neurogenic radial glia in the outer subventricular zone of human neocortex. *Nature* 464: 554–561

Hardcastle Z & Papalopulu N (2000) Distinct effects of XBF-1 in regulating the cell cycle inhibitor p27(XIC1) and imparting a neural fate. *Development* 127: 1303–14

Harris L & Guillemot F (2019) HES1, two programs: promoting the quiescence and proliferation of adult neural stem cells. *Genes Dev* 33: 479–481

Hatta M & Cirillo LA (2007) Chromatin opening and stable perturbation of core histone:DNA contacts by FoxO1. *J Biol Chem* 282: 35583–35593

Hegi ME, Diserens AC, Gorlia T, Hamou MF, de Tribolet N, Weller M, Kros JM, Hainfellner JA, Mason W, Mariani L *et al* (2005) MGMT Gene Silencing and Benefit from Temozolomide in Glioblastoma. *N Engl J Med* 352: 997–1003

van der Heide LP, Jacobs FM, Burbach JP, Hoekman MF & Smidt MP (2005) FoxO6 transcriptional activity is regulated by Thr 26 and Ser 184, independent of nucleo-cytoplasmic shuttling. *Biochem J* 391: 623–629

Heide LP Van Der & Smidt MP (2005) Regulation of FoxO activity by CBP / p300-mediated acetylation. *Trends Biochem Sci* 30: 81–86

Heinrich MA, Bansal R, Lammers T, Zhang YS, Michel Schiffelers R & Prakash J (2019) 3D-Bioprinted Mini-Brain: A Glioblastoma Model to Study Cellular Interactions and Therapeutics. *Adv Mater* 31: e1806590

Hemmati HD, Nakano I, Lazareff JA, Masterman-smith M, Geschwind DH, Bronner-Fraser M & Kornblum HI (2003) Cancerous stem cells can arise from pediatric brain tumors. *Proc Natl Acad Sci USA* 100: 15178-83

Hochedlinger K & Jaenisch R (2015) Induced Pluripotency and Epigenetic Reprogramming. *Cold Spring Harb Perspect Biol* 7: pii. a019448

Hochedlinger K & Plath K (2009) Epigenetic reprogramming and induced pluripotency. *Development* 136: 509–523

Hoekman MF, Jacobs FM, Smidt MP & Burbach JP (2006) Spatial and temporal expression of FoxO transcription factors in the developing and adult murine brain. *Gene Expr Patterns* 6: 134–140

Holland EC (2000) Glioblastoma multiforme: The terminator. *Proc Natl Acad Sci* 97: 6242–6244

Hong CS & Saint-Jeannet JP (2007) The Activity of Pax3 and Zic1 Regulates Three Distinct Cell Fates at the Neural Plate Border. *Mol Biol Cell* 18: 2192-202

Hornsveld M, Dansen TB, Derksen PW & Burgering BM (2018) Seminars in Cancer Biology Re-evaluating the role of FOXOs in cancer. *Semin Cancer Biol* 50: 90–100

van der Horst A, de Vries-Smits AM, Brenkman AB, van Triest MH, van den Broek N, Colland F, Maurice MM & Burgering BM (2006) FOXO4 transcriptional activity is regulated by monoubiquitination and USP7/HAUSP. *Nat Cell Biol* 8: 1064–1073

Hottinger AF, Abdullah KG & Stupp R (2016) Current Standards of Care in Glioblastoma Therapy. In *Glioblastoma.* Elsevier Inc. (pp. 73-80).

Hu H, Wang B, Borde M, Nardone J, Maika S, Allred L, Tucker PW & Rao A (2006) Foxp1 is an essential transcriptional regulator of B cell development. *Nat Immunol* 7: 819–826

Huang H & Tindall DJ (2007) Dynamic FoxO transcription factors. *J Cell Sci* 120: 2479–2487

Huse JT, Phillips HS & Brennan CW (2011) Molecular subclassification of diffuse gliomas: Seeing order in the chaos. *Glia* 59: 1190–1199

Inamoto I & Shin JA (2018) Peptide therapeutics that directly target transcription factors. *Pept Sci* 111: 1-11

Ishii A, Kimura T, Sadahiro H, Kawano H, Takubo K, Suzuki M & Ikeda E (2016) Histological Characterization of the tumorigenic 'peri-necrotic niche' harboring quiescent stem-like tumor cells in glioblastoma. *PLoS One* 11: e0147366

Ivanov AA, Khuri FR & Fu H (2014) Targeting protein-protein interactions as an anticancer strategy. *Trends Pharmacol Sci* 34: 393–400

Iwafuchi-Doi M & Zaret KS (2014) Pioneer transcription factors in cell reprogramming. *Genes Dev* 28: 2679–2692

Jackson BC, Carpenter C, Nebert DW & Vasiliou V (2010) Update of human and mouse forkhead box (FOX) gene families. *Hum Genomics* 4: 345–52

Jackson M, Hassiotou F & Nowak A (2014) Glioblastoma stem-like cells: At the root of tumor recurrence and a therapeutic target. *Carcinogenesis* 36: 177–185

Jacobi AM, Rettig GR, Turk R, Collingwood MA, Zeiner SA, Quadros RM, Harms DW, Bonthuis PJ, Gregg C, Ohtsuka M *et al* (2017) Simplified CRISPR tools for efficient genome editing and streamlined protocols for their delivery into mammalian cells and mouse zygotes. *Methods* 121-122: 16-28

Jacobs FM, van der Heide LP, Wijchers PJ, Burbach JP, Hoekman MF & Smidt MP (2003) FoxO6, a novel member of the FoxO class of transcription factors with distinct shuttling dynamics. *J Biol Chem* 278: 35959–35967

Jacques TS, Swales A, Brzozowski MJ, Henriquez NV, Linehan JM, Mirzadeh Z, O'Malley C, Naumann H, Alvarez-Buylla A & Brandner S (2010) Combinations of genetic mutations in the adult neural stem cell compartment determine brain tumour phenotypes. *EMBO* 29: 222–235

Jane EP, Premkumar DR, Addo-Yobo SO & Pollack IF (2009) Abrogation of Mitogen-Activated Protein Kinase and Akt Signaling by Vandetanib Synergistically Potentiates Histone Deacetylase Inhibitor-Induced Apoptosis in Human Glioma Cells. *J Pharmacol Exp Ther* 331: 327–337

Jang HS, Shin WJ, Lee JE & Do JT (2017) CpG and non-CpG methylation in epigenetic gene regulation and brain function. *Genes (Basel)* 8: pii E148

Ji Z & Sharrocks AD (2015) Changing partners: transcription factors form different complexes on and off chromatin. *Mol Syst Biol* 11: 782

Johnson BE, Mazor T, Hong C, Barnes M, Aihara K, McLean CY, Fouse SD, Yamamoto S, Ueda H, Tatsuno K *et al* (2014) Mutational analysis reveals the origin and therapy-driven evolution of recurrent glioma. *Science* 343: 189-193

Johnson MB, Wang PP, Atabay KD, Murphy EA, Doan RN, Hecht JL & Walsh CA (2015) Single-cell analysis reveals transcriptional heterogeneity of neural progenitors in human cortex. *Nat Neurosci* 18: 637–647

Kaestner KH, Knöchel W & Martínez DE (2000) Unified nomenclature for the winged helix/forkhead transcription factors. *Genes Dev* 14: 142–146

Karadedou CT, Gomes AR, Chen J, Petkovic M, Ho KK, Zwolinska AK, Feltes A, Wong SY, Chan KY, Cheung YN *et al* (2012) FOXO3a represses VEGF expression through FOXM1-dependent and -independent

mechanisms in breast cancer. *Oncogene* 31: 1845–1858

Kastury K, Li J, Drunk T, Su H, Vogt PK, Croce CM & Huebner K (1994) The human homologue of the retroviral oncogene qin maps to chromosome 14q13. *Proc Natl Acad Sci USA* 91: 3616–3618

Katz C, Levy-Beladev L, Rotem-Bamberger S, Rito T, Rüdiger SG & Friedler A (2011) Studying protein-protein interactions using peptide arrays. *Chem Soc Rev* 40: 2131–2145

Keenen B & de la Serna IL (2009) Chromatin remodeling in Embryonic stem cells: regulating the balance between pluripotency and differentiation. *J Cell Physiol* 219: 1–7

Kelava I & Lancaster MA (2016) Stem Cell Models of Human Brain Development. *Stem Cell* 18: 736–748

Kelley ML, Strezoska Z, He K, Vermeulen A, Smith Av (2016) Versatility of chemically synthesized guide RNAs for CRISPR-Cas9 genome editing. *J Biotechnol* 233: 74-83

Kempermann G, Gage FH, Aigner L, Song H, Curtis MA, Thuret S, Kuhn HG, Jessberger S, Frankland PW, Cameron HA *et al* (2018) Human Adult Neurogenesis : Evidence and Remaining Questions *Cell Stem Cell* 23: 25–30

Kim DH, Perdomo G, Zhang T, Slusher S, Lee S, Phillips BE, Fan Y, Giannoukakis N, Gramignoli R, Strom S *et al* (2011a) FoxO6 Integrates Insulin Signaling With Gluconeogenesis in the Liver. *Diabetes* 60: 2763–2774

Kim DH, Zhang T, Lee S & Dong HH (2013) FoxO6 in glucose metabolism. *J Diabetes* 5: 233–240

Kim H, Zheng S, Amini SS, Virk SM, Mikkelsen T, Brat DJ, Grimsby J, Sougnez C, Muller F, Hu J *et al* (2015c) Whole-genome and multisector exome sequencing of primary and post-treatment glioblastoma reveals patterns of tumor evolution. *Genome Res* 25:316-27

Kim J, Lee IH, Cho HJ, Park CK, Jung YS, Kim Y, Nam SH, Kim BS, Johnson MD, Kong DS *et al* (2015a) Spatiotemporal Evolution of the Primary Glioblastoma Genome. *Cancer Cell* 28: 318–328

Kim JH, Lee SR, Li LH, Park HJ, Park JH, Lee KY, Kim MK, Shin BA & Choi SY (2011b) High cleavage efficiency of a 2A peptide derived from porcine teschovirus-1 in human cell lines, zebrafish and mice. *PLoS One* 6: e18556

Kim SH, Joshi K, Ezhilarasan R, Myers TR, Siu J, Gu C, Nakano-Okuno M, Taylor D, Minata M, Sulman EP *et al* (2015b) EZH2 protects Glioma stem cells from radiation-induced cell death in a MELK/FOXM1-dependent manner. *Stem Cell Reports* 4: 226–238

Kim ME, Cho JH, Lee JS (2019) Forkhead box O 6 modulates immunological functions of Dendritic cells. *J Immuno.* 202: (1 Supplement) 58.7

Kleinsmith LJ & Pierce GB Jr (1964) Multipotentiality of Single Embryonal Carcinoma Cells. *Cancer Res* 24*:* 1544-51.

Klose RJ, Kallin EM & Zhang Y (2006) JmjC-domain-containing proteins and histone demethylation. *Nat Rev Genet* 7: 715–727

Koehler AN (2010) A complex task? Direct modulation of transcription factors with small molecules. *Curr Opin Chem Biol* 14: 331–340

Koshy M, Villano JL, Dolecek TA, Howard A, Mahmood U, Chmura SJ, Weichselbaum RR & McCarthy BJ (2012) Improved survival time trends for glioblastoma using the SEER 17 population-based registries. *J Neurooncol* 107: 207–212

Kramer A & Schneider-Mergener J (1998) Synthesis and screening of peptide libraries on continuous cellulose membrane supports. *Methods Mol Biol* 87:25-39

Kreso A & Dick JE (2014) Evolution of the cancer stem cell model. *Cell Stem Cell* 14: 275–291

Kretzschmar M & Massague J (1998) SMADs : mediators and regulators of TGF-13 signaling. *Curr Opin Genet Dev* 8: 103–111

Kriegstein A & Alvarez-Buylla A (2009) The Glial Nature of Embryonic and Adult Neural Stem Cells. *Annu Rev Neurosci* 32: 149–184

Kristensen LH, Nielsen AL, Helgstrand C, Lees M, Cloos P, Kastrup JS, Helin K, Olsen L & Gajhede M (2012) Studies of H3K4me3 demethylation by KDM5B/Jarid1B/PLU1 reveals strong substrate recognition in vitro and identifies 2,4-pyridine-dicarboxylic acid as an in vitro and in cell inhibitor. *FEBS J* 279: 1905–1914

Krivtsov AV, Twomey D, Feng Z, Stubbs MC, Wang Y, Faber J, Levine JE, Wang J, Hahn WC, Gilliland DG *et al* (2006) Transformation from committed progenitor to leukaemia stem cell initiated by MLL – AF9. *Nature* 442: 818–822

Kumamoto T, Toma K, Gunadi, McKenna W, Kasukawa T, Katzman S, Chen B & Hanashima C (2013) Foxg1 Coordinates the Switch from Non-Radially to Radially Migrating Glutamatergic Subtypes in the Neocortex through Spatiotemporal Repression. *Cell Rep* 3: 931–945

Kumar N, Tsai Y, Chen L, Zhou A, Banerjee KK, Saxena M, Huang S, Toke NH, Xing J, Shivdasani RA *et al* (2019) The lineage-specific transcription factor CDX2 navigates dynamic chromatin to control distinct stages of intestine development. *Development* 146: pii: dev172189

Lai AY & Wade PA (2011) Cancer biology and NuRD: A multifaceted chromatin remodelling complex. *Nat Rev Cancer* 11: 588–596

Lai RK, Chen Y, Guan X, Nousome D, Sharma C, Canoll P, Bruce J, Sloan AE, Cortes E, Vonsattel JP *et al* (2014) Genome-wide methylation analyses in glioblastoma multiforme. *PLoS One* 9: e89376

Lallemand F, Petitalot A, Vacher S, de Koning L, Taouis K, Lopez BS, Zinn-Justin S, Dalla-Venezia N, Chemlali W, Schnitzler A *et al* (2018) Involvement of the FOXO6 transcriptional factor in breast carcinogenesis. *Oncotarget* 9: 7464–7475

Lam EW, Brosens JJ, Gomes AR & Koo CY (2013) Forkhead box proteins : tuning forks for transcriptional harmony. *Nat Rev Cancer* 13: 482–495

Lam EW & Gomes AR (2014) Forkhead box transcription factors in cancer initiation, progression and chemotherapeutic drug response. *Front Oncol* 4: 305

Lambert M, Jambon S, Depauw S & David-Cordonnier MH (2018a) Targeting Transcription Factors for Cancer Treatment. *MDPI Mol* 23: pii: E1479

Lambert SA, Jolma A, Campitelli LF, Das PK, Yin Y, Albu M, Chen X, Taipale J, Hughes TR & Weirauch MT (2018b) The Human Transcription Factors. *Cell* 172: 650–665

Lan X, Jörg DJ, Cavalli FMG, Richards LM, Nguyen V, Vanner RJ, Guilhamon P, Lee L, Kushida M, Pellacani D *et al* (2017) Fate mapping of human glioblastoma reveals an invariant stem cell hierarchy. *Nature* 549: 227–232

Lapidot T, Sirard C, Vormoor J, Murdoch B, Hoang T, Caceres-Cortes J, Mindent M, Paterson B, Caligiuri MA & Dick JE (1994) A cell initiating human acute myeloid leukaemia after transplantation into SCID mice. *Nature* 362: 645-8

Lathia JD, Mack SC, Mulkearns-Hubert EE, Valentim CL & Rich JN (2015) Cancer stem cells in glioblastoma. *Genes Dev* 29: 1203–1217

Le Lay J & Kaestner KH (2010) The Fox Genes in the Liver: From Organogenesis to Functional Integration. *Physiol Rev* 90: 1–22

Lee EQ, Kaley TJ, Duda DG, Schiff D, Lassman AB, Wong ET, Mikkelsen T, Purow BW, Muzikansky A, Ancukiewicz M *et al* (2015) A multicenter, phase II, randomized, noncomparative clinical trial of

radiation and temozolomide with or without vandetanib in newly diagnosed glioblastoma patients. *Clin Cancer Res* 21: 3610–3618

Lee J, Kotliarova S, Kotliarov Y, Li A, Su Q, Donin NM, Pastorino S, Purow BW, Christopher N, Zhang W *et al* (2006) Tumor stem cells derived from glioblastomas cultured in bFGF and EGF more closely mirror the phenotype and genotype of primary tumors than do serum-cultured cell lines. *Cancer Cell* 9: 391–403

Lee J, Son MJ, Woolard K, Donin NM, Li A, Cheng CH, Kotliarova S, Kotliarov Y, Walling J, Ahn S *et al* (2008) Epigenetic-Mediated Dysfunction of the Bone Morphogenetic Protein Pathway Inhibits Differentiation of Glioblastoma-Initiating Cells. *Cancer Cell* 13: 69–80

Lee JH, Lee JE, Kahng JY, Kim SH, Park JS, Yoon SJ, Um JY, Kim WK, Lee JK, Park J *et al* (2018) Human glioblastoma arises from subventricular zone cells with low-level driver mutations. *Nature* 560: 243–247

Lee N, Erdjument-Bromage H, Tempst P, Jones RS & Zhang Y (2009) The H3K4 Demethylase Lid Associates with and Inhibits Histone Deacetylase Rpd3. *Mol Cell Biol* 29: 1401–1410

Lehmann OJ, Sowden JC, Carlsson P, Jordan T & Bhattacharya SS (2003) Fox's in development and disease. *Trends Genet* 19: 339–344

Levine M & Tjian R (2003) Transcription regulation and animal diversity. *Nature* 424: 147–151

Li B, Samanta A, Song X, Iacono KT, Bembas K, Tao R, Basu S, Riley JL, Hancock WW, Shen Y *et al* (2007) FOXP3 interactions with histone acetyltransferase and class II histone deacetylases are required for repression. *Proc Natl Acad Sci* 104: 4571–4576

Li J, Chang HW, Lai E, Parker EJ & Vogt PK (1995) The Oncogene qin Codes for a Transcriptional Repressor. *Cancer Res* 55: 5540–5545

Li J V., Chien CD, Garee JP, Xu J, Wellstein A & Riegel AT (2013) Transcriptional Repression of AIB1 by FoxG1 Leads to Apoptosis in Breast Cancer Cells. *Mol Endocrinol* 27: 1113–1127

Li Q, Tang H, Hu F & Qin C (2019) Silencing of FOXO6 inhibits the proliferation, invasion, and glycolysis in colorectal cancer cells. *J Cell Biochem* 120: 3853–3860

Li S, Weidenfeld J & Morrisey EE (2004) Transcriptional and DNA Binding Activity of the Foxp1/2/4 Family Is Modulated by Heterotypic and Homotypic Protein Interactions. *Mol Cell Biol* 24: 809–822

Li X, Wang W, Wang J, Malovannaya A, Xi Y, Li W, Guerra R, Hawke DH, Qin J & Chen J (2015) Proteomic analyses reveal distinct chromatin- associated and soluble transcription factor complexes. *Mol Syst Biol* 11: 775

Li Y, Min W, Li M, Han G, Dai D, Zhang L, Chen X, Wang X, Zhang Y, Yue Z *et al* (2016) Identification of hub genes and regulatory factors of glioblastoma multiforme subgroups by RNA-seq data analysis. *Int J Mol Med* 38: 1170-8

Liau BB, Sievers C, Donohue LK, Gillespie SM, Flavahan WA, Miller TE, Venteicher AS, Hebert CH, Carey CD, Rodig SJ *et al* (2017) Adaptive Chromatin Remodeling Drives Glioblastoma Stem Cell Plasticity and Drug Tolerance. *Cell Stem Cell* 20: 233-246.e7

Liau LM, Ashkan K, Tran DD, Campian JL, Trusheim JE, Cobbs CS, Heth JA, Salacz M, Taylor S, D'Andre SD *et al* (2018) First results on survival from a large Phase 3 clinical trial of an autologous dendritic cell vaccine in newly diagnosed glioblastoma. *J Transl Med* 16: 142

Liberti MV & Locasale JW (2016) The Warburg Effect: How Does it Benefit Cancer Cells? *Trends Biochem Sci* 41: 211–218

Ligon KL, Alberta JA, Kho AT, Weiss J, Kwaan MR, Nutt CL, Louis DN, Stiles CD & Rowitch DH (2004) The oligodendroglial lineage marker OLIG2 is universally expressed in diffuse gliomas. *J Neuropathol Exp*

Neurol 63: 499–509

Linkous A, Balamatsias D, Snuderl M, Edwards L, Miyaguchi K, Milner T, Reich B, Cohen-Gould L, Storaska A, Nakayama Y *et al* (2019) Modeling Patient-Derived Glioblastoma with Cerebral Organoids. *Cell Reports* 26: 3203-3211.e5

Lister R, Pelizzola M, Dowen RH, Hawkins RD, Hon G, Tonti-Filippini J, Nery JR, Lee L, Ye Z, Ngo QM *et al* (2009) Human DNA methylomes at base resolution show widespread epigenomic differences. *Nature* 462: 315–322

Liu C, Sage JC, Miller MR, Verhaak RG, Hippenmeyer S, Vogel H, Foreman O, Bronson RT, Nishiyama A, Luo L *et al* (2011) Mosaic Analysis with Double Markers Reveals Tumor Cell of Origin in Glioma. *Cell* 146: 209–221

Liu F, Hon GC, Villa GR, Turner KM, Ikegami S, Yang H, Ye Z, Li B, Kuan S, Lee AY *et al* (2015) EGFR Mutation Promotes Glioblastoma through Epigenome and Transcription Factor Network Remodeling. *Mol Cell* 60: 307–318

Liu X, Chen X, Shi L, Shan Q, Cao Q, Yue C, Li H, Li S, Wang J, Gao S *et al* (2019) The third-generation EGFR inhibitor AZD9291 overcomes primary resistance by continuously blocking ERK signaling in glioblastoma. *J Exp Clin Cancer Res* 38: 219

Liu X, Greer C & Secombe J (2014) KDM5 Interacts with Foxo to Modulate Cellular Levels of Oxidative Stress. *PLoS Genet* 10: e1004676

Lodato MA, Ng CW, Wamstad JA, Cheng AW, Thai KK, Fraenkel E, Jaenisch R & Boyer LA (2013) SOX2 Co-Occupies Distal Enhancer Elements with Distinct POU Factors in ESCs and NPCs to Specify Cell State. *PLoS Genet* 9: e1003288

Louis DN, Perry A, Reifenberger G, von Deimling A, Figarella-Branger D, Cavenee WK, Ohgaki H, Wiestler OD, Kleihues P & Ellison DW (2016) The 2016 World Health Organization Classification of Tumors of the Central Nervous System: a summary. *Acta Neuropathol* 131: 803–820

Love MI, Huber W & Anders S (2014) Moderated estimation of fold change and dispersion for RNA-seq data with DESeq2. *Genome Biol* 15: 550

Lu C & Allis CD (2017) SWI/SNF Complex in Cancer: 'Remodeling' Mechanisms Uncovered. *Nat Genet* 49: 178–179

Lu QR, Park JK, Noll E, Chan JA, Alberta J, Yuk D, Alzamora MG, Louis DN, Stiles CD, Rowitch DH *et al* (2001) Oligodendrocyte lineage genes (OLIG) as molecular markers for human glial brain tumors. *Proc Natl Acad Sci* 98: 10851–10856

Lujan E, Chanda S, Ahlenius H, Sudhof TC & Wernig M (2012) Direct conversion of mouse fibroblasts to self-renewing, tripotent neural precursor cells. *Proc Natl Acad Sci* 109: 2527–2532

Ma K, Deng X, Xia X, Fan Z, Qi X, Wang Y, Li Y, Ma Y, Chen Q, Peng H *et al* (2018) Direct conversion of mouse astrocytes into neural progenitor cells and specific lineages of neurons. *Transl Neurodegener* 7: 29

Mabonga L & Kappo AP (2020) Peptidomimetics: A Synthetic Tool for Inhibiting Protein–Protein Interactions in Cancer. *Int J Pept Res Ther* 26: 225-241

Mack SC, Singh I, Wang X, Hirsch R, Wu Q, Villagomez R, Bernatchez JA, Zhu Z, Gimple RC, Kim LJY *et al* (2019) Chromatin landscapes reveal developmentally encoded transcriptional states that define human glioblastoma. *J Exp Med* 216: 1071–1090

MacLeod G, Bozek DA, Rajakulendran N, Monteiro V, Ahmadi M, Steinhart Z, Kushida MM, Yu H, Coutinho FJ, Cavalli FMG *et al* (2019) Genome-Wide CRISPR-Cas9 Screens Expose Genetic Vulnerabilities and Mechanisms of Temozolomide Sensitivity in Glioblastoma Stem Cells. *Cell Rep* 27: 971-986.e9

Madhavan S, Zenklusen J-C, Kotliarov Y, Sahni H, Fine HA & Buetow K (2009) Rembrandt: Helping

Personalized Medicine Become a Reality through Integrative Translational Research. *Mol Cancer Res* 7: 157–167

Madureira PA, Varshochi R, Constantinidou D, Francis RE, Coombes RC, Yao KM & Lam EW (2006) The forkhead box M1 protein regulates the transcription of the estrogen receptor α in breast cancer cells. *J Biol Chem* 281: 25167–25176

Major ML, Lepe R & Costa RH (2004) Forkhead Box M1B Transcriptional Activity Requires Binding of Cdk-Cyclin Complexes for Phosphorylation-Dependent Recruitment of p300/CBP Coactivators. *Mol Cell Biol* 24: 2649–2661

Manuel M, Martynoga B, Yu T, West JD, Mason JO & Price DJ (2010) The transcription factor Foxg1 regulates the competence of telencephalic cells to adopt subpallial fates in mice. *Development* 137(3): 487–497

Manuel MN, Martynoga B, Molinek MD, Quinn JC, Kroemmer C, Mason JO & Price DJ (2011) The transcription factor Foxg1 regulates telencephalic progenitor proliferation cell autonomously, in part by controlling Pax6 expression levels. *Neural Dev* 6:9

Marcal N, Patel H, Dong Z, Belanger-Jasmin S, Hoffman B, Helgason CD, Dang J & Stifani S (2005) Antagonistic Effects of Grg6 and Groucho/TLE on the Transcription Repression Activity of Brain Factor 1/FoxG1 and Cortical Neuron Differentiation. *Mol Cell Biol* 25: 10916–10929

Martella A, Matjusaitis M, Auxillos J, Pollard SM & Cai Y (2017) EMMA: An Extensible Mammalian Modular Assembly Toolkit for the Rapid Design and Production of Diverse Expression Vectors. *ACS Synth Biol* 6: 1380–1392

Martin M (2011) Cutadapt removes adapter sequences from high-throughput sequencing reads. *EM.net.journal* 17: 10–12

Martynoga B, Andersen J, Achimastou A, Urbán N, van den Berg D, Guillemot F, Mateo JL, Wittbrodt J, Ettwiller L, Zhou B *et al* (2013) Epigenomic enhancer annotation reveals a key role for NFIX in neural stem cell quiescence. *Genes Dev* 27: 1769–1786

Martynoga B, Morrison H, Price DJ & Mason JO (2005) Foxg1 is required for specification of ventral telencephalon and region-specific regulation of dorsal telencephalic precursor proliferation and apoptosis. *Dev Biol* 283: 113–127

Massagué J (2008) TGFβ in Cancer. *Cell* 134: 215–230

Masui K, Tanaka K, Akhavan D, Babic I, Gini B, Matsutani T, Iwanami A, Liu F, Villa GR, Gu Y *et al* (2013) MTOR complex 2 controls glycolytic metabolism in glioblastoma through FoxO acetylation and upregulation of c-Myc. *Cell Metab* 18: 726–739

Mateo JL, van Den Berg DL, Haeussler M, Drechsel D, Gaber ZB, Castro DS, Robson P, Crawford GE, Flicek P, Ettwiller L *et al* (2015) Characterization of the neural stem cell gene regulatory network identifies OLIG2 as a multifunctional regulator of self-renewal. *Genome Res.* 25: 41–56

McGranahan N & Swanton C (2017) Clonal Heterogeneity and Tumor Evolution: Past, Present, and the Future. *Cell* 168: 613–628

Mehta S, Huillard E, Kesari S, Maire CL, Golebiowski D, Harrington EP, Alberta JA, Kane MF, Theisen M, Ligon KL *et al* (2011) The Central Nervous System-Restricted Transcription Factor Olig2 Opposes p53 Responses to Genotoxic Damage in Neural Progenitors and Malignant Glioma. *Cancer Cell* 19: 359–371

Meijer DH, Kane MF, Mehta S, Liu H, Harrington E, Taylor CM, Stiles CD & Rowitch DH (2012) Separated at birth? the functional and molecular divergence of OLIG1 and OLIG2. *Nat Rev Neurosci* 13: 819–831

Meijsing SH, Pufall MA, So AY, Bates DL, Chen L & Yamamoto KR (2009) DNA Binding Site Sequence Structure and Activity. *Science* 324: 407–411

Meissner A, Mikkelsen TS, Gu H, Wernig M, Hanna J, Sivachenko A, Zhang X, Bernstein BE, Nusbaum C, Jaffe

DB *et al* (2008) Genome-scale DNA methylation maps of pluripotent and differentiated cells. *Nature* 454: 766–770

Mencarelli MA, Spanhol-Rosseto A, Artuso R, Rondinella D, De Filippis R, Bahi-Buisson N, Nectoux J, Rubinsztajn R, Bienvenu T, Moncla A *et al* (2010) Novel FOXG1 mutations associated with the congenital variant of Rett syndrome. *J Med Genet* 47: 49–53

Menendez JA & Alarcon T (2014) Metabostemness: A New Cancer Hallmark. *Front Oncol* 4: 262

Le Mercier M, Hastir D, Moles Lopez X, de Nève N, Maris C, Trepant AL, Rorive S, Decaestecker C & Salmon I (2012) A Simplified Approach for the Molecular Classification of Glioblastomas. *PLoS One* 7: e45475

Merkle FT & Alvarez-Buylla A (2006) Neural stem cells in mammalian development. *Curr Opin Cell Biol* 18: 704–709

Merkle FT, Tramontin AD, Garcıa-Verdugo JM, & Alvarez-Buylla A (2004) Radial glia give rise to adult neural stem cells in the subventricular zone. *PNAS* 101: 17528–17532

Mikkelsen TS, Hanna J, Zhang X, Ku M, Wernig M, Schorderet P, Bernstein BE, Jaenisch R, Lander ES & Meissner A (2008) Dissecting direct reprogramming through integrative genomic analysis. *Nature* 454: 49–55

Mirzadeh Z, Merkle FT, Soriano-Navarro M & Garcia-Verdugo JM & Alvarez-Buylla A (2008) Neural Stem Cells Confer Unique Pinwheel Architecture to the Ventricular Surface in Neurogenic Regions of the Adult Brain. *Cell Stem Cell* 3: 265–278

Mitter D, Pringsheim M, Kaulisch M, Plümacher KS, Schröder S, Warthemann R, Abou Jamra R, Baethmann M, Bast T, Büttel HM *et al* (2018) FOXG1 syndrome: Genotype-phenotype association in 83 patients with FOXG1 variants. *Genet Med* 20: 98–108

Miyoshi G & Fishell G (2012) Dynamic FoxG1 Expression Coordinates the Integration of Multipolar Pyramidal Neuron Precursors into the Cortical Plate. *Neuron* 74: 1045–1058

Modrek AS, Bayin NS & Placantonakis DG (2014) Brain stem cells as the cell of origin in glioma. *World J Stem Cells* 6: 43-52

Mohammed H, D'Santos C, Serandour AA, Ali HR, Brown GD, Atkins A, Rueda OM, Holmes KA, Theodorou V, Robinson JL *et al* (2013) Endogenous Purification Reveals GREB1 as a Key Estrogen Receptor Regulatory Factor. *Cell Rep* 3: 342–349

Mohammed H, Taylor C, Brown GD, Papachristou EK, Carroll JS & D'Santos CS (2016) Rapid immunoprecipitation mass spectrometry of endogenous proteins (RIME) for analysis of chromatin complexes. *Nat Protoc* 11: 316–326

Molofsky AV, Krenick R, Ullian E, Tsai H, Deneen B, Richardson WD, Barres BA & Rowitch DH (2012) Astrocytes and disease : a neurodevelopmental perspective. *Genes Dev* 26: 891–907

Morrison AM, Nutt SL, Thévenin C, Rolink A & Busslinger M (1998) Loss- and gain-of-function mutations reveal an important role of BSAP (Pax-5) at the start and end of B cell differentiation. *Semin Immunol* 10: 133–142

Murphy DB, Wiese S, Burfeind P, Schmunt D, Mattei M-G, Schulz-Schaeffer W & Thies U (1994) Human Brain Factor 1, a New members of the Fork Head Gene family. *Genomics* 21: 551–557

Myatt SS & Lam EW (2007) The emerging roles of forkhead box (Fox) proteins in cancer. *Nat Rev Cancer* 7: 847–859

Nam JS, Yang H, Kim NH, Sun Y, Choi BS & Huh SO (2010) A Winged-Helix Transcription Factor Foxg1 Induces Expression of Mss4 Gene in Rat Hippocampal Progenitor Cells. *Exp Neurobiol* 19: 75-82

National Cancer Intelligence Network (2013) NCIN: Astrocytic Brain Tumours - surival rates in England.

NCIN Data Briefing. Retrieved from: https://www.ncin.org.uk/publications/data_briefings/astrocytic_brain_tumours_survival_rates_in_england

Neftel C, Laffy J, Filbin MG, Hara T, Shore ME, Rahme GJ, Richman AR, Silverbush D, Shaw ML, Hebert CM *et al* (2019) An Integrative Model of Cellular States, Plasticity, and Genetics for Glioblastoma. *Cell* 178: 835–849

Neyns B, Sadones J, Joosens E, Bouttens F, Verbeke L, Baurain JF, D'Hondt L, Strauven T, Chaskis C, In't Veld P *et al* (2009) Stratified phase II trial of cetuximab in patients with recurrent high-grade glioma. *Ann Oncol* 20: 1596–1603

Nielsen S, Nagelhus EA, Amiry-Moghaddam M, Bourque C, Agre P & Ottersen OP (1997) Specialized Membrane Domains for Water Transport in Glial Cells : High-Resolution Immunogold Cytochemistry of Aquaporin-4 in Rat Brain. *J Neurosci* 17: 171–180

Nutt CL, Mani DR, Betensky RA, Tamayo P, Cairncross JG, Ladd C, Pohl U, Hartmann C, McLaughlin ME, Batchelor TT *et al* (2003) Gene expression-based classification of malignant gliomas correlates better with survival than histological classification. *Cancer Res* 63: 1602–1607

O'Duibhir E, Carragher NO & Pollard SM (2017) Accelerating glioblastoma drug discovery: Convergence of patient-derived models, genome editing and phenotypic screening. *Mol Cell Neurosci* 80: 198–207

Obayashi S, Tabunoki H, Kim SU & Satoh J (2009) Gene Expression Profiling of Human Neural Progenitor Cells Following the Serum-Induced Astrocyte Differentiation. *Cell Mol Neurobiol* 29: 423–438

Obendorf M, Meyer R, Henning K, Mitev YA, Schroder J, Patchev VK & Wolf SS (2007) FoxG1 , a member of the forkhead family , is a corepressor of the androgen receptor. *J Steroid Biochem Mol Biol* 104: 195–207

Olar A & Aldape KD (2014) Using the molecular classification of glioblastoma to inform personalized treatment. *J Pathol* 232: 165–177

Orkin SH & Hochedlinger K (2011) Chromatin connections to pluripotency and cellular reprogramming. *Cell* 145: 835–850

Ostrom QT, Gittleman H, Truitt G, Boscia A, Kruchko C & Barnholtz-Sloan JS (2018) CBTRUS statistical report: Primary brain and other central nervous system tumors diagnosed in the United States in 2011-2015. *Neuro Oncol* 20: iv1–iv86

Ozawa T, Riester M, Cheng YK, Huse JT, Squatrito M, Helmy K, Charles N, Michor F & Holland EC (2014) Most human non-GCIMP glioblastoma subtypes evolve from a common proneural-like precursor glioma. *Cancer Cell* 26: 288–300

Paap RH, Oosterbroek S, Wagemans CMRJ, von Oerthel L, Schellevis RD, Vastenhouw-van der Linden AJA, Groot Koerkamp MJA, Hoekman MFM & Smidt MP (2016) FoxO6 affects Plxna4-mediated neuronal migration during mouse cortical development. *Proc Natl Acad Sci* 113: E7087–E7096

Pancrazi L, Di Benedetto G, Colombaioni L, Della Sala G, Testa G, Olimpico F, Reyes A, Zeviani M, Pozzan T & Costa M (2015) Foxg1 localizes to mitochondria and coordinates cell differentiation and bioenergetics. *Proc Natl Acad Sci* 112: 13910–13915

Pang ZP, Yang N, Vierbuchen T, Ostermeier A, Fuentes DR, Yang TQ, Citri A, Sebastiano V, Marro S, Südhof TC *et al* (2011) Induction of human neuronal cells by defined transcription factors. *Nature* 476: 220–223

Papachristou EK, Kishore K, Holding AN, Harvey K, Roumeliotis TI, Chilamakuri CSR, Omarjee S, Chia KM, Swarbrick A, Lim E *et al* (2018) A quantitative mass spectrometry-based approach to monitor the dynamics of endogenous chromatin-associated protein complexes. *Nat Commun* 9: 1–13

Park AK, Kim P, Ballester LY, Esquenazi Y & Zhao Z (2019) Subtype-specific signaling pathways and genomic aberrations associated with prognosis of glioblastoma. *Neuro Oncol* 21: 59–70

Pastrana E, Silva-Vargas V & Doetsch F (2011) Protocol Review Eyes Wide Open : A Critical Review of Sphere-Formation as an Assay for Stem Cells. *Cell Stem Cell* 8: 486–498

Patel AP, Tirosh I, Trombetta JJ, Shalek AK, Gillespie SM, Wakimoto H, Cahill DP, Nahed BV, Curry WT, Martuza RL *et al* (2014) Single-cell RNA-seq highlights intratumoral heterogeneity in primary glioblastoma. *Science* 344: 1396–1401

Patil V, Ward RL & Hesson LB (2014) The evidence for functional non-CpG methylation in mammalian cells. *Epigenetics* 9: 823–828

Pearson JRD & Regad T (2017) Targeting cellular pathways in glioblastoma multiforme. *Signal Transduct. Target Ther* 2: 17040

Peck B, Ferber EC & Schulze A (2013) Antagonism between FOXO and MYC Regulates Cellular Powerhouse. *Front Oncol* 3: 96

Peñuelas S, Anido J, Prieto-Sánchez RM, Folch G, Barba I, Cuartas I, García-Dorado D, Poca MA, Sahuquillo J, Baselga J *et al* (2009) TGF-β Increases Glioma-Initiating Cell Self-Renewal through the Induction of LIF in Human Glioblastoma. *Cancer Cell* 15: 315–327

Phillips HS, Kharbanda S, Chen R, Forrest WF, Soriano RH, Wu TD, Misra A, Nigro JM, Colman H, Soroceanu L *et al* (2006) Molecular subclasses of high-grade glioma predict prognosis, delineate a pattern of disease progression, and resemble stages in neurogenesis. *Cancer Cell* 9: 157–173

Pollard SM (2013) In Vitro Expansion of Fetal Neural Progenitors as Adherent Cell Lines. In Reynolds BA & Deleyrolle LP (eds) *Neural Progenitor Cells: Methods in Molecular Biology (Methods and Protocols)*, vol 1059. Humana Press, Totowa, NJ.

Pollard SM & Conti L (2007) Investigating radial glia in vitro. *Prog Neurobiol* 83: 53–67

Pollard SM, Conti L, Sun Y & Smith A (2006) Adherent Neural Stem (NS) Cells from Fetal and Adult Forebrain. *Cereb Cortex* 16: i112–i120

Pollard SM, Yoshikawa K, Clarke ID, Danovi D, Stricker S, Russell R, Bayani J, Head R, Lee M, Bernstein M *et al* (2009) Glioma Stem Cell Lines Expanded in Adherent Culture Have Tumor-Specific Phenotypes and Are Suitable for Chemical and Genetic Screens. *Cell Stem Cell* 4: 568–580

Puchalski RB, Miller J, Dalley R, Smith KA, Bertagnolli D, Bickley K, Boe AF, Brouner K, Butler S, Caldejon S *et al* (2018) An anatomic transcriptional atlas of human glioblastoma. *Science* 360: 660–663

Qin H, Zhao A, Zhang C & Fu X (2016) Epigenetic Control of Reprogramming and Transdifferentiation by Histone Modifications. *Stem Cell Rev Reports* 12: 708–720

Qinyu L, Long C, Zhen-Dong D, Min-Min S, Wei-Ze W, Wei-Ping Y & Cheng-Hong P (2013) FOXO6 promotes gastric cancer cell tumorigenicity via upregulation of C-myc. *FEBS Lett* 587: 2105–2111

Raciti M, Granzotto M, Duc M Do, Fimiani C, Cellot G, Cherubini E & Mallamaci A (2013) Reprogramming fibroblasts to neural-precursor-like cells by structured overexpression of pallial patterning genes. *Mol Cell Neurosc.* 57: 42–53

Rahdar M, McMahon MA, Prakash TP, Swayze EE, Frank Bennett C & Cleveland DW (2015) Synthetic CRISPR RNA-Cas9-guided Genome Editing in Human cells. *Pro Natl Acad USA* 112**:** E7110-7

Rebetz J, Tian D, Persson A, Widegren B, Salford LG, Englund E, Gisselsson D & Fan X (2008) Glial progenitor-like phenotype in low-grade glioma and enhanced CD133-expression and neuronal lineage differentiation potential in high-grade glioma. *PLoS One* 3: e1936

Regad T, Roth M, Bredenkamp N, Illing N & Papalopulu N (2007) The neural progenitor-specifying activity of FoxG1 is antagonistically regulated by CKI and FGF. *Nat Cell Biol* 9: 531–540

Renault M, Rafalski VA, Morgan AA, Salih DA, Brett JO, Webb AE, Villeda SA, Thekkat PU, Guillerey C, Denko

NC *et al* (2009) FoxO3 Regulates Neural Stem Cell Homeostasis. *Cell Stem Cell* 5: 527–539

Reya, T, Morrison SJ, Clarke MF & Weissman IL (2001) Stem cells, cancer, and cancer stem cells. *Nature* 414: 105-11

Reynolds BA & Weiss S (1992) Generation of Neurons and Astrocytes from Isolated Cells of the Adult Mammalian Central Nervous System. *Science* 255: 1707–1710

Rheinbay E, Suvà ML, Gillespie SM, Wakimoto H, Patel AP, Shahid M, Oksuz O, Rabkin SD, Martuza RL, Rivera MN *et al* (2013) An Aberrant Transcription Factor Network Essential for Wnt Signaling and Stem Cell Maintenance in Glioblastoma. *Cell Rep* 3: 1567–1579

Rich JN (2016) Cancer stem cells: Understanding tumor hierarchy and heterogeneity. *Medicine (Baltimore)* 95: S2–S7

Riddick G, Kotliarova S, Rodriguez V, Kim HS, Linkous A, Storaska AJ, Ahn S, Walling J, Belova G & Fine HA (2017) A Core Regulatory Circuit in Glioblastoma Stem Cells Links MAPK Activation to a Transcriptional Program of Neural Stem Cell Identity. *Sci Rep* 7: 43605

Ring KL, Tong LM, Balestra ME, Javier R, Andrews-Zwilling Y, Li G, Walker D, Zhang WR, Kreitzer AC & Huang Y (2012) Direct reprogramming of mouse and human fibroblasts into multipotent neural stem cells with a single factor. *Cell Stem Cell* 11: 100–109

Robertson E, Perry C, Doherty R & Madhusudan S (2015) Transcriptomic Profiling of Forkhead Box Transcription Factors in Adult Glioblastoma Multiforme. *Cancer Genomics and Proteomics* 12: 103–112

Robinson JL, MacArthur S, Ross-Innes CS, Tilley WD, Neal DE, Mills IG & Carroll JS (2011) Androgen receptor driven transcription in molecular apocrine breast cancer is mediated by FoxA1. *EMBO J* 30: 3019–3027

Rodriguez C, Huang LJS, Son JK, McKee A, Xiao Z & Lodish HF (2001) Functional Cloning of the Proto-oncogene Brain Factor-1 (BF-1) As a Smad-binding Antagonist of Transforming Growth Factor-β Signaling. *J Biol Chem* 276: 30224–30230

Rodriguez P, Bonte E, Krijgsveld J, Kolodziej KE, Guyot B, Heck AJ, Vyas P, de Boer E, Grosveld F & Strouboulis J (2005) GATA-1 forms distinct activating and repressive complexes in erythroid cells. *EMBO J* 24: 2354–2366

Roesch A, Mueller AM, Stempfl T, Moehle C, Landthaler M & Vogt T (2008) RBP2-H1/JARID1B is a transcriptional regulator with a tumor suppressive potential in melanoma cells. *Int J Cancer* 122: 1047–1057

Romanelli MG, Tato L, Lorenzi P & Morandi C (2003) Nuclear localization domains in human thyroid transcription factor 2. *Biochim Biophys Acta - Mol Cell Res* 1643: 55–64

Romani M, Pistillo MP & Banelli B (2018) Epigenetic Targeting of Glioblastoma. *Front Oncol* 8: 448

Rosenfeld MG, Lunyak VV & Glass CK (2006) Sensors and signals : a coactivator / corepressor / epigenetic code for integrating signal-dependent programs of transcriptional response. *Genes Dev* 20: 1405–1428

Roth M, Bonev B, Lindsay J, Lea R, Panagiotaki N, Houart C & Papalopulu N (2010) FoxG1 and TLE2 act cooperatively to regulate ventral telencephalon formation. *Development* 137: 1553–1562

Rothenberg MS, Concannon K, Cullen S, Boulay G, Turke AB, Faber AC, Lockerman EL, Rivera MN, Engelman JA, Maheswaran S *et al* (2015) Inhibition of mutant EGFR in lung cancer cells triggers SOX2-FOXO6-dependent survival pathways. *Elife* 4: e06132

Rousso DL, Pearson CA, Gaber ZB, Miquelajauregui A, Li S, Portera-Cailliau C, Morrisey EE & Novitch BG (2012) Foxp-Mediated Suppression of N-Cadherin Regulates Neuroepithelial Character and

Progenitor Maintenance in the CNS. *Neuron* 74: 314–330

Safa AR, Saadatzadeh MR, Cohen-Gadol AA, Pollok KE & Bijangi-Vishehsaraei K (2016) Emerging targets for glioblastoma stem cell therapy. *J Biomed Res* 30: 19–31

Salih DA, Rashid AJ, Colas D, de laTorre-Ubieta L, Zhu RP, Morgan AA, Santo EE, Ucar D, Devarajan K, Cole CJ *et al* (2012) FoxO6 regulates memory consolidation and synaptic function. *Genes Dev* 26: 2780–2801

Samanta J & Kessler JA (2004) Interactions between ID and OLIG proteins mediate the inhibitory effects of BMP4 on oligodendroglial differentiation. *Development* 131: 4131–4142

Sampson JH, Aldape KD, Archer GE, Coan A, Desjardins A, Friedman AH, Friedman HS, Gilbert MR, Herndon JE, Mclendon RE *et al* (2011) Greater chemotherapy-induced lymphopenia enhances tumor-specific immune responses that eliminate EGFRvIII-expressing tumor cells in patients with glioblastoma. *Neuro Oncol* 13: 324–333

Santisteban P, Recacha P, Metzger DE & Zaret KS (2010) Dynamic expression of Groucho-related genes Grg1 and Grg3 in foregut endoderm and antagonism of differentiation. *Dev Dyn* 239: 980–986

Sauer F, Fondell JD, Ohkuma Y, Roeder RG & Jackle H (1995) Control of transcription by Kriippel through interactions with TFIIB and TFIIEP. *Nature* 375: 162–164

Sauer F & Jäckle H (1991) Concentration-dependent transcriptional activation or repression by Kriippel from a single binding site. *Nature* 353: 563–566

Savic D, Partridge EC, Newberry KM, Smith SB, Meadows SK, Roberts BS, Mackiewicz M, Mendenhall EM & Myers RM (2015) CETCh-seq: CRISPR epitope tagging ChIP-seq of DNA-binding proteins. *Genome Res* 25: 1581–1589

Schmitges FW, Radovani E, Najafabadi HS, Barazandeh M, Campitelli LF, Yin Y, Jolma A, Zhong G, Guo H, Kanagalingam T *et al* (2016) Multiparameter functional diversity of human C2H2 zinc finger proteins. *Genome Res* 26: 1742–1752

Schmitz SU, Albert M, Malatesta M, Morey L, Johansen JV, Bak M, Tommerup N, Abarrategui I & Helin K (2011) Jarid1b targets genes regulating development and is involved in neural differentiation. *EMBO J* 30: 4586–4600

Scott CE, Wynn SL, Sesay A, Cruz C, Cheung M, Gomez Gaviro MV, Booth S, Gao B, Cheah KS, Lovell-Badge R *et al* (2010) SOX9 induces and maintains neural stem cells. *Nat Neurosci* 13: 1181–1189

Secombe J, Li L, Carlos L & Eisenman RN (2007) The Trithorax group protein Lid is a trimethyl histone H3K4 demethylase required for dMyc-induced cell growth. *Genes Dev* 21: 537–551

Sell S (2010) On the stem cell origin of cancer. *Am J Pathol* 176: 2584–2594

Seoane J, Le H, Shen L, Anderson SA & Massagué J (2004) Integration of Smad and Forkhead Pathways in the Control of Neuroepithelial and Glioblastoma Cell Proliferation. *Cell* 117: 211–223

Seth KA & Majzoub JA (2001) Repressor Element Silencing Transcription Factor / Neuron- restrictive Silencing Factor (REST / NRSF) Can Act as an Enhancer as Well as a Repressor of Corticotropin-releasing Hormone Gene Transcription. *J Biol Chem* 276: 13917–13923

Shen Q, Wang Y, Dimos JT, Fasano CA, Phoenix TN, Lemischka IR, Ivanova NB, Stifani S, Morrisey EE & Temple S (2006) The timing of cortical neurogenesis is encoded within lineages of individual progenitor cells. *Nat Neurosci* 9: 743–751

Shoichet SA, Kunde SA, Viertel P, Schell-Apacik C, von Voss H, Tommerup N, Ropers HH & Kalscheuer VM (2005) Haploinsufficiency of novel FOXG1B variants in a patient with severe mental retardation, brain malformations and microcephaly. *Hum Genet* 117: 536–544

Shoshan Y, Nishiyama A, Chang A, Mork S, Barnett GH, Cowell JK, Trapp BD & Staugaitis SM (2002)

Expression of oligodendrocyte progenitor cell antigens by gliomas: Implications for the histogenesis of brain tumors. *Proc Natl Acad Sci* 96: 10361–10366

Sidaway P (2017) CNS cancer: Glioblastoma subtypes revisited. *Nat Rev Clin Oncol* 14: 587

Siegenthaler JA & Miller MW (2008) Generation of Cajal-Retzius neurons in mouse forebrain is regulated by transforming growth factor β-Fox signaling pathways. *Dev Biol* 313: 35–46

Singh DK, Kollipara RK, Vemireddy V, Yang XL, Sun Y, Regmi N, Klingler S, Hatanpaa KJ, Raisanen J, Cho SK *et al* (2017) Oncogenes Activate an Autonomous Transcriptional Regulatory Circuit That Drives Glioblastoma. *Cell Rep* 18: 961–976

Singh SK, Clarke ID, Terasaki M, Bonn VE, Hawkins C, Squire J & Dirks PB (2003) Identification of a Cancer Stem Cell in Human Brain Tumors. *Cancer Res* 63: 5821–5828

Singh SK, Hawkins C, Clarke ID, Squire JA, Bayani J, Hide T, Henkelman MR, Cusimano MD & Dirks PB (2004) Identification of human brain tumour initiating cells. *Nature* 432: 396–401

Sonderegger CK & Vogt PK (2003) Binding of the corepressor TLE1 to Qin enhances Qin-mediated transformation of chicken embryo fibroblasts. *Oncogene* 22: 1749–1757

Soneson C, Love MI & Robinson MD (2016) Differential analyses for RNA-seq: Transcript-level estimates improve gene-level inferences [version 2]. *F1000Research* 4: 1521

Sottoriva A, Spiteri I, Piccirillo SG, Touloumis A, Collins VP, Marioni JC, Curtis C, Watts C & Tavaré S (2013) Intratumor heterogeneity in human glioblastoma reflects cancer evolutionary dynamics. *Proc Natl Acad Sci* 110: 4009–4014

Soufi A (2014) Mechanisms for enhancing cellular reprogramming. *Curr Opin Genet Dev* 25: 101–109

Spitz F & Furlong EE (2012) Transcription factors: From enhancer binding to developmental control. *Nat Rev Genet* 13: 613–626

Srinivasan R, Mager GM, Ward RM, Mayer J & Svaren J (2006) NAB2 represses transcription by interacting with the CHD4 subunit of the nucleosome remodeling and deacetylase (NuRD) complex. *J Biol Chem* 281: 15129–15137

Stiles CD & Rowitch DH (2008) Glioma Stem Cells: A Midterm Exam. *Neuron* 58: 832–846

Stricker SH, Feber A, Engström PG, Carén H, Kurian KM, Takashima Y, Watts C, Way M, Dirks P, Bertone P *et al* (2013) Widespread resetting of DNA methylation in glioblastoma-initiating cells suppresses malignant cellular behavior in a lineage-dependent manner. *Genes Dev* 27: 654–669

Stricker SH & Pollard SM (2014) Reprogramming cancer cells to pluripotency: An experimental tool for exploring cancer epigenetics. *Epigenetics* 9: 798–802

Stroud JC, Wu Y, Bates DL, Han A, Nowick K, Paabo S, Tong H & Chen L (2006) Structure of the forkhead domain of FOXP2 bound to DNA. *Structure* 14: 159–166

Stupp R, Hegi ME, Mason WP, van den Bent MJ, Taphoorn MJ, Janzer RC, Ludwin SK, Allgeier A, Fisher B, Belanger K *et al* (2009) Effects of radiotherapy with concomitant and adjuvant temozolomide versus radiotherapy alone on survival in glioblastoma in a randomised phase III study: 5-Year analysis of the EORTC-NCIC trial. *Lancet Oncol* 10: 459–466

Stupp R, Mason WP, van den Bent MJ, Weller M, Fisher B, Taphoorn MJ, Belanger K, Brandes AA, Marosi C *et al* (2005) Radiotherapy plus Concomitant and Adjuvant Temozolomide for Glioblastoma. *N Engl J Med* 352: 987-96

Stupp R, Tonn JC, Brada M, Pentheroudakis G; ESMO Guidelines Working Group (2010) High-grade malignant glioma: ESMO clinical practice guidelines for diagnosis, treatment and follow-up. *Ann Oncol* 21: v190-3

Sun Y, Hu J, Zhou L, Pollard SM & Smith A (2011) Interplay between FGF2 and BMP controls the self-renewal , dormancy and differentiation of rat neural stem cells. *J Cell Sci* 124: 1867–1877

Sun Y, Kong W, Falk A, Hu J, Zhou L, Pollard S & Smith A (2009) CD133 (Prominin) negative human neural stem cells are clonogenic and tripotent. *PLoS One* 4: e5498

Sun Y, Pollard S, Conti L, Toselli M, Biella G, Parkin G, Willatt L, Falk A, Cattaneo E & Smith A (2008) Long-term tripotent differentiation capacity of human neural stem (NS) cells in adherent culture. *Mol Cell Neurosci* 38: 245–258

Sun Z, de Fontoura CSG, Moreno M, Holton NE, Sweat M, Sweat Y, Lee MK, Arbon J, Bidlack FB, Thedens DR *et al* (2018) FoxO6 regulates Hippo signaling and growth of the craniofacial complex. *PLoS Genet* 14: e1007675

Sundar SJ, Hsieh JK, Manjila S, Lathia JD & Sloan A (2014) The role of cancer stem cells in glioblastoma. *Neurosurg Focus* 37: E6

Suvà ML, Rheinbay E, Gillespie SM, Patel AP, Wakimoto H, Rabkin SD, Riggi N, Chi AS, Cahill DP, Nahed BV *et al* (2014) Reconstructing and Reprogramming the Tumor-Propagating Potential of Glioblastoma Stem-like Cells. *Cell* 157: 580–594

Suvà ML, Riggi N & Bernstein BE (2013) Epigenetic Reprogramming in Cancer. *Science* 339: 1567–1571

Suvà ML, Riggi N, Janiszewska M, Radovanovic I, Provero P, Stehle JC, Baumer K, Le Bitoux MA, Marino D, Cironi L *et al* (2009) EZH2 is essential for glioblastoma cancer stem cell maintenance. *Cancer Res* 69: 9211–9218

Swanton C (2012) Intratumor heterogeneity: Evolution through space and time. *Cancer Res* 72: 4875–4882

Takahashi K & Yamanaka S (2006) Induction of Pluripotent Stem Cells from Mouse Embryonic and Adult Fibroblast Cultures by Defined Factors. *Cell* 126: 663–676

Tan K, Shaw AL, Madsen B, Jensen K, Taylor-Papadimitriou J & Freemont PS (2003) Human PLU-1 Has Transcriptional Repression Properties and Interacts with the Developmental Transcription Factors BF-1 and PAX9. *J Biol Chem* 278: 20507–20513

Tan Y, Raychaudhuri P & Costa RH (2007) Chk2 Mediates Stabilization of the FoxM1 Transcription Factor To Stimulate Expression of DNA Repair Genes. *Mol Cell Biol* 27: 1007–1016

Team BC, Maintainer BP (2019). TxDb.Hsapiens.UCSC.hg38.knownGene: Annotation package for TxDb object(s). R package version 3.4.6.

Temple S (1989) Division and differentiation of isolated eNS blast cells in microculture. *Nature* 340: 471–473

The Cancer Gencome Atlas Research Network (2008) Comprehensive genomic characterization defines human glioblastoma genes and core pathways. *Nature* 455: 1061–1068

Tohyama J, Yamamoto T, Hosoki K, Nagasaki K, Akasaka N, Ohashi T, Kobayashi Y & Saitoh S (2011) West syndrome associated with mosaic duplication of FOXG1 in a patient with maternal uniparental disomy of chromosome 14. *Am J Med Genet* 155A: 2584–2588

Toms SA, Kim CY, Nicholas G & Ram Z (2019) Increased compliance with tumor treating fields therapy is prognostic for improved survival in the treatment of glioblastoma: a subgroup analysis of the EF-14 phase III trial. *J Neurooncol* 141: 467–473

Tsai KL, Huang CY, Chang CH, Sun YJ, Chuang WJ & Hsiao CD (2006) Crystal structure of the human FOXK1a-DNA complex and its implications on the diverse binding specificity of winged helix/forkhead proteins. *J Biol Chem* 281: 17400–17409

Tykocki T & Eltayeb M (2018) Ten-year survival in glioblastoma. A systematic review. *J Clin Neurosci* 54: 7–

Vakoc CR, Mandat SA, Olenchock BA & Blobel GA (2005) Histone H3 lysine 9 methylation and HP1γ are associated with transcription elongation through mammalian chromatin. *Mol Cell* 19: 381–391

Vegas N, Cavallin M, Maillard C, Boddaert N, Toulouse J, Schaefer E, Lerman-Sagie T, Lev D, Magalie B, Moutton S *et al* (2018) Delineating FOXG1 syndrome: From congenital microcephaly to hyperkinetic encephalopathy. *Neurol Genet* 4: e281

Verginelli F, Perin A, Dali R, Fung KH, Lo R, Longatti P, Guiot M, Del Maestro RF, Rossi S, di Porzio U *et al* (2013) Transcription factors FOXG1 and Groucho/TLE promote glioblastoma growth. *Nat Commun* 4: 2956

Verhaak RG, Hoadley KA, Purdom E, Wang V, Qi Y, Wilkerson MD, Miller CR, Ding L, Golub T, Mesirov JP *et al* (2010) Integrated Genomic Analysis Identifies Clinically Relevant Subtypes of Glioblastoma Characterized by Abnormalities in PDGFRA, IDH1, EGFR, and NF1. *Cancer Cell* 17: 98–110

Vezzali R, Weise SC, Hellbach N, Machado V, Heidrich S & Vogel T (2016) The FOXG1/FOXO/SMAD network balances proliferation and differentiation of cortical progenitors and activates Kcnh3 expression in mature neurons. *Oncotarget* 7: 37436-37455

Visvader JE & Lindeman GJ (2008) Cancer stem cells in solid tumours: Accumulating evidence and unresolved questions. *Nat Rev Cancer* 8: 755–768

Wainwright EN & Scaffidi P (2017) Epigenetics and Cancer Stem Cells: Unleashing, Hijacking, and Restricting Cellular Plasticity. *Trends in Cancer* 3: 372–386

Walz W & Lang MK (1998) Immunocytochemical evidence for a distinct GFAP-negative subpopulation of astrocytes in the adult rat hippocampus. *Neurosci Lett* 257: 127–130

Wang F, Marshall CB, Li GY, Yamamoto K, Mak TW & Ikura M (2009) Synergistic Interplay between Promoter Recognition and CBP/p300 Coactivator Recruitment by FOXO3a. *ACS Chem Biol* 4: 1017–1027

Wang F, Marshall CB, Yamamoto K, Li GY, Gasmi-Seabrook GM, Okada H, Mak TW & Ikura M (2012) Structures of KIX domain of CBP in complex with two FOXO3a transactivation domains reveal promiscuity and plasticity in coactivator recruitment. *Proc Natl Acad Sci* 109: 6078–6083

Wang JH, Tang H-S, Li XS, Zhang XL, Yang XZ, Zeng LS, Ruan Q, Huang YH, Liu GJ, Wang J *et al* (2017a) Elevated FOXO6 expression correlates with progression and prognosis in gastric cancer. *Oncotarget* 8: 31682–31691

Wang J, Ma Y & Cooper MK (2013) Cancer stem cells in glioma: Challenges and opportunities. *Transl Cancer Res* 2: 429–441

Wang J, Scully K, Zhu X, Cai L, Zhang J, Prefontaine GG, Krones A, Ohgi KA, Zhu P, Garcia-Bassets I *et al* (2007) Opposing LSD1 complexes function in developmental gene activation and repression programmes. *Nature* 446: 882-7

Wang J, Wakeman TP, Lathia JD, Hjelmeland AB, Wang XF, White RR, Rich JN & Sullenger BA (2010) Notch promotes radioresistance of glioma stem cells. *Stem Cells* 28: 17–28

Wang L, Wang J, Jin T, Zhou Y & Chen Q (2018) FoxG1 facilitates proliferation and inhibits differentiation by downregulating FoxO / Smad signaling in glioblastoma. *Biochem Biophys Res Commun* 504: 46–53

Wang Q, Hu B, Hu X, Kim H, Squatrito M, Scarpace L, deCarvalho AC, Lyu S, Li P, Li Y *et al* (2017b) Tumor Evolution of Glioma-Intrinsic Gene Expression Subtypes Associates with Immunological Changes in the Microenvironment. *Cancer Cell* 32: 152

Wang Y, Wang F, Wang R, Zhao P & Xia Q (2015) 2A self-cleaving peptide-based multi-gene expression system in the silkworm Bombyx mori. *Sci Rep* 5: 16273

Weigel D, Jürgens G, Küttner F, Seifert E & Jäckle H (1969) The Homeotic Gene fork head Encodes a Nuclear Protein and Is Expressed in the Terminal Regions of the Drosophila Embryo. *Cell* 57: 645–658

Westphal M, Maire CL & Lamszus K (2017) EGFR as a Target for Glioblastoma Treatment: An Unfulfilled Promise. *CNS Drugs* 31: 723–735

Wick W & Kessler T (2018) New glioblastoma heterogeneity atlas — a shared resource. *Nat Rev Neurol* 14: 453-454

Widschwendter M, Fiegl H, Egle D, Mueller-Holzner E, Spizzo G, Marth C, Weisenberger DJ, Campan M, Young J, Jacobs I *et al* (2007) Epigenetic stem cell signature in cancer. *Nat Genet* 39: 157-8

Wiese S, Murphy DB, Schlung A, Burfeind P, Schmundt D, Schniille V, Mattei M & Thies U (1995) The genes for human brain factor 1 and 2, members of the fork head gene family, are clustered on chromosome 14q. *Biochim Biophys Acta* 1262: 105–112

Wijchers PJ, Burbach JP & Smidt MP (2006) In control of biology : of mice , men and Foxes. *Biochem J* 397: 233–246

de Winter JCF (2013) Using the Student's t-test with Extremely Small Sample sizes. *Practical Assessment, Research and Evaluation*, 18(10) ISSN-1531-7714.

Wolfrum C, Besser D, Luca E & Stoffel M (2003) Insulin regulates the activity of forkhead transcription factor Hnf-3 /Foxa-2 by Akt-mediated phosphorylation and nuclear/cytosolic localization. *Proc Natl Acad Sci* 100: 11624–11629

Xiang Y, Zhu Z, Han G, Ye X, Xu B, Peng Z, Ma Y, Yu Y, Lin H, Chen *AP et al* (2007) JARID1B is a histone H3 lysine 4 demethylase up-regulated in prostate cancer. *Proc Natl Acad Sci* 104: 19226–19231

Xie W, Barr CL, Kim A, Yue F, Lee AY, Eubanks J, Dempster EL & Ren B (2012) Base-resolution analyses of sequence and parent-of-origin dependent DNA methylation in the mouse genome. *Cell* 148: 816–831

Xie Y, Bergström T, Jiang Y, Johansson P, Marinescu VD, Lindberg N, Segerman A, Wicher G, Niklasson M, Baskaran S *et al* (2015) The Human Glioblastoma Cell Culture Resource: Validated Cell Models Representing All Molecular Subtypes. *EBioMedicine* 2: 1351–1363

Xu F, Mao C, Ding Y, Rui C, Wu L, Shi A, Zhang H, Zhang L & Xu Z (2010) Molecular and Enzymatic Profiles of Mammalian DNA Methyltransferases: Structures and Targets for Drugs. *Curr Med Chem* 17: 4052–4071

Xuan S, Baptista CA, Balas G, Tao W, Soares VC & Lai E (1995) Winged Helix Transcription Factor BF-1 Is Essential for the Development of the Cerebral Hemispheres. *Neuron* 14: 1141–1152

Yamane K, Tateishi K, Klose RJ, Fang J, Fabrizio LA, Erdjument-Bromage H, Taylor-Papadimitriou J, Tempst P & Zhang Y (2007) PLU-1 Is an H3K4 Demethylase Involved in Transcriptional Repression and Breast Cancer Cell Proliferation. *Mol Cell* 25: 801–812

Yan C & Higgins PJ (2013) Drugging the undruggable: Transcription therapy for cancer. *Biochim Biophys Acta - Rev Cancer* 1835: 76–85

Yang H, Wang H, Shivalila CS, Cheng AW, Shi L & Jaenisch R (2013) One-step generation of mice carrying reporter and conditional alleles by CRISPR/cas-mediated genome engineering. *Cell* 154: 1370-9

Yang R, Wu Y, Zou J, Zhou J, Wang M, Hao X & Cui H (2016) The Hippo transducer TAZ promotes cell proliferation and tumor formation of glioblastoma cells through EGFR pathway. *Oncotarget* 7: 36255-36265

Yang Q, Kong Y, Rothermel B, Garry DJ, Bassel-Duby R, Williams RS (2000) The winged-helix/forkhead protein myocyte nuclear factor beta (MNF-beta) forms a co-repressor complex with mammalian sin3B. *Biochem J* 345: 335-43

Yao J, Lai E & Stifani S (2001) The Winged-Helix Protein Brain Factor 1 Interacts with Groucho and Hes Proteins To Repress Transcription. *Mol Cell Biol* 21: 1962–1972

Yao J, Liu Y, Lo R, Tretjakoff I, Peterson A & Stifani S (2000) Disrupted development of the cerebral hemispheres in transgenic mice expressing the mammalian Groucho homologue Transducin-like-Enhancer of split 1 in postmitotic neurons. *Mech Dev* 93: 105–115

Yeo H, Lyssiotis CA, Zhang Y, Ying H, Asara JM, Cantley LC & Paik JH (2013) FoxO3 coordinates metabolic pathways to maintain redox balance in neural stem cells. *EMBO J* 32: 2589–2602

Ying Q, Stavridis M, Griffiths D, Li M & Smith A (2003) Conversion of embryonic stem cells into neuroectodermal precursors in adherent monoculture. *Nat Biotechnol* 21: 183–186

Yuan X, Curtin J, Xiong Y, Liu G, Waschsmann-Hogiu S, Farkas DL, Black KL & Yu JS (2004) Isolation of cancer stem cells from adult glioblastoma multiforme. *Oncogene* 23: 9392–9400

Yun M, Wu J, Workman JL & Li B (2011) Readers of histone modifications. *Cell Res* 21: 564–578

Zeng F, Xue M, Xiao T, Li Y, Xiao S, Jiang B & Ren C (2016) MiR-200b promotes the cell proliferation and metastasis of cervical cancer by inhibiting FOXG1. *Biomed Pharmacother* 79: 294–301

Zhang SC, Wernig M, Duncan ID, Brüstle O & Thomson JA (2001) In vitro differentiation of neural precursors from human embryonic stem cells. *Nat Biotechnol* 19: 1129–1133

Zhang X, Zhang W, Cao WD, Cheng G & Zhang YQ (2012) Glioblastoma multiforme: Molecular characterization and current treatment strategy (Review). *Exp Ther Med* 3: 9–14

Zhang Y, Liang J & Li Q (2014) Coordinated Regulation of Retinoic Acid Signaling Pathway by KDM5B and Polycomb Repressive Complex 2. *J Cell Biochem* 115: 1528–1538

Zhou Q, Obana EA, Radomski KL, Sukumar G, Wynder C, Dalgard CL & Doughty ML (2016) Inhibition of the histone demethylase Kdm5b promotes neurogenesis and derepresses Reln (reelin) in neural stem cells from the adult subventricular zone of mice. *Mol Biol Cell* 27: 627–639

Zong H, Parada LF & Baker SJ (2015) Cell of origin for malignant gliomas and its implication in therapeutic development. *Cold Spring Harb Perspect Biol* 7: pii: a020610

APPENDICES

I. CRISPR gRNA sequences

Target gene	Purpose	Sequence (5' to 3')	PAM	Species	Additional ID
FoxO6	Gene-tagging	GGCACCCAGGCTGTGTAGGG	TGG	Mouse	2
Foxg1	Gene-tagging	TTTAATACATTAACATCCGG	GGG	Mouse	M85
FOXG1	Gene-tagging	TCACTTACAGTCTGGTCCCA	GGG	Human	2
FOXG1	Gene disruption	GACAACCACCACGCGAGCCA	CGG	Human	-
Foxg1	Gene disruption (5' end)	GACAACCACCACGCGAGCCA	CGG	Mouse	sp322
Foxg1	Gene disruption (3' end)	GAAATAATCAGACAGTCCCC	CGG	Mouse	sp199

II. CRISPR donor DNA sequences

Target gene	Purpose	Sequence (5' to 3')	Species
FoxO6	HA-tagging	ACTTCGACTCAGCCCTGCCTCCGCCACCCCCGG GCCTGGCTGGGGCGCCGCCCCCTAACCAGAGCT GGGTGCCAGGCTACCCATACGACGTACCAGATT ACGCTTGAGGGGCACCCTACACAGCCTGGGTGC CCCGGTCCCGTCCCCATGGGGCCTCTGTCTTCCCA TCCCGATCCCCGGGTCC	Mouse
Foxg1	V5-tagging	CTGGACTTATTTTTTTAATTATCATTTACAATGC AAATGTGTGTAAAACGTTCACTTACAGTCTGCTC CCCCGGATGTTACGTAGAATCGAGACCGAGGAGA GGGTTAGGGATAGGCTTACCATGTATTAAAGGGT TGGAAGAAGACCCCTGATTTTGATGTGTGAAATA ATCAGACAGTCCCCCGGACAGTCCTGTCG	Mouse
FOXG1	V5-tagging	GGACTTATTTTTTTAATTATCATTTACAATGCAA ATGTGTGTAAAACGTTCACTTACAGTCTGCTCCC AGGCATGTTACGTAGAATCGAGACCGAGGAGAGG GTTAGGGATAGGCTTACCATGTATTAAAGGGTTG	Human

		GAAGAAGACCCCTGATTTTGATGTGTGAAATAAT CAGACAGTCCCCCAGACAGTCCCGTCG	
FOXG1	3xFLAG-HA-p2A-eGFP	GCACTTTGAGTTACAACGGCACCACGTCGGCCTAC CCCAGCCACCCCATGCCCTACAGCTCCGTGTTGACT CAGAACTCGCTGGGCAACAACCACTCCTTCTCCACC GCCAACGGCCTGAGCGTGGACCGGCTGGTCAACGGG GAGATCCCGTACGCCACGCACCACCTCACGGCCGCC GCGCTAGCCGCCTCGGTGCCCTGCGGCCTGTCGGTG CCCTGCTCTGGGACCTACTCCCTCAACCCCTGCTCC GTCAACCTGCTCGCGGGCCAGACCAGTTACTTTTT CCCCCACGTCCCGCACCCGTCAATGACTTCGCAGA GCAGCACGTCCATGAGCGCCAGGGCCGCGTCCTCC TCCACGTCGCCGCAGGCCCCCTCGACCCTGCCCTG TGAGTCTTTAAGACCCTCTTTGCCAAGTTTTACG ACGGGACTGTCTGGGGGACTGTCTGATTATTTCAC ACATCAAAATCAGGGGTCTTCTTCCAACCCTTTAA TACATGGATCCGACTACAAAGACCATGACGGTGAT TATAAAGATCATGACATCGATTACAAGGATGACGA TGACAAGGGATCCTACCCATACGATGTTCCAGATT ACGCTGGATCCGGCGCAACAAACTTCTCTCTGCTG AAACAAGCCGGAGATGTCGAAGAGAATCCTGGAC CGATGGTGAGCAAGGGCGAGGAGCTGTTCACCGG GGTGGTGCCCATCCTGGTCGAGCTGGACGGCGAC GTAAACGGCCACAAGTTCAGCGTGTCCGGCGAGG GCGAGGGCGATGCCACCTACGGCAAGCTGACCCT GAAGTTCATCTGCACCACCGGCAAGCTGCCCGTG CCCTGGCCCACCCTCGTGACCACCCTGACCTACG GCGTGCAGTGCTTCAGCCGCTACCCCGACCACATGA AGCAGCACGACTTCTTCAAGTCCGCCATGCCCGAAG GCTACGTCCAGGAGCGCACCATCTTCTTCAAGGACG ACGGCAACTACAAGACCCGCGCCGAGGTGAAGTTCG AGGGCGACACCCTGGTGAACCGCATCGAGCTGAAGG GCATCGACTTCAAGGAGGACGGCAACATCCTGGGG CACAAGCTGGAGTACAACTACAACAGCCACAACGT CTATATCATGGCCGACAAGCAGAAGAACGGCATCA AGGTGAACTTCAAGATCCGCCACAACATCGAGGAC GGCAGCGTGCAGCTCGCCGACCACTACCAGCAGAA CACCCCCATCGGCGACGGCCCCGTGCTGCTGCCCG ACAACCACTACCTGAGCACCCAGTCCGCCCTGAGC AAAGACCCCAACGAGAAGCGCGATCACATGGTCC TGCTGGAGTTCGTGACCGCCGCCGGGATCACTCT CGGCATGGACGAGCTGTACAAGTAACATGCCTGG GACCAGACTGTAAGTGAACGTTTTACACAC ATTTGCATTGTAAATGATAATTAAAAAAA TAAGTCCAGGTATTTTTTATTAAGCCCCCC CCTCCCATTTCTGTACGTTTGTTCAGTCTC TAGGGTTGTTTATTATTCTAACAAGGTGT GGAGTGTCAGCGAGGTGCAATGTGGGGAG AATACATTGTAGAATATAAGGTTTGGAAG TCAAATTATAGTAGAATGTGTATCTAAAT AGTGACTGCTTTGCCATTTCATTCAAACC TGACAAGTCTATCTCTAAGAGCCGCCAGA TTTCCATGTGTGCAGTATTATAAGTTATC ATGGAACTATATGGTGGACGCAGACCTTG AGAACAACCTAAATTATGGGGAGAATTTT AAAATGTTAAACTGTAATTTGTATTTAAA AAGCATTCGTAGTAAAGGTGCCCAAGAAA TTATTTTGGCCATTTATTGTTTTGTCCTT TTCTTTAAAGAACTGTTTTTT	Human

III. Plasmids

Plasmid name	Bacterial selection	Mammalian selection	SMP Library ID
pCMV-pBase	Ampicillin	N/A	sp59
pCAG-Tet3G	Ampicillin	Zeocin	sp169
PB TRE-FOXG1V5 (TetOn-FOXG1_V5)	Ampicillin	Blasticidin	sp171
CAG-WTCas9-2A-mCherry	Ampicillin	N/A	sp404
pU6-BsaI-mFoxg1-guide-1	Kanamycin	N/A	sp199
mFoxg1_gRNA_B-U6BSAIbackbone	ClonNAT	N/A	sp322

IV. Cell lines

Cell lines are listed as 'parental' if not genetically-engineered, or have been gifted following genetic engineering elsewhere. 'Engineered' cell lines have been genetically engineered by a member of the Pollard lab.

Cell line	Species	Parental/ engineered	Modification	Notes
FS3	Mouse	Engineered	Dox-inducible *FOXG1-V5* and *SOX2* overexpression	Clonal, ANS4-derived. Made by Dr Harry Bulstrode.
F6	Mouse	Engineered	Dox-inducible *FOXG1-V5* overexpression	Clonal, ANS4-derived. Made by Dr Harry Bulstrode.
F11-19	Mouse	Engineered	Dox-inducible *FOXG1-V5* overexpression	Clonal, ANS4-derived. F11 clonal line made by Dr Harry Bulstrode. F11-19 clonal line re-derived by K. Ferguson.
IENS-GFP	Mouse	'Parental'	EGFRvIII overexpression and *Ink4a/Arf* deletion.	Gift from Prof M. Lohuizen (Bruggeman *et al*, 2007). SVZ NSCs from *Cdkn2a*$^{-/-}$ adult mice were transduced

			Stably express GFP from a constitutive promoter.	with EGFRvIII retrovirus.
IENS-GFP *Foxg1* KO Clone 58	Mouse	Engineered	CRISPR/Cas9 KO of *Foxg1*	Clonal cell line
IENS-GFP *Foxg1* KO Clone 59	Mouse	Engineered	CRISPR/Cas9 KO of *Foxg1*	Clonal cell line
FF-IEK	Mouse	Engineered	*Ink4a/Arf* deletion and EGFRvIII overexpression (+mKate) by Dr Ester Gangoso.(FF-I clone 8+EGFRVIII+mKate (PiggyBac-mediated overexpression).	Derived from 'FF' cell line, an adult SVZ *Foxg1*$^{fl/fl}$ cell line derived by H.Bulstrode using mice provided by V.Fotski, from Fischell lab (Miyoshi & Fishell, 2012).
FF-IEK *Foxg1* KO	Mouse	Engineered	Cre-mediated deletion of *Foxg1*	Cre-mediated deletion of *Foxg1* performed by Dr Ester Gangoso
ANS4	Mouse	Parental	N/A	Derived from SVZ of adult mouse
Foxo6 KO Clone 53	Mouse	Engineered	Bi-allelic *Foxo6* disruption	Clonal, ANS4-derived. Made by Claudia-Garcia Diaz
ANS4 FOXG1-V5 ind.	Mouse	Engineered	Dox-inducible FOXG1-V5 overexpression	Bulk population.
Foxo6 KO Clone 53 FOXG1-V5 ind.	Mouse	Engineered	Dox-inducible FOXG1-V5 overexpression	Bulk population.
G7	Human	Parental	N/A	Patient-derived GNS cell line
G7 *FOXG1* null	Human	Engineered	CRISPR/Cas9 KO of *FOXG1*, previously engineered by Dr Raul Bardini Bressan	Patient-derived GNS cell line, clonal.
G313	Human	Parental	N/A	Patient-derived GNS cell line from GCGR.
G313 *FOXG1* KO clone 42	Human	Engineered	CRISPR/Cas9 KO of *FOXG1*, aided by S. VijayKumar and K.Benjasupawan	Patient-derived GNS cell line, clonal.
G313 *FOXG1* KO clone 44	Human	Engineered	CRISPR/Cas9 KO of *FOXG1*, aided by S. VijayKumar and K.Benjasupawan	Patient-derived GNS cell line, clonal.
G313 *FOXG1* KO clone 47	Human	Engineered	CRISPR/Cas9 KO of *FOXG1*, aided by S. VijayKumar and K.Benjasupawan	Patient-derived GNS cell line, clonal.
G301-B	Human	Parental	N/A	Patient-derived GNS cell line from GCGR.
G317	Human	Parental	N/A	Patient-derived GNS cell line from GCGR.

G325	Human	Parental	N/A	Patient-derived GNS cell line from GCGR.
G326	Human	Parental	N/A	Patient-derived GNS cell line from GCGR.
G327	Human	Parental	N/A	Patient-derived GNS cell line from GCGR.
G328	Human	Parental	N/A	Patient-derived GNS cell line from GCGR.
G330	Human	Parental	N/A	Patient-derived GNS cell line from GCGR.
CB152	Human	Parental	N/A	Human foetal NS cell line.
CB11130	Human	Parental	N/A	Human foetal NS cell line.
Jarid1b$^{F/F}$; *Rosa26::CreERT2* (-4OHT)	Mouse	Parental	Previously engineered to contain *Jarid1b* alleles with exon 6 floxed, and heterozygous for *CreERT2* at the *Rosa26* locus through mice breeding.	Gifted by Prof. Kristian Helin. (Schmitz *et al*, 2011). NS cells derived from the cerebral cortex of E12.5 mouse embryos
Jarid1b$^{-/-}$; *Rosa26::CreERT2* (+4OHT)	Mouse	Parental	*Jarid1b*$^{F/F}$; *Rosa26::CreERT2* previously treated with 4OHT to achieve *Jarid1B* deletion.	Gifted by Prof. Kristian Helin. (Schmitz *et al*, 2011). NS cells derived from the cerebral cortex of E12.5 mouse embryos
Jarid1B WT -4OHT FOXG1-V5 ind.	Mouse	Engineered	Dox-inducible FOXG1-V5 overexpression	Bulk population.
Jarid1B KO +4OHT FOXG1-V5 ind.	Mouse	Engineered	Dox-inducible FOXG1-V5 overexpression	Bulk population.
IENS-GFP Foxg1-V5 clone 11	Mouse	Engineered	V5-tag insertion at *Foxg1* 3' end	Clonal, derived from IENS-GFP
IENS-GFP Foxg1-V5 clone 18	Mouse	Engineered	V5-tag insertion at *Foxg1* 3' end	Clonal, derived from IENS-GFP
IENS-GFP Foxg1-V5 clone 23	Mouse	Engineered	V5-tag insertion at *Foxg1* 3' end	Clonal, derived from IENS-GFP
G7-CAG-Luc-GFP	Human	Parental	Constitutive GFP expression	Patient-derived GNS cell line
G7-GFP FOXG1-V5 clone 16	Human	Engineered	V5-tag insertion at *FOXG1* C terminus	Clonal, derived from G7-GFP
G7-GFP FOXG1-V5 clone 50	Human	Engineered	V5-tag insertion at *FOXG1* 3' end	Clonal, derived from G7-GFP
G7-GFP FOXG1-V5 clone 62	Human	Engineered	V5-tag insertion at *FOXG1* 3' end	Clonal, derived from G7-GFP
G7 FOXG1-3xFLAG-HA-p2A-eGFP	Human	Engineered	3xFLAG-HA-p2A-eGFP-tag insertion at *FOXG1* 3' end	Bulk population, sorted for eGFP expressing cells.
G313 FOXG1-3xFLAG-HA-p2A-eGFP	Human	Engineered	3xFLAG-HA-p2A-eGFP-tag insertion at *FOXG1* 3' end	Bulk population, sorted for eGFP expressing cells.

V. Antibodies

Primary antibodies

Antigen	Species and Isotype	Application	Dilution	Manufacturer	Catalogue
V5 tag	Mouse IgG2b	WB/ ICC	1:1000/1:2000	eBioscience	14-6796
GFAP	Rabbit IgG	ICC	1:1000	Sigma	G9269
GFAP	Mouse	ICC	1:1000	Sigma	G3893
Nestin	Mouse IgG1	ICC	1:10	DSHB	Rat-401
Foxg1	Mouse IgG2a	WB/ ICC/IP	1:1000/1:100/ ~100µl =10 µg / IP	SMP lab	17B12 hybridoma
Foxg1	Rabbit IgG polyclonal	IP	10 µg per IP	Abcam	ab18259
Gapdh	Mouse IgG2b	WB	1:1000	GenTex	GTX627408
Olig2	Rabbit IgG polyclonal	ICC	1:300	Millipore	ab9610
Sox2	Rabbit IgG polyclonal	ICC	1:100	Abcam	ab92492
Tuj1	Mouse IgG2a	ICC	1:1000	Biolegend	801202
Blbp	Rabbit IgG polyclonal	ICC	1:200	Santa Cruz	sc30088
Jarid1b	Rabbit IgG polyclonal	WB	1:1000	Novus Biologicals	NBP1-84352
Jarid1b	Rabbit IgG polyclonal	WB	1:1000	Helin lab	DAIN78
Jarid1b	Rabbit IgG polyclonal	WB	1:1000	Cell Signaling Technology	3273
Ki67	Rabbit IgG	ICC	1:200	Thermo Fisher	RB-9043-P0
FLAG	Mouse IgG1 monoclonal	ICC	1:2000	Sigma	F3165
HA	Mouse IgG1 monoclonal	WB/ ICC	1:1000/1:100	Cell Signaling Technology	(6E2) 2367
HA	Mouse	IP	5 µg / IP	Abcam	ab9110
Mouse IgG	From mouse serum	IP	10 µg / IP	Sigma	I5381

Secondary antibodies

Antigen	Species and Isotype	Application	Dilution	Conjugation	Manufacturer
Various IgG	Goat	ICC	1:1000	Alexa Fluor™ 488/594/647	Invitrogen
ECL anti-mouse IgG	Goat	WB	1:10000 (1:50000 for Gapdh)	HRP-linked	R & D
ECL anti-rabbit IgG	Goat	WB	1:10000	HRP-linked	GE

VI. Primers

Locus	Modification	Forward (5' to 3')	Reverse (5' to 3')	Species
FoxO6	C terminal (3') HA-tag	GGATCTGGACCTCGACATGT	ATCTGGTACGTCGTATGGGT	Mouse
FoxO6	Gene disruption at 5' end	CCTCACTGCCTGGGTCTTT	CGGACCATCCAGTCGTAGAT	Mouse
Foxg1	Gene disruption	CAAGTCCTCGTTCAGCATCA	CAACACTGCCCATTCAATTG	Mouse
Foxg1	C terminal (3') V5-tag	TCAATGACTTCGCAGACCAG	ATTCTCCCACATTGCACCTC	Mouse
FOXG1	C terminal (3') V5-tag	TCAATGACTTCGCAGACCAG	ACCGAGGAGAGGGTTAGGGAT	Human
FOXG1	C terminal (3') 3xFLAG-HA-p2A-eGFP-tag	CGACAACCACTACCTGAGCA	ACCAAGTGCATTTTCTAGAACCC	Human
FOXG1	Primers to amplify 3xFLAG-HA-p2A-eGFP-tag dsDNA	ACAGCTCCGTGTTGACTCAGAAC	TTGGGCACCTTTACTACGAATGC	Human
Rosa26	ROSA26-CreERT2	AAAGTCGCTCTGAGTTGTTAT	CCTGATCCTGGCAATTTCG	Mouse
Jarid1B	Exon 6 deletion	CAGTACCCAGGAAGCAGAGTG	CCCAAAATGGACATAACAAG	Mouse
Jarid1B (qRT-PCR)	Exon 6 deletion	TCCGACACAAAGGACAAGGA	GCTTCTGTTGCCTCTTCTGG	Mouse

VII. TaqMan assays

Gene	Species	Dye	Order number
Gapdh	Mouse	FAM-MGB	Mm99999915_g1
FOXG1	Human	FAM-MGB	Hs01850784_s1
Foxo6	Mouse	FAM-MGB	Mm00809934_s1
Foxo3	Mouse	FAM-MGB	Mm01185722_m1
NMyc	Mouse	FAM-MGB	Mm00476449_m1
Plk1	Mouse	FAM-MGB	Mm00440924_g1
Chd3	Mouse	FAM-MGB	Mm01332658_m1
Tet3	Mouse	FAM-MGB	Mm00805756_m1
Dnmt1	Mouse	FAM-MGB	Mm01151063_m1
Dnmt3b	Mouse	FAM-MGB	Mm01240113_m1
Dnmt3a	Mouse	FAM-MGB	Mm00432881_m1
Hdac7	Mouse	FAM-MGB	Mm00469527_m1
Ezh2	Mouse	FAM-MGB	Mm00468464_m1
Nestin	Mouse	FAM-MGB	Mm00450205_m1
Blbp (Fabp7)	Mouse	FAM-MGB	Mm00445225_m1
Olig2	Mouse	FAM-MGB	Mm01210556_m1
Aqp4	Mouse	FAM-MGB	Mm00802131_m1
S100	Mouse	FAM-MGB	Mm00485897_m1
Gfap	Mouse	FAM-MGB	Mm01253033_m1
FOXO6	Human	FAM-MGB	Hs01010449_s1
CHD3	Human	FAM-MGB	Hs01050212_m1
GAPDH	Human	FAM-MGB	Hs02758991_g1

VIII. Supplementary RNA-seq data

Figure 4-12 with cell line labels

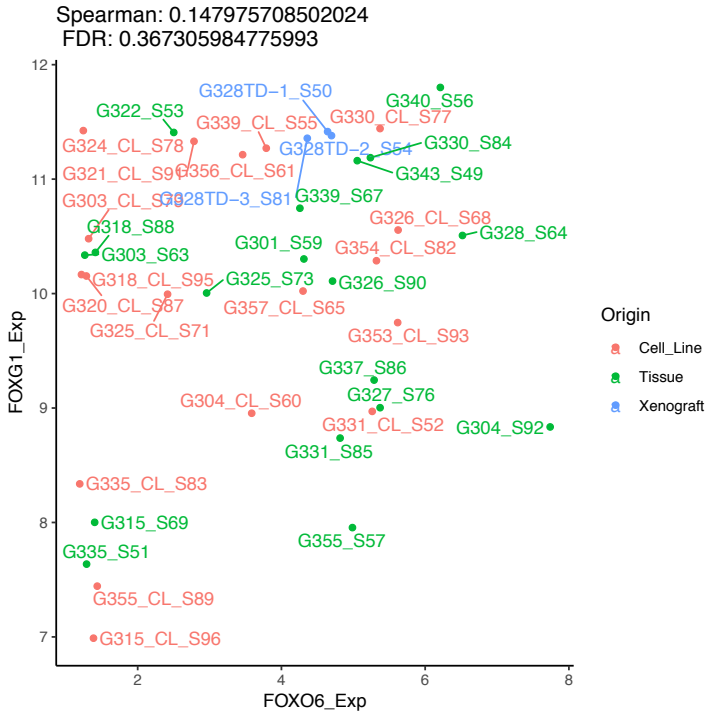

Figure 4-16 with cell line labels

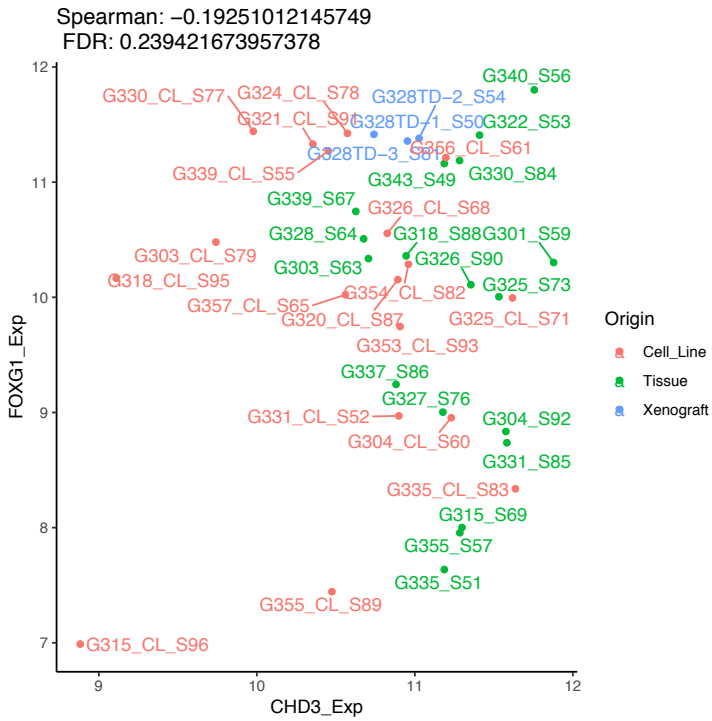

Original GNS cell line names and new GCGR names

Original name	GCGR name
G301B	GCGR-E1
G303B	GCGR-E3
G304B	GCGR-E4
G313	GCGR-E13
G315	GCGR-E15
G317	GCGR-E17
G322	GCGR-E22
G326	GCGR-E26
G327	GCGR-E27
G328	GCGR-E28
G318	GCGR-E18
G320	GCGR-E20
G321	GCGR-E21

Original name	GCGR name
G324	GCGR-E24
G325	GCGR-E25
G330	GCGR-E30
G335	GCGR-E35
G331	GCGR-E31
G334	GCGR-E34
G337	GCGR-E37
G339	GCGR-E39
G343	GCGR-E43
G351	GCGR-E51
G353	GCGR-E53
G354	GCGR-E54
G355	GCGR-E55